Space-Time Codes for High Data Rate Wireless Communications

Ran Gozali

Dissertation submitted to the Faculty of the
Virginia Polytechnic Institute and State University
in partial fulfillment of the requirements for the degree of

Doctor of Philosophy
in
Electrical Engineering

Brian D. Woerner, Chair
Jeffrey H. Reed
Theodore S. Rappaport
William J. Ebel
Warren L. Stutzman
Werner Kohler

April 24, 2002
Blacksburg, Virginia

Keywords: Space-Time Coding, MIMO Channels, VT-STAR, Iterative Processing,
Wireless Communications

Space-Time Codes for High Data Rate Wireless Communications

by
Ran Gozali
Committee Chairman: Brian D. Woerner
Electrical Engineering

Abstract

Space-time codes (STC) are a class of signaling techniques, offering coding and diversity gains along with improved spectral efficiency. These codes exploit both the spatial and the temporal diversity of the wireless link by combining the design of the error correction code, modulation scheme and array processing. STC are well suited for improving the downlink performance, which is the bottleneck in asymmetric applications such as downstream Internet.

Three original contributions to the area of STC are presented in this dissertation. First, the development of analytic tools that determine the fundamental limits on the performance of STC in a variety of channel conditions. For trellis-type STC, transfer function based techniques are applied to derive performance bounds over Rayleigh, Rician and correlated fading environments. For block-type STC, an analytic framework that supports various complex orthogonal designs with arbitrary signal cardinalities and array configurations is developed. In the second part of the dissertation, the Virginia Tech Space-Time Advanced Radio (VT-STAR) is designed, introducing a multi-antenna hardware laboratory test bed, which facilitates characterization of the multiple-input multiple-output (MIMO) channel and validation of various space-time approaches. In the third part of the dissertation, two novel space-time architectures paired with iterative processing principles are proposed. The first scheme extends the suitability of STC to outdoor wireless communications by employing iterative equalization/decoding for time dispersive channels and the second scheme employs iterative interference cancellation/decoding to solve the error propagation problem of Bell-Labs Layered Space-Time Architecture (BLAST). Results show that remarkable energy and spectral efficiencies are achievable by combining concepts drawn from space-time coding, multiuser detection, array processing and iterative decoding.

Acknowledgments

This work has been made possible by the MPRG Industrial Affiliates program, the Defense Advanced Research Projects Agency (DARPA), the Office of Naval Research through the NAVCIITI program and Rafael Inc., Israel.

I would first like to thank my advisor and mentor, Dr. Woerner, who has provided me with guidance and freedom to create. His consistent encouragement, support and excellent advice have allowed me to develop my research capabilities, writing skills and teaching experience. On a personal note, his attitude towards his students, staff and colleagues will serve me as a model throughout my professional career. I am grateful to the other professors on my committee for their time, counsel and insight into my research. Special thanks to the outstanding MPRG staff, who have created a good atmosphere for effective work environment. One of the great benefits of working in MPRG is the quality of students and level of interaction among students. It has been a pleasure for me to collaborate with many bright students during the development of the Virginia Tech Space-Time Advanced Radio. Special thanks to R. Mostafa and R.C. Palat, who have diligently continued the work and brought the system into a fruitful stage. I would also like to thank Dr. Buehrer for his collaboration on the work presented in Chapter 9.

Finally, on a personal note, I would like to thank my family; my wife, Tsofit, who has supported me with encouragement and love, my children, Tsach and Noa, who have brought happiness into our lives, my parents in law, Nili and Rimon, who have helped us during the last year of our studies, my siblings, Atara, Tsachi and Rama, who have been a source of inspiration for me, and finally, my parents, Rafael and Shoshana, who invested their whole life in loving, caring and educating us, and to whom I dedicate this thesis.

Contents

List of Tables

List of Figures

Chapter 1

Introduction

The whole is greater than the sum of its parts

Ida P. Rolf

The use of antenna array systems may be one of the last remaining frontiers that promises to deliver substantial increase in capacity of wireless systems. Antenna arrays offer the ability to suppress interfering signals, to improve signal reception, and to increase data rate of transmisssion [1]. Over the last decade, the field of wireless communications has expanded explosively in terms of the number of portable devices around the globe, allowing ubiquitous communications by offering voice and data services in both indoor and outdoor environments. Advancements in RF circuit technologies and large-scale integrated processing platforms facilitate the implementation of sophisticated signal processing algorithms that improve the reliability and data rate of current wireless networks. Multimedia applications represent a challenging task for system designers in the 21st century, as they require broadening of the narrow and condensed wireless pipe. Sparked by recent information theoretic results on the multiple-input multiple-output (MIMO) channel[1] [2], a new class of codes, termed space-time codes (STC), has been shown to exploit the spatial and temporal characteristics of this channel, offering improvements in throughput and link reliability.

This chapter begins by presenting a brief overview of the history of personal wireless communications. Next, the importance of diversity in wireless system design is discussed. A comparison of coded modulation methods for single antenna systems in additive white Gaussian noise (AWGN) is offered as a reference for the results that will be presented in this dissertation for multi-antenna systems operating over fading channels. We discuss the tradeoffs between spectral and energy efficiency and give various examples for schemes that are well-suited for power-limited or bandwidth-limited channels. An overview of the active

[1]The MIMO channel corresponds to the use of multiple element arrays in both ends of the wireless link.

research area of STC and MIMO channels is presented, addressing some of the classical proposed schemes for multi-antenna systems. This chapter concludes with the purpose and outline of the dissertation.

1.1 Wireless Personal Communications

Wireless personal communications has developed significantly over the last two decades since the inception of its first generation analog mobile phones, through second generation digital wireless systems and up to current efforts towards implementation of third generation digital wireless networks. A common theme of this evolution has been the need for more capacity, which motivates the exploration of MIMO techniques in this thesis.

The concept of cellular mobile systems, which was originally proposed in 1968 by AT&T to the Federal Communications Commission (FCC) [3], was based on breaking each market into small geographic zones or "cells" that use a fraction of the total available radio spectrum. In each cell, a centralized base station manages the communications with each one of the users through a certain Common Air Interface (CAI). The CAI is based on a multiple access technique that shares the time, frequency or code resources among users.

The first U.S. cellular system was deployed in 1983 by Ameritech in Chicago, IL and known as the first generation Advanced Mobile Phone System (AMPS). The FCC allocated a total of 40 MHz of spectrum in the 800 MHz band to cover 666 full duplex channels. The AMPS system uses a 7-cell reuse pattern with options for sectoring and cell splitting [4]. AMPS is based on Frequency Division Multiple Access (FDMA) where each channel uses frequency modulation (FM) with maximum frequency deviation of ± 12 KHz. In order to increase capacity in AMPS markets, Motorola introduced the N-AMPS (narrowband AMPS), which provides three simultaneous users within a bandwidth of 30 KHz. This is achieved by using FDMA with 10 KHz channels and a decreased frequency deviation per channel, which results in a slightly reduced audio quality as compared to AMPS, altough N-AMPS never achieved widespread acceptance in the North America market.

Cellular phones have evolved from a product associated with connotations of wealth into a mass-market consumer product. By the late 1980's, it was clear that the first generation analog AMPS could not support the massive demand for wireless services. That was the impetus for the second generation cellular systems, which were all digital. The key advantage of digital communications over analog communications is its ability to provide higher spectral efficiencies, thus accommodating more users within a given spectrum allocation. This is achieved by the use of advanced source coding techniques along with channel coding that provides immunity to errors occured in the channel. In addition, digital communications

enables the multiplexing of various data types from different information sources.

In the early 1990's, the United States Digital Cellular System (USDC) was developed to support more users (as compared to AMPS) within a fixed spectrum. USDC is a Time-Division Multiple Access (TDMA) system which supports three full rate users or six-half rate users on each AMPS channel. Thus, USDC increases capacity by a factor of 6 as compared with analog AMPS. In 1990, the dual mode USDC/AMPS system was standardized as Interim Standard 54 (IS-54) or IS-136 by the Electronic Industries Association (EIA). The USDC system was designed to share the same frequencies, frequency reuse plan and base stations of AMPS, so that dual mode USDC base station equipment could support backwards compatibility. Because of this compatability with AMPS, USDC is also called D-AMPS (digital AMPS) and its control channels use exactly the same signaling format as AMPS. The voice channels however, employ $\pi/4$ DQPSK modulation with an aggregate data rate of 48.6 kbps. The channel coding includes a rate 1/2, constraint length 6 convolutional code and a 7 bit CRC error detection code.

The Pan European digital cellular standard, known as the GSM (Global System Mobile), was deployed in Europe in 1991. GSM is currently the world's most popular standard for cellular radio and personal communications. GSM services include voice, data and supplementary ISDN services. GSM uses frequency division duplexing (FDD) and a combination of 8 slots TDMA, with frequency hopping employed for frequency diversity in some markets. An aggregate Transmission rate of 270.83 kbps is achieved using a binary GMSK modulation with bandwidth to symbol duration product of 0.3 [3]. The effective transmission rate per user is 33.8 kbps where the end user data rate (after reduction of overheads, pilot symbols, etc.) is 24.7 kbps. GSM uses a convolutional code with rate 1/2 and constraint length 5, along with interleaving for the data channels. Since the channel bandwidth used by GSM networks is higher than the channel coherence bandwidth[2], the channel appears to be frequency selective. To mitigate the channel-induced Intersymbol Interference (ISI), GSM receivers apply a Viterbi equalizer that performs MLSE equalization prior to the decoding process.

Code Division Multiple Access (CDMA) was originally proposed by Qualcomm as a promising technique to enhance capacity significantly. A long debate across the wireless communications community with respect to capacity comparisons of AMPS, USDC, GSM and CDMA led to the development of different architectures and multiple standards. In the CDMA standard, known as Interim Standard IS-95, and later as cdmaOne, all users transmit simultaneously (same time and frequency), but each user is assigned with a unique

[2]Coherence bandwidth is defined as the range of frequencies in which the channel response appears to be "flat" (same gain and phase response) [5].

code that performs spreading of the original information spectrum. At the receiver, users can be separated from each other since they appear to be orthogonal or exhibit low cross-correlation. This is achieved by correlation processing of the signature code that extracts the desired user information sequence. Similar to IS-54, IS-95 system is designed to be compatible with the existing U.S. analog cellular systems (AMPS), such that mobile phones and base stations can be economically produced to support dual mode operation. In its original version, the maximum user data rate was 9.6 kbps, while in subsequent versions 13.4 kbps was used for voice. The chip rate (after spreading) is 1.2288 Mchips/s (spreading factor of 128) and the modulation process is different for the forward and reverse links. On the forward link, the user data stream is encoded using a rate 1/2 convolutional code, interleaving, and spreading using one of 64 orthogonal spreading sequences. The forward channel is assumed to be synchronous since the transmission from the base station to multiple users is performed simultaneously and is originated from a single location. In the reverse link, multiple users appear to be asynchronous at the base station since they are separated geographically in the service area and each signal travels a different path with different delay. In this link, the message is first encoded with a rate 1/3 convolutional code with interleaving. Following, groups of six coded bits are mapped into 64-ary orthogonal signaling (using Walsh functions) and a final 4-fold spreading is performed with a mobile-to-base station specific spreading code to achieve a chip rate of 1.288 Mchips/s.

In CDMA systems, tight power control is essential to reduce the "near-far" problem that arises from users with large difference in received power levels. Since CDMA utilizes wideband channels, the delayed echoes of the signal (multipath) are resolvable (delays are larger than the chip duration) and thus the channel exhibits time dispersion or frequency selectivity. Rather than mitigating this channel-induced ISI, Rake reception technology exploits the resolvable multipath by coherently combining their energy with distinct "finger" receivers, each of which is "tuned" to the delay of a single multipath component.

The fundamental goal of mobile communications in the 21st century is to provide multi-services to anyone, anywhere, anytime. In order to achieve that with a single wireless device, there is a need to consolidate the multiple standards into a single unified standard that will enable global roaming, high capacity and reliable wireless links for multiple services and applications (e.g., voice, data, video, etc.). Towards that end, the third generation mobile radio standard, originally termed the Future Public Land Mobile Telecommunications System (FPLMTS), and later renamed for brevity IMT-2000, for International Mobile Telecommunications by the year 2000, was presented by the International Telecommunications Union (ITU). The common technology for third generation is Wideband CDMA, which

is backward compatible with GSM networks [6]. In the U.S. however, cdma2000 standard was proposed to be backward compatible with USDC. The standard supports adaptive data rates and flexible operation with multiple services. Small cells are designed for low mobility type applications (e.g., cordless phones) while large cells will be used by high mobility users (e.g., vehicular communications). Support for many advanced technologies is incorporated into the standard including smart antennas, interference cancellation, transmit diversity and turbo coding.

As digital integrated circuit technology continues to evolve, additional advanced signal processing techniques are incorporated into the standards to offer higher data rates and more reliable wireless connectivity. In the same time, wireless systems are to operate reliably in diverse environments, such as indoor and outdoor; urban, suburban and rural; macro, micro and picocellular networks. These diverse wireless environments introduce variety of impairments to the transmitted signal, including multipath fading and Multiple Access Interference (MAI). The best remedy for these imperfections is to apply different forms of diversity, which is the topic of the next section.

1.2 The Role of Diversity in Wireless Systems

Compared with the Gaussian channel, Rayleigh fading introduces severe performance degradations to a digital communication receiver, measured in tens of decibels, in terms of the mean SNR required to achieve bit error probability within given specifications. Increasing the transmitter power or the size of antennas are not economically feasible approaches for combatting this problem. An alternative to increased power, is the use of special modulation and reception techniques which are less vulnerable to fading effects. One widely used example is multiple receive antenna combining techniques, categorized as spatial diversity techniques. Another example, is error correction codes with interleaving, which provide a form of time diversity. The terms "diversity advantage" or "diversity order" are used frequently in this dissertation, although they have no standard definition. By "diversity advantage", we refer to the negative power of SNR in the error rate expressions. That is, the asymptotic slope of the error rate curves when plotted vs. signal-to noise ratio in decibels. It is well known that the error rate of a binary digital communication system operating over a Rayleigh fading channel has inverse linear dependence on SNR (unlike the exponential waterfall dependency in the case of Gaussian channel). However, as we introduce a form of diversity to the system (by means of spatial, time or any other form of diversity) operating under fading conditions, the error rate curve is inversely proportional to the lth power of SNR, where l is the diversity order (e.g., l may be the number of antenna elements in

maximal ratio receive combining). The diversity principle is aimed towards reducing the probability of near zero fades, or "deep fades" as often termed. It is important to note that large scale fading, corresponding to movement of the terminal over large areas can not be compensated by the use of diversity mechanisms. This is due to the fact that all diversity channels are affected identically by the large scale fading. The goal is to compensate or mitigate small scale fading effects. The following various forms of diversity have been proposed in the literature.

- **Spatial Diversity -**

Spatial diversity is based on reception or transmission via multiple antenna elements along with appropriate signal processing that combines the signals from the various antennas. The effect of spatial diversity with multiple receive antenna elements was observed originally in 1927 during experiments with spatially separated receive antennas at High Frequency (HF) [7]. It was observed that with sufficient spacing between antennas, the fading fluctuations of the received signals are independent of one another. It was then demonstrated that appropriate switching between the two replicas of the received signal greatly reduces the probability of having a "deep fade". The concept of "switched diversity", known later as selection diversity, assumes that at each instant in time, the best signal is selected. Note that the term "instant" refers to the time constant in the order of the estimation process involved in the combiner, which should be shorter than the coherence time[3] of the channel. Extension of the selection diversity to linear combining yields the well known maximal-ratio combining (MRC) approach. This technique weights the signal received by each diversity branch according to the actual channel estimates in order to maximize SNR at the combiner output. MRC is known to be optimal in the SNR sense. Equal gain combining is a degenerated form of MRC in which equal weights are assigned to all diversity branches. It is suboptimal but simple to implement as it does not depend on channel estimation.

- **Frequency (Multipath) Diversity -**

In frequency selective channels[4], transmission of the signal in sufficiently spaced carrier frequencies allows reception of independently faded replicas of the signal, thus a form of frequency diversity. To obtain relatively high decorrelation, it is desirable to space the carriers an order of magnitude larger than the coherence bandwidth. The bandwidth of each carrier can be narrow enough such that fading is flat on each individual branch. The

[3]Coherence time is the duration of time in which the channel appears to be static.

[4]Also known as time dispersive channels

cost of frequency diversity lies in the increased bandwidth occupancy, the multiple transmitters and receivers per user and overall lower efficiency in usage of spectrum. Wideband communications (e.g., spread spectrum) exploits form of frequency diversity as the channel introduces resolvable multipaths that can be coherently combined using Rake receiver. From frequency domain perspective, the channel exhibits different responses for different frequencies. In the time, this translates to time dispersion or channel-induced ISI. In some texts, this form of diversity is referred to as multipath diversity.

- **Time Diversity -**

One common form of time diversity is acheived by employing error correction code with interleaving such that errors occurring in the channel are well separated compared with the reciprocal of the average fading rate. Since the fade levels associated with various repetitions of the information bit are essentially independent, an appropriate decoding of these repetitions provides a diversity effect. The use of error correction codes to achieve temporal diversity results in bandwidth expansion due to the transmission of redundant bits.

- **Polarization Diversity -**

Polarization diversity implies a single polarization at the transmitter, with depolarization in the propagation medium. The receiver is composed of two orthogonal polarizations such that the two resulting signals do not fade in a correlated manner. For practical applications, the diversity is limited to dual diversity as any third polarization is a linear combination of the other two and hence can not contribute to the diversity effectiveness.

- **Angle Diversity -**

Angle diversity requires antenna beamwidths that are narrow compared to the transmitted beamwidth, such that the two beams are oriented towards different portions of the transmitted signal, and thus the signals received via the multiple beams appear to be decorrelated.

To summarize, diversity techniques play a significant role in the design of wireless systems. Although it can take multiple forms (time, frequency, space, polarization, etc.), not all forms of diversity are possible at all times. For example, Rake reception is effective only if the channel is frequency selective such that multipath components are resolvable. Time diversity is not effective for delay-sensitive applications, operating in slow fading channels. In this dissertation, it will be shown that it is beneficial to combine different forms of diversity (spatial, temporal and also multipath diversity) in a joint design rather than employing

these techniques indpendently. The next section defines two key performance metrics, the spectral and energy efficiency, which are used in the performance evaluation of any digital communications system.

1.3 Comparison of Coded Modulation Methods

Most digital communication systems concatenate error correction codes and digital modulation techniques to transport information over the channel. The error correction code introduces redundant information to the bit stream, thus expanding the bandwidth to facilitate error recovery capability at the decoder. The modulation maps a sequence of binary digits into a set of corresponding signal waveforms. The binary digits are represented by the phase, frequency, amplitude (or combination) of the transmitted waveforms.

There are numerous ways to compare the performance of digital communication systems. For example, it is possible to determine the signal-to-noise-ratio (SNR) required to achieve a specific probability of error[5]. This energy efficiency measure, though important, would not result in a meaningful comparison, unless it is performed based on the same constraints of bandwidth or data rate of transmission. To that end, we shall also consider the spectral efficiency of the scheme, which corresponds to the data rate of the scheme per a fixed bandwidth use.

The bandwidth of the transmitted signal in a coded system is a function of the channel code rate, the number of bits per transmission interval (symbol duration) and the characteristics of the pulse shaping used. For a fixed channel bandwidth, increasing data rate is possible by expanding the signal set to a larger alphabet (e.g., MPSK, QAM), such that each symbol carries more bits per transmission interval. This operation increases bandwidth efficiency[6] at the expense of energy efficiency since the Euclidean distance between constellation points is reduced (assuming constant transmitted power). On the other hand, reducing the code rate results in an enhanced error correction capability at the expense of increased bandwidth.

Coded digital communication systems were originally designed by independently specifying the encoder/decoder and the modulator/demodulator. It was in 1974, when J.L. Massey suggested that a joint design of these entities may result in superior performance. To quote Massey in [8]: "Sometimes the communication engineer presumes that the purpose of coding is to correct errors made by the demodulator. He somehow believes that if the error probability is unacceptably large, then coding should be able to rescue his design and

[5]Usually termed the energy efficiency of the scheme.

[6]The terms spectral efficiency and bandwidth efficiency are used interchangeably in this text.

he is inevitably disappointed to learn that the necessary code redundancy is so large that his overall system is quite inefficient."

An example for a joint coded modulation scheme that strives to improve its energy efficiency without sacrificing bandwidth efficiency was proposed in 1982 by Ungerboeck [9]. In his scheme, known as trellis coded modulation (TCM), the redundant bits necessary for coding come from expansion of the signal set. The design of a trellis code is based on the set partitioning approach [10], which groups signals into subsets with large Euclidean distance. In this way, TCM achieves considerable coding gains over conventional uncoded multilevel modulation without compromising bandwidth.

When comparing the performance of various coded systems, it is desired to capture both the spectral and energy efficiencies of these schemes. A compact and meaningful comparison is to plot the normalized data rate, denoted R/W (in bits per second per hertz of bandwidth) versus the SNR per bit, denoted E_b/N_0 (in decibels). The right upper part of such a two-dimensional space corresponds to schemes that achieve high spectral efficiency but poor energy efficiency. These schemes may be suited for channels that are strictly band-limited but are not particularly constraint by power (e.g., microwave links, where power is cheap, but available bandwidth is restricted by regulation). On the contrary, the left lower part of the bandwidth-energy space corresponds to schemes that achieve good energy efficiency with poor spectral efficiency. These schemes may be suited for power-limited channels that have no strict constraints on bandwidth (e.g., deep-space communications where power is expensive to generate[7] and transmission distances are enormous). Figure 1.1 illustrates such a plot for few coded and uncoded schemes at a fixed symbol error probability of 10^{-5}. Results for uncoded M-ary Phase Shift Keying (MPSK), coded Binary Phase Shift Keying (BPSK), uncoded Quadrature Amplitude Modulation (QAM), TCM with MPSK and TCM with M-ary Amplitude Shift Keying (MASK) are included. The curve labeled "Shannon Capacity Bound" is the theoretical maximum normalized data rate where reliable communications can be achieved over band-limited AWGN channels [11].

We observe that for uncoded MPSK and QAM, increasing M results in a higher normalized data rate at the cost of an increased SNR per bit. In particular, it is shown that uncoded 64 and 16 QAM schemes require SNRs of 19 and 14.5 dB, respectively, to deliver 6 and 4 [bps/Hz] at symbol error probability of 10^{-5}. While both 16 QAM and 16 PSK modulation schemes carry 4 [bps/Hz] of spectral efficiency, the energy efficiency of QAM is better than PSK by nearly 4 dB. When BPSK is used without any correction code, $E_b/N_0 = 9.6$ dB is required to achieve $P_b = 10^{-5}$. Note that QPSK doubles the spectral efficiency of

[7] $1 Million per dB has been a rule of thumb

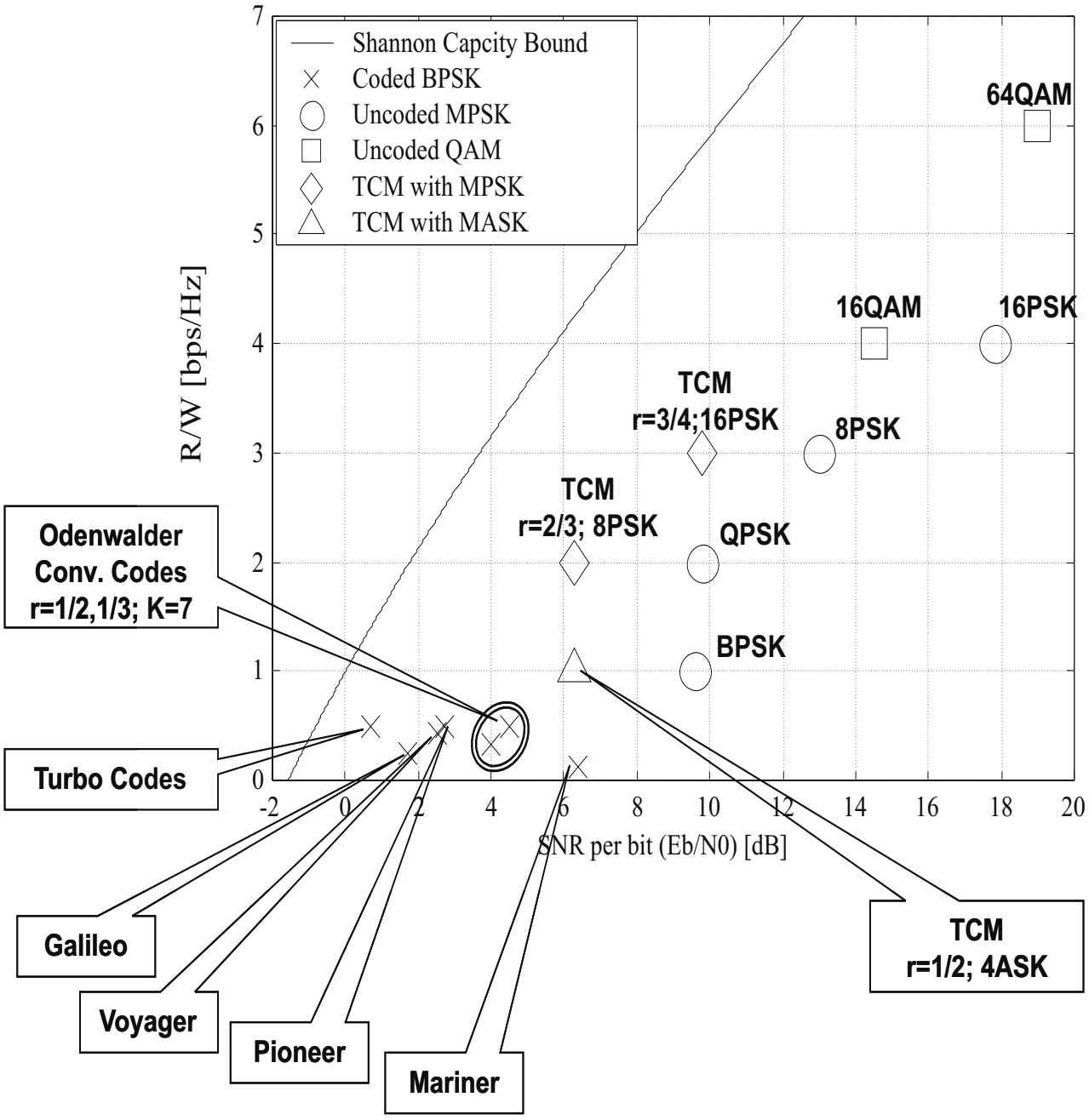

Figure 1.1: Comparison of several coded modulation methods for single antenna systems in AWGN at 10^{-5} symbol error probability

BPSK without affecting the energy efficiency, since it is composed of two orthogonal BPSK signal sets.

Coded BPSK schemes are shown to achieve good energy efficiency results and are intended mainly for power-limited channels. The savings in E_b/N_0 due to coding is termed the coding gain of the scheme. In 1969, the first operational code was employed into the Mariner mission to Mars. This was the $(32, 6)$ Reed-Muller code with code rate of $1/8$ that achieves coding gain of 3.2 dB. In Pioneer missions, the rate $1/2$ constraint length 32 convolutional code provided 6.9 dB of coding gain. Other coded schemes include the Odenwalder convolutional codes with constraint length 7 and rates $1/2$ and $1/3$, which achieve coding gains of 5.1 and 5.4 dB, respectively. These codes have been adopted by numerous satellite communication systems. The communication link for the Voyager missions was based on a serial concatenation of the rate $1/2$ Odenwalder code and a Reed Solomon outer error correction code [12], providing coding gain of 7.1 dB at a composite code rate of 0.44. The Galileo mission to Jupiter used a coded system with rate $1/4$, constraint length 15 convolutional code that achieves 7.9 dB coding gain [13]. An important advancement in coding theory was introduced in 1993 by a group of researchers from France [14], who termed their new class of codes as "turbo" codes. These codes, which are based on parallel concatenation of two or more component codes, nonuniform interleaving, and iterative decoding algorithms, were shown to close the gap between practical coding systems and Shannon's theoretical limit. For these codes, E_b/N_0 of only 0.7 dB is required to achieve bit-error rate of 10^{-5}.

Figure 1.1 also includes results for a few TCM schemes. It is shown that the rate $2/3$ TCM with 8 PSK (jointly designed coded modulation scheme) outperforms uncoded QPSK by 3 dB, keeping the same spectral efficiency (2 [bps/Hz]). A similar trend is shown for 3 [bps/Hz] schemes as the rate $3/4$ TCM paired with 16 PSK outperforms uncoded 8 PSK.

We emphasize that the results presented in Figure 1.1 are for AWGN channels only. In wireless channels, in addition to thermal noise, the receiver has to cope with multipath fading, multiple access interference (MAI) and other external interfering sources. In the same time, wireless systems must be both power and bandwidth efficient since power is costly (impacts battery life and size) and bandwidth is also limited (e.g., regulation, cost). An effective coded-modulation technique for wireless channels has been proposed recently as space-time coding, where the spatial (antenna) dimension is incorporated into the process of signaling design, introducing both spatial and temporal forms of diversity to improve the spectral and energy efficiency of the system. Space-time codes have attracted huge attention from the communications community in the recent five years, for their holistic approach to

system design, combining the error correction code, modulation scheme and array processing principles into a single design problem. Following the inventions of TCM by Ungerboeck in 1982 and Turbo Codes by Berrou, Glavieux and Thitimajshima in 1993, STC extend the notion of looking at traditionally separated entities such as modulator/demodulator, encoder/decoder and transmit/receive diversity as a combined entity. In the next section, an overview of this class of codes, which employs multi-transmit multi-receive antenna arrays is provided, describing the rich active research area of multi-antenna systems for high data rate wireless communications.

1.4 Space-Time Coding and MIMO Channels: An Overview

With the integration of Internet and multimedia applications in next generation wireless communications, the demand for reliable high data rate services is rapidly growing. The Multiple-Input Multiple-Output (MIMO) channel model in wireless communications corresponds to the use of multiple element arrays in both ends of the wireless link [2]. Space-time coding exploits the diversity provided by the MIMO channel in both space (antenna) and time domains, thus significantly increasing the system capacity as well as improving the reliability of the wireless link.

Current cellular systems use antenna diversity at the base station for improving the reception and the capacity of the uplink channel. However, it becomes apparent that the weak link is the downlink channel. Furthermore, as data type services (e.g., downstream Internet) continue to evolve, the requirements for throughput in a cellular system are asymmetrical. In data applications, users frequently access the wireless network with relatively short messaging requesting large amounts of data to be sent. This leads to the question of how to broaden the band-limited wireless pipe for the downlink channel. In many applications, antenna receive diversity at the mobile handset is not a feasible option due to limitations on the simplicity, size and cost of the handset. Moreover, implementation of multiple antenna elements at the handset is often difficult, resulting in non-equal gain and correlated channels, which lead to ineffective diversity mechanisms. This has motivated researchers and wireless designers to propose solutions in the form of transmit diversity where multiple antenna elements (possibly the same physical elements used for reception) are used in conjuction with appropriate signal processing at the receiver to achieve higher spectral efficiency, diversity advantage and possibly coding gain.

Information theoretic aspects of transmit diversity were addressed by Foschini and Gans [2], Teletar [15], Marzetta [16], and Narula, Trott and Wornell in [17]. In this work, the capacity of MIMO channels as compared with the Shannon capacity for Single-Input Single

Output (SISO) channels was investigated. It was shown in [2] that the capacity grows at least linearly with the number of transmit antennas as long as the number of receive antennas is greater than or equal to the number of transmit antennas. This framework has led to the development of many transmit-receive diversity architectures, space-time codes and advanced signal processing techniques - all aiming to exploit the unprecedented capacity offered by the MIMO channel. Major approaches that exploit the capabilities of MIMO channels are:

- Bell Labs Layered Space-Time Architecture, proposed by Foschini et al. [2].
- Space-Time Trellis Codes (STTC), proposed by Tarokh et al. [18].
- Space-Time Block Codes (STBC), proposed by Alamouti [19].

The BLAST test bed system (with 8 or 16 antenna elements at each side of the wireless link) was the first prototype to prove the significant capacity enhancements of wireless systems in indoor environments. In BLAST, the receiver applies multi-user detection techniques preceded by a sorting algorithm in order to decouple successively the sub-channels arriving from different transmit antennas. The BLAST transmitter does not introduce any orthogonality across multiple transmit antennas. The propagation environment itself, which is assumed to exhibit significant multipath, is exploited to separate the signals at the receiver. To quote the BLAST designers: "BLAST exploits multipath rather than mitigates it" or "the more multipath the better the performance of BLAST is". It was demonstrated that over "rich-scattering" indoor environments, the BLAST system achieves a throughput of 621 Kbps over a narrowband channel of 30 KHz. Thus, unprecedented spectral efficiency is achieved. It has been shown that the main problem of BLAST is its poor energy efficiency [20], requiring very high SNR to guarantee acceptable level of error probability.

Space-time trellis coding (STTC) [18, 21, 22, 23, 24, 25, 26, 27, 28] is a class of signaling techniques that combines the design of the channel code with transmit and optionally receive antenna diversity. Coding theory suggests [2, 29] that in the context of random channels, even if there is not any a-priori channel state information (CSI) at the transmitter, a single channel code can cope well with a broad range of channel realizations. In this context, the term outage probability is used to describe the extent of channel realizations in which the code performs well. The transmit diversity advantage offered by STTC is equivalent to receiver antenna diversity with optimal combining (MRC). In addition to the diversity advantage, a certain amount of coding gain can be achieved by a well-constructed STTC.

Code design criteria for STTC were derived in [18, 30] based upon upper bounds on the pair-wise error probability. The two design criteria are the rank criterion, corresponding

to maximization of diversity advantage and the determinant criterion, corresponding to maximization of coding gain.

In analogue to Multiple Trellis-Coded Modulation (MTCM), a STTC has multiple symbols associated with a single trellis transition. However, in STTC signaling, the multiple symbols are transmitted over space (antenna) domain rather than over time domain. Therefore, assuming the same alphabet is used, the spectral efficiency of STTC is n_T times higher than the corresponding spectral efficiency of MTCM, where n_T corresponds to the number of antenna elements at the transmitter.

The STTC creates inter-relations between signals transmitted over the space domain (different transmit antennas) and signals transmitted over time domain (consecutive time symbols). The encoder is composed of n_T different generator polynomials that determine the simultaneously transmitted symbols. The receiver is based upon estimation of the channel fade coefficients followed by a Maximum Likelihood Sequence Estimation (MLSE) decoder, which determines the lowest accumulated Euclidean distance metric to extract the most likely transmitted sequence.

In hope of reducing the exponential decoder complexity of STTC, Alamouti proposed a simple transmit diversity scheme [19], which was later expanded by Tarokh et al. [27] for an arbitrary number of array elements to form the class of Space-Time Block Codes (STBC). These codes achieve the same diversity advantage of Maximal Ratio Receive Combining (MRRC). STBC are defined by a mapping operation of a block of input symbols into space and time domains, creating orthogonal sequences that are transmitted from different transmit antennas. The receiver is composed of channel estimation, a combining procedure (in both time and space) and a maximum likelihood (ML) symbol-by symbol detection rule. The STBC decoder has a remarkably simple structure and yet achieves the same diversity advantage as that of MRRC. Note that there is no memory between consecutive blocks and the typical block length is very short. Thus, a very limited coding gain is expected. Also, the low decoder complexity lends itself naturally to concatenation with a powerful outer error correction code [31]. In order to relax the requirement for instantaneous channel estimation at the receiver, a differential space-time block coding (D-STBC) technique was proposed in [28]. The performance of D-STBC is inferior to the performance of coherent STBC (C-STBC) by 3 dB under ideal conditions but is much more robust to frequency and phase errors and does not rely on instantaneous tracking of channel state information.

The development of space-time coding and MIMO channels uses a new paradigm for combining the benefits of coded-modulation with full diversity gains over wireless links. If this technology is to be incorporated in next generation wireless systems many issues need

to be investigated. Active research areas include: performance evaluation over correlated fading paths, performance evaluation over flat and frequency selective channels in conjunction with channel estimation techniques, characterization of space-time channel vector models, performance in the presence of MAI, hybrid space-time coding with beamforming and implementation issues on reconfigurable hardware and DSP platforms. Also, possible integrations of STC schemes with other known techniques such as: turbo codes and iterative decoding [31], multi-user interference rejection [32] and OFDM [22] are under intensive investigation. In the next section, the purpose and outline of this dissertation is presented, emphasizing original contributions to the area of space-time coding.

1.5 Purpose and Overview of Thesis

The purpose of this thesis is threefold. First, it intends to provide analytic tools that determine the fundamental limits on the performance of space-time codes in a variety of channel conditions. This analysis facilitates rapid calculation of error rate curves, leading to insights into the behavior of the schemes in various environments (e.g., Rayleigh, Rician, AWGN, correlated channels, etc.), and into parameter optimization in code design. Second, it examines the practical implications of incorporating these schemes onto current wireless systems by implementing a multi-transmit multi-receive antenna laboratory test bed, known as the Virginia Tech Space-Time Advanced Radio (VT-STAR). This architecture allows for characterization of the MIMO channel and validation of various space-time approaches. Third, it proposes novel techniques that combine concepts drawn from space-time code design, iterative processing and multiuser detection techniques in order to improve both the energy and spectral efficiency of multi-antenna systems operating over flat and frequency selective fading channels.

In the introductory part of this thesis, the fundamentals of STC and MIMO channels are presented. Chapter 2 presents capacity analysis and outage probability results for MIMO flat and frequency selective channels. These information theoretic results, originally derived by Foschini and Gans in [2] and El Gamal et al. in [33], have sparked the search for efficient space-time codes that exploit portion of the theoretical capacity growth. Chapter 3 introduces fundamental concepts of space-time architectures such as code design criteria, performance analysis and decoder complexity for both trellis and block-type STC. The architecture of the Bell-Labs Space-Time Layered system is also described, demonstrating huge enhancement of throughput via the use of multiple antenna elements at both ends of the wireless link.

Original performance analyses for both STTC and STBC are presented in Chapters 4 and 5, respectively. Chapter 4 includes a derivation of analytical performance results for the bit-error probability of STTC, operating over Rayleigh, Rician and correlated flat fading channels. In the uncorrelated case, the concept of Generating Function Techniques (G.F.T) is applied to upper bound the bit-error probability of the scheme. In the correlated case, bit-error probability approximations are derived by determining an upper bound on the pair-wise error probability of short error events. These analytic results are shown to be a function of the number of antenna elements in both ends of the link, the signal-to-noise ratio, the eigenvalues of a certain code distance matrix and the covariance matrix of the fade coefficients. Bit-error probability is found to be inversely proportional to the lth power of E_b/N_0 in Rayleigh fading environments, where l corresponds to the diversity advantage of the scheme. For the Rician case, as the channel tends towards AWGN (dominant Line-of-Sight component), bit-error probability decreases exponentially with E_b/N_0. Both analytic and simulation results indicate that even when high correlation across transmit antenna elements exists, the diversity advantage offered by the STTC is maintained. Since these analytic results are found to be tight to the simulated performance, these tools may be used (in conjunction with Monte Carlo simulation techniques) to verify the performance of many proposed codes operating over a variety of channel conditions.

Chapter 5 introduces performance analysis of Space-Time Block Coding, based on the probability density function of the effective signal-to-noise ratio at the space-time combiner output. This framework supports various complex orthogonal designs operating with M-ary PSK modulation and practical array configurations over independent or correlated flat Rayleigh fading channels. Using the analytic results, we study the benefits associated with employing more than two antenna elements at the transmitter and quantify the robustness of the scheme to spatial correlation. Monte Carlo simulation results are presented for STBC schemes in a variety of configurations. This includes schemes paired with QAM signaling format for high spectral efficiency applications, schemes concatenated with an outer error correction code (e.g., TCM) for improved energy efficiency (without sacrificing spectral efficiency) and schemes operating with imperfect channel estimation and carrier recovery mismatch. It is shown that differential STBC (D-STBC) does not rely on channel estimation, has relaxed requirements on the accuracy of the carrier recovery mechanism and achieves the same diversity advantage as coherent STBC.

Based on the D-STBC approach, the Virginia Tech Space-Time Advanced Radio (VT-STAR) is designed, introducing a 2×2 antenna element array architecture, which allows exploitation of transmit and receive diversity mechanisms at the signal processing level. The

VT-STAR design, described in Chapter 6, includes DSP implementation, Radio Frequency (RF) section, multi-channel data conversion design and system level design. Based on software defined radio (SDR) concepts, the test bed supports two modes of operation: a real-time mode for testing the interactions of practical algorithms (e.g., timing recovery, channel estimation, automatic gain control) with space-time demodulation and a measurement tool for the characterization of the MIMO channel. Representative results for the capacity of a narrowband MIMO channel, measured in our indoor laboratory settings are provided and compared with theoretical bounds.

In the remainder of this dissertation, we propose novel techniques for iterative ("turbo"-like) processing paired with space-time coding, including iterative equalization/decoding scheme for high delay spread environments and iterative interference cancellation/decoding schemes for Bell Labs Layered Space-Time Architecture (BLAST). Since frequency selective fading channels introduce severe performance degradations to all of these schemes, we consider in Chapter 7 a concatenation of equalization and decoding techniques. The scheme is based on an iterative processing of two Aposteriori Probability (APP) algorithms separated by block interleaving/deinterleaving, aiming to compensate the channel induced ISI of high delay spread environments. Performance results indicate that the scheme does not only compensate for the channel-induced ISI, rather, it exploits multipath diversity by gathering energy from all channel tap coefficients. The improvement introduced by the scheme relies on sharing soft information between the two stages in an iterative manner.

In Chapter 8, iterative processing is applied to BLAST receivers in order to reduce the error propagation problem, which is found to be the dominant reason for their poor energy efficiency. Two candidate schemes that support successive and parallel interference cancellation (SIC and PIC) BLAST detectors are proposed. Both schemes rely on introducing channel coding with appropriate interleaving over the layers. In the SIC case, since the reliability of previously detected layers is crucial to the diversity advantage of successive layers, we place a more powerful code over the layer to be detected first. This unequal error protection facilitates an increased level of diversity with minimum penalty in spectral efficiency. For PIC BLAST detectors, a constant rate channel code is placed over each layer and iterative parallel interference cancellation decoding is incorporated at the receiver. Upon completion of the fourth iteration, almost error-free decisions are fed into the interfere cancellation unit, thus offering maximum diversity level to all detected layers.

Similar to the comparison of coded modulation schemes for single antenna systems operating in AWGN, Chapter 9 concludes the dissertation with a unified comparison of various multi-antenna systems operating in fading channels, using a metric that encapsulates

both the spectral and energy efficiency of the scheme. Observing the benefits associated with joint rather than segregated design in the physical layer of a digital communications system (e.g. TCM, STC), the interactions between functions, executed in multiple layers of the wireless network (e.g., PHY and MAC), may be a research topic whose time has come. As an example, Chapter 9 explores the interactions between scheduling algorithms, performed at the MAC layer of the network, and space-time architectures, employed at the PHY layer of the system. Results indicate that these modules should not be designed independently since the scheduling algorithm gives rise to a multiuser diversity process, which affects the performance of the space-time architecture and the overall system.

Finally, Chapter 10 summarizes the dissertation and provides suggestions for extension of the work.

Chapter 2

The Multiple Input Multiple Output (MIMO) Channel

This chapter presents information theoretic results that demonstrate the potential for an enormous growth in the capacity of wireless systems through the use of Multiple Element Array (MEA) technology [2, 33]. These results have motivated the search for practical structures and schemes that achieve a portion of this theoretical capacity growth. For a given channel bandwidth and total transmitted power, we explore the capacity of various antenna array architectures in flat and frequency selective fading MIMO channels. In particular, the capacity of the MIMO channel is compared with the capacity of receive diversity, transmit diversity, single antenna systems and the Shannon capacity for band-limited Gaussian channels. Since capacity is a function of the channel realization, which is modeled by a set of complex Gaussian random variables, its cumulative distribution function (CDF) and outage probability are evaluated. Outage probability represents the probability that the capacity does not exceed a given threshold.

A general block diagram for a MIMO channel system is given in Figure 2.1.

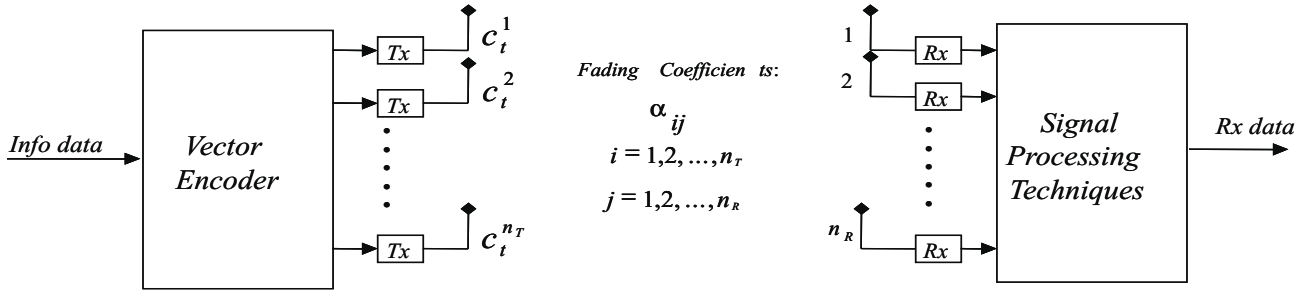

Figure 2.1: MIMO channel model

2.1 Flat Fading MIMO Channel

The MIMO flat fading channel is modeled by a channel matrix H, in which its $ijth$ entry represents the complex fade coefficient from transmit antenna $i, i = [1, 2, \cdots, n_T]$ to receive antenna $j, j = [1, 2, \cdots, n_R]$, where n_T and n_R correspond to the number of antenna elements at the transmitter and at the receiver, respectively. In the analysis that follows, α_{ij} are assumed to be independent identically distributed (i.i.d) zero mean complex Gaussian random variables with variance 0.5 per dimension.

The channel is assumed to be slow (compared to the system baud rate), flat (no channel-induced ISI) with decorrelation across fade coefficients associated with multiple antenna elements. It is assumed that the environment is composed of a large number of scatterers such that the fade coefficients are Rayleigh distributed. These idealized channel conditions may represent the class of indoor channels with fixed terminals that might be part of a WLAN network. The channel is assumed to be quasi-static[1] such that its time coherence is larger than the duration of a symbol. It is also assumed that no feedback link is present and thus CSI is available only at the receiver. The total power is thus distributed uniformly across multiple transmit antenna elements. This assures that the SNR per receive branch is not a function of the number of transmit antenna elements and comparison with various antenna configurations (i.e., single transmit antenna systems) is meaningful.

A key result for the capacity of MIMO channels was obtained originally by Foschini and Gans in [2]. Assuming that the transmitted signal vector is composed of n_T statistically independent spatially separated equal power components each with a Gaussian distribution, the capacity is described by (see [2])

$$C = log_2 det \left[I_{n_R} + (SNR/n_T) H^{\dagger} H \right]. \tag{2.1}$$

where $H^{\dagger}$ corresponds to the transpose conjugate of H, and SNR is the signal-to-noise ratio at the jth receive branch. I_{n_R} is an $n_R \times n_R$ identity matrix. In order to get insight into the meaning of the above result, we apply it to few special cases.

• Case I: Single-Input Single-Output (SISO) Channel

In this case, a single antenna element is used at each side of the wireless link and thus H is a complex scalar.

$$C = log_2(1 + SNR\,|H|^2), \tag{2.2}$$

where $|H|^2$ is the normalized channel power characteristic. In the AWGN channel, $H = 1$,

[1] Quasi-static means that the fading coefficients are constant over a frame length (or block length) of l symbols and are changed independently between consecutive frames or blocks.

and thus we get the well known Shannon capacity formula [11] for SISO channel. Note that in this case, an increase of 3 dB in SNR results in additional 1 bit/cycle in capacity.

• Case IIa: Single-Input Multiple-Output ; Optimal Combining (SIMO-OC)

The SIMO-OC channel corresponds to receive diversity with optimal combining (maximal ratio combining). In optimal combining, the receiver employs linear combining with the channel fade coefficients as weights in order to maximize the SNR at the output of the combining stage. That is, while the signal components are coherently combined, the noise terms are not added coherently (noise terms across multiple receive elements are independent). Thus, the capacity of a Single-Input Multiple-Output (SIMO) channel with optimal combining at the receiver is described by:

$$C = log_2 \left[1 + SNR \sum_{j=1}^{n_R} |H_j|^2 \right]. \tag{2.3}$$

By applying appropriate weights at the receiver, H_j terms are summed coherently and thus the effective SNR is maximized.

• Case IIb: Single-Input Multiple-Output ; Selection Diversity (SIMO-SD)

The SIMO-SD channel corresponds to receive diversity with selection diversity mechanism, such that the best branch is selected instantaneously out of n_R possible branches. Although selection diversity is inferior to maximal ratio combining in terms of performance, its complexity is lower since it does not require detailed knowledge of the channel fade coefficients. The capacity of the SIMO channel with selection diversity at the receiver is described by:

$$C = max_m log_2 \left[1 + SNR\,|H_m|^2 \right] = log_2 \left[1 + SNR(max_m\,|H_m|^2) \right], \tag{2.4}$$

where $m \in \{1, \cdots, n_R\}$.

• Case III: Multiple-Input Single-Output (MISO) Channel

The MISO channel corresponds to transmit diversity. By applying n_T transmit antennas and a single receive antenna to Eq. (2.1), we get

$$C = log_2 \left[1 + (SNR/n_T) \sum_{i=1}^{n_T} |H_i|^2 \right]. \tag{2.5}$$

Note that it is assumed that the total radiated power is divided uniformly over n_T transmit elements, such that the average SNR at the receiver is not a function of the number of elements at the transmitter.

• Case IV: Multiple-Input Multiple-Output (MIMO) Uncoupled Channel

Let us assume $n = n_T = n_R$ elements, the MIMO uncoupled channel corresponds to the artificial case of n parallel pipes (channels), each of which has line-of-sight between transmit antenna element i and receive antenna element $j = i$. That is, the channel matrix is the diagonal identity matrix, $H = I_n$. Plugging this into the capacity formula of Eq. (2.1), we get:

$$C = nlog_2(1 + (SNR/n)) \ \rightarrow \ SNR/ln(2) \ as \ n \rightarrow \infty. \tag{2.6}$$

Note that capacity increases linearly with the number of antenna elements. Also, asymptotically (large number of antenna elements) capacity scales linearly with SNR, rather than logarithmically. The parallelism of the channel assumed here is not realistic as these multi-dimensional channels are coupled and subject to fading. In fact, for large array size (more than 4 antenna elements), the full MIMO channel outperforms the uncoupled case, as some of the cross channels enhance capacity further. However, with this artificial model, we can observe that capacity reflects an approximately n-fold increase over Shannon's capacity for SISO AWGN channel with a power penalty due to the distribution of power across transmit antenna elements.

In order to illustrate the above results, we turn to computer simulation. Since capacity is a function of the channel matrix , it is treated as a random variable. Complementary Cumulative Distribution Functions (CCDFs) are computed for this random variable for various antenna configurations. We randomly generate sufficient statistics of channel realizations in a Monte Carlo manner in order to evaluate capacity CCDFs. Capacity is measured in terms of outage probability, which represents the percentage of channels in which the capacity does not exceed a given threshold. Outage probability indicates the confidence level of the result stated. For example, outage probability of 1% denotes a confidence level of 99%, meaning that 99% of channel realizations allow capacity that is greater or equal a given threshold. Only 1% of channel realizations will not meet the specified capacity result. Capacity results are presented as a function of the signal-to-noise ratio for a given outage probability. Figures 2.2, 2.3 depict the complementary CDF of the capacity for received SNR of 20 dB in the cases of $(n_T, n_R) = (2, 2)$ and $(n_T, n_R) = (4, 4)$, respectively. Each Figure presents a comparison of the CCDF for the single-input single-output (SISO) capacity expression given in Eq. (2.2), the single-input multiple-output (SIMO) capacity expression given in Equations (2.3) and (2.4) for optimal combining (OC) and selection diversity (SD), respectively, the multiple-input single-output (MISO) capacity expression given in Eq. (2.5) and the multiple-input multiple-output (MIMO) capacity expression given in Eq. (2.1).

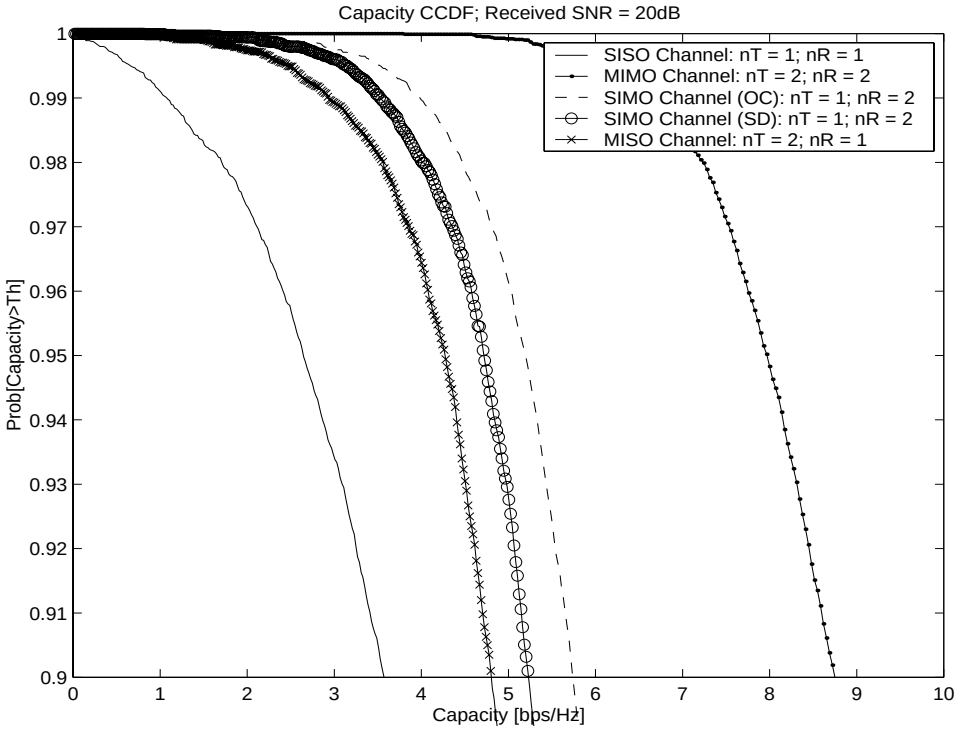

Figure 2.2: MIMO channel - complementary CDF for $(n_T, n_R) = (2, 2)$

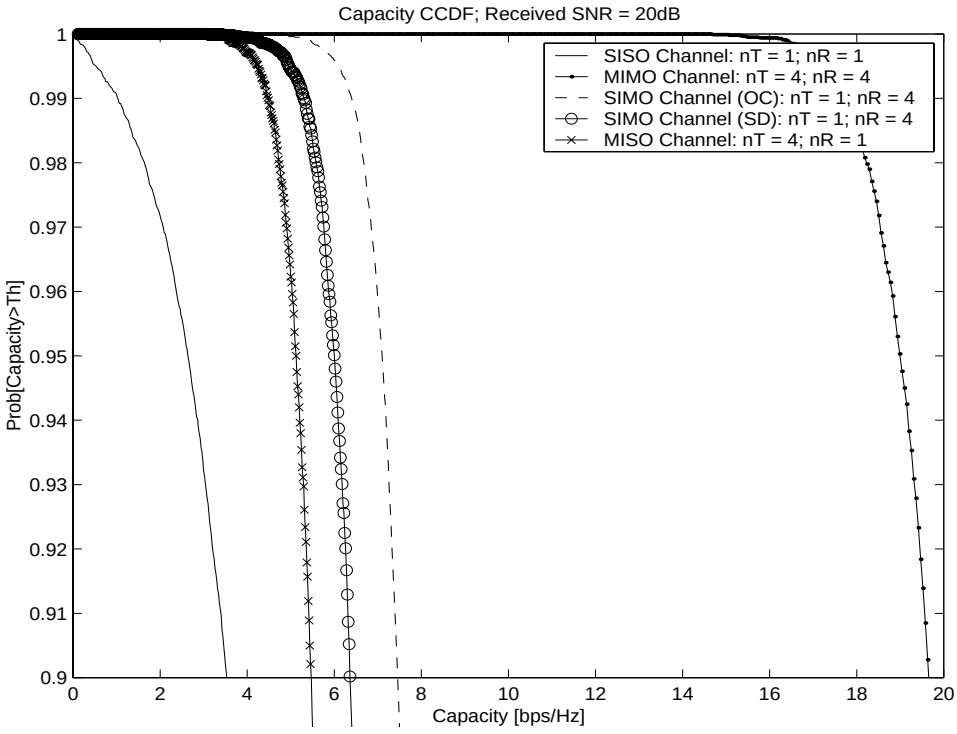

Figure 2.3: MIMO channel - complementary CDF for $(n_T, n_R) = (4, 4)$

It is observed that the MIMO channel capacity outperforms all other configurations and boosts capacity significantly. Also, it is observed that the capacity of the transmit diversity only (MISO channel) is inferior to capacity obtained by receive diversity (SIMO channel). This is due to the fact that the total radiated power is kept the same (P watts) regardless of the number of elements at the transmitter, and thus transmit diversity, unlike receive diversity, does not achieve antenna aperture gain. Also, capacity of optimal receive diversity (SIMO-OC) outperforms the capacity provided by receive diversity selection (SIMO-SD). We observe that an enhancement of the signal-to-noise ratio by diversity techniques translates into capacity enhancements. It is shown that for outage probability of 5%, the capacity of the 2×2 MIMO channel is 7.9 [bps/Hz] while the capacity of the SISO channels for the same outage probability is 2.7 [bps/Hz], which corresponds to nearly 3-fold capacity increase. For the 4×4 MIMO channel, $P_{outage} = 5\%$ yields capacity of 19 [bps/Hz] as compared with 2.7 [bps/Hz] of the SISO channel, 7.1 [bps/Hz] of the SIMO-OC channel and 5.0 [bps/Hz] of the MISO channel.

Next, we fix the outage probability to $10\%, 5\%, 1\%$ and present capacities of the SISO, MISO, SIMO-OC and MIMO channels as a function of signal-to-noise ratio. These are given in Figures 2.4, 2.5 for the cases of $(n_T, n_R) = (2, 2)$ and $(n_T, n_R) = (4, 4)$, respectively.

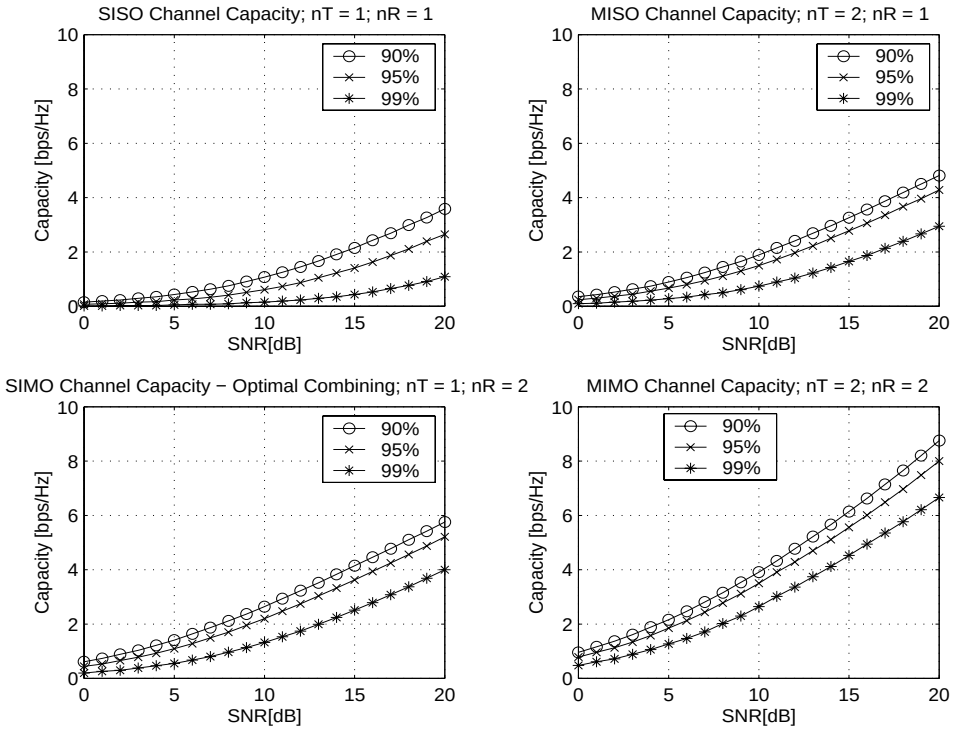

Figure 2.4: MIMO capacity as a function of SNR for $(n_T, n_R) = (2, 2)$

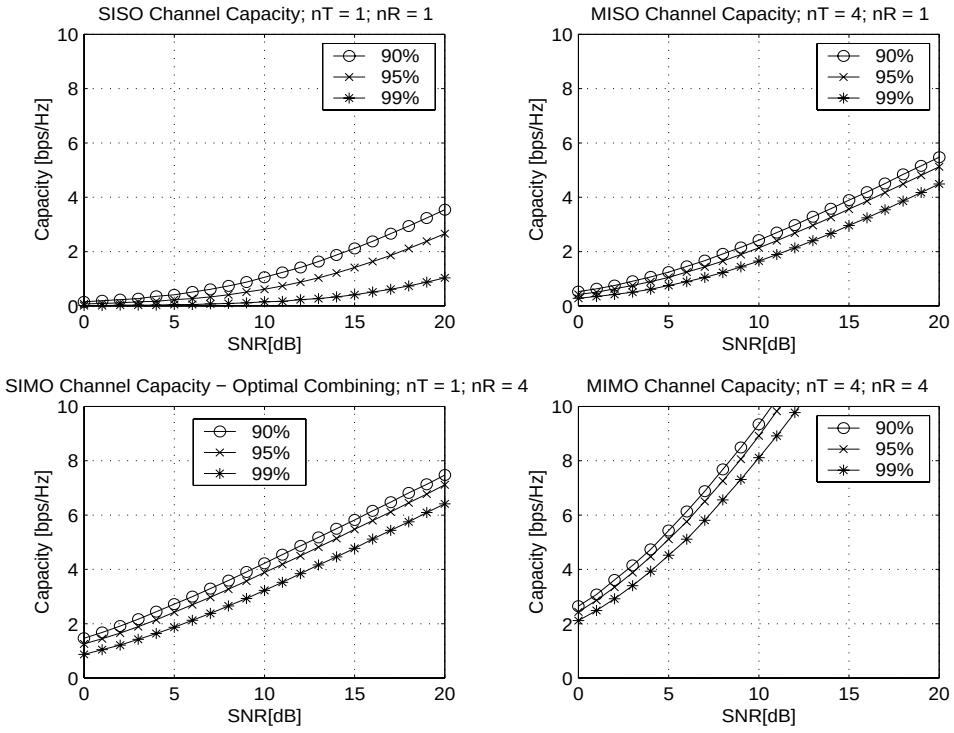

Figure 2.5: MIMO capacity as a function of SNR for $(n_T, n_R) = (4, 4)$

The legend in these figures represents the confidence level (complementary of outage probability). For example, 99% corresponds to an outage probability of 1%, which means that only 1% of channel realizations will have capacity that does not exceed a given abscissa. The MIMO channel capacity significantly outperforms all other configurations. For example, in SNR of 15 dB and outage probability of 1%, the capacity offered by the $(n_T, n_R) = (4, 4)$ MIMO channel is 8 [bps/Hz] where in the same conditions the SISO channel provides less than 1 [bps/Hz]. Thus, almost an order of magnitude in capacity growth is observed.

Figures 2.6, 2.7 compare capacities for outage probability of 1%. Here, we also include the classical Shannon capacity formula for AWGN ($C_{AWGN} = log_2(1 + SNR)$). We observe that the MIMO channel capacity in flat Rayleigh fading channels outperforms the AWGN capacity for the case of $(n_T, n_R) = (4, 4)$ antenna array configuration. Furthermore, we observe that receive diversity with optimal combining (SIMO-OC) converts the SIMO Rayleigh fading channel into a SISO AWGN channel.

Finally, we present results for the transmit diversity case (MISO channel capacity). Assuming a limited number of antenna elements at the receiver, the underlying question is whether it is beneficial to add more and more antenna elements at the transmitter. Figure 2.8 demonstrates that for a single receive antenna systems, adding more than 4 elements to

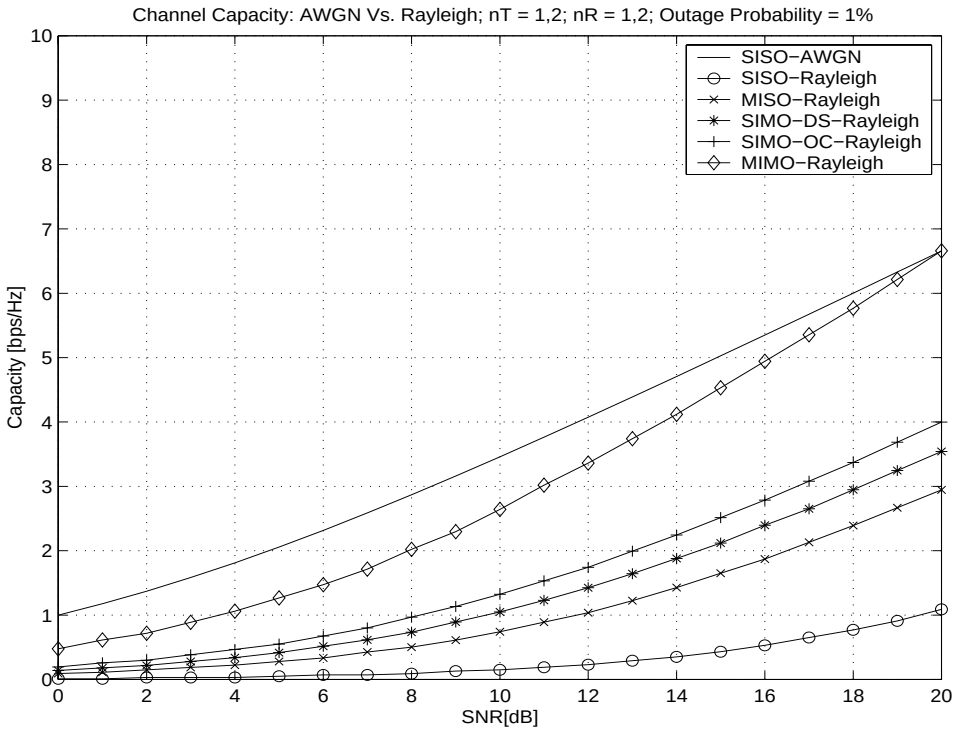

Figure 2.6: Capacity comparison - Rayleigh Vs. AWGN; $(n_T, n_R) = (2, 2)$,$P_{outage} = 1\%$

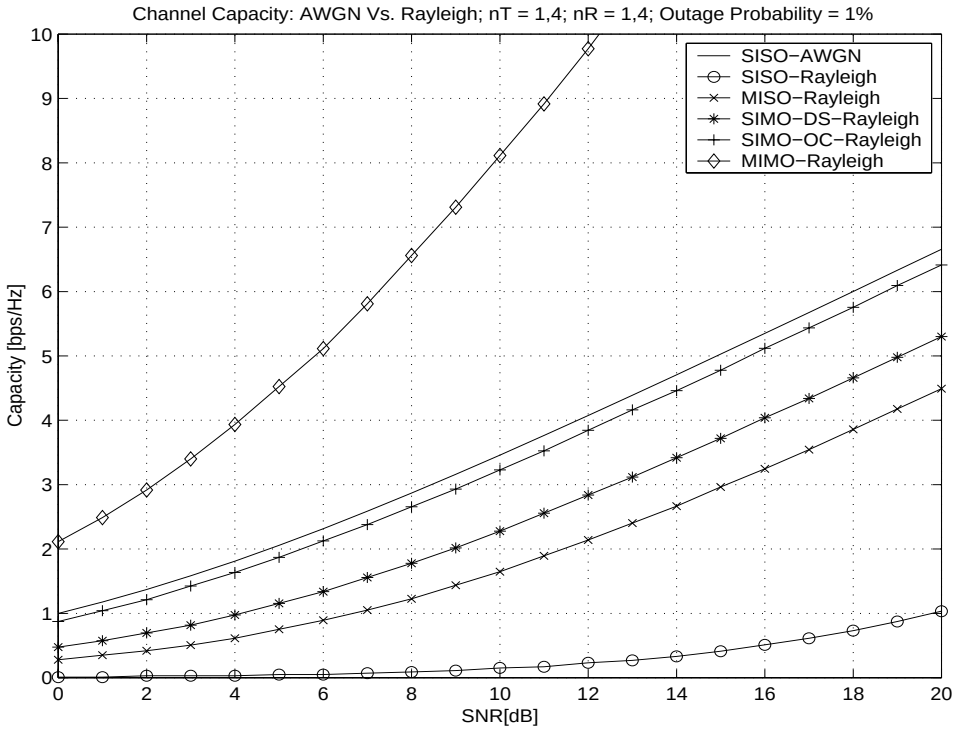

Figure 2.7: Capacity comparison - Rayleigh Vs. AWGN; $(n_T, n_R) = (4, 4)$,$P_{outage} = 1\%$

the transmitter results in diminishing returns in capacity. Similarly, Figure 2.9 demonstrates that with two elements at the receiver, more than six elements at the transmitter results in limited enhancements. This convergence can be also observed mathematically. Applying the strong low of large numbers to Eq. (2.5), as $n_T \to \infty$, the sample mean $1/n_T \sum_{i=1}^{n_T} |H_i|^2$ tends towards the expected value of $|H_i|^2$, which is 1 by definition (complex Gaussian R.V. with variance 0.5 per dimension). In this case, Eq. (2.5) simplifies to the Shannon capacity formula for SISO AWGN channel. Therefore, the capacity of MISO channel can not exceed the AWGN Shannon capacity. Indeed, this phenomena is demonstrated in Figure 2.8.

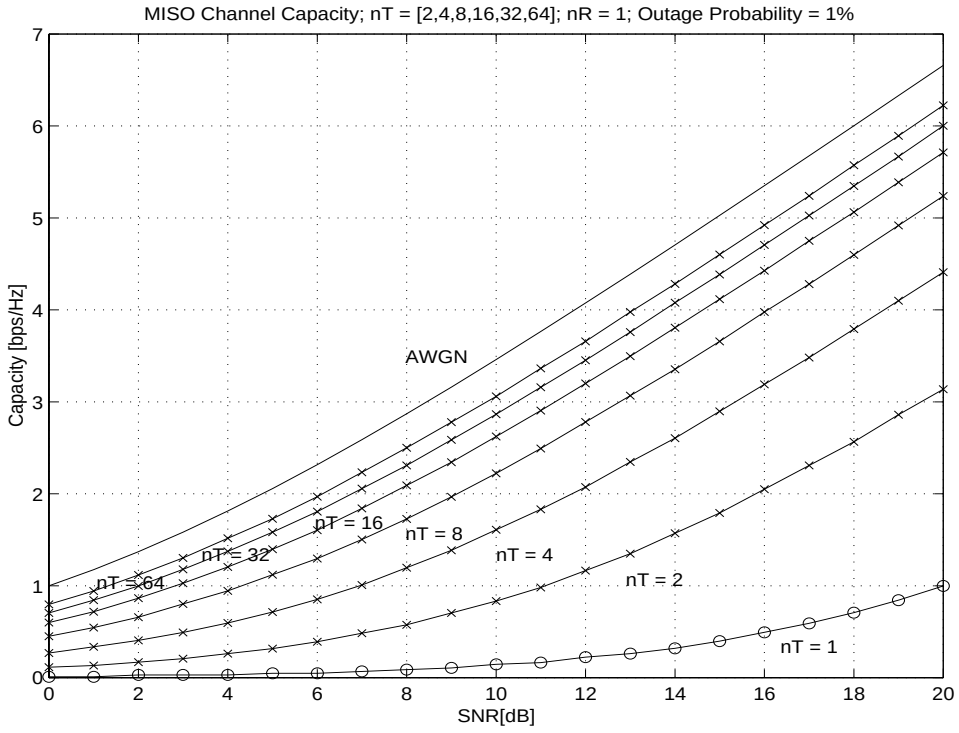

Figure 2.8: Capacity of MISO channel, $n_T = [2, 4, 8, 16, 32, 64]; n_R = 1, P_{outage} = 1\%$

2.2 Frequency Selective Fading MIMO Channels

In this section, the channel between transmit antenna i and receive antenna j is modeled by a Finite Impulse Response (FIR) filter with L_{ISI} taps. All channels are assumed to have the same channel memory. The lth tap of the $(i, j)th$ channel is denoted $\alpha_{i,j}(l)$ and is modeled as a zero mean complex Gaussian random variable with variance 0.5 per dimension. The taps of each FIR channel are normalized ($\sum_{l=0}^{L_{ISI}-1} |\alpha_{i,j}(l)|^2 = 1$) such that the channel has unit energy gain.

The outage probability of frequency selective MIMO channels is compared with that of

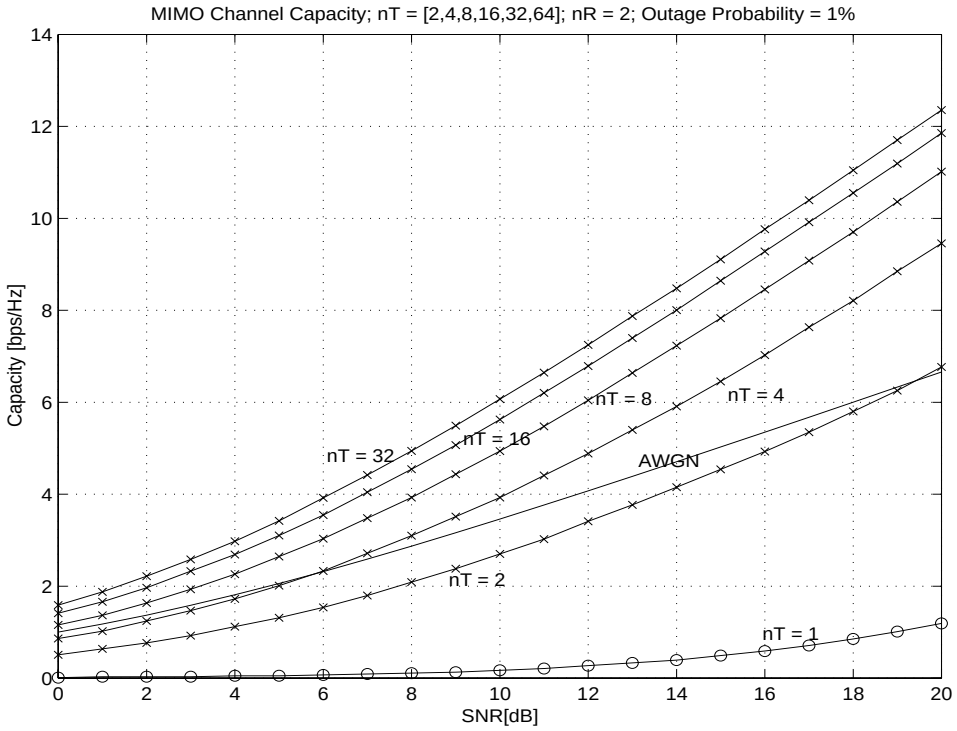

Figure 2.9: Capacity of MIMO channel, $n_T = [2, 4, 8, 16, 32, 64]; n_R = 2$, $P_{outage} = 1\%$

a MIMO flat fading channel. The objectives of this section are two fold: 1) demonstrating the potential for enhanced capacity in the case of frequency selective MIMO channels. 2) obtaining the outage probability of an L_{ISI}-tap frequency selective MIMO channel for a fixed spectral efficiency. This outage probability will serve us in Chapter 7 as a lower bound on the frame error rate of an arbitrary code with the same fixed spectral efficiency.

In [33], the authors have extended the result of Eq. (2.1) to frequency selective MIMO channels:

$$C = \frac{1}{N}\sum_{m=0}^{N-1} log_2 \left\{ det \left[I_{n_R} + \frac{SNR}{n_T} \tilde{H}_m^{\dagger} \tilde{H}_m \right] \right\}, \tag{2.7}$$

where L_{ISI} is the number of independent taps of the FIR filter which models the time dispersive channel, $\tilde{H}_m = \sum_{l=0}^{L_{ISI}-1} H(l) exp\left(-j\frac{2\pi}{N} lm\right)$, N is the frame length and $H(l)$ is the $n_T \times n_R$ MIMO channel matrix of the lth tap, $l \in [0, 1, \ldots, L_{ISI} - 1]$.

Figure 2.10 depicts the CCDF of the capacity for a fixed SNR of 13 dB. In this Figure, in addition to the SISO, SIMO-OC, SIMO-DS, MISO, MIMO flat fading channels, we also present the 2-taps frequency selective MISO case. It can be seen that for a threshold of 2 [bps/Hz], the frequency selective MISO channel has lower outage probability than that of spatial diversity only with either receive or transmit diversity mechanisms.

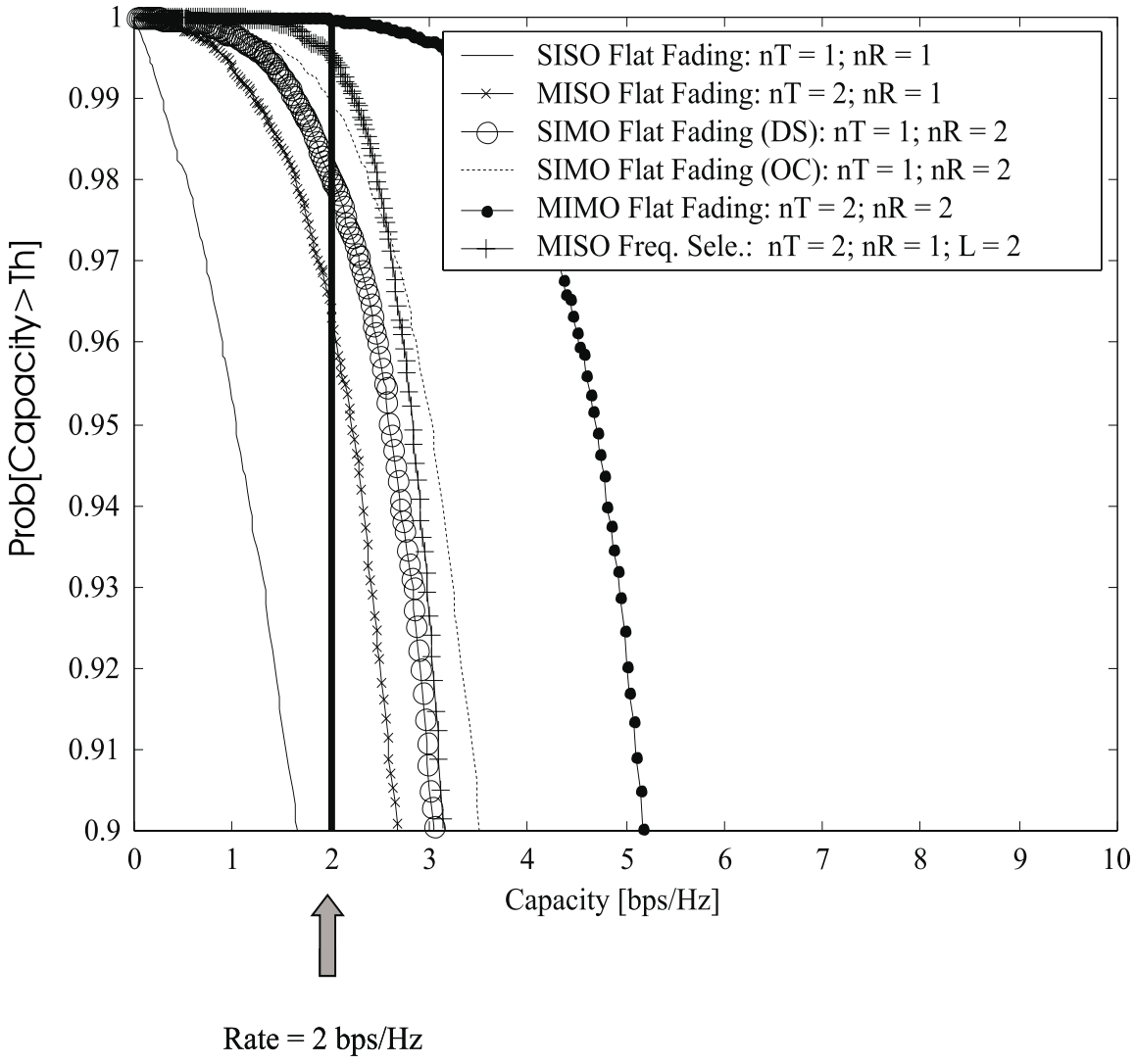

Figure 2.10: CCDF of MIMO channel capacity; $SNR = 13$dB

To illustrate this phenomena further, we plot in Figure 2.11 the outage probability versus SNR for the various cases for a fixed spectral efficiency of 2 [bps/Hz]. It is shown that the asymptotic slope of the frequency selective MISO channel achieves full spatial and frequency diversity level. That is, diversity level of 4 is achieved, as attributed to 2 transmit antennas elements and 2-tap time dispersive channel. In fact, the slope of the curve follows the asymptotic slope of MISO flat fading with 4 transmit antenna elements.

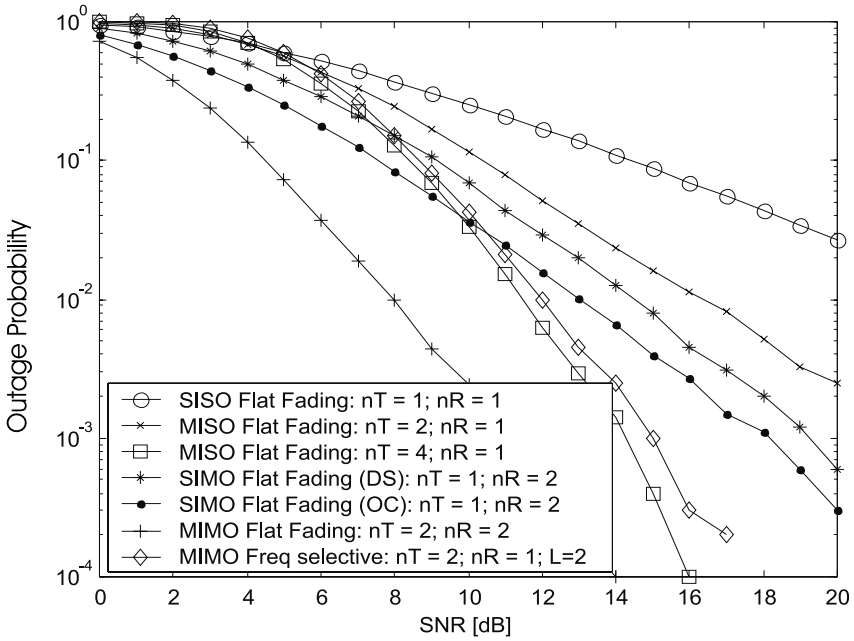

Figure 2.11: Outage probability of MIMO channel; frequency selective versus flat fading

2.3 Chapter Summary

The chapter presents an overview of the fundamental theory of the multi-input multi-output (MIMO) wireless channel. Results of capacity analysis, in terms of outage probability, are presented along with comparisons across various antenna configurations and channel conditions. The comparison illuminates significant capacity gains offered by exploiting the spatial-temporal properties of the MIMO channel. Outage probability results for MIMO frequency selective fading channels will be used in Chapter 7 as lower bounds on the frame error rate. These capacity results have motivated researchers to develop practical schemes for the MIMO channel. The next chapter introduces the fundamentals of space-time coding techniques, which achieve a portion of the theoretical capacity growth demonstrated herein.

Chapter 3

Space-Time Coding Fundamentals

Transmit-receive diversity schemes can be categorized into the two following groups.

- Closed loop schemes that employ feedback between receiver and transmitter
- Open loop schemes with no feedback

In time-division duplexing (TDD) systems, the reciprocity property of the channel can be leveraged by reusing channel estimates that were measured over the uplink channel for the transmission mechanism in the downlink. This is known as the Weight Reuse Technique (WRT), where downlink weights are a scaled version of the uplink weights, and the channel is assumed to exhibit slow fading characteristics such that weights that were measured in the uplink slot are still valid for downlink transmission.

In frequency-division duplexing (FDD) type of systems, channel reciprocity does not exist. Therefore, channel estimation is necessary at the mobile receiver. The receiver performs channel estimation of the fade coefficients (based on training sequences, pilot symbols or blind techniques) and sends this information via a feedback link to the transmitter. The feedback link has to be fast enough so that the CSI is still valid when applied at the transmitter. In other words, the coherence time of the channel must be longer than the required time to estimate, send and apply feedback side information. The transmitter can use the feedback information to weight the amplitudes and phases of the multi-element transmitter in order to maximize signal-to-noise ratio at the receiver. Other use of feedback information might include switched diversity where the transmitter switches in between multiple antennas or beam forming techniques. Feedback type schemes introduce an additional level of complexity by adding another layer of processing.

Another approach for transmit diversity is to measure angle-of-arrival (AOA) information from a given mobile to the base station based on direction finding (DF) algorithms

and to direct transmit energy towards the desired mobile. This is possible since AOA information is relatively similar for the uplink and the downlink, even in FDD systems.

Space-Time Coding techniques are categorized as an open loop architectures. They do not require a feedback link and are not based on measuring information at the receiver prior to transmission. Space-time codes introduce a signal structure that is exploited at the receiver to offer spatial and temporal diversity. Unlike traditional error correction codes, the redundant information is distributed over space (antenna) and time domains, thus leading to an increased bandwidth efficiency. Since in a space-time coded system the transmit array emits waveforms that operate over the same frequency and time, a superposition of signals appear at the receiver coupled with noise and other interfering sources such as multiple access interference, and channel induced ISI. The underlying question is how to suppress the sources of interference and decouple this superposition such that each sub-stream can be decoded. One approach might be introducing linear processing at the transmitter to map information across antennas. The mapping rule may introduce orthogonality across sequences transmitted from distinct antenna elements, which can be exploited at the receiver with the appropriate combing rule [19]. The receiver is composed of linear processing followed by maximum likelihood decoding techniques. This technique is know as the class of Space-Time Block Codes (STBC).

The orthogonality can be also implemented via time multiplexing [34], frequency multiplexing [35] or by using orthogonal spreading sequences for different antennas [36]. However, as will be described in this chapter, the orthogonality requirement can be relaxed by a joint design of the channel code, modulation and array processing. The time multiplexing approach is the delay diversity scheme, originally proposed by Seshadri and Winters [34]. In this scheme, delayed replicas of the same symbol are transmitted through different antenna elements such that a flat fading channel is transformed into a frequency selective fading channel. The receiver uses a maximum likelihood sequence estimator (MLSE) equalizer to offer a diversity order similar to maximal ratio receive combining (MRRC).

Tarokh and Calderbank extended the delay-diversity approach to the joint design of error-correction codes, modulation and array processing [18]. These codes are known as Space-Time Trellis Codes, which achieve both diversity advantage and coding gain and leads to an increased bandwidth efficiency. In space-time coded systems, there is not a mandatory requirement for multiple antenna elements at the receiver. The design and structure of STTC and STBC is the topic of the following sections.

3.1 Space-Time Trellis Coding (STTC)

3.1.1 Encoding and Decoding Algorithms

A system model for a Space-Time Trellis Code is given in Figure 3.1.

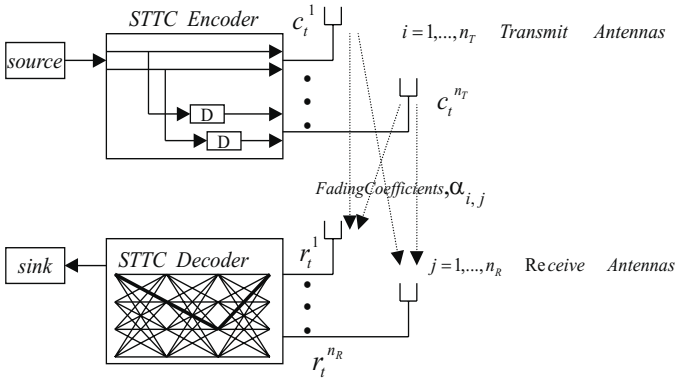

Figure 3.1: STTC system model

The STTC scheme contains n_T transmit antennas and possibly n_R receive antenna elements. The data stream is encoded by the channel code and then split into n_T parallel transmission chains. This channel code creates the inter-relations between signals in the space domain (different transmit antennas) and signals in the time domain (consecutive time symbols). A space-time trellis encoder maps each k input bits into n_T M-ary symbols which are simultaneously transmitted using n_T transmit antennas. Each transition in the trellis diagram corresponds to n_T symbols that are transmitted simultaneously over the channel. The values of these n_T M-ary symbols are based on the k input bits, ν state bits and generator polynomials $g_i, i = [1, 2, \ldots, n_T]$. Thus, a generator matrix with size $(k+\nu) \times n_T$ can entirely define the STTC. In Figure 3.1, $c_t^i, i = 1, 2, \ldots, n_T$ are the n_T symbols that are simultaneously transmitted at symbol time t over the wireless link. As examples, trellis diagrams of STTC with 4 or 8 state, QPSK modulation, and 2 transmit antenna elements are described in Figure 3.2. Note that each trellis transition is labeled with a pair of QPSK symbols that are transmitted simultaneously from antennas 1 and 2, respectively. Also, the four transitions that diverge from and merge into each node correspond to all possible combinations of 2 information bits.

Assuming a flat fading channel, the signal at each receive antenna $j, j = [1, 2, \ldots, n_R]$, is a linear superposition of the n_T simultaneously transmitted signals, weighted by fade coefficients and corrupted by noise. The signal received by antenna j, at time t, can be

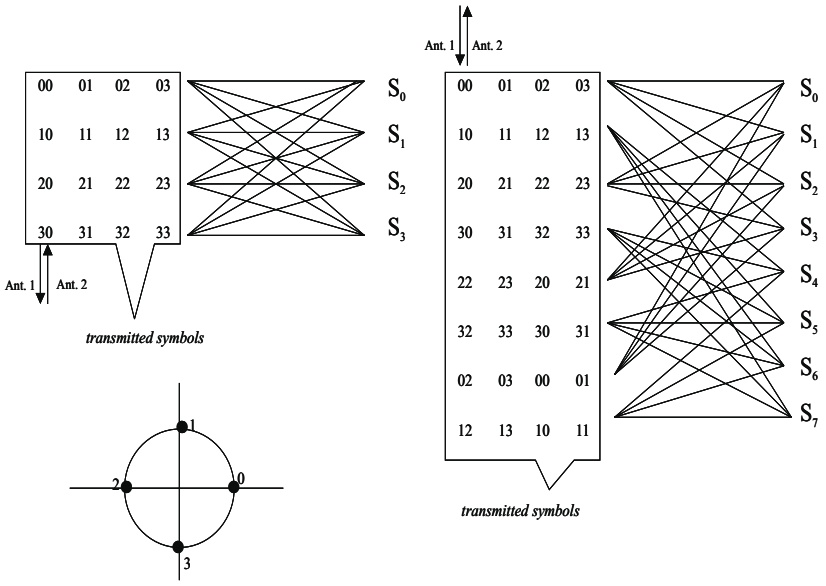

Figure 3.2: 4 and 8 state STTC, QPSK mapping

modeled by:

$$r_t^j = \sum_{i=1}^{n_T} \alpha_{i,j} c_t^i + \eta_t^j, \tag{3.1}$$

where η_t^j denotes the AWGN term and is modeled as independent samples of a zero mean complex Gaussian random variable with variance $[\frac{N_0}{2}]$ per dimension.

The channel is modeled by a $n_T \times n_R$ matrix $\Omega = [\alpha_{i,j}]$, whose entry $\alpha_{i,j}$ represents the complex fade coefficient for the path from transmit antenna i to receive antenna j. These fade coefficients are assumed to be independent complex Gaussian random variables with possibly nonzero complex mean and variance 0.5 per dimension. The channel is assumed to be quasi-static, flat fading such that no channel induced ISI term is present.

The receiver is based upon estimation of the channel fade coefficients followed by a Maximum Likelihood Sequence Estimation (MLSE) decoder, which computes the lowest accumulated squared Euclidean distance metric to extract the most likely transmitted sequence. The branch metric of the MLSE decoder is based on the squared Euclidean distance between the received signal and each candidate set of n_T transmitted codeword, denoted $e_t^i, i = 1, 2, \ldots, n_T$. Assuming perfect knowledge of CSI (channel coefficients $\alpha_{i,j}$) at the receiver, this metric is given by,

$$\sum_{j=1}^{n_R} \left| r_t^j - \sum_{i=1}^{n_T} \alpha_{i,j} e_t^i \right|^2 . \tag{3.2}$$

Note that the receive diversity takes the form of equal gain combining.

3.1.2 Performance Analysis

Assume the following codeword (of length l) was transmitted :

$$c = c_1^1 c_1^2 \cdots c_1^n c_2^1 c_2^2 \cdots c_2^n \cdots c_l^1 c_l^2 \cdots c_l^n, \tag{3.3}$$

and assume that the maximum likelihood decoder has decided (erroneously) in favor of

$$e = e_1^1 e_1^2 \cdots e_1^n e_2^1 e_2^2 \cdots e_2^n \cdots e_l^1 e_l^2 \cdots e_l^n. \tag{3.4}$$

Then, the Chernoff bound for the conditional pair-wise error probability (PWEP) is given by [37],

$$P(c \to e|\alpha_{i,j}) \leq exp\left[-d^2(c,e|\alpha_{i,j})\frac{E_s}{4N_0}\right] \tag{3.5}$$

where E_s and $N_0/2$ are the symbol energy and the noise variance per dimension, respectively, and $d^2(c,e|\alpha_{i,j})$ is the conditional squared Euclidean distance in between pair of codewords which is given by,

$$d^2(c,e|\alpha_{i,j}) = \sum_{j=1}^{n_R}\sum_{t=1}^{l}\left|\sum_{i=1}^{n_T}\alpha_{i,j}(c_t^i - e_t^i)\right|^2, \tag{3.6}$$

Note that the expression in (3.6) is a sum of quadratic forms as both squared terms associated with single transmit antenna and cross terms associated with products across various transmit antenna elements are present. This sum can be described in matrix notation by:

$$d^2(c,e|\alpha_{i,j}) = \sum_{j=1}^{n_R}\Omega_j^\dagger A \Omega_j \tag{3.7}$$

where Ω_j is defined as a column vector with dimensions $n_T \times 1$ whose entries are the fade coefficients associated with all transmit antennas and single receive antenna j and $\Omega_j^\dagger = \overline{\Omega_j^T}$ (conjugate transpose). A is $n_T \times n_T$ code distance matrix whose p,q element is given by:

$$A_{pq} = \sum_{t=1}^{l}(c_t^p - e_t^p)\overline{(c_t^q - e_t^q)} \tag{3.8}$$

Note that A is an Hermitian matrix and therefore it is diagonalizable. Also, by construction, the square root of A is given by,

$$B(c,e) = \begin{bmatrix} e_1^1 - c_1^1 & e_2^1 - c_2^1 & \cdots & e_l^1 - c_l^1 \\ e_1^2 - c_1^2 & e_2^2 - c_2^2 & \cdots & e_l^2 - c_l^2 \\ \cdots & \cdots & \cdots & \cdots \\ e_1^{n_T} - c_1^{n_T} & e_2^{n_T} - c_2^{n_T} & \cdots & e_l^{n_T} - c_l^{n_T} \end{bmatrix}, \tag{3.9}$$

where $A(c,e)$ is called the distance matrix and is given by,

$$A(c,e) = B(c,e)B(c,e)^\dagger \tag{3.10}$$

Thus, the principle axis theorem [38, 39] is used to perform the following change of coordinates:

$$\beta_j = (\beta_{1,j}, \ldots, \beta_{n_T,j}) = U^{\dagger}\Omega_j, \tag{3.11}$$

where U is the unitary matrix which diagonalizes A. The linear transformation with an orthonormal matrix U, described in Eq. (3.11), preserves the statistical properties of the fade coefficients. Therefore, if $\alpha_{i,j}$ are assumed to be zero mean independent complex Gaussian random variables with variance 0.5 per dimension so are $\beta_{i,j}$. This change of coordinates transforms the quadratic form into a standard form without cross terms,

$$d^2(c_t, e_t|\alpha_{i,j}) = \sum_{j=1}^{n_R} \beta_j^{\dagger}\Lambda\beta_j = \sum_{j=1}^{n_R}\sum_{i=1}^{n_T} \lambda_i \left|\beta_{i,j}\right|^2, \tag{3.12}$$

where Λ is the diagonal matrix with eigenvalues of A in its diagonal.
Then, for Rayleigh fading channel the pair-wise error probability is given by:

$$P(c \to e) \leq \left(\prod_{i=1}^{r} \lambda_i\right)^{-n_R} \left(\frac{E_s}{4N_0}\right)^{-rn_R}, \tag{3.13}$$

where $\lambda_i, i = [1, 2, \ldots, r]$ are the nonzero eigenvalues of the distance matrix $A(c, e)$, and r is the rank of $A(c, e)$ or $B(c, e)$ (Note that the ranks of $B(c, e)$ and $A(c, e)$ are equal). Thus, for a given number of receive antenna elements, n_R, the exponent of the SNR term is a function of the rank of $B(c, e)$. Therefore, the rank of the difference matrix determines the asymptotic error rate slope which corresponds to the diversity advantage of the STTC scheme. In addition, $(\prod_{i=1}^{r} \lambda_i)^{1/r}$ determines the offset in SNR from the equivalent uncoded system with the same diversity order, corresponding to the coding gain of the STC scheme.

3.1.3 Code Design Criteria

A. Slow Rayleigh/Rician Fading

The design criteria for space-time trellis codes operating over Rayleigh fading channel are:
• **The Rank criterion:** In order to maximize diversity advantage the difference matrix $B(c, e)$ has to be full rank over all possible pairs of codewords. The maximal diversity order in that case is $n_T \times n_R$.
Remark: An example of a violation of the full rank may occur in case of an all zero row of $B(c, e)$. This is the case where the symbols transmitted from the kth antenna element are equal across the two codewords c and e. In such a case, the kth antenna link can not provide a form of diversity to the other links since it conveys the same information for two distinct codewords.
• **The Determinant criterion:** In order to maximize coding gain the minimum of the product of the non-zero eigenvalues of $A(c, e)$ over all possible codewords has to be maximized.
Remark: Since the code distance matrix A represents the distance between codewords across different transmit antenna elements, the determinant criteria corresponds to increasing the distance across codewords. The name determinant criteria was given since the product of the eigenvalues of a full rank matrix equals its determinant (see Appendix B for proof).

B. Fast Fading

• **The distance criterion:** In order to achieve diversity of qn_R in a rapid fading environment, for any two codewords c and e the strings $[c_t^1, c_t^2, \cdots, c_t^{n_T}]$ and $[e_t^1, e_t^2, \cdots, e_t^{n_T}]$ must be different at least q times within the duration of a codeword.
Remark: This design criteria exploits the temporal diversity provided by the rapid fading environment and thus the diversity order of qn_R is a combined spatial-temporal diversity.
• **The product criterion:** In order to maximize coding gain, the product of distances across trellis transitions labeled with non-equal sets of symbols should be maximized.
Remark: Note that there are similarities between the above code design criteria and those derived for trellis coded modulation (TCM) in Rayleigh fading channels. These are given in [40, 41, 42] as: 1) the length of the shortest error event path, and 2) the product of branch distances along that path. The maximization of free Euclidean distance is a secondary design criteria. In AWGN channels however, the design criteria is the maximization of the free Euclidean distance.

3.1.4 STTC Example

As an example of evaluating STTC design criteria, we consider the 4-state delay diversity 2 space-time trellis code described in Figure 3.3. For a given node (state) in the trellis, the

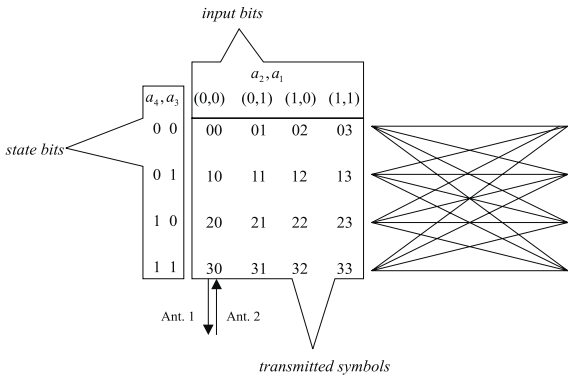

Figure 3.3: Trellis diagram of the 4-state delay diversity STTC, 2 Tx antennas, 2 [bps/Hz]

four pairs of symbols associated with the branches emanating from that node represent the n_T (in this specific case $n_T = 2$) simultaneous transmitted symbols for all possible values of input bits. The first symbol of each pair will be transmitted from antenna 1, while the second symbol will be transmitted (simultaneously) from antenna 2. Antenna 2 symbols are determined by the *current input bits only* while antenna 1 symbols are determined by the *states bits only* (which are the previous input bits). This is the reason for the name delay-diversity in which current and previous bits are transmitted simultaneously from two distinct antennas.

In order to guarantee that the rank criterion is met for this scheme and therefore that maximum diversity advantage is achieved, two heuristic design rules can be specified:

1. Diverging branches from the same node differ in the second symbol while constant in the first symbol.

2. Merging branches differ in the first symbol while constant in the second symbol.

The rank order for this code is 2. In order to prove this, we need to show that for any pair of codewords the two rows of the difference matrix are linearly independent. This is apparent from the two heuristic design rules as the first rule guarantees that $(e^1_{t=1} - c^1_{t=1}) = 0$ and $(e^2_{t=1} - c^2_{t=1}) \neq 0$ and the second rule guarantees that $(e^1_{t=l} - c^1_{t=l}) \neq 0$ and $(e^2_{t=l} - c^2_{t=l}) = 0$. Thus, the difference matrix, $B(c, e)$ will have the form:

$$B(c,e) = \begin{bmatrix} 0 & * & \cdots & * & e^1_l - c^1_l \\ e^2_1 - c^2_1 & * & \cdots & * & 0 \end{bmatrix} \tag{3.14}$$

It is clear that the two rows of $B(c,e)$ are linearly independent. Next, in order to evaluate the determinant criterion, we need to find the codewords $\{c,e\}$ in which the determinant,

$$\det\left(\sum_{t=1}^{l}\begin{bmatrix}(e_t^1-c_t^1)(e_t^1-c_t^1)^* & (e_t^1-c_t^1)(e_t^2-c_t^2)^*\\ (e_t^2-c_t^2)(e_t^1-c_t^1)^* & (e_t^2-c_t^2)(e_t^2-c_t^2)^*\end{bmatrix}\right) \tag{3.15}$$

is minimized. Forming the A matrix per trellis transition, the corresponding state diagram for the 4 state code is described in Figure 4.11. Carrying out the summation and determi-

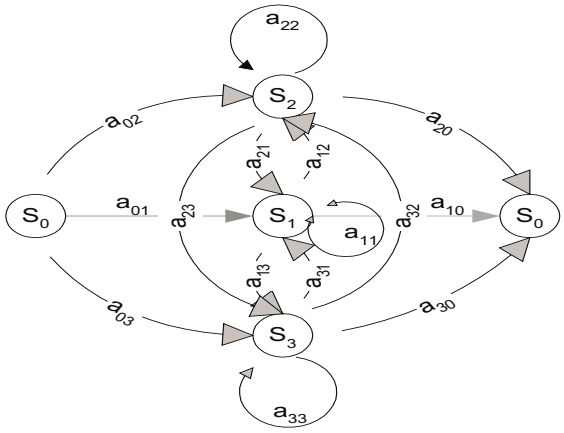

Figure 3.4: Modified state diagram of 4 state STTC

nant of Eq. (3.15) for all possible codewords, it can be seen that the minimum determinant of this code is 4 (1.3 dB), which provides a measure of the expected coding gain.

3.1.5 Decoding Complexity

The decoder complexity of the Viterbi algorithm is known to scale exponentially with the number of states in the trellis. The decoder of STTC is a maximum likelihood sequence detector, which can be implemented with the Viterbi algorithm. An important question is what is the minimum number of trellis states required for a space-time trellis code to guarantee transmit diversity order of r. To answer this question, we examine the minimum constraint length of a STTC with transmit diversity level of r. Recall that in order to guarantee diversity level of r, the rank of $B(c,e)$ (dimensions $n_T \times l$) must be r for any pair of codewords. This means that at least r rows (and r columns) of this matrix should be linearly independent or non-zero. If the constraint length of the code is less than $r-1$, two paths (codewords) in the trellis merge back after $r-1$ transitions, resulting in only $r-1$ non-zero columns in the $B(c,e)$ matrix and thus a violation of the rank criterion. Therefore,

the minimum constraint length of a space-time trellis code with transmit diversity order r is $r-1$. Next, assume a spectral efficiency of b bits per second per hertz, the number of branches leaving each state are 2^b. Thus, according to the minimum constraint length criteria, at time $r-1$, there are $2^{b(r-1)}$ paths that can not merge back to the same state. In other words, there are at least $2^{b(r-1)}$ states in the trellis of a space-time trellis code with spectral efficiency b [bps/Hz] that achieves transmit diversity order of r. Therefore, the decoder complexity of a STTC is growing exponentially with the spectral efficiency of the scheme.

In the next section, the second family of STC is introduced, demonstrating a remarkably simple decoder structure. This class is known as the orthogonal space-time block codes.

3.2 Space-Time Block Coding (STBC)

Seeking low decoder complexity, Alamouti in [19] proposed a simple dual transmit diversity scheme that achieves the same diversity advantage of dual branch Maximal Ratio Receive Combining (MRRC). The scheme was generalized by Tarokh et al. in [27] for arbitrary number of transmit antennas elements by applying the theory of orthogonal design. The novelty of this family of codes is its simple maximum likelihood decision rule, which is preceded by linear processing only. The scheme is defined by its encoder matrix, which maps k input M-ary symbols into n_T orthogonal sequences of length p, thus creating a rate $r = k/p$ code. The encoder matrix, denoted G_{n_T}, is called the orthogonal design of the STBC for the orthogonality property across its columns.

A block diagram of the full rate orthogonal design transmit diversity scheme with 2 transmit and 1 receive antenna elements (G_2) is illustrated in Figure 3.5.

The orthogonality across sequences of symbols, transmitted simultaneously form the two antenna elements, is exploited at the receiver by the combining rule. The objectives of this combiner are two fold: 1) decouple the received superposition of symbols to create separate decision statistics, and 2) coherently combine the fade coefficients associated with each transmitted symbol to allow for diversity order. The derived decision statistics are fed into a symbol-by symbol Maximum Likelihood (ML) decoder. It is noted that the STBC scheme relies on quasi-static flat channel conditions, or a slow time-varying channel such that the coherence time of the channel is greater than the duration of a block (p consecutive symbols). This is a reasonable assumption in most practical systems since the block length of STBC is relatively short.

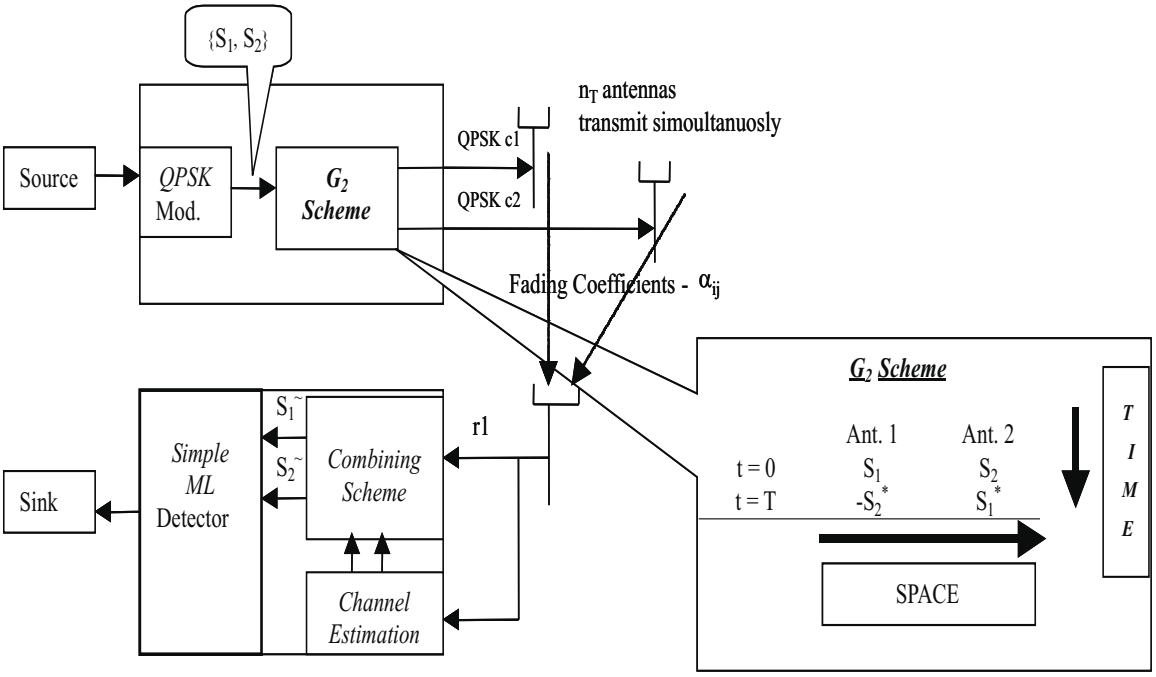

Figure 3.5: STBC block diagram

3.2.1 Coherent Space-Time Block Coding (C-STBC)

A. Encoding Algorithm

Each set of b bits is mapped to form a M-ary PSK or QAM symbol with cardinality 2^b. The space-time block encoding algorithm of Figure 3.5 is described by the encoder matrix G_2, which maps a block of $k = 2$ symbols into $n_T = 2$ sequences of length $p = 2$ each. G_2 is given by

$$G_2 = \begin{pmatrix} x_1 & x_2 \\ -x_2^* & x_1^* \end{pmatrix}, \tag{3.16}$$

where x_1 and x_2 denote a pair of symbols at the encoder input (denoted S_0, S_1 in Figure 3.5). The encoder output is denoted by s_t^i, where $1 \leq t \leq p$ corresponds to the time instant within a block of length p symbols and i corresponds to the ith antenna element at the transmitter. The G_2 matrix implies a rate 1 ($r = k/p$) code that does not expand bandwidth to transmit the redundant information. The first and second rows of the encoder matrix are transmitted at times t and $t+T$ from the two antennas, respectively. The orthogonality criteria corresponds to a zero inner product of the two columns.

B. Decoding Algorithm

The received signal at receive antenna j at time t is modeled by,

$$r_t^j = \sum_{i=1}^{n_T} \alpha_{i,j} s_t^i + \eta_t^j, \tag{3.17}$$

where η_t^j denotes the AWGN term and is modeled as independent samples of a zero mean complex Gaussian random variable with variance $[\frac{N_0}{2}]$ per dimension. Assuming ideal CSI at the receiver, the following decision metric is evaluated

$$\sum_{t=1}^{p} \sum_{j=1}^{n_R} \left| r_t^j - \sum_{i=1}^{n_T} \alpha_{i,j} s_t^i \right|^2. \tag{3.18}$$

In the case of G_2 matrix, the ML detection rule is the minimization process of the following decision metric:

$$\sum_{j=1}^{n_R} (\left| r_1^j - \alpha_{1,j} s_1 - \alpha_{2,j} s_2 \right|^2 + \left| r_2^j - \alpha_{1,j} s_2^* - \alpha_{2,j} s_1^* \right|^2). \tag{3.19}$$

Note that the fade coefficients are assumed to be constant over the block duration of $p = 2$ symbols. This is a reasonable assumption for typical coherence time and baud rate of practical systems. Expanding the above metric and simplifying, the minimization of Eq. (3.19) is equivalent to the following two separate minimization processes:

$$\left| \left[\sum_{j=1}^{n_R} (r_1^j \alpha_{1,j}^* + (r_2^j)^* \alpha_{2,j}) \right] - s_1 \right|^2 + \left(-1 + \sum_{j=1}^{n_R} \sum_{i=1}^{2} |\alpha_{i,j}|^2 \right) |s_1|^2 \tag{3.20}$$

for decoding s_1, and

$$\left| \left[\sum_{j=1}^{n_R} (r_1^j \alpha_{2,j}^* - (r_2^j)^* \alpha_{1,j}) \right]^2 - s_2 \right|^2 + \left(-1 + \sum_{j=1}^{n_R} \sum_{i=1}^{2} |\alpha_{i,j}|^2 \right) |s_2|^2 \tag{3.21}$$

for decoding s_2.

Thus, the receiver structure for STBC includes channel estimates of the fade coefficients in the following linear processing rule:

$$\begin{aligned} \tilde{s}_1 &= \sum_{j=1}^{n_R} \left(\alpha_{1,j}^* r_1^j + \alpha_{2,j} (r_2^j)^* \right) \\ \tilde{s}_2 &= \sum_{j=1}^{n_R} \left(\alpha_{2,j}^* r_1^j - \alpha_{1,j} (r_2^j)^* \right) \end{aligned} \tag{3.22}$$

Plugging Eq. (5.1) into the combining rule of Eq. (3.22) yields

$$\begin{aligned} \tilde{s}_1 &= \left(\sum_{j=1}^{n_R} \sum_{i=1}^{2} |\alpha_{i,j}|^2 \right) s_1 + N_1, \\ \tilde{s}_2 &= \left(\sum_{j=1}^{n_R} \sum_{i=1}^{2} |\alpha_{i,j}|^2 \right) s_2 + N_2; \end{aligned} \tag{3.23}$$

where N_1 and N_2 are noisy terms given by

$$\begin{aligned} N_1 &= \sum_{j=1}^{n_R} \left(\alpha_{1,j}^* \eta_1^j + \alpha_{2,j} (\eta_2^j)^* \right), \\ N_2 &= \sum_{j=1}^{n_R} \left(-\alpha_{1,j} (\eta_2^j)^* + \alpha_{2,j}^* \eta_1^j \right). \end{aligned} \tag{3.24}$$

Note that the fade coefficients are added coherently, yielding optimal combining and diversity order of $2 \times n_R$. Also, note that the linear combining rule takes advantage of the orthogonality of the columns of G_2 in order to decouple the estimates for s_1 and s_2. Once decision statistics for s_1 and s_2 are obtained, the optimum detection rule is described by:
Choose $s_1 = s_i; i = [1, \cdots, 2^b]$ if and only if

$$\left(-1 + \sum_{j=1}^{n_R} \sum_{i=1}^{2} |\alpha_{i,j}|^2 \right) |s_i|^2 + d^2(\tilde{s_1}, s_i) \leq \left(-1 + \sum_{j=1}^{n_R} \sum_{i=1}^{2} |\alpha_{i,j}|^2 \right) |s_k|^2 + d^2(\tilde{s_2}, s_k), \ \forall i \neq k. \tag{3.25}$$

For PSK signals (equal energy constellations) the decision rule in Eq. (3.25) is simplified to:
Choose $s_1 = s_i$ if and only if

$$d^2(\tilde{s_1}, s_i) \leq d^2(\tilde{s_1}, s_k), \ \forall i \neq k, \tag{3.26}$$

and a separate identical decision rule for s_2: choose $s_2 = s_i$ if and only if

$$d^2(\tilde{s_2}, s_i) \leq d^2(\tilde{s_2}, s_k), \ \forall i \neq k. \tag{3.27}$$

3.2.2 Orthogonal Designs

A complex orthogonal design G is defined as a $p \times n_T$ orthogonal transmission matrix with entries the indeterminants $[\pm x1, \pm x_2, \cdots, \pm x_n]$, their conjugates $[\pm x_1^*, \pm x_2^*, \cdots, \pm x_n^*]$ and the superposition of those. In the previous section, a full rate $(G_2, r = 1)$ complex orthogonal design was described for 2 transmit antenna elements. Following the theory of orthogonal design by Radon and Hurwitz [43], Tarokh et al. generalized in [27] these schemes for an arbitrary number of antenna elements. While a full rate orthogonal design exists for real

alphabets (i.e., PAM) with arbitrary number of elements, it does not exist for an arbitrary complex alphabet (i.e., PSK or QAM) with more than 2 antenna elements. This has motivated researchers to search for sporadic complex orthogonal designs, which accommodate rates as close to 1 as possible, yet achieve full spatial diversity order. Table 3.1 summarizes the characteristics of few sporadic complex orthogonal designs, proposed originally in [27], for $2, 3$ and 4 transmit antenna elements. Following Table 3.1, the orthogonal transmission matrices are described.

Table 3.1: Orthogonal designs for STBC

Orthogonal Design	n_T	*rate*	*k - input block length*	*p - output block length*
G_2	2	1	2	2
G_3	3	1/2	4	8
G_4	4	1/2	4	8
H_3	3	3/4	3	4
H_4	4	3/4	3	4

• **Orthogonal Design I:** 2 transmit antenna elements, $r = 1$.

$$G_2 = \begin{pmatrix} x_1 & x_2 \\ -x_2^* & x_1^* \end{pmatrix} \tag{3.28}$$

• **Orthogonal Design IIa:** 3 transmit antenna elements, $r = 1/2$.

$$G_3 = \begin{pmatrix} x_1 & x_2 & x_3 \\ -x_2 & x_1 & -x_4 \\ -x_3 & x_4 & x_1 \\ -x_4 & -x_3 & x_2 \\ x_1^* & x_2^* & x_3^* \\ -x_2^* & x_1^* & -x_4^* \\ -x_3^* & x_4^* & x_1^* \\ -x_4^* & -x_3^* & x_2^* \end{pmatrix} \tag{3.29}$$

• **Orthogonal Design IIb:** 3 transmit antenna elements, $r = 3/4$.

$$H_3 = \begin{pmatrix} x_1 & x_2 & x_3/\sqrt{2} \\ -x_2^* & x_1^* & x_3/\sqrt{2} \\ x_3^*/2 & x_3^*/2 & (-x_1 - x_1^* + x_2 - x_2^*)/2 \\ x_3^*/2 & -x_3^*/2 & (x_2 + x_2^* + x_1 - x_1^*)/2 \end{pmatrix} \tag{3.30}$$

• **Orthogonal Design IIIa:** 4 transmit antenna elements, $r = 1/2$.

$$G_4 = \begin{pmatrix} x_1 & x_2 & x_3 & x_4 \\ -x_2 & x_1 & -x_4 & x_3 \\ -x_3 & x_4 & x_1 & -x_2 \\ -x_4 & -x_3 & x_2 & x_1 \\ x_1^* & x_2^* & x_3^* & x_4^* \\ -x_2^* & x_1^* & -x_4^* & x_3^* \\ -x_3^* & x_4^* & x_1^* & -x_2^* \\ -x_4^* & -x_3^* & x_2^* & x_1^* \end{pmatrix} \tag{3.31}$$

• **Orthogonal Design IIIb:** 4 transmit antenna elements, $r = 3/4$.

$$H_4 = \begin{pmatrix} x_1 & x_2 & x_3/\sqrt{2} & x_3/\sqrt{2} \\ -x_2^* & x_1^* & x_3/\sqrt{2} & -x_3/\sqrt{2} \\ x_3^*/2 & x_3^*/2 & (-x_1 - x_1^* + x_2 - x_2^*)/2 & (-x_2 - x_2^* + x_1 - x_1^*)/2 \\ x_3^*/2 & -x_3^*/2 & (x_2 + x_2^* + x_1 - x_1^*)/2 & -(x_1 + x_1^* + x_2 - x_2^*)/2 \end{pmatrix} \tag{3.32}$$

It can be verified that the columns of these matrices meet the orthogonality requirement. These codes have a simple linear processing rule, followed by a maximum likelihood decoder. As an example, the decoder for G_3 minimizes the following decision metrics:

$$\begin{aligned} &\left| \left[\sum_{j=1}^{n_R} \left(r_1^j \alpha_{1,j}^* + r_2^j \alpha_{2,j}^* + r_3^j \alpha_{3,j}^* + (r_5^j)^* \alpha_{1,j} + (r_6^j)^* \alpha_{2,j} + (r_7^j)^* \alpha_{3,j} \right) \right] - s_1 \right|^2 \\ &\qquad + \left(-1 + \sum_{j=1}^{n_R} \sum_{i=1}^{3} |\alpha_{i,j}|^2 \right) |s_1|^2 , \end{aligned} \tag{3.33}$$

for decoding s_1,

$$\begin{aligned} &\left| \left[\sum_{j=1}^{n_R} \left(r_1^j \alpha_{2,j}^* - r_2^j \alpha_{1,j}^* + r_4^j \alpha_{3,j}^* + (r_5^j)^* \alpha_{2,j} - (r_6^j)^* \alpha_{1,j} + (r_8^j)^* \alpha_{3,j} \right) \right] - s_2 \right|^2 \\ &\qquad + \left(-1 + \sum_{j=1}^{n_R} \sum_{i=1}^{3} |\alpha_{i,j}|^2 \right) |s_2|^2 , \end{aligned} \tag{3.34}$$

for decoding s_2,

$$\begin{aligned} &\left| \left[\sum_{j=1}^{n_R} \left(r_1^j \alpha_{3,j}^* - r_3^j \alpha_{1,j}^* - r_4^j \alpha_{2,j}^* + (r_5^j)^* \alpha_{3,j} - (r_7^j)^* \alpha_{1,j} - (r_8^j)^* \alpha_{2,j} \right) \right] - s_3 \right|^2 \\ &\qquad + \left(-1 + \sum_{j=1}^{n_R} \sum_{i=1}^{3} |\alpha_{i,j}|^2 \right) |s_3|^2 , \end{aligned} \tag{3.35}$$

for decoding s_3, and

$$\begin{aligned} &\left| \left[\sum_{j=1}^{n_R} \left(-r_2^j \alpha_{3,j}^* + r_3^j \alpha_{2,j}^* - r_4^j \alpha_{1,j}^* - (r_6^j)^* \alpha_{3,j} + (r_7^j)^* \alpha_{2,j} - (r_8^j)^* \alpha_{1,j} \right) \right] - s_4 \right|^2 \\ &\qquad + \left(-1 + \sum_{j=1}^{n_R} \sum_{i=1}^{3} |\alpha_{i,j}|^2 \right) |s_4|^2 , \end{aligned} \tag{3.36}$$

for decoding s_4.

Additional decoding rules for G_4, H_3, H_4 can be found in the Appendix of [25]. Performance analysis of these codes with M-ary PSK or QAM and various spectral efficiencies are presented in Chapter 5.

3.2.3 Differential Space-Time Block Coding (D-STBC)

Differential demodulation techniques are widely used in contemporary communications systems, offering robust performance in the presence of unknown phase and CSI. In contrast, coherent demodulation implies stringent requirements for accurate carrier recovery and channel estimation in order to compensate the instantaneous phase and allow for optimal detection. Carrier recovery and channel estimation can be performed with data-aided type techniques (i.e., transmission of pilot symbols) or non data-aided (blind) techniques. In the former, additional overhead is introduced to provide robust tracking of signal parameters, while in the latter additional complexity is added to the system. In addition, instantaneous tracking of phase and CSI is a challenging task in time varying channels. Under ideal conditions, coherent demodulation outperforms differential demodulation by approximately 3 dB. In differential modulation schemes, the information is carried out in the phase difference between consecutive symbols rather than in the absolute phase. Demodulation is performed by using the previous received symbol as a noisy reference signal to the incoming current symbol. Since both previous and current symbols undergo the same channel conditions, the demodulator extracts the difference between consecutive phases to yield the information sequence. This process causes error propagation, which leads to degradation in performance as compared with coherent demodulation. While differential demodulation has been primarily used in single transmit antenna systems, the concept can be also applied to transmit diversity schemes to solve practical issues such as the need for accurate channel estimation at the receiver and carrier recovery. Differential space-time modulation approaches have been proposed and investigated in [28, 44, 45, 46]. Here, we adopt the scheme proposed in [28] as an extension to the family of space-time block codes.

A. The Encoding Algorithm

The transmitter block diagram for differential STBC is illustrated in Figure 3.6.

The information bits are packed into groups of b bits each and mapped by the following M-ary PSK mapper:

$$A = \left\{ \frac{1}{\sqrt{2}} \exp^{\frac{j2\pi k}{M}} \right\} \tag{3.37}$$

We denote (a_1, a_2) as our reference pair (constant and known to the receiver) of M-ary PSK symbols. Grouping a pair of new M-ary PSK constellation symbols, denoted (a_3, a_4),

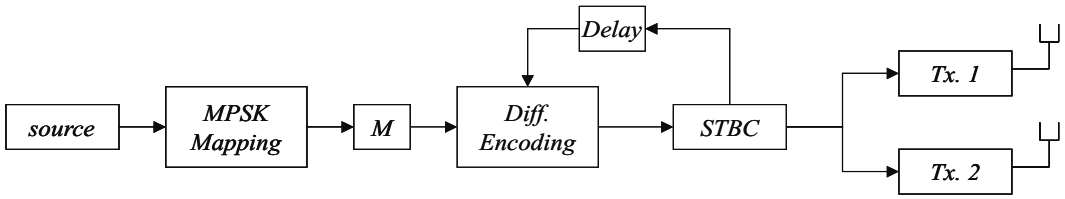

Figure 3.6: D-STBC encoder block diagram

the mapping M performs change of basis according to G_2 orthogonal design. That is, the columns of G_2, (x_1, x_2) and $(-x_2^*, x_1^*)$, are used as orthonormal vectors to span the new basis. The pair of symbols (a_3, a_4) in the new basis are denoted (A, B) and given by

$$\begin{aligned} A &= a_3 a_1^* + a_4 a_2^*, \\ B &= -a_3 a_2 + a_4 a_1. \end{aligned} \tag{3.38}$$

Note that this mapping is an isometric mapping, thus preserving distance properties. That is, distance between two vectors in the natural basis is equal to distance between vectors in the new basis. This property will be used by performing maximum likelihood decoding over the vector (A,B) to decode for the pair (a_3, a_4). Next, differential encoding is performed across set of symbols:

$$\begin{aligned} s_{2t+1} &= A s_{2t-1} - B s_{2t}^*, \\ s_{2t+2} &= A s_{2t} + B s_{2t-1}^*, \end{aligned} \tag{3.39}$$

where (A, B) is the pair of new symbols in the G_2 basis, (s_{2t}, s_{2t-1}) is the previously transmitted pair of symbols from antennas 1 and 2 respectively at time $2t-1$, and (s_{2t+1}, s_{2t+2}) is the current differentially encoded pair of symbols to be transmitted next. This new pair of symbols is fed into the space-time block encoder, described by G_2, to create the following two pairs of symbols: $(s_{2t+1}, -s_{2t+2}^*)$ and (s_{2t+2}, s_{2t+1}^*) that are transmitted from antennas 1 and 2 respectively at times $2t+1$ and $2t+2$. The pair (s_{2t+1}, s_{2t+2}) is fed back to the differential encoder for the next iteration where the set (s_{2t+3}, s_{2t+4}) is produced. This process continues in an inductive manner until the end of the frame.

B. The Decoding Algorithm

The receiver block diagram for differential STBC is illustrated in Figure 3.7.

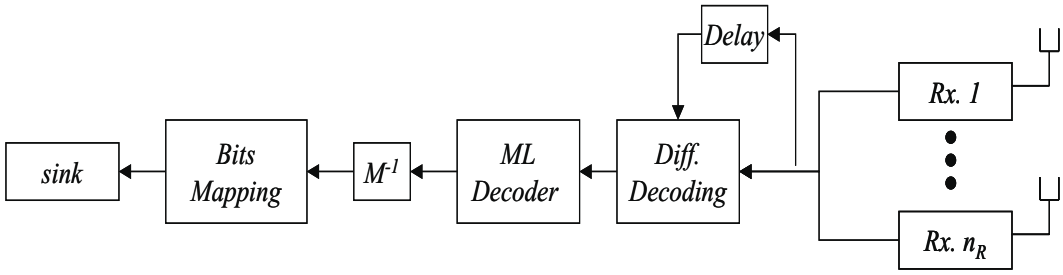

Figure 3.7: D-STBC decoder block diagram

Let us assume that the receiver is equipped with a single antenna element. The extension to n_R receive antenna elements is straightforward. Let us denote $r_{2t-1}, r_{2t}, r_{2t+1}$ and r_{2t+2} as four consecutive samples at the matched filter output. In quasi-static flat fading channel, the received signals are modeled by:

$$\begin{aligned} r_{2t-1} &= \alpha_1 s_{2t-1} + \alpha_2 s_{2t} + \eta_{2t-1}, \\ r_{2t} &= \alpha_1(-s^*_{2t}) + \alpha_2 s^*_{2t-1} + \eta_{2t}, \\ r_{2t+1} &= \alpha_1 s_{2t+1} + \alpha_2 s_{2t+2} + \eta_{2t+1}, \\ r_{2t+2} &= \alpha_1(-s^*_{2t+2}) + \alpha_2 s^*_{2t+1} + \eta_{2t+2}, \end{aligned} \tag{3.40}$$

where $\eta_i, i = [2t-1, 2t, 2t+1, 2t+2]$ represents the AWGN term in consecutive time samples. Differential decoding is performed by the following operations:

$$\begin{aligned} R_1 &= r_{2t+1} r^*_{2t-1} + r^*_{2t+2} r_{2t}, \\ R_2 &= r_{2t+1} r^*_{2t} - r^*_{2t+2} r_{2t-1}. \end{aligned} \tag{3.41}$$

Plugging Eq. (3.40) into Eq. (3.41) and some algebraic manipulations, R_1 and R_2 are simplified to:

$$\begin{aligned} R_1 &= \left(|\alpha_1|^2 + |\alpha_2|^2\right) A + N_1, \\ R_2 &= \left(|\alpha_1|^2 + |\alpha_2|^2\right) B + N_2, \end{aligned} \tag{3.42}$$

where N_1 and N_2 represent the effective noise terms (composed of noise cross signal terms and noise cross noise terms) of the decision statistics R_1 and R_2. Thus, the differential decoding procedure, described by Eq. (3.41), performs decoupling of the pair of symbols and yields separate decision statistics for A and B, respectively. Moreover, observing Eq.

(3.42), we see the optimal combining of the fade coefficients, similar to 2-fold diversity of maximal ratio receive combining.

Since the vector (A, B) has a unit length regardless of the sequence of $2b$ information bits associated with it, a maximum likelihood decision rule is applied by choosing the closest vector (A, B) to (R_1, R_2) out of the 2^{2b} possible candidates. The decision $(\hat{A}, \hat{B})$ is transformed back to $2b$ decoded bits by inverse M-mapping rule. The differential decoding followed by ML detection rule continues in an inductive manner until all frame components are decoded.

The extension to n_R elements at the receiver is performed by the following equal gain combining rule over the decision statistics:

$$\begin{aligned} \tilde{R}_1 &= \sum_{j=1}^{n_R} R_1^j \\ \tilde{R}_2 &= \sum_{j=1}^{n_R} R_2^j \end{aligned} \tag{3.43}$$

where R_1^j and R_2^j are computed per receive antenna j using Eq. (3.41). $(\tilde{R}_1, \tilde{R}_2)$ is the combined decision statistics vector which can be described by:

$$\begin{aligned} \tilde{R}_1 &= \left(\sum_{j=1}^{n_R} \sum_{i=1}^{2} |\alpha_{i,j}|^2 \right) A + \tilde{N}_1 \\ \tilde{R}_2 &= \left(\sum_{j=1}^{n_R} \sum_{i=1}^{2} |\alpha_{i,j}|^2 \right) B + \tilde{N}_2 \end{aligned} \tag{3.44}$$

Thus, diversity advantage of $2 \times n_R$ is achieved. Note that the decoding scheme is not based on knowledge or tracking of the fade coefficients. Also, as will be shown in Chapter 5, this scheme is robust to frequency and phase errors. In Chapter 6, implementation of D-STBC on DSP platform is described as part of the Virginia Tech Space-Time Advanced Radio (VT-STAR) test bed.

3.3 Bell Labs Layered Space-Time Architecture (BLAST)

The design of the BLAST test bed system was motivated by the information theoretic results of Foschini and Gans in [2](see also section 2.1), showing the enormous capacity growth with the use of multiple element array technology. The BLAST architecture (with 8 or 16 antenna elements in both ends of the wireless link) demonstrates unprecedented data rates over a rich scattering environment such as indoor wireless channel. A throughput of 621 Kbps over a narrowband channel of 30 KHz was demonstrated in an indoor environments.

Thus, spectral efficiencies at the order of 20 [bps/Hz] are achieved. An essential feature of BLAST is that there is no mechanism, such as time-, frequency- or code-division multiplexing that assures an orthogonality across sequences transmitted from the different transmitter antenna elements. Rather, the propagation environment itself, which is assumed to exhibit significant multipath, is exploited to separate the signals at the receiver. Two main BLAST schemes were proposed in the literature. The V-BLAST scheme [47] known as the vertical BLAST and corresponds to a vertical mapping of symbols onto the space domain such that a simultaneous transmission from all transmit antennas is performed without any sub-stream coding. That is, each transmitter operates as a conventional QAM transmitter. The second scheme, known as D-BLAST [48], is a diagonally layered space time architecture, in which inter sub-stream coding is introduced across diagonals in space-time. The structure of these schemes is the subject of the next subsections.

3.3.1 V-BLAST Architecture

A generic block diagram for V-BLAST is illustrated in Figure 3.8. A model for the received

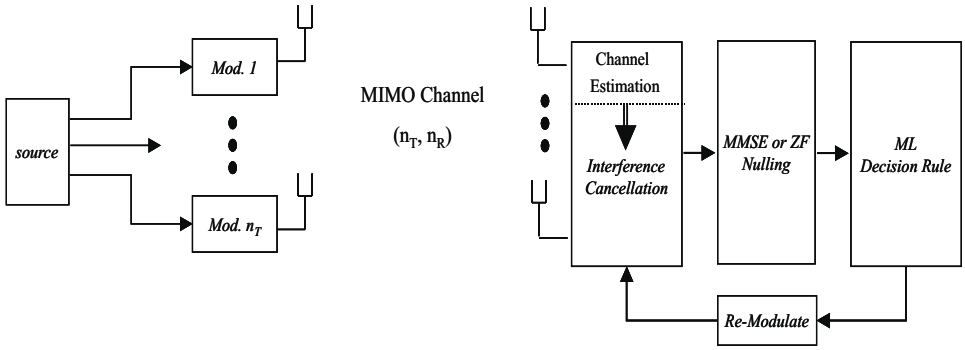

Figure 3.8: V-BLAST Architecture

vector is given by the following matrix equation:

$$\overline{r} = H\overline{a} + \overline{\nu}, \tag{3.45}$$

where H represents the channel fade coefficients matrix with size $n_R \times n_T$, $\overline{a}$ is the transmitted vector with size $n_T \times 1$, which is composed of a set of symbols, each of which is a member of a QAM constellation. $\overline{\nu}$ represents a vector of independent samples of AWGN over n_R receive antenna chains.

The V-BLAST receiver performs channel estimation based on pilot symbols and then sorts the channels based on these channel estimates. The sorting algorithm determines the order in which the various transmitted components will be decoded. Nulling is performed by

linearly weighting the received signals in order to minimize a given cost function. Candidate criteria are the minimum mean-squared error (MMSE) or zero-forcing (ZF). As an example, zero forcing nulling is performed by finding the weight vector, $\overline{w_i}$, which satisfies:

$$\overline{w_i}^T (H)_j = \delta_{ij}, \tag{3.46}$$

where $(H)_j$ is the jth column of the channel matrix H, and δ_{ij} is the Kronecker delta. Thus, the decision statistics for the ith sub-stream (signal from transmit antenna i) is given by:

$$\overline{y_i} = \overline{w_i}^T \overline{r}. \tag{3.47}$$

Next, the receiver slices y_i to perform decision for a_i and regenerates the contribution of a_i in order to subtract it from the received vector. This is described by,

$$\overline{r_{i+1}} = \overline{r_i} - \hat{\overline{a_i}}(H)_i, \tag{3.48}$$

where $\hat{\overline{a_i}}$ are the decisions for $\overline{a_i}$. The process of linear nulling, decision rule and symbol cancelation is performed successively until all components of the $\overline{a}$ vector are recovered. Note that the sorting algorithm is performed each iteration and enhances system performance. For example, Wolniansky et al. have shown in [47] that ordering based on maximum SNR at each stage of the successive cancelation process yields optimal results. Reported results for the V-BLAST are summarized in the table 3.2.

Table 3.2: V-BLAST spectral efficiency: 8×8 antenna array architecture

BLAST Parameter	*Value*
Environment	Indoor
Coding	No
Modulation	16QAM
Training Sequence Overhead	20%
Bandwidth	30KHz
(n_T, n_R)	$(8, 8)$
Symbol Rate	24.3 Ksym/sec
SNR	25 dB
Block Error Rate	10^{-2}
Bit Error Rate	10^{-5}
Spectral Efficiency	26 [bps/Hz]
Net Data Rate	621 kbps

It is observed that over a narrowband channel of 30 KHz, net rate of 621 kbps is achieved using 8×8 antenna array architecture. This is an unprecedented bandwidth efficiency. Note

however that the SNR required to guarantee acceptable error rate of 10^{-5} is at the order of 25 dB. Chapter 8 proposes two novel schemes that apply iterative processing principles and channel coding to improve the poor energy efficiency of BLAST detectors.

3.3.2 D-BLAST Architecture

The D-BLAST architecture, proposed originally by Foschini in [48], is presented next. The encoding process is illustrated in Figure 3.9.

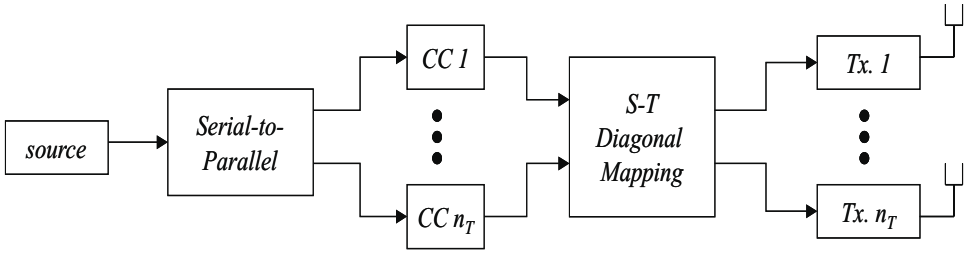

Figure 3.9: D-BLAST encoder structure

The information bit stream is first vertically mapped (serial-to-parallel converter) to produce n_T substreams which are encoded by parallel constituent codes (CC). Each codeword is layered in diagonals in space-time such that the output symbols from the kth CC are transmitted from transmit antennas $1, 2, \cdots, n_T$ in turns. The corresponding decoder can be either a hard-decision feedback decoder or a soft-decision feedback decoder with iterative processing. A hard decision decoder for D-BLAST is shown in Figure 3.10.

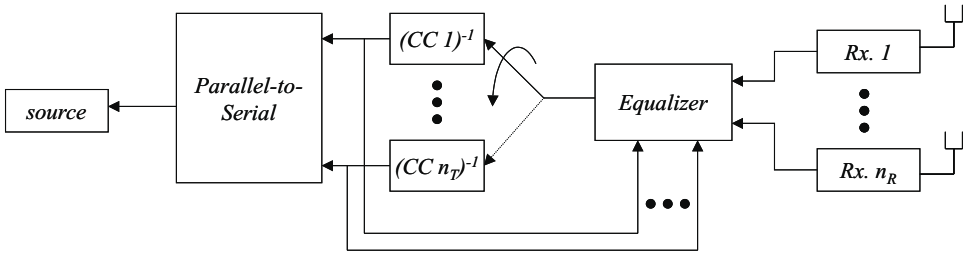

Figure 3.10: D-BLAST hard-decision decoder structure

Similarly to the detection of V-BLAST, channel estimation is followed by sorting algorithm and linear nulling (equalization) to produce decision statistics for the ith transmitted scheme. In D-BLAST, the equalizer generates decision statistics for the first diagonal. Based on these decision statistics, the first CC decoder decodes the diagonal, which is fed back in order to successively cancel its contribution from the received signal. In an inductive manner, the next diagonal is equalized and sent to the second CC decoder for decoding.

The complexity of this decoder is quadratic with the number of elements at the transmitter, which is low compared to the ML decoder complexity.

A second approach to detect D-BLAST type encoders is by exchanging soft decision between the nulling processing (equalizer) and the decoding stage in an iterative manner [49]. Block diagram for iterative decoding of D-BLAST is given in Figure 3.11. Since the

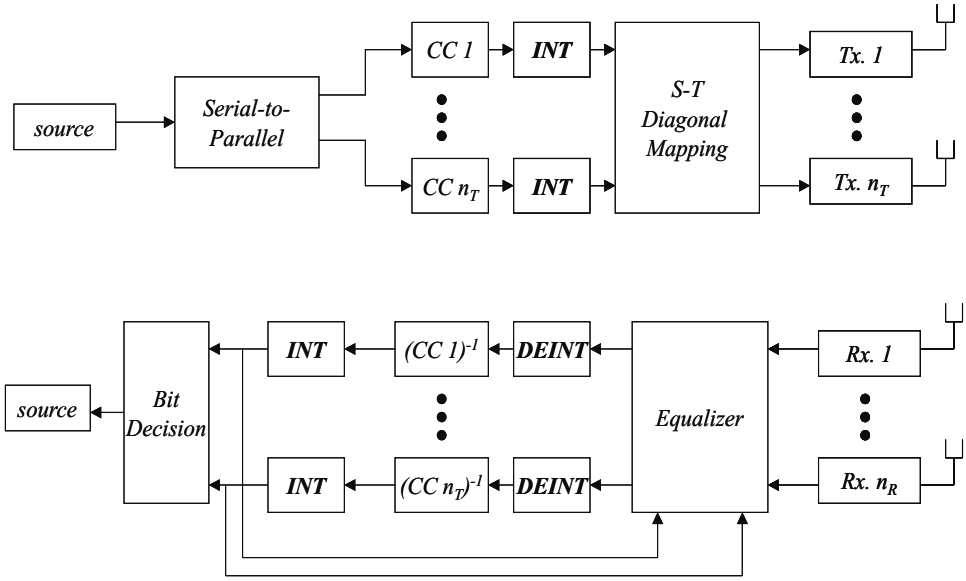

Figure 3.11: D-BLAST encoder-decoder structure with iterative decoding

encoder and the channel are viewed as a serially concatenated code, the equalization and decoding stages exchange soft decision information in an iterative manner to improve the reliability of the nulling and decoding process.

3.4 Chapter Summary

Fundamentals of space-time coding techniques were introduced in this chapter. The encoding-decoding mechanisms of space-time trellis codes were described followed by performance analysis and code design criteria. The two design criteria are the rank criterion, corresponding to maximization of diversity advantage and the determinant criterion, corresponding to maximization of coding gain. Decoder complexity was addressed and shown to increase exponentially with spectral efficiency.

The class of space-time block coding was shown to be a simple transmit diversity mechanism that achieves the same diversity advantage of maximal ratio combining (MRC). STBC is composed of three stages: encoding procedure which is based on orthogonal design, a combining procedure in time domain that decouples the symbols associated with the received superposition and a symbol-by-symbol ML detection rule. Orthogonal designs for more than two antenna elements at the transmitter were presented. Differential STBC was introduced as an option for transmit diversity scheme that does not require explicit knowledge of CSI and is robust to carrier recovery mismatch.

Finally, the BLAST architecture was presented, achieving high data rates using multiple antenna array technology. Armed with the fundamentals of space-time coding techniques, the next six chapters of this dissertation introduce original contributions to the theoretical and practical aspects of STTC, STBC, and BLAST architectures.

Chapter 4

STTC: Code Structure and Bit-Error Probability Analysis

The application of coded modulation to multiple antenna elements requires the development of effective analytical tools for the calculation of the error probabilities of these schemes. In this chapter, analytic tools that were widely used in the area of Trellis-Coded Modulation are shown to be applicable to STTC. Examples include the Calderbank-Mazo (CM) algorithm, transfer function bounding techniques and truncation of the union bound. As will be seen in the sequel, certain modifications are needed to support the transmit-receive diversity mechanisms of STTC.

A main building block for this analysis is the Pair-Wise Error Probability (PWEP), which can be used in the derivation of the upper (union) bound on the bit or frame error probabilities of the coded scheme. The design of STTC has so far been based on optimizing the worst case PWEP [18, 30]. This analysis led to the so-called rank criterion (to insure diversity) and the determinant criterion (to maximize coding gain) for designing and/or searching for good space-time codes. Since most of the STTC obtained are hand-crafted, it is necessary to find a systematic approach that translates the trellis diagrams into closed analytic forms. The Calderbank-Mazo algorithm [50], is applied to STTC to create the generator matrix of the code using simple linear algebra computations [51]. Using this generator matrix representation, an extensive computer search can be performed to find the best space-time trellis codes according to the rank/determinant criteria [52].

It is noted, however, that designing STTC solely based on optimizing the worst case PWEP does not necessarily result in superior performance. Rather, it is important to develop performance analysis tools that take into account all or at least dominant PWEPs.

This chapter provides an original derivation of analytical performance results for the bit-error probability of Space-Time Trellis Codes (STTC), operating over Rayleigh, Rician and correlated fading channels. In the uncorrelated fading case, the Generating[1] Function Technique (GFT) is applied, taking into consideration all PWEPs of the code [53]. Similar work was reported in [54], where the "distance spectrum" of the STTC is computed, enumerating product measures across error events, weighted by the relative frequency of their occurrence. Since these bounding techniques are based on the error-state diagram of the code, codes with high number of states require reduced state techniques [55]. Analytic results show that in the Rayleigh case, bit-error probability is inversely proportional to the lth power of E_b/N_0, where l corresponds to the diversity advantage of the scheme. In the Rician case, we vary the specular-to-diffuse component ratio, from one extreme case (dominant diffuse component, Rayleigh fading) to the other extreme (dominant specular component, Line-of-Sight case). Results indicate that as the channel tends towards AWGN, BER decreases exponentially with E_b/N_0. Also, upper bounds are shown to be as tight as 2 dB to simulated performance. In the correlated fading case, bit-error probability is derived by determining an upper bound on the PWEP of dominant short error events [56]. Bit-error probability is approximated by a truncation of the infinite series used in calculating the union bound. Through simulations, we show that this approximation is valid for high signal to noise ratios, as short error events determine the diversity advantage as well as the coding gain of the scheme. Various cross-correlation coefficients for the fading channels are considered, representing the limited physical separation across transmit antenna elements. Both analytic and simulation results indicate that for cross-correlation coefficient values less than 0.75, the diversity advantage is still maintained and proportional to the number of antenna elements, while coding gain is penalized by less than 1.5 dB.

In determining the PWEP itself, two main approaches were proposed in the literature. The first one, used in this chapter, is based on the computation of the Chernoff bound. The second, used in [57] and [58], applies the moment-generating function (MGF) and residue methods, respectively, to determine an exact value of the PWEP. A comprehensive treatment of the derivation of exact PWEP over fading channels is addressed in [59].

This chapter is organized as follows. Section 4.1 presents the application of the CM algorithm to STTC. Section 4.2 applies the transfer function bounding technique to STTC in independent Rayleigh and Rician fading channels. In section 4.3, performance analysis of STTC operating over correlated Rayleigh fading channels is carried out, based on truncation of the union bound.

[1] also known as the enumerating or transfer function

4.1 Code Structure

4.1.1 The Calderbank-Mazo (CM) Algorithm

A trellis code can be seen as a "sliding window" method of encoding binary data stream to sequence of channel input symbols. Trellis code is a real valued function of n bits that are composed of k current input bits and $\nu = n - k$ state bits. Formally

$$f_j = f(a_1, a_2, \ldots, a_n), \tag{4.1}$$

where $n = k + \nu$, $(a_1, a_2, \ldots, a_k)$ are the current input bits and $(a_{k+1}, \ldots, a_n)$ are the ν preceding bits. $a_i \in \{0, 1\}$ and f_j is an M-ary constellation symbol. It was shown in [50] that any real valued function can be written as a sum of products of a_i:

$$f(a_1, \ldots, a_n) = k_0 + \sum_{i=1}^{n} k_i a_i + \sum_{i,j=1, j>i}^{n} k_{ij} a_i a_j + \cdots + k_{12\ldots n} a_1 a_2 \ldots a_n. \tag{4.2}$$

There are $\sum_{i=0}^{n} \binom{n}{i} = 2^n$ coefficients for this expansion. These coefficients will be determined according to the values that $f(a_1, a_2, \ldots, a_n)$ can take, which correspond to the M-ary channel symbols described to the left of the trellis diagram. As described in [50], the coefficients may be determined iteratively as follows. First, set all of the bits a_i to be zero and obtain $k_0 = f(0, 0, \ldots, 0)$. Next, evaluate the function n times when only one $a_i = 1, i = 1, \ldots, n$ and the rest are set to zero, to obtain n first order coefficients. Continuation of this process determines all 2^n coefficients.

For trellis codes, it is more convenient to use $\{\pm 1\}$ representation of binary data rather than $\{0, 1\}$ representation. Substituting the simple transformation $a_i = [\frac{1-b_i}{2}]$ to (4.2) yields

$$f(b_1, \ldots, b_n) = \tilde{k}_0 + \sum_{i=1}^{n} \tilde{k}_i b_i + \sum_{i,j=1, j>i}^{n} \tilde{k}_{ij} b_i b_j + \cdots + \tilde{k}_{12\ldots n} b_1 b_2 \ldots b_n. \tag{4.3}$$

Note that there is a different set of coefficients after this transformation. Equation (4.3) can be written in a vector-matrix form. Let f denote a column vector whose 2^n components are all possible values that f can take(according to all combinations of input and state bits). Next, let $\tilde{K}$ be the vector of the unknown coefficients. Finally, let B be an $2^n \times 2^n$ matrix where each row represents the 2^n values of all the products of the n-tuple bits: $[b_1, b_2, \ldots, b_n]$. That is, a given row of B is described by

$$B = [1, b_1, b_2, \cdots, b_n, b_1 b_2, b_1 b_3, \cdots, b_1 b_n, \cdots, \prod_{i=1}^{n} b_i]. \tag{4.4}$$

It can be verified that B is a Hadamard matrix. That is, the rows (and columns) of B are orthogonal, and $BB^T = 2^n I$ where the superscript T denotes transpose and I is a $2^n \times 2^n$

identity matrix. Then, Eq. (4.3) can be written in matrix form as:

$$f = B\tilde{K}, \tag{4.5}$$

and thus

$$\tilde{K} = B^{-1}f = \frac{1}{2^n}B^T f. \tag{4.6}$$

An appropriate interpretation of the last equation is that $\tilde{K}$ is the Hadamard transform of the vector f. Thus, for a given trellis diagram, a simple computer program can perform the above matrix algebra computations to derive the coefficients $\tilde{K}$ and yield the closed analytic form of the code. One last remark must be made. After determining $\tilde{K}$ we need to derive the original set of coefficients K, which corresponds to the original binary data over $\{0, 1\}$. We will substitute the linear transformation $b_i = 1 - 2a_i$ to the analytic form in order to obtain the appropriate relationships between the trellis diagram and the analytic form.

4.1.2 STTC Generator Matrix Construction using the CM algorithm

In this section we present the application of the Calderbank Mazo algorithm to STTC via three examples, the $4, 8$ and 16 state STTC with 2 Tx antennas and QPSK signaling format.

• 4-state STTC, 2 Tx Antenna

We revisit the 4-state delay-diversity STTC with 2 transmit antennas that was described in section 3.1.4. The signal constellation is QPSK and thus the bandwidth efficiency is 2 [bps/Hz]. The trellis diagram for this code was given in Figure 4.1.

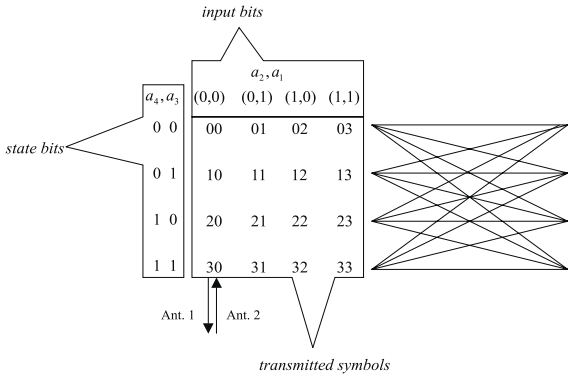

Figure 4.1: Trellis diagram of the 4-state delay diversity STTC, 2 Tx antennas, 2 [bps/Hz]

The Calderbank-Mazo algorithm for this code is performed as follows:

1. Apply the linear transformation $b_i = 1 - 2a_i$ on the input and state bits.

2. Evaluate the input-output (I/O) function from the trellis diagram. In this example, according to Figure 4.1, we have summarized the I/O function in the following table.

Input Bits		*State bits*		*Channel Symbols*	
b_2	b_1	b_4	b_3	f_1 {Antenna # 1}	f_2 {Antenna # 2}
-1	-1	-1	-1	0	0
-1	1	-1	-1	0	1
1	-1	-1	-1	0	2
1	1	-1	-1	0	3
-1	-1	-1	1	1	0
-1	1	-1	1	1	1
1	-1	-1	1	1	2
1	1	-1	1	1	3
-1	-1	1	-1	2	0
-1	1	1	-1	2	1
1	-1	1	-1	2	2
1	1	1	-1	2	3
-1	-1	1	1	3	0
-1	1	1	1	3	1
1	-1	1	1	3	2
1	1	1	1	3	3

Figure 4.2: I/O function of trellis diagram

The channel symbols, $f_i, i = \{1, 2\}$, can be written in matrix form

$$f = \begin{bmatrix} 0\,0\,0\,0\,1\,1\,1\,1\,2\,2\,2\,2\,3\,3\,3\,3 \\ 0\,1\,2\,3\,0\,1\,2\,3\,0\,1\,2\,3\,0\,1\,2\,3 \end{bmatrix}, \tag{4.7}$$

where the $1st$ and $2nd$ rows contain the M-ary symbols of antenna 1 and antenna 2, respectively.

3. Build the Hadamard matrix, B, with dimensions 16×16 ($n = 4$) by creating the appropriate products of the b_i

4. Derive the vectors of the desired coefficients ,$\tilde{K}$, by computing Equation (4.6) and then transform to $\{0, 1\}$ bits to obtain K:

$$K = \begin{bmatrix} 0\,0\,2\,1\,0\,0\,0\,0\,0\,0\,0\,0\,0\,0\,0\,0 \\ 2\,1\,0\,0\,0\,0\,0\,0\,0\,0\,0\,0\,0\,0\,0\,0 \end{bmatrix}. \tag{4.8}$$

5. The closed analytic form for the code are described by

$$\begin{aligned} x_t^2 &= 2a_2(t) + a_1(t), \\ x_t^1 &= 2a_4(t) + a_3(t), \end{aligned} \tag{4.9}$$

Therefore, the generator matrix of the code is

$$G = \begin{bmatrix} 2 & 1 & 0 & 0 \\ 0 & 0 & 2 & 1 \end{bmatrix}^T. \tag{4.10}$$

Once the closed analytic form was obtained, the implementation of the encoder, shown in Figure 4.3, is straightforward.

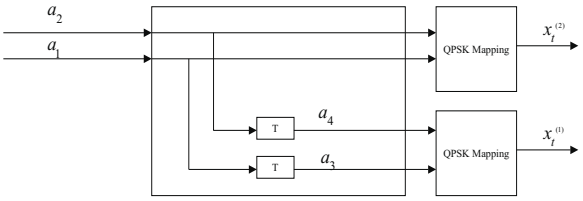

Figure 4.3: Encoder block diagram of the 4-state STTC, 2 Tx antennas, 2 [bps/Hz]

Note that in this example the encoding procedure and the mapping to M-ary symbols are performed together in a single step, where the addition in Equation (4.9) takes place over Z_4. This closed analytic form is found to be more tractable than the original trellis diagram, as it enables a systematic search for codes with maximum coding gain (the determinant criterion) in conjunction with full diversity gain (rank criterion).

• **8-state STTC, 2 Tx Antenna**

The 8-state trellis STTC is given in Figure 4.4.

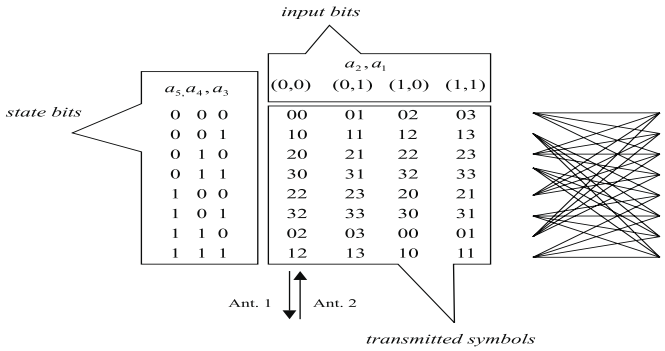

Figure 4.4: Trellis diagram of the 8-state STTC, 2 Tx antennas, 2 [bps/Hz]

Using the same technique, the appropriate closed analytic forms that describe this code are:

$$\begin{aligned} x_t^2 &= 2a_5 + 2a_2 + a_1 = 2(a_5 + a_2) + a_1, \\ x_t^1 &= 2a_5 + 2a_4 + a_3 = 2(a_5 + a_4) + a_3, \end{aligned} \tag{4.11}$$

which corresponds to the following generator matrix:

$$G = \begin{bmatrix} 2 & 2 & 1 & 0 & 0 \\ 2 & 0 & 0 & 2 & 1 \end{bmatrix}^T. \tag{4.12}$$

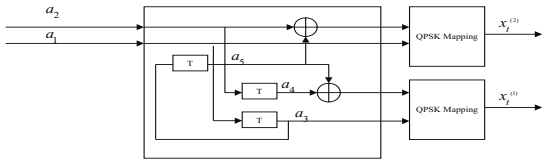

Figure 4.5: Encoder block diagram of the 8-state STTC, 2 Tx antennas, 2 [bps/Hz]

The encoder block diagram is drawn in Figure 4.5.

• **16-state STTC, 2 Tx Antenna**

The 16-state trellis STTC is given in Figure 4.6.

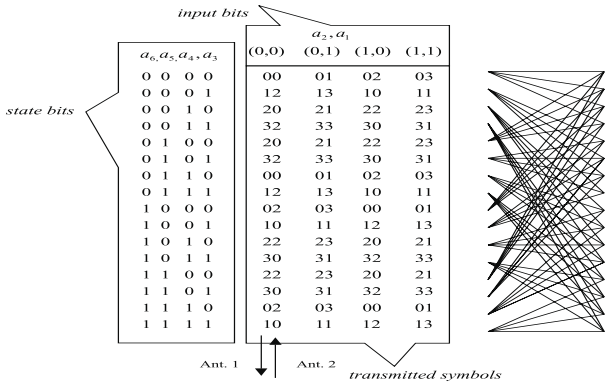

Figure 4.6: Trellis diagram of the 16-state STTC, 2 Tx antennas, 2 [bps/Hz]

The closed analytic forms are:

$$\begin{aligned} x_t^2 &= 2a_6 + 2a_3 + 2a_2 + a_1 = 2(a_6 + a_3 + a_2) + a_1, \\ x_t^1 &= 2a_5 + 2a_4 + a_3 = 2(a_5 + a_4) + a_3, \end{aligned} \tag{4.13}$$

Therefore, the generator matrix is:

$$G = \begin{bmatrix} 0 & 2 & 2 & 1 & 0 & 0 \\ 2 & 0 & 0 & 2 & 2 & 1 \end{bmatrix}^T, \tag{4.14}$$

and the encoder block diagram is drawn in Figure 4.7.

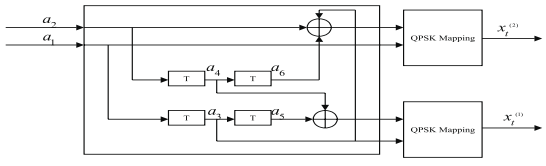

Figure 4.7: Encoder block diagram of the 16-state STTC, 2 Tx antennas, 2 [bps/Hz]

4.1.3 The Rank and Determinant Criterion: Re-evaluation

The closed analytic form can be used in the evaluation process of the rank and determinant criterion of STTC. For the 4 state code described in previous subsection, the difference matrix can be written as:

$$B(c,e) = \begin{bmatrix} e_1^1 - c_1^1 & e_2^1 - c_2^1 & \cdots & e_l^1 - c_l^1 \\ e_1^2 - c_1^2 & e_2^2 - c_2^2 & \cdots & e_l^2 - c_l^2 \end{bmatrix} \tag{4.15}$$

The minimum rank of this matrix over all possible codewords determines the diversity advantage of the system. Assuming QPSK modulation, we can express the entries of the difference matrix as:

$$\begin{aligned} c_t^k &= \exp(j * \pi/2 * 0) = j^0 = 1, \\ e_t^k &= \exp(j * \pi/2 * x_t^k) = j^{x_t^k}. \end{aligned} \tag{4.16}$$

For the 4-state delay-diversity example in previous subsection, substituting the closed analytic form of Equation (4.9) yields

$$\begin{aligned} e_t^2 &= j^{2a_2(t)+a_1(t)}, \\ e_t^1 &= j^{2a_4(t)+a_3(t)}, \end{aligned} \tag{4.17}$$

where $\{a_1(t), a_2(t)\}$ and $\{a_3(t), a_4(t)\}$ are the input and state bits, respectively, at time t. Recall that at time $t = 0$ (diverging from state 0 in the trellis) the state bits are zero, thus $e_t^1 = c_t^1 = 1$ or $e_t^1 - c_t^1 = 0$ while $e_t^2 - c_t^2 \neq 0$. At time $t = l$ (merging to state 0 in the trellis) the input bits are zero and therefore $e_t^2 = c_t^2 = 1$ or $e_t^2 - c_t^2 = 0$ while $e_t^1 - c_t^1 \neq 0$. Thus, the two rows of the difference matrix are linearly independent, corresponding to full rank or maximum diversity advantage.

As described in section 3.1.4, in order to evaluate the determinant criterion, we need to find codewords $\{c, e\}$, which minimize the determinant in Equation (3.15). By substituting the algebraic description of this code, given in Equation (4.9), we can generate 2^n distinct matrices for any combination of k input bits and ν state bits. We call these matrices the branch matrices as for each branch in the trellis there is a corresponding matrix. Then, we find the path in the trellis with the minimum determinant of the cumulative branch matrix. This is the determinant, which determines the coding gain of the scheme. Applying the described approach produces determinants of 4,12 and 20 for the $4, 8$ and 16 state codes, respectively.

To summarize, a systematic approach for the translation of the trellis diagrams of STTC to closed analytic forms is done by applying the Calderbank-Mazo algorithm to STTC. We

have shown the simplicity in using this technique in order to determine the block diagram of the space-time trellis encoder. In practice, for a given trellis diagram of STTC, a computer program using simple matrix algebra can be used to calculate the coefficients of the algebraic description. In addition, for a given diversity advantage (number of transmit and receive antenna fixed), it is possible to use these forms to perform a systematic code search in order to maximize the coding gain (determinant criterion).

4.2 Upper Bounds using Generating Function Techniques

Generating Function Techniques (GFT) have been extensively used in the performance analysis of convolutional codes [60], and trellis codes [61, 62, 63, 64], for AWGN, Rayleigh and Rician channels. The generating function enumerates the distance of any incorrect path (as compared with the correct path) in each step of the Viterbi decoding algorithm to form a closed form description for the distance profile of the code. This function is usually denoted by $T(D, L, I)$ where D, L &I correspond to arbitrary variables whose powers represent the distance between codewords, the length in trellis transitions and the distance between information bits, respectively.

In applying GFT to STTC we restrict ourselves to the class of geometrically uniform STTC [18]. To quote Forney and Slepian [65], a geometrically uniform code is a code that "has the same distance profile from any codepoint" or "the maximum likelihood decision regions are all congruent". As an illustration, consider a two-dimension signal space, with either M-ary PSK or QAM modulation as described in Figure 4.8. In the M-PSK case, all

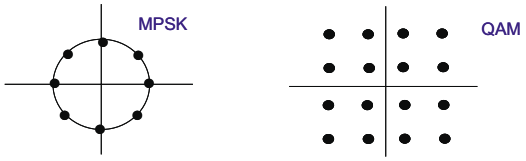

Figure 4.8: Geometric uniformity

symbols in the alphabet "see" the same distance profile to all other symbols. However, in a QAM signal constellation, the distance profile seen is different and is a function of the reference symbol. Extending this concept to codespace, a geometrically uniform code is a code where the probability of error is not a function of the transmitted codeword and therefore we can assume, without any loss of generality, that the all-zero codeword was transmitted. All other codewords are referred to as error events. This enables us to form the modified state diagram of the code with the same number of states as the original code trellis. For codes that are not geometrically uniform, the derivation of the generating

function is cumbersome as all possible transmitted sequences in the code trellis must be considered. Fortunately, most of the proposed STTC in the literature have been shown to be geometrically uniform.

The label of each branch in the modified state diagram is conditional upon the fade coefficients and therefore an averaging over the Rayleigh or Rician pdf is required. We assume a memoryless channel (infinite depth interleaving) to allow an averaging on a per branch basis. The averaged generating function, denoted by $\overline{T(D, L, I)}$, is differentiated with respect to I (App. C) to yield an upper (union) bound on the bit error probability.

As examples, we consider 4 and 8 state STTC with 2 transmit antenna elements and 1 or 2 receive antenna elements. Analytic results show that the bit-error probability is inversely proportional to the lth power of E_b/N_0, where l corresponds to the diversity advantage of the scheme. Moreover, comparing analysis and simulation results, we conclude that these analytic results are within 2 dB of the performance of STTC in Rayleigh and Rician fading channels.

The system model is described in Figure 4.9. The information bit stream is partitioned

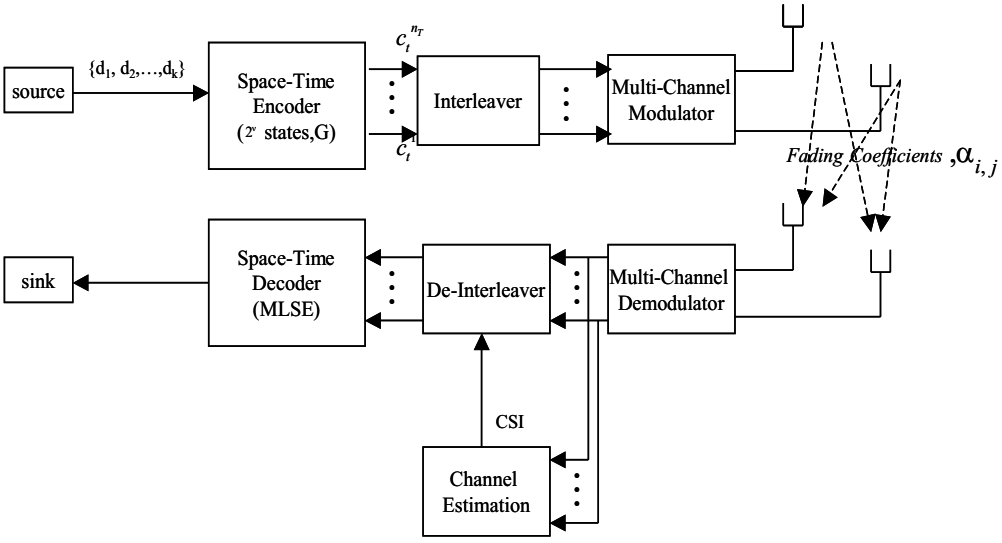

Figure 4.9: STTC system model with interleaving

into blocks of k information bits. Each block is encoded by a 2^ν state space-time encoder with generator matrix G to create n_T symbols that are transmitted simultaneously from n_T transmit antennas. The space-time encoder is followed by a block interleaver (which breaks up channel burst errors) and a multi-channel modulator. It is important to note that interleaving is performed according to an identical rule for all transmit antennas such that the rank criterion is not affected [66].

The channel is modeled by an $n_T \times n_R$ matrix $\Omega = [\alpha_{i,j}]$, whose entry $\alpha_{i,j}$ represents the complex fade coefficient for the path from transmit antenna i to receive antenna j. These fade coefficients are assumed to be independent complex Gaussian random variables with possibly nonzero complex mean (to support the case of Rician fading) and variance 0.5 per dimension. The received signal at each receive antenna is a linear superposition of the simultaneously transmitted symbols (with fade coefficients as weights) corrupted by AWGN. The receiver front end is composed of an array of n_R receive antenna elements. The processing at the receiver includes channel estimation of the fade coefficients followed by de-interleaving and Maximum Likelihood Sequence Estimation (MLSE) decoder, which computes the lowest accumulated squared Euclidean distance metric to extract the most likely transmitted sequence.

In order to simplify the analysis, the following assumptions are made. First, we assume perfect knowledge of CSI at the receiver. Second, an ideal interleaver (with infinite depth) is assumed such that the channel is memoryless and thus an averaging (with respect to Rayleigh or Rician pdf) on a per branch basis (of the modified state diagram) is made possible. Third, a flat fading channel is assumed such that no channel-induced ISI term is present.

Branch labels of the modified state diagram contain information about the squared Euclidean distance between multiple symbols associated with trellis transitions and the corresponding Hamming distance between information bits. Thus, it provides insight to follow the operation of the MLSE decoder, which evaluates branch metrics and accumulates those metrics to decide in favor of the most likely transmitted sequence. In the next section, we derive the branch label of the modified state diagram of the code, average it with respect to Rayleigh or Rician pdf and incorporate the result into the generating function, which is differentiated to obtain an upper (union) bound on the bit-error probability of the scheme.

4.2.1 Performance Analysis

The branch label of the modified state diagram is described by

$$a(D, I) = I^{n_d} D^{d^2(c_t, e_t|\alpha_{i,j})}, \tag{4.18}$$

where c_t corresponds to the transmitted set at time t of n_T all-zero symbols, e_t corresponds to the erroneously decided set of n_T coded symbols, n_d is the Hamming distance (between information bits) and $d^2(c_t, e_t|\alpha_{i,j})$ is the conditional squared Euclidean distance between the two sets.
The signal received at antenna $j, j = 1, 2, \ldots, n_R$, is modeled by

$$r_t^j = \sum_{i=1}^{n_T} \alpha_{i,j} c_t^i + \eta_t^j, \tag{4.19}$$

where η_t^j denotes the AWGN term and is modeled as independent samples of a zero mean complex Gaussian random variable with variance $N_0/2$ per dimension.

The branch metric of the MLSE decoder is based on the squared Euclidean distance between the received signal and each candidate set of n_T transmitted symbols, denoted $e_t^i, i = 1, 2, \ldots, n_T$. Assuming perfect knowledge of CSI at the receiver, this metric is given by

$$\sum_{j=1}^{n_R} \left| r_t^j - \sum_{i=1}^{n_T} \alpha_{i,j} e_t^i \right|^2. \tag{4.20}$$

Note that the receive diversity here takes the form of equal gain combining. Combining (4.19) and (4.20), we write the conditional squared Euclidean distance between trellis branch sets at time t as

$$d^2(c_t, e_t|\alpha_{i,j}) = \sum_{j=1}^{n_R} \left| \sum_{i=1}^{n_T} \alpha_{i,j} (c_t^i - e_t^i) \right|^2. \tag{4.21}$$

Note that the expression in (4.21) is a sum of quadratic forms as both squared terms associated with an individual transmit antenna and cross terms associated with products across various transmit antenna elements are present. Matrix representation of this sum of quadratic forms is given by

$$d^2(c_t, e_t|\alpha_{i,j}) = \sum_{j=1}^{n_R} \Omega_j^\dagger A \Omega_j, \tag{4.22}$$

where Ω_j is defined as the jth column of the channel matrix Ω, $\Omega_j^\dagger = \overline{\Omega_j^T}$ (conjugate transpose) and A is $n_T \times n_T$ branch distance matrix whose (p, q) element is given by

$$A_{pq} = (c_t^p - e_t^p)\overline{(c_t^q - e_t^q)}. \tag{4.23}$$

Note that A is Hermitian and therefore it is diagonalizable. Thus, using the principle axis theorem [38], we perform the following change of coordinates:

$$\beta_j = (\beta_{1,j}, \ldots, \beta_{n_T,j})^T = U^\dagger \Omega_j, \tag{4.24}$$

where U is the unitary matrix which diagonalizes A. The linear transformation with an orthonormal matrix U, described in (4.24), preserves the statistical properties of the fade coefficients such that if Ω_j is assumed to be a non-zero mean uncorrelated complex Gaussian random vector with variance 0.5 per dimension, so is β_j. This change of coordinates transforms the quadratic form into a standard form without cross terms. That is given by

$$d^2(c_t, e_t|\alpha_{i,j}) = \sum_{j=1}^{n_R} \beta_j^\dagger \Lambda \beta_j = \sum_{j=1}^{n_R} \sum_{i=1}^{n_T} \lambda_i \left|\beta_{i,j}\right|^2, \tag{4.25}$$

where Λ is the diagonal matrix with eigenvalues of A in its diagonal.

We can now substitute the result in (4.25) into (4.18) to obtain the following expression for the branch label

$$a(D, I) = I^{n_d} D^{\sum_{j=1}^{n_R} \sum_{i=1}^{n_T} \lambda_i |\beta_{i,j}|^2}. \tag{4.26}$$

Recall from [42] that $D = e^{-\gamma} = e^{-E_s/4N_0}$ where E_s and $N_0/2$ represent the symbol energy and the noise variance per dimension, respectively.

According to the memoryless channel assumption, we can average the branch label of (4.26) with respect to the distribution of $|\beta_{i,j}|$.

A. Rayleigh Channel

Averaging (4.26) with respect to Rayleigh pdf, we obtain:

$$\overline{a(D, I)} = I^{n_d} \prod_{i=1}^{n_T} (1 + \gamma \lambda_i)^{-n_R}. \tag{4.27}$$

Note that the averaged branch label is a function of the number of antenna elements in both ends of the link, the signal-to-noise ratio (γ), the eigenvalues of the A matrix and the number of information bits in error.

B. Rician Channel

Rician fading channel arises from the presence of a specular component in addition to the diffuse component. The Rician pdf of a random variable r is nonzero for $r \geq 0$ and is given by

$$f(r) = 2(1 + K) r \exp\left[-K - r^2(1 + K)\right] I_0\left[2r\sqrt{K(1 + K)}\right], \tag{4.28}$$

where K denotes the ratio of specular-to-diffuse component. Note that $K \to 0$ corresponds to the case of negligible specular component which corresponds to a Rayleigh fading, and $K \to \infty$ corresponds to the case of dominant specular component and thus an AWGN channel. $I_0(x)$ is the zero-order modified Bessel function of the first kind.
Averaging (4.26) with respect to Rician pdf of (4.28), we obtain:

$$\overline{a(D,I)} = I^{n_d} \prod_{i=1}^{n_T} \left[\frac{(1+K)}{(1+K+\gamma\lambda_i)} D^{\frac{\lambda_i K}{(1+K+\gamma\lambda_i)}} \right]^{-n_R}. \tag{4.29}$$

The average branch label in Eq. (4.27) and Eq. (4.29) for Rayleigh and Rician channels, respectively is incorporated into the modified state diagram, so that the averaged transfer function of the code, denoted $\overline{T(D,L,I)}$, is derived. This average transfer function is then differentiated with respect to I [42] to obtain the desired bit-error probability upper bound

$$P_b \leq \frac{1}{2n} \frac{\partial \overline{T(D,L,I)}}{\partial I}\bigg|_{I=1, D=e^{-E_s/4N_0}}. \tag{4.30}$$

The above procedure is illustrated by example in the following section. A step-by-step summary is provided here.

For a given geometrically uniform STTC with n_T transmit antenna elements, n_R receive antenna elements, 2^ν state and encoder matrix G:

1. Form the modified state diagram of the code.
2. Evaluate the matrix A per trellis branch.
3. Compute the corresponding eigenvalues $\lambda(A)$.
4. Label the modified state diagram with the averaged branch labels (Eq. (4.27),(4.29)).
5. Write the state equations to compute $\overline{T(D,L,I)}$.
6. Evaluate an upper bound for the code (Eq. (4.30)).

4.2.2 Case Study

As an example of the analysis technique, we consider STTC with 4 or 8 states, QPSK mapping, 2 transmit antenna elements and 1 or 2 receive antenna elements. The trellises of 4 and 8 state STTC with QPSK mapping are given in Figure 4.10. The corresponding modified state diagrams for the 4 state code is described in Figure 4.11.

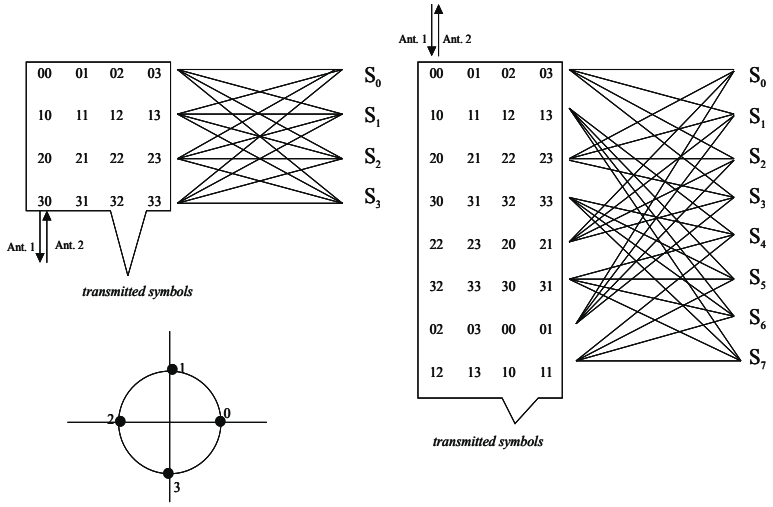

Figure 4.10: 4 and 8 state STTC, QPSK mapping

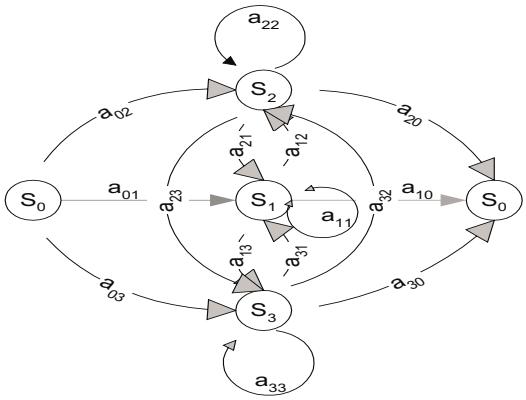

Figure 4.11: Modified state diagram of 4 state STTC

Following the derivation in section 4.2, we evaluate the hermitian matrix A on a per trellis branch basis and compute the corresponding eigenvalues. Next, we use Eq. (4.27) to find the average branch label of the modified state diagram with respect to Rayleigh pdf. These are described in table 4.1.

Table 4.1: Averaged branch labels of the modified state diagram in Figure 4.11

Transition	*Averaged Branch Label*
a_{01}	$\overline{a_{01}} = I(1+2\gamma)^{-n_R}$
a_{02}	$\overline{a_{02}} = I(1+4\gamma)^{-n_R}$
a_{03}	$\overline{a_{03}} = I^2(1+2\gamma)^{-n_R}$
a_{11}	$\overline{a_{11}} = I(1+4\gamma)^{-n_R}$
a_{12}	$\overline{a_{12}} = I(1+6\gamma)^{-n_R}$
a_{13}	$\overline{a_{13}} = I^2(1+4\gamma)^{-n_R}$
a_{21}	$\overline{a_{21}} = I(1+6\gamma)^{-n_R}$
a_{22}	$\overline{a_{22}} = I(1+8\gamma)^{-n_R}$
a_{23}	$\overline{a_{23}} = I^2(1+6\gamma)^{-n_R}$
a_{31}	$\overline{a_{31}} = I(1+4\gamma)^{-n_R}$
a_{32}	$\overline{a_{32}} = I(1+6\gamma)^{-n_R}$
a_{33}	$\overline{a_{33}} = I^2(1+4\gamma)^{-n_R}$
a_{10}	$\overline{a_{10}} = (1+2\gamma)^{-n_R}$
a_{20}	$\overline{a_{20}} = (1+4\gamma)^{-n_R}$
a_{30}	$\overline{a_{30}} = (1+2\gamma)^{-n_R}$

Assuming $\xi = [\xi_1 \ \xi_2 \ \xi_3]^T$ to be the state vector of the finite state machine of Figure 4.11, the state equations are given by

$$\begin{bmatrix} \xi_1 \\ \xi_2 \\ \xi_3 \end{bmatrix} = \begin{bmatrix} 1-\overline{a_{11}} & \overline{a_{21}} & \overline{a_{31}} \\ \overline{a_{12}} & 1-\overline{a_{22}} & \overline{a_{32}} \\ \overline{a_{13}} & \overline{a_{23}} & 1-\overline{a_{33}} \end{bmatrix} \begin{bmatrix} \overline{a_{01}} \\ \overline{a_{02}} \\ \overline{a_{03}} \end{bmatrix}, \tag{4.31}$$

and the averaged transfer function from state s_0 (input) to state s_0 (output) is given by

$$\overline{T(D,L,I)} = \overline{a_{10}}\xi_1 + \overline{a_{20}}\xi_2 + \overline{a_{30}}\xi_3. \tag{4.32}$$

Differentiating the averaged transfer function according to Eq. (4.30) yields the desired upper bound.

4.2.3 Analytic and Simulation Results

Figure 4.12 compares the derived upper bounds with Monte Carlo simulations.

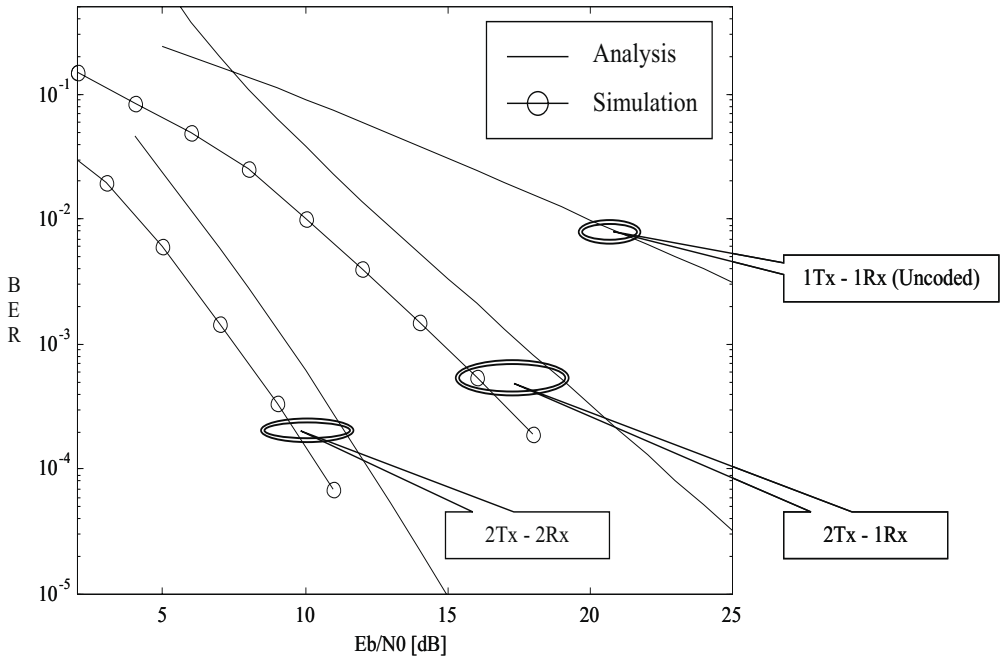

Figure 4.12: Error bounds for 4 state STTC over flat Rayleigh fading channel

It is observed that the upper bounds are inversely proportional to the lth power of E_b/N_0, as compared with the inverse linear dependence for the case of no diversity. This illustrates the diversity advantage, which is proportional to the number of antenna elements at both ends of the link and can be observed as the asymptotic slope of the error rate curves ($l = 1, 2, 4$ for 1Tx-1Rx, 2Tx-1Rx, 2Tx-2Rx, respectively). Furthermore, these bounds are as tight as 2 dB to the simulated performance of STTC over flat Rayleigh fading channel.

Next, we present results for the 8 state STTC with 2 transmit antenna elements and 1 or 2 receive antenna elements. The upper bounds, given in Figure 4.13, are again inversely proportional to the lth power of E_b/N_0 and are as tight as 2 dB to the performance of 8 state STTC over flat Rayleigh fading channel as observed by simulations. Comparing with results for the 4-state code, coding gain of 2 dB is observed.

The difference between the simulation results and the analytic bounds is attributed to the averaging process of the branch label with respect to the Rayleigh pdf. Similar gaps between simulation and analysis results were observed in bounding techniques of Trellis codes operating in Rayleigh fading environment [42].

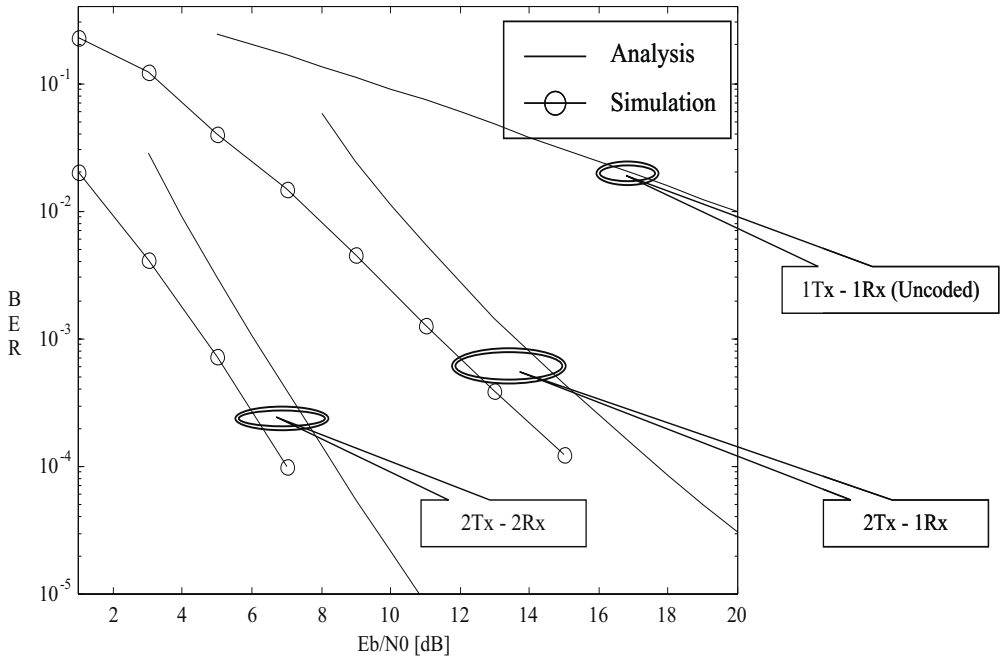

Figure 4.13: Error bounds for 8 state STTC over flat Rayleigh fading channel

Results are extended to support the case of a Rician fading channel. We use Eq. (4.29) in averaging the branch label with respect to the Rician pdf and evaluate the averaged transfer function. Figures 4.14 and 4.15 illustrate upper bounds for 4 state STTC, operating over Rician channel with various ratios of specular to diffuse component, for 1 and 2 receive antenna elements, respectively. It can be seen that as $K \to 0$, the channel tends towards the Rayleigh fading channel and therefore the error rate curves are inversely proportional to the lth power of E_b/N_0 ($l = 2, 4$ for 2Tx-1Rx, 2Tx-2Rx, respectively). However, as $K \to \infty$, the channel tends towards AWGN and therefore the error rate curves are exponentially decreasing with respect to E_b/N_0. Also, as a sanity check, it is noted that over AWGN channel, the 2Tx-2Rx scheme outperforms the 2Tx-1Rx scheme by 3 dB as expected from the additional receiver antenna gain.

It is noticed that the upper bounds become tighter to the simulated performance as the channel tends towards AWGN. The reason is that the averaging with respect to the Rician pdf in large specular-to-diffuse components ratios is equivalent to the case of no averaging (AWGN), which results in tighter upper bounds. A similar trend was also observed in [42] for MTCM operating over Rician fading channel.

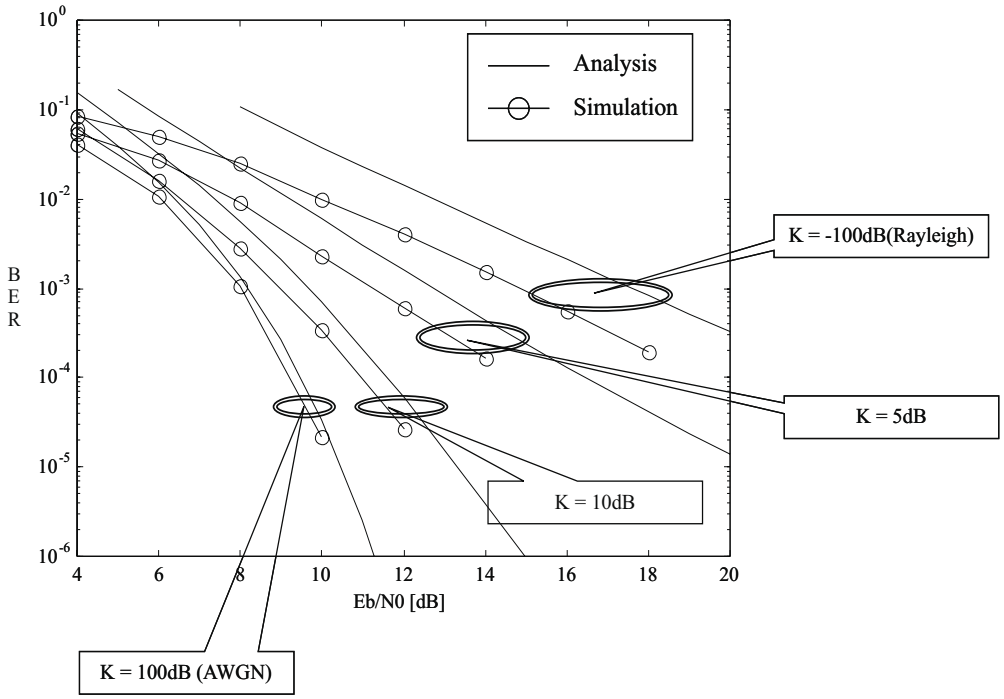

Figure 4.14: Error bounds for 4 state STTC, 2Tx-1Rx over Rician fading channel

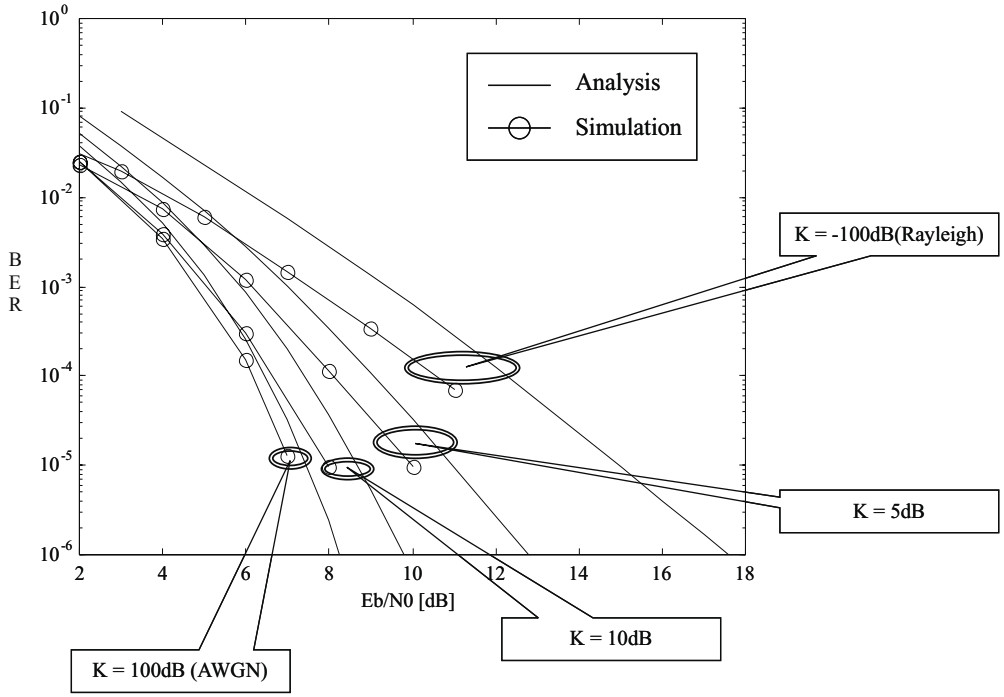

Figure 4.15: Error bounds for 4 state STTC, 2Tx-2Rx, over Rician fading channel

4.3 Performance Analysis in Correlated Fading Channels

Most of the work on STTC has assumed independence across fading paths. However, a legitimate practical question is to what extent independence among the fading paths is required to maintain the diversity advantage offered by STTC. The goal of this section is to answer this question in a quantitative manner. An analytic tool is developed to evaluate the expected degradation due to correlation among fading paths. Analytic results are confirmed with Monte Carlo simulations.

Our intuition suggests that the performance of the scheme is strongly determined by the occurrence of "deep fades" across the multiple paths. However, since these "deep fades" are rare probabilistic events, even high correlation across fading paths may not imply that the Rayleigh envelopes undergo simultaneous "fades". Thus, we expect that the effectiveness of transmit diversity offered by STTC may be maintained even when significant correlation exists. In fact, this result is demonstrated below.

The analysis includes evaluation of bit-error probability based on the Pair-Wise Error Probability (PWEP). The PWEP takes the form of a characteristic function of the pair-wise squared Euclidean distance. As will be shown in the sequel, this distance is a quadratic form of a zero mean Correlated Complex Gaussian Random Vector (CCGRV), with a certain covariance matrix. This allows us to find a closed form upper bound on the PWEP, which is shown to be a function of the number of antenna elements in both ends of the link, the signal-to-noise ratio, the code distance matrix and the covariance matrix of the fade coefficients. In evaluating the bit-error probability, we weight the PWEP with the corresponding Hamming distance for a small set of dominant short error events. Through simulations, we show that asymptotically, this approximation is valid as the short error events determine the diversity advantage as well as the coding gain of the scheme.

Unlike the work of Uysal and Georghiades in [67], where infinite depth interleaving was assumed, here a quasi-static channel model is used. Although both works indicate that the STC scheme is robust to spatial fading correlation, the nature of the analysis and results differ. While the authors in [67] have derived exact expression for the PWEP, we propose a systematic procedure to derive a closed form upper bound for the PWEP. This results in different bit-error probability approximations, especially asymptotically when the cross correlation factor ρ is driven toward 1. In our analytic results, the diversity advantage is eliminated (as one would expect) while in [67] a small amount of degradation (< 2dB) is observed. One can view the analytic bit-error probability result as a truncation of the infinite series of the generating function used in calculating the union bound.

As examples, we consider 4 and 8 state STTC with 2 transmit antenna elements and 1

or 2 receive antenna element. Various correlation coefficients among the fade coefficients, which represent the limited physical separation between transmit antenna elements, are considered.

The system model is described in Figure 4.16.

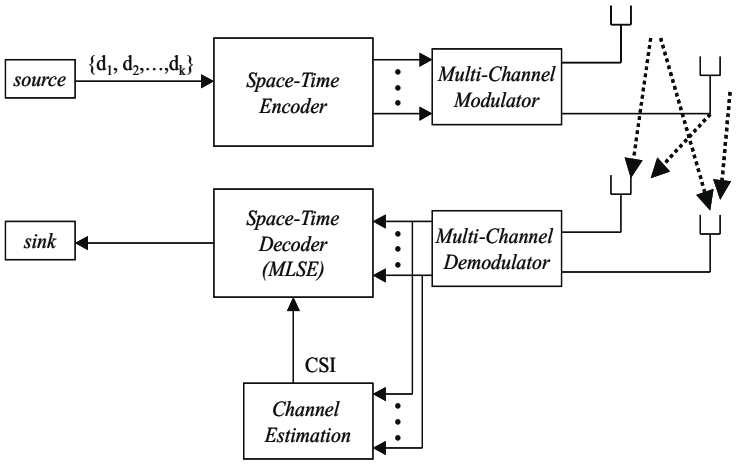

Figure 4.16: STTC system model

The channel is modeled by an $n_T \times n_R$ matrix $\Omega = [\alpha_{i,j}]$, whose entry $\alpha_{i,j}$ represents the quasi-static complex fade coefficient for the path from transmit antenna i to receive antenna j. For a given receive antenna j, the fade coefficients across multiple transmit antennas (the jth column vector of Ω) are assumed to be correlated complex Gaussian random variables with covariance matrix C. We focus on the effect of correlation across transmit antenna elements and thus assume that the fade coefficients across multiple receive antenna elements are uncorrelated. The received signal at each receive antenna is a linear superposition of the simultaneously transmitted symbols (with correlated fade coefficients as weights) corrupted by AWGN.

In simulating the channel, we adopt the procedure proposed in [68, 69], for generating equal power correlated Rayleigh fading envelopes. The procedure extends the classical Jakes model [70] by converting two uncorrelated Rayleigh envelopes to correlated ones with a given covariance matrix.

4.3.1 Performance Analysis

The pair-wise error probability of a maximum-likelihood receiver is well approximated by the Chernoff bound [42, 71, 37]

$$P(c \to e) = \overline{P(c \to e \mid \alpha_{i,j})} \leq \overline{\exp(-d^2(c,e|\alpha_{i,j})\gamma)}, \tag{4.33}$$

where c and e are the transmitted and erroneously decided sequences, respectively, the overbar indicates an expectation with respect to the fade coefficients, $\alpha_{i,j}$ and $\gamma = E_s/4N_0$, where E_s and $N_0/2$ represent the symbol energy and the noise variance per dimension, respectively.

The conditional squared Euclidean distance between codewords, denoted $d^2(c,e|\alpha_{i,j})$, can be written [18] as the following sum of quadratic forms:

$$d^2(c,e|\alpha_{i,j}) = \sum_{j=1}^{n_R} \Omega_j^\dagger A \Omega_j, \tag{4.34}$$

where Ω_j is defined as the jth column vector of the channel matrix Ω, and A is $n_T \times n_T$ code distance matrix whose (p,q) element is given by

$$A_{pq} = \sum_{t=1}^{l} (c_t^p - e_t^p)\overline{(c_t^q - e_t^q)}. \tag{4.35}$$

Note that A is a Hermitian matrix and therefore it is diagonalizable. Now, let us define Q_j as the jth quadratic form, such that

$$Q_j = \Omega_j^\dagger A \Omega_j. \tag{4.36}$$

Again, Ω_j is a $n_T \times 1$ *correlated* complex Gaussian random vector with covariance matrix C. Reformulating the result in [72, 7] (see Appendix **??**), which is based on Turin's Theorem [73], we can write the characteristic function of Q_j

$$\Phi_{Q_j}(t) = \overline{exp(itQ_j)} = \frac{1}{det(I_N - itCA)}, \tag{4.37}$$

where C is the covariance matrix of Ω_j, $i = \sqrt{-1}$ and I_N is an $N \times N$ identity matrix.

Substituting $it = -\gamma$ in Eq. (5.10) and summing over j, we obtain the characteristic function of the squared Euclidean distance

$$\Phi_{d^2}(\gamma) = \overline{exp(-d^2(c,e|\alpha_{i,j})\gamma)} = \frac{1}{[det(I_N + \gamma CA)]^{n_R}}. \tag{4.38}$$

Note that the fade coefficients across multiple receive antennas are assumed to be uncorrelated. It can be seen that the characteristic function of Eq. (4.38) is the desired pair-wise

error probability bound, defined in Eq. (4.33). Defining $W = CA$ in Eq. (4.38), the pair-wise error probability bound is simplified to

$$P(c \to e) \leq \prod_{i=1}^{n_T} (1 + \gamma\lambda_i)^{-n_R}, \tag{4.39}$$

where λ_i are the eigenvalues of $W = CA$.

The pair-wise error probability bound of (4.39) is a function of the number of antenna elements in both ends of the link (n_T, n_R), the signal-to-noise ratio (γ) the code distance matrix (A) and the covariance matrix (C) of the fade coefficients.

In order to obtain an upper bound for the averaged bit-error probability, one must evaluate the pair-wise error probability over all possible error events and plug the results into an upper (union) bound via classical transfer function techniques. Rather than performing the above tedious task, we restrict ourselves to a small set of dominant error events and show through simulations that in high SNR this approximation is valid, since the short error events determine the diversity advantage as well as the coding gain of the scheme. An approximation to the bit error probability is given by

$$P_b \approx \frac{1}{k} \sum_{n:L_n \leq N} m_n P(c_n \to e_n), \tag{4.40}$$

where $P(c_n \to e_n)$, m_n and L_n are the PWEP, Hamming distance and length of the nth error event, respectively. N denotes the maximum length of the encoding intervals to be considered and k is the number of information bits per encoding interval.

In fact, Eq. (4.40) represents a truncation of the infinite series used in calculating the union bound on the bit-error probability. The above procedure will be illustrated by example in the following section. A step-by-step summary is provided here.

For the nth dominant error event (shorter than N transitions) perform:

1. Evaluate the pair-wise code distance matrix A.
2. Evaluate the matrix W by multiplying the covariance matrix C with the code distance matrix A.
3. Compute the corresponding eigenvalues λ_i of W.
4. Evaluate an upper bound on the PWEP (Eq. (4.39)).
5. Compute m_n, the associated Hamming distance.
6. Weight the PWEP with the corresponding Hamming distances to obtain an approximation for the bit-error probability (Eq.(4.40)).

4.3.2 Case Study

As an example of the analysis technique, STTC with 4 or 8 state, QPSK modulation, 2 transmit antenna elements and 1 or 2 receive antenna elements are considered. The trellises of a 4 and 8 state STTC and the QPSK mapping were given in Figure 3.2.

In our error analysis, we identify all error events whose lengths are less than or equal to N encoding intervals. Table 4.2 summarizes the error events for the code in Figure 3.2 up to $N = 3$.

Table 4.2: The list of error events for the STTC in Figure 3.2; $N = 3$

nth Error Event	L_n	m_n	A
$S_0 \to S_1 \to S_0$	2	1	$\begin{bmatrix} 2 & 0 \\ 0 & 2 \end{bmatrix}$
$S_0 \to S_2 \to S_0$	2	1	$\begin{bmatrix} 4 & 0 \\ 0 & 4 \end{bmatrix}$
$S_0 \to S_3 \to S_0$	2	2	$\begin{bmatrix} 2 & 0 \\ 0 & 2 \end{bmatrix}$
$S_0 \to S_1 \to S_1 \to S_0$	3	2	$\begin{bmatrix} 4 & 2 \\ 2 & 4 \end{bmatrix}$
$S_0 \to S_1 \to S_2 \to S_0$	3	2	$\begin{bmatrix} 6 & 2-2i \\ 2+2i & 6 \end{bmatrix}$
$S_0 \to S_1 \to S_3 \to S_0$	3	3	$\begin{bmatrix} 4 & -2i \\ 2i & 4 \end{bmatrix}$
$S_0 \to S_2 \to S_1 \to S_0$	3	2	$\begin{bmatrix} 6 & 2+2i \\ 2-2i & 6 \end{bmatrix}$
$S_0 \to S_2 \to S_2 \to S_0$	3	2	$\begin{bmatrix} 8 & 4 \\ 4 & 8 \end{bmatrix}$
$S_0 \to S_2 \to S_3 \to S_0$	3	3	$\begin{bmatrix} 6 & 2-2i \\ 2+2i & 6 \end{bmatrix}$
$S_0 \to S_3 \to S_1 \to S_0$	3	3	$\begin{bmatrix} 4 & 2i \\ -2i & 4 \end{bmatrix}$
$S_0 \to S_3 \to S_2 \to S_0$	3	3	$\begin{bmatrix} 6 & 2+2i \\ 2-2i & 6 \end{bmatrix}$
$S_0 \to S_3 \to S_3 \to S_0$	3	4	$\begin{bmatrix} 4 & 2 \\ 2 & 4 \end{bmatrix}$

For each error event (with respect to the all-zero transmitted codeword), we evaluate the length of the error event L_n, the corresponding Hamming distances m_n and the associated Hermitian matrix A. Next, we evaluate the eigenvalues of the matrix $W = CA$, where C is

the normalized covariance matrix of the fade coefficients and is given by

$$C = \begin{bmatrix} 1 & \rho \\ \rho & 1 \end{bmatrix}. \tag{4.41}$$

Note that ρ is the cross-correlation coefficient across the two transmit antenna elements. Applying Eq. (4.39) for various cross-correlation coefficients $0 \leq \rho \leq 1$, we obtain upper bounds on the pair-wise error probabilities for the 4 state code over a correlated Rayleigh fading channel, and use these bounds in Eq. (4.40) to obtain the desired bit-error probability result.

4.3.3 Analytic and Simulation Results

Analytic results are plotted in Figure 4.17. It is observed that for $\rho \leq 0.75$, bit-error probability is inversely proportional to the quadratic and fourth power of E_b/N_0 for the 2Tx-1Rx and 2Tx-2Rx, respectively. This implies that the diversity advantage is still achieved and is proportional to the number of antenna elements. Furthermore, for $\rho \leq 0.75$, the observed degradation is less than 1.5 dB and can be interpreted as a penalty in coding gain rather than a loss of diversity order. Nevertheless, as ρ tends towards 1, the diversity advantage of the scheme is eliminated.

Next, we present results for the 8 state STTC with 2 transmit antenna elements and 1 or 2 receive antenna elements. The analytic results, presented in Figure 4.18, are again inversely proportional to the squared and fourth power of E_b/N_0 for the 2Tx-1Rx and 2Tx-2Rx, respectively, as long as $\rho \leq 0.75$.

Simulation results for the 4 and 8 state STTC, operating over correlated Rayleigh fading channels are provided to support our analytic results. Modeling of the channel requires construction of correlated fading envelopes with a given cross-correlation coefficient ρ. This is done by adopting the procedure proposed in [68, 69, 74] for generating N correlated Rayleigh fading envelopes. The procedure is summarized in Appendix E. The starting point is the desired covariance matrix of the Rayleigh envelopes. A look-up table is used to convert this covariance matrix to the covariance matrix of the complex Gaussian random variables. A Cholesky decomposition of this new covariance matrix, produces a lower triangular "coloring" matrix, which multiplies the uncorrelated complex Gaussian vectors to produce correlated ones with the desired covariance matrix. For detailed description of the algorithm see Appendix E.

Figure 4.19 presents the correlated Rayleigh envelopes for two extreme cases of cross-correlation coefficient. In the upper subplot, the Rayleigh envelopes appear to be uncorre-

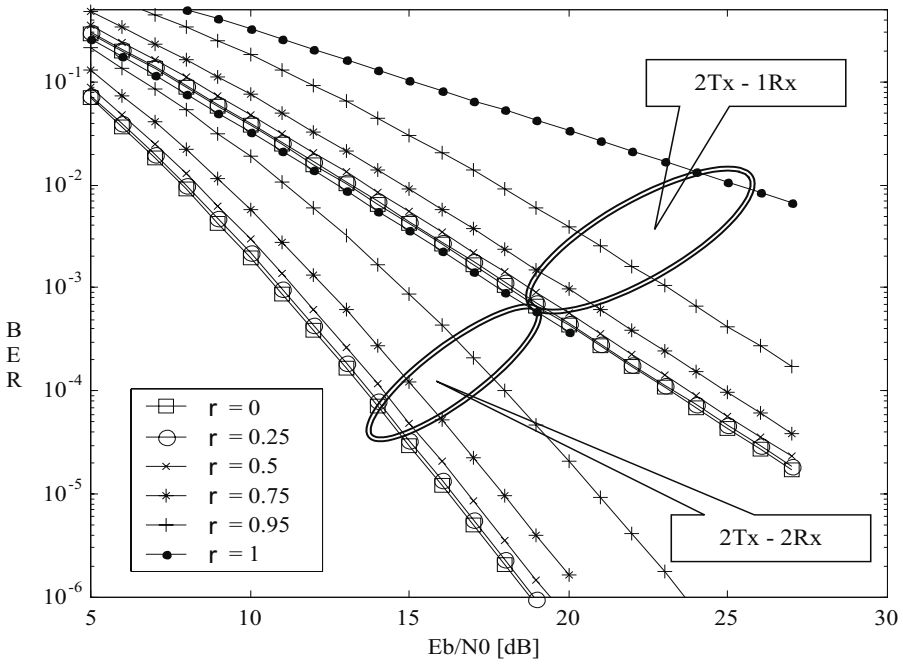

Figure 4.17: Analytic results for 4 state STTC over correlated Rayleigh fading channel

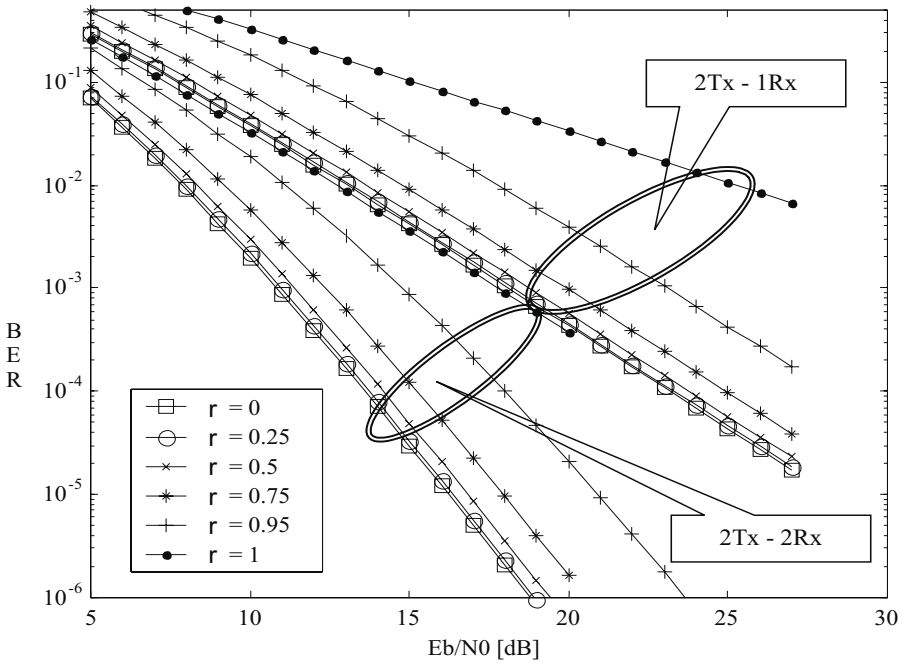

Figure 4.18: Analytic results for 8 state STTC over correlated Rayleigh fading channel

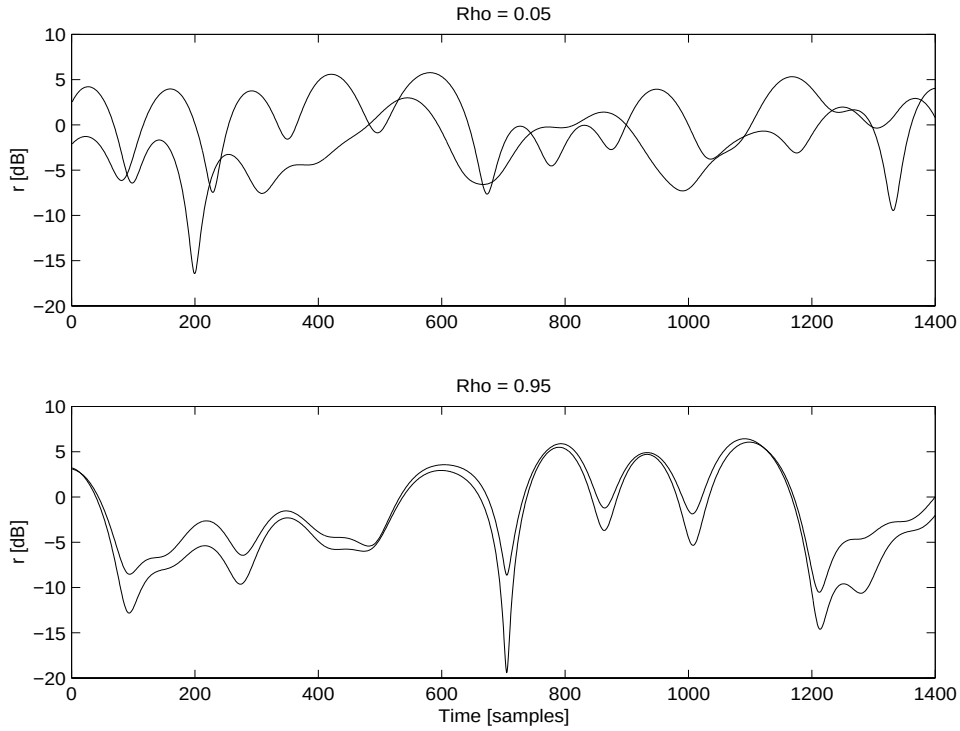

Figure 4.19: Correlated Rayleigh envelopes, $\rho = 0.05, 0.95$

lated, as expected in the case of low cross-correlation coefficient ($\rho = 0.05$) while in the lower subplot the two are almost identical, implying high cross-correlation coefficient ($\rho = 0.95$).

Figure 4.20 presents Monte Carlo simulation results for the 4 state STTC with 2 transmit antennas and 1 or 2 receive antennas, operating over a correlated Rayleigh fading channel with varying cross-correlation coefficients ($\rho = 0.05, 0.75, 0.95$). Simulation results indicate that the effectiveness of STTC transmit diversity schemes is retained for cross-correlation coefficients as high as 0.75, with a limited penalty in coding gain (< 1 dB). Furthermore, comparing simulation results with the derived analytic approximations, we observe that by considering only small set of dominant error events ($N = 3$) the analytic results are as tight as $2 - 3$ dB to the simulated performance.

Figure 4.21 presents Monte Carlo simulation results for the 8 state STTC. Similar to the results of the 4 state code, the diversity advantage is maintained even for cross-correlation coefficient as high as 0.75, with a limited penalty in coding gain. Also, comparing simulation results with the analytic performance results for the same code (Figure 4.18), we conclude that these results are as tight as $2 - 3$ dB to the performance of the code.

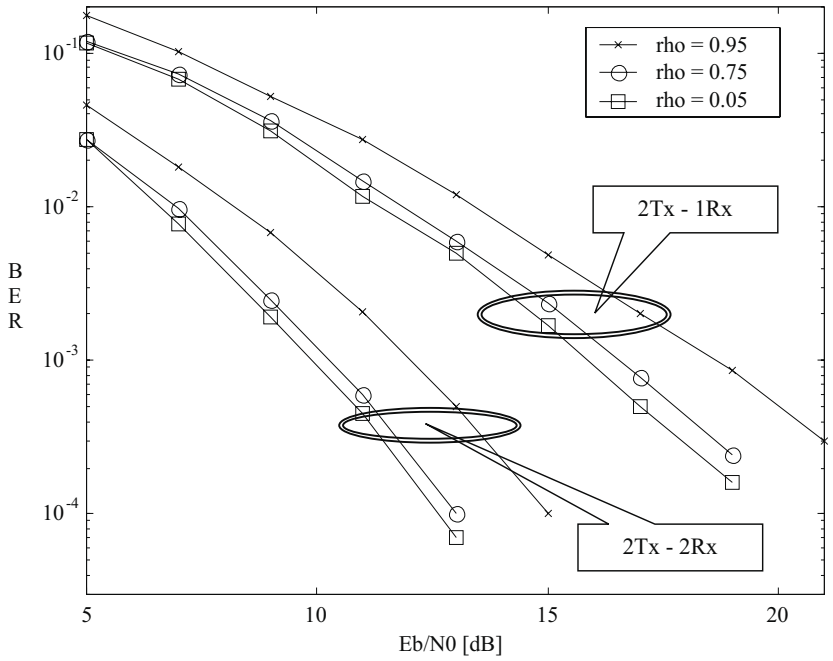

Figure 4.20: Simulation results for 4 state STTC over correlated Rayleigh fading channel

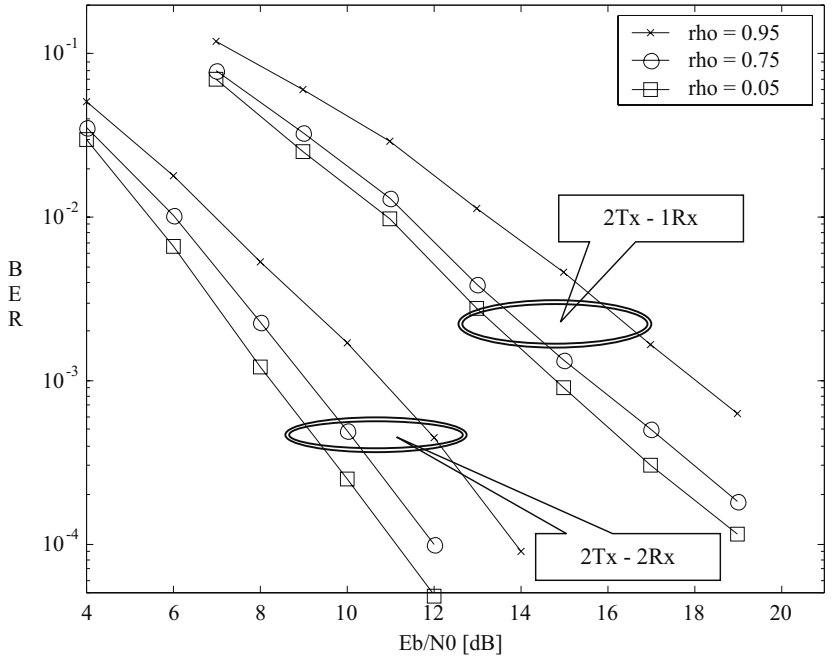

Figure 4.21: Simulation results for 8 state STTC over correlated Rayleigh fading channel

4.4 Chapter Summary

Various analysis techniques, which are adopted from the area of trellis coded modulation, have been applied to STTC in order to develop insights for the structure and performance of these codes in Rayleigh, Rician and correlated fading channels. First, we presented a method to construct the block diagram of space-time trellis codes from its trellis diagram, which is usually designed by hand to guarantee full rank and maximum determinant criteria. The technique is based on the Calderbank-Mazo algorithm [50], which finds the generator matrix of the code using simple linear algebra computations. This method was presented at the 2000 IEEE Southeast Conference in Nashville, Tennessee [51].

Following, transfer function techniques are developed to upper bound the bit-error probability of the scheme in independent Rayleigh or Rician fading channels. Using these analytic tools, we evaluate the performance of the codes over a wide span of channel realizations from Rayleigh fading (no specular component) to AWGN (dominant specular component, no diffuse component). This performance analysis technique was presented at the 2001 Spring Vehicular Technology Conference (VTC) in Rhodes, Greece [53].

In the correlated case, bit-error probability is derived by determining an upper bound on the pair-wise error probability of dominant short error events. Since only a number of pair-wise error events are included, the resulting analysis leads to approximations rather than into true upper bounds; However, in all cases examined, the analytic results did indeed upper bound the simulation results. Analytic results of the bit-error probability are found to be inversely proportional to the lth power of E_b/N_0, where l corresponds to the diversity advantage of the scheme. Both analytic and simulation results indicate that for cross-correlation coefficient values less than 0.75, the diversity advantage is retained while coding gain is penalized by less than 1.5 dB. This work will be presented at the 2002 Spring International Conference on Third Generation Wireless and Beyond, San Francisco, California [56]. The combined performance analysis over independent and correlated fading channels was submitted to *IEEE Transactions on Communications* [75].

The analytic results derived herein are shown to be functions of the number of antenna elements in both ends of the link, the signal-to-noise ratio, the eigenvalues of the code distance matrix and the covariance matrix of the fade coefficients. While a wealth of analytic tools are available for evaluating the performance of trellis-coded modulation, to date these tools have yet to be fully exploited for the analysis of STTC. The techniques presented in this chapter, along with the work in [18, 58, 67, 72, 76, 77, 57] initiate the studies of the theoretical limits of STTC and provide insights into efficient code design criteria in a variety of channel conditions.

Chapter 5

Performance Analysis of Space-Time Block Codes (STBC)

The encoding and decoding algorithms of STBC were discussed in details in Chapter 3. This family introduces a simple, elegant transmit diversity mechanism that allows the designer to move the diversity burden from the mobile units to the base station, while achieving the same diversity advantage of Maximal Ratio Receive Combining (MRRC). These schemes were recently adopted by the 3G standardization committees [78], as they retain the property of having a very simple maximum likelihood decision rule preceded by linear processing.

In this chapter, error rate analysis of various STBC architectures is presented based on an original derivation of analytical bounds and Monte Carlo simulation methods. The performance analysis presented herein is based on the probability density function of the effective signal-to-noise ratio at the space-time combiner output. This framework supports various complex orthogonal designs operating with M-ary PSK modulation and practical array configurations over independent or correlated flat Rayleigh fading channels. Using the analytic results, we study the benefits associated with employing more than two antenna elements at the transmitter and quantify the robustness of the scheme to spatial correlation. Next, Monte Carlo simulation results are presented for coherent STBC schemes in a variety of configurations. This includes schemes paired with QAM signaling format for high spectral efficiency applications, schemes concatenated with an outer error correction code (e.g., TCM) for improved energy efficiency and schemes operating with imperfect channel estimation and carrier recovery mismatch. It is shown that a coherent STBC scheme requires stringent requirements on the frequency and phase offsets of a carrier recovery loop. On the other hand, differential STBC (D-STBC) does not rely on channel estimation and have relaxed requirements on the accuracy of the carrier recovery mechanism. The D-STBC

scheme is shown to achieve the same diversity advantage as coherent STBC with a penalty of 3 dB in performance. D-STBC has been implemented as the first core algorithm on the MIMO hardware laboratory testbed architecture, which is described in Chapter 6.

5.1 Theoretic Bounds of STBC over Independent and Correlated Fading Channels

In this section, tight upper bounds on the error probability of space-time block codes, also known as orthogonal design transmit diversity, are derived. These analytic bounds facilitate rapid calculation of error rates, leading to useful insights into system behavior in a variety of channel conditions.

Let us first introduce notations that will be used in the performance analysis that follows. The orthogonal design maps k input M-ary symbols, denoted $\{s_q, q \in [1, \cdots, k]\}$, to n_T orthogonal sequences of length p each, yielding a Space-Time Block Code (STBC) of rate $r = k/p$. A complex orthogonal design G_{n_T} is defined by a $p \times n_T$ transmission matrix with entries $[\pm s_1, \pm s_2, \cdots, \pm s_k]$, their conjugates $[\pm s_1^*, \pm s_2^*, \cdots, \pm s_k^*]$ and superposition of those. While a full rate orthogonal design exists for real alphabets (i.e., PAM) with arbitrary number of elements, it does not exist for an arbitrary complex alphabet (i.e., PSK or QAM) with more than 2 antenna elements. This has motivated researchers to search for sporadic complex orthogonal designs, which accommodate rates as close to 1 as possible, yet achieve full spatial diversity order. Table 3.1 summarized the characteristics of few sporadic complex orthogonal designs, proposed originally in [27], for $2, 3$ and 4 transmit antenna elements.

In [25], the performance of these orthogonal designs was reported using Monte Carlo simulation methods and assuming uncorrelated fading scenarios. Performance analysis for the error rate of these schemes was drawn from analysis of receive diversity combining schemes [71, 7]. In these classical results, the moment generating function (MGF) or characteristic function of the effective SNR at the combiner output played a key role in determining the error rate of the scheme. In [79], the authors present a unified framework for the calculation of exact error rate expressions of multichannel reception over Nakagami-m fading channels. In [80], the authors have derived a closed form expression for the error probability of STBC under spatial fading correlation conditions. Their analysis is confined however to binary PSK modulation and full rate orthogonal designs only. Similar analysis was also used in [81] to obtain pairwise symbol error probability for binary PSK signaling over two correlated fading channels in receive diversity settings. In [82], necessary and sufficient conditions for the minimization of the conditional error probability of linear space-time codes were

provided, demonstrating that within this category, space-time block codes satisfy the conditions and thus are optimal. In this section, tight upper bounds are derived to support arbitrary complex orthogonal designs paired with M-ary PSK modulation and linear or circular antenna array configuration [83]. We further remove the assumption of uncorrelated fading paths and investigate the robustness of the scheme to spatial correlation [84]. The novelty of our analytic result is in modeling the effects of distributing the transmitted power equally across transmit antenna elements, the rate loss of the orthogonal design, the alphabet size, and the antenna array configuration in terms of size and geometry.

The performance analysis presented herein is based on the distribution of the effective SNR at the output of the receiver combining stage. In the case of independent fading channels, this SNR is a chi-square random variable with $n_T n_R$ degrees of freedom, where n_T and n_R represent the number of antenna elements at the transmitter and receiver, respectively. In the correlated fading case, the effective SNR takes the form of Hermitian quadratic form in complex correlated Gaussian variates. Thus, its characteristic function has a closed form solution [7], which is processed by an inverse Laplace transform to yield its probability density function (pdf). Finally, the pdf of the effective SNR is used in averaging the upper (union) bound of the conditional error probability of the scheme.

Results indicate that for systems with low spectral efficiency requirements (e.g., 1 [bps/Hz]), it is beneficial to increase the number of antenna elements at the transmitter. For example, increasing the number of antenna elements at the transmitter from 2 to 4 in single receive antenna element systems enhances performance by 8.5 dB at SER of 10^{-5}. Higher spectral efficiencies however (e.g., $2, 3$ [bps/Hz]) require higher signal cardinalities, especially for orthogonal designs with a rate loss ($n_T > 2$), thus resulting in limited to no improvement in energy efficiency. It is also observed that the effective diversity order in the case of correlated fading environment is determined by the geometric mean of the covariance matrix eigenvalues. The performance of the scheme with practical array configurations (e.g., linear or circular) is computed, demonstrating the versatility of the analytic result and the robustness of the codes to spatial fading correlation.

5.1.1 Performance Analysis

Assuming quasi-static frequency non-selective (flat) fading channel, the received signal at receive antenna j at time t is modeled by

$$r_t^j = \sum_{i=1}^{n_T} \alpha_{i,j} c_t^i + \eta_t^j, \tag{5.1}$$

where η_t^j denotes the AWGN term and is modeled as a zero mean i.i.d. complex Gaussian random variable with variance $\frac{n_T}{2SNR}$ per dimension. The average energy of c_t^i, which denotes the symbol transmitted from transmit antenna i at time t, is normalized to one. The block of k M-ary symbols at the input to the orthogonal design is denoted $\{s_q, q \in [1, \cdots, k]\}$. The channel is modeled by an $n_T \times n_R$ matrix $\Omega = [\alpha_{i,j}]$, whose entry $\alpha_{i,j}$ represents the complex fade coefficient for the path from transmit antenna i to receive antenna j. These fade coefficients are assumed to be zero mean independent or correlated complex Gaussian random variables with variance 0.5 per dimension.

Assuming ideal CSI at the receiver, the maximum likelihood decision rule minimizes the following decision metric:

$$\sum_{j=1}^{n_R} \sum_{t=1}^{p} \left| r_t^j - \sum_{i=1}^{n_T} \alpha_{i,j} c_t^i \right|^2 . \tag{5.2}$$

Expanding the above metric and using Eq. (5.1), the decoder uses the following k separate decision statistics:

$$\tilde{s}_q = \frac{1}{r} \left(\sum_{j=1}^{n_R} \sum_{i=1}^{n_T} |\alpha_{i,j}|^2 \right) s_q + \tilde{N}, \quad q \in [1, \cdots, k], \tag{5.3}$$

where r is the rate of the orthogonal design and $\tilde{N}$ is the effective noise at the combining stage output. It is easy to verify that $\tilde{N}$ is a zero mean complex Gaussian random variable with variance $\sigma_{\tilde{N}}^2 = \frac{n_T}{2rSNR} \sum_{j=1}^{n_R} \sum_{i=1}^{n_T} |\alpha_{i,j}|^2$ per dimension. The effective SNR at the space-time combiner output is thus given by

$$\Gamma = \frac{SNR}{r n_T} \sum_{j=1}^{n_R} \sum_{i=1}^{n_T} |\alpha_{i,j}|^2 . \tag{5.4}$$

Assuming M-ary PSK signals (equal energy constellation), the maximum likelihood decision rule is based on the minimum Euclidean distance, denoted d_{min}, of the decision statistics in Eq. (5.3) to all possible signal constellation points in the alphabet. The conditional error probability is upper (union) bounded by

$$P(e|\Gamma) \leq 2Q\left(\frac{d_{min}/2}{\sigma_{\tilde{N}}}\right) = 2Q\left(\frac{\frac{1}{r}\sum_{j=1}^{n_R}\sum_{i=1}^{n_T}|\alpha_{i,j}|^2 \, sin(\frac{\pi}{M})}{\sqrt{\frac{n_T}{2rSNR}\sum_{j=1}^{n_R}\sum_{i=1}^{n_T}|\alpha_{i,j}|^2}}\right) = 2Q\left(\sqrt{\eta\Gamma}\right), \tag{5.5}$$

where $\eta = 2 \; sin^2\left(\frac{\pi}{M}\right)$.

A. Independent fading channels

In this case, the effective SNR (defined in Eq. (5.4) as Γ) is a chi-square random variable with $n_T n_R$ degrees of freedom. The probability density function of this random variable is

given by [71, 85]

$$f_\Gamma(\Gamma) = \frac{1}{(n_T n_R - 1)! \left(\frac{SNR}{r n_T}\right)^{n_T n_R}} \Gamma^{n_T n_R - 1} e^{-\frac{\Gamma}{SNR/(r n_T)}}. \tag{5.6}$$

Thus, the error probability of a rate r complex orthogonal design, paired with M-ary PSK modulation, n_T antenna elements at the transmitter and n_R receive antenna elements, is given by

$$P_e = \int_{\Gamma=0}^{\infty} P(e|\Gamma) f_\Gamma(\Gamma) d\Gamma \leq 2\frac{\mu^{n+1}}{n!} \int_{\Gamma=0}^{\infty} Q\left(\sqrt{\eta\Gamma}\right) \Gamma^n e^{-\mu\Gamma} d\Gamma, \tag{5.7}$$

where $\mu = \frac{r n_T}{SNR}$ and $n = n_T n_R - 1$. This integral can be easily solved using numeric integration methods or using a mathematical software package. Exemplary performance results for few sporadic space-time block codes are provided in section 5.1.2 (Figure 5.1 and Table 5.1).

B. Correlated fading channels

In order to derive upper bounds on the error probability of the scheme under spatial fading correlation conditions, we first restructure the channel matrix Ω to form an $n_T n_R \times 1$ column vector of fade coefficients:

$$\tilde{\Omega} = \left[\{\alpha_{11}, \cdots, \alpha_{n_T 1}\}, \{\alpha_{12}, \cdots, \alpha_{n_T 2}\}, \cdots, \{\alpha_{1 n_R}, \cdots, \alpha_{n_T n_R}\}\right]^T. \tag{5.8}$$

We express the $\sum_{j=1}^{n_R} \sum_{i=1}^{n_T} |\alpha_{i,j}|^2$ as a matrix quadratic form in complex correlated Gaussian variates, denoted by F:

$$\sum_{j=1}^{n_R} \sum_{i=1}^{n_T} |\alpha_{i,j}|^2 = \tilde{\Omega}^T \tilde{\Omega} = F. \tag{5.9}$$

Note that $F = \mu\Gamma$. Applying the result of Appendix B of [7] (see Appendix **??**), the characteristic function of F is given by

$$\Psi_F(s) = \frac{1}{det(I_{n_T n_R} + sR)} = \frac{1}{\prod_{m=1}^{n_T n_R}(1 + s\lambda_m)}, \tag{5.10}$$

where $I_{n_T n_R}$ is an $n_T n_R \times n_T n_R$ identity matrix and R is the covariance matrix of $\tilde{\Omega}$ with $n_T n_R$ eigenvalues, denoted λ_m. Assuming multiplicity 1 to these eigenvalues, the partial fraction decomposition of the characteristic function in (5.10) yields:

$$\Psi_F(s) = \sum_{m=1}^{n_T n_R} \frac{a_m}{(1 + s\lambda_m)}, \tag{5.11}$$

where $a_m = \frac{\lambda_m^{(n_T n_R - 1)}}{\prod_{m=1}^{n_T n_R - 1}(\lambda_m - \lambda_l)}, \lambda_l \neq \lambda_m$. Taking the inverse Laplace transform of this characteristic function, we compute the distribution of F:

$$f_F(F) = L^{-1}(\Psi_F(s)) = \sum_{m=1}^{n_T n_R} \frac{a_m}{\lambda_m} \exp\left(-\frac{F}{\lambda_m}\right). \tag{5.12}$$

The pdf of (5.12) is used in averaging the conditional error probability of (5.5):

$$P_e = \int_{F=0}^{\infty} P(e|F) f_F(F) dF \leq 2 \sum_{m=1}^{n_T n_R} \frac{a_m}{\lambda_m} \int_{F=0}^{\infty} \exp\left(-\frac{F}{\lambda_m}\right) Q(\sqrt{\frac{\eta}{\mu}F}) dF. \tag{5.13}$$

To simplify notation, let us define $\gamma_{eq} = \frac{\eta}{\mu} = \frac{2SNR\ sin^2(\frac{\pi}{M})}{r\ n_T}$ as a parameter that encapsulates the M-ary signaling, the orthogonal design rate and the averaged SNR per receive antenna branch. The above integration has a closed form solution [86], which is given by

$$P_e \leq \sum_{m=1}^{n_T n_R} a_m \left[1 - \frac{1}{\sqrt{1 + \frac{1}{\lambda_m \gamma_{eq}}}}\right]. \tag{5.14}$$

Note that asymptotically, as $SNR \to \infty$:

$$\sqrt{1 + \frac{2}{\lambda_m \gamma_{eq}}} \approx 1 + \frac{1}{\lambda_m \gamma_{eq}} \tag{5.15}$$

and thus,

$$\begin{aligned} P_e &\leq \sum_{m=1}^{n_T n_R} \frac{a_m}{1 + \lambda_m \gamma_{eq}} \\ &= \prod_{m=1}^{n_T n_R} \frac{1}{(1 + \lambda_m \gamma_{eq})} \\ &\approx \frac{1}{\left(\prod_{m=1}^{n_T n_R} \lambda_m\right) \gamma_{eq}^{n_T n_R}}. \end{aligned} \tag{5.16}$$

This result demonstrates that in order to get an effective diversity order of $n_T n_R$ from the orthogonal design, two conditions have to be met: 1) The geometric mean of the covariance matrix eigenvalues has to be as large as possible, and 2) the smallest eigenvalue should be reasonably large above the threshold from which the diversity performance is being referred. A similar conclusion was also drawn in [7] for maximal ratio receive combining schemes. In the next section, we compare this analytic result with Monte Carlo simulations and apply different antenna array configurations that imply various covariance matrix forms.

5.1.2 Analytic and Simulation Results

A. Independent fading channels

Figure 5.1 presents the performance of various complex orthogonal designs for a fixed spectral efficiency of 1 [bps/Hz], operating over uncorrelated fading channels. We consider $2, 3$ and 4 transmit antenna elements with 1 receive antenna element paired with G_2, G_3 and G_4 orthogonal designs, respectively. Since the G_2 scheme is based on a full rate code, BPSK modulation is used while for the rate 1/2 codes (G_3 and G_4), QPSK signaling format is used.

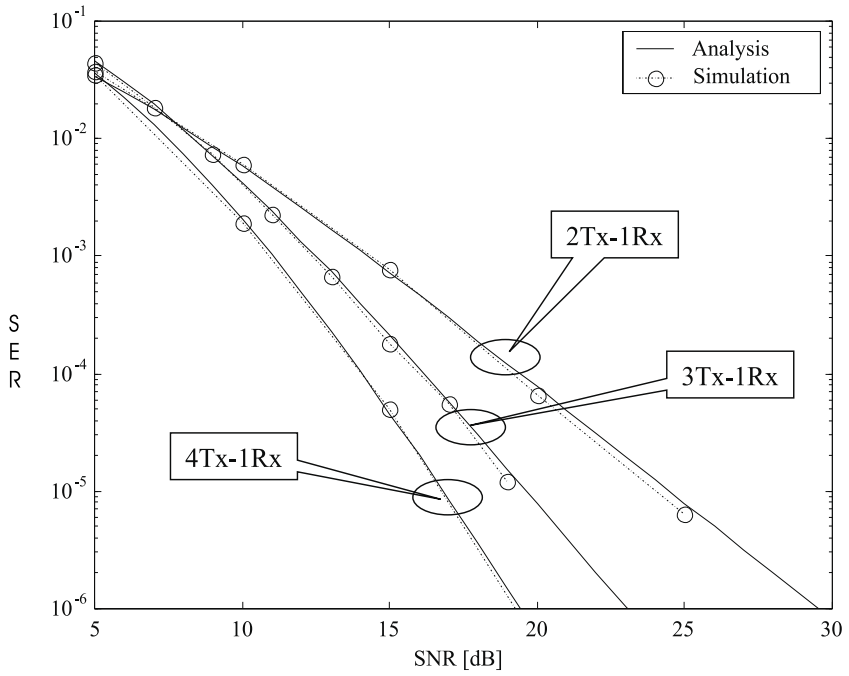

Figure 5.1: Uncorrelated Fading Conditions; 1 [bps/Hz]; 2Tx-1Rx, 3Tx-1Rx, 4Tx-1Rx

The diversity advantage of the above schemes is $2, 3$ and 4 as seen by the asymptotic slope of the error rate curves and as attributed to the antenna array size. Furthermore, an excellent match is demonstrated between the analytic results of Eq. (5.7) and the Monte Carlo simulation results.

To further demonstrate the versatility and effectiveness of the analytic result, Table 5.1 summarizes the performance of various complex orthogonal designs paired with M-ary PSK modulation and various number of antenna elements. The table describes both the spectral efficiency of the scheme in [bps/Hz] and the energy efficiency in terms of the required SNR

for a fixed symbol error probability of 10^{-5} and 10^{-7}.

Table 5.1: Spectral and Energy Efficiency of Orthogonal Design Transmit Diversity Schemes

Scheme (rate)	n_T	n_R	*Modulation*	*bps/Hz*	*SNR[dB] @* $P_e = 10^{-5}$	*SNR[dB] @* $P_e = 10^{-7}$
G_2 (1.0)	2	1	BPSK	1	25	35.5
G_3 (0.5)	3	1	QPSK	1	19	26.3
G_4 (0.5)	4	1	QPSK	1	16.5	22
G_2 (1.0)	2	1	QPSK	2	28.5	38.5
G_3 (0.5)	3	1	16PSK	2	30.5	37.1
G_4 (0.5)	4	1	16PSK	2	28	33.3
G_2 (1.0)	2	1	8PSK	3	34	44
H_3(0.75)	3	1	16PSK	3	32.3	39.5
H_4(0.75)	4	1	16PSK	3	29.5	34.8
G_2 (1.0)	2	4	BPSK	1	7	10.2
G_3 (0.5)	3	4	QPSK	1	5.7	8.3
G_4 (0.5)	4	4	QPSK	1	5.2	7.5
G_2 (1.0)	2	4	QPSK	2	10	13.2
G_3 (0.5)	3	4	16PSK	2	17	19.4
G_4 (0.5)	4	4	16PSK	2	16.5	18.7
G_2 (1.0)	2	4	8PSK	3	15.1	18.2
H_3(0.75)	3	4	16PSK	3	18.6	21.3
H_4(0.75)	4	4	16PSK	3	18.2	20.4

The results presented in this table indicate that for systems with low spectral efficiency requirements (e.g., 1 [bps/Hz]), it is beneficial to increase the number of antenna elements at the transmitter. For example, for single receive antenna element systems, transmit diversity with 4 antenna elements enhances performance by 8.5dB (at $P_e = 10^{-5}$) as compared to dual transmit diversity scheme. Higher spectral efficiencies however (e.g., $2, 3$ [bps/Hz]) require higher signal cardinalities, especially for orthogonal designs with a rate loss ($n_T > 2$). These larger symbol alphabets lead to no improvement in energy efficiency at a symbol error rate of 10^{-5}. However, note that asymptotically ($P_e = 10^{-7}$ column), higher diversity order is the dominant factor in determining performance.

For systems with multiple receive antenna elements (e.g., $n_R = 4$), increasing the number of antenna elements at the transmitter is beneficial only for low spectral efficiency requirements. Note that for high spectral efficiency cases, systems that employ receive diversity would not gain from employing more than two antenna elements at the transmitter.

B. Correlated fading channels

Applying the result of Eq. (5.14) to the case of a full rate orthogonal design (G_2) with 2 transmit and 1 receive antenna elements (2Tx-1Rx) and M-ary PSK modulation yields:

$$P_e \leq \frac{1}{\lambda_1 - \lambda_2}\left[\lambda_1\left(1 - \frac{1}{\sqrt{1+\frac{1}{\lambda_1 SNR\sin^2(\frac{\pi}{M})}}}\right) - \lambda_2\left(1 - \frac{1}{\sqrt{1+\frac{1}{\lambda_2 SNR\sin^2(\frac{\pi}{M})}}}\right)\right], \quad (5.17)$$

where λ_1, λ_2 are the eigenvalues of the channel covariance matrix, SNR is the signal-to-noise ratio per receive antenna branch, and M is the alphabet size. Figure 5.2 compares the analytic performance results of Eq. (5.17) with Monte Carlo simulation results for binary and 8-ary PSK modulation. Excellent agreement is demonstrated for various correlation coefficients across fading paths. Both analytic and simulation results indicate that the effective diversity order of the scheme is retained for cross-correlation coefficients as high as 0.75, with a limited penalty of 1dB at a target symbol error rate of 10^{-4}. However, as the cross correlation factor ρ tends toward 1, the diversity advantage is eliminated.

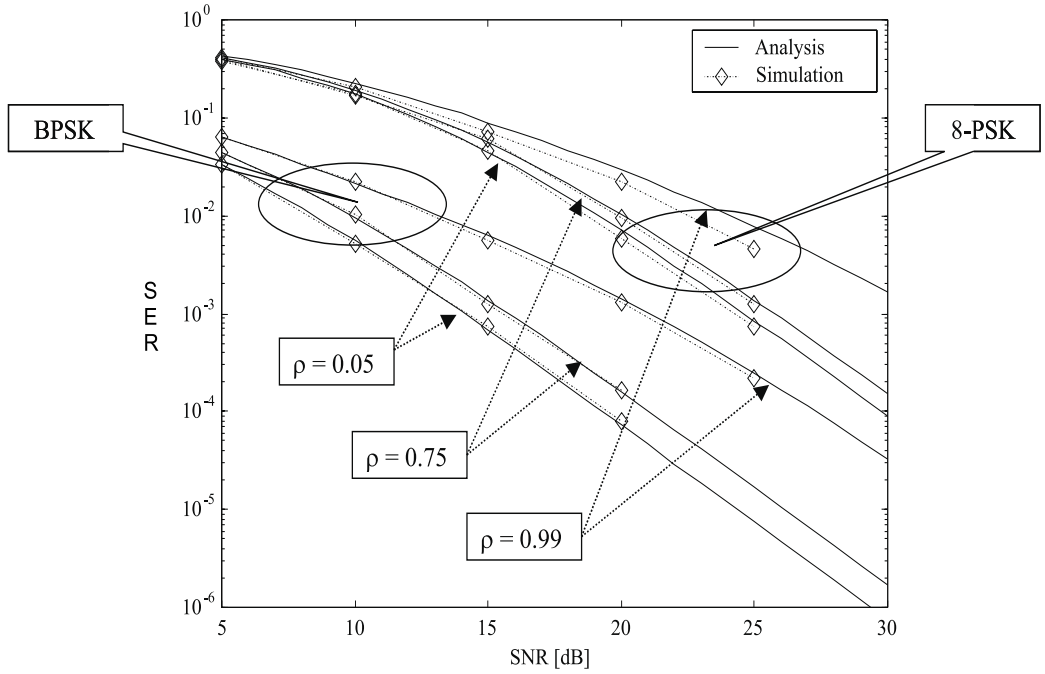

Figure 5.2: STBC over correlated fading channels; 1 and 3 [bps/Hz], 2Tx-1Rx

In simulating spatially correlated fade coefficients, we adopt the procedure proposed in [68, 69], which is based on multiplying independent complex Gaussian random vectors with

a lower triangular "coloring" matrix that is obtained from a Cholesky decomposition of the desired covariance matrix.

Next, we address the case of uniformly spaced linear or circular antenna array configuration paired with orthogonal design transmit diversity. For linear array geometry at the transmitter with 1 antenna element at the receiver, the covariance matrix of $\tilde{\Omega}$ takes the following Toeplitz form:

$$R_{mm'} = \begin{cases} 1, & m = m' \\ \rho^{|m-m'|}, & m \neq m' \end{cases}, \tag{5.18}$$

where ρ represents the cross-correlation coefficient between the fade coefficients associated with two adjacent antenna elements. In the circular array case, the covariance matrix is still Hermitian and has a well-known general eigenvalue solution [39]. The circulant matrix takes the following form:

$$R_{mm'} = \begin{cases} 1, & m = m' \\ \rho^{min\{|m-m'|, n_T - |m-m'|\}}, & m \neq m' \end{cases}, \tag{5.19}$$

Figure 5.3 compares analytic and simulation performance results for the orthogonal design G_4 with 4Tx-1Rx and QPSK signaling format using linear array or circular array.

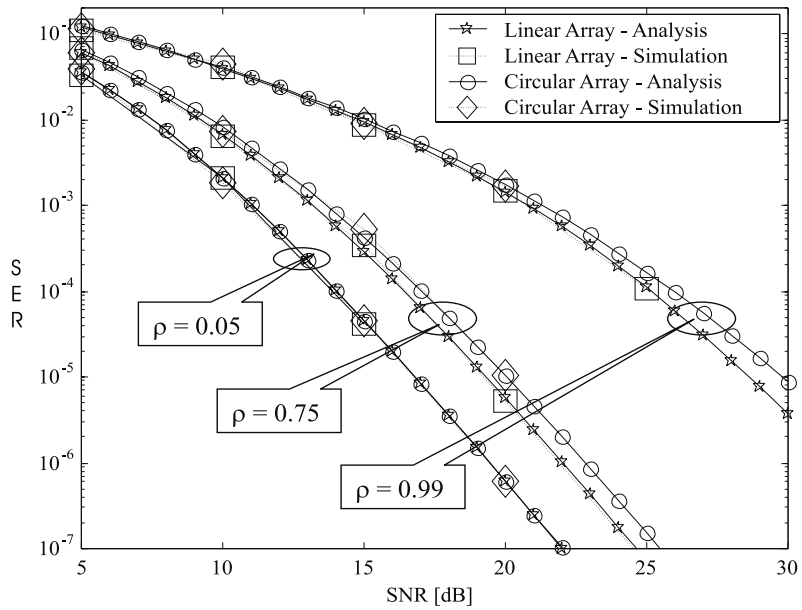

Figure 5.3: Linear vs. Circular Antenna Array; G_4 Orthogonal Design, QPSK Modulation, 4Tx-1Rx

It is shown that the scheme with a uniformly spaced linear array outperforms the scheme with the circular array. The gap in performance is increased as the cross correlation factor increases but is bounded to 1dB. For both array configurations, it is shown that cross correlation of 0.75 results in $2-3$dB degradation while $\rho = 0.99$ results in a loss of diversity advantage. Again, an excellent match between analytic and simulation results is demonstrated.

5.2 Coherent STBC (C-STBC) in Various Configurations

In this section, performance comparison of coherent STBC with MRRC is performed, illuminating the effect of distributing the power equally across transmit antenna elements. This phenomenon was also described in previous section, where the equivalent SNR at the output of the space-time combiner (Eq. (5.4)) was normalized to n_T. Following, simulation results for STBC with QAM signaling format and multiple element at the receiver are reported, demonstrating that the diversity advantage offered by placing multiple elements at both ends of the link has the order of $n_T n_R$. Next, a concatenated trellis coded modulation with STBC scheme is presented, showing that the simple ML decoder structure of the STBC lends itself naturally for concatenation with an outer error correction code. This architecture "enjoys" both spatial diversity order and coding gain without sacrificing bandwidth efficiency. Furthermore, it was demonstrated in [87] that such concatenation outperforms some of the best trellis type space-time codes with the same complexity and spectral efficiency. The sensitivity of the C-STBC to carrier recovery mismatch is also quantified in this section, demonstrating the need for STBC schemes that employ non-coherent detection.

5.2.1 C-STBC versus MRC

The STBC scheme simulated in this section is based on the G_2 orthogonal design paired with BPSK signaling format. For comparison purposes, results for maximal ratio receive combining with two and four receive antenna elements, are presented. The simulation assumptions include quasi-static flat Rayleigh fading channel and perfect knowledge of CSI at the receiver. As seen in Figure 5.4, the STBC with 2Tx-1Rx antenna array configuration has the same asymptotic slope as the error rate curve of the 1Tx-2Rx MRC architecture.

In addition, the same diversity advantage is experienced by 2Tx-2Rx STBC and 1Tx-4Rx MRC. We note however that the performance of STBC is inferior to the performance of MRC by 3 dB. This penalty is attributed to the fact that transmit diversity systems, unlike receive diversity schemes, does not provide antenna gain. The total transmitted power,

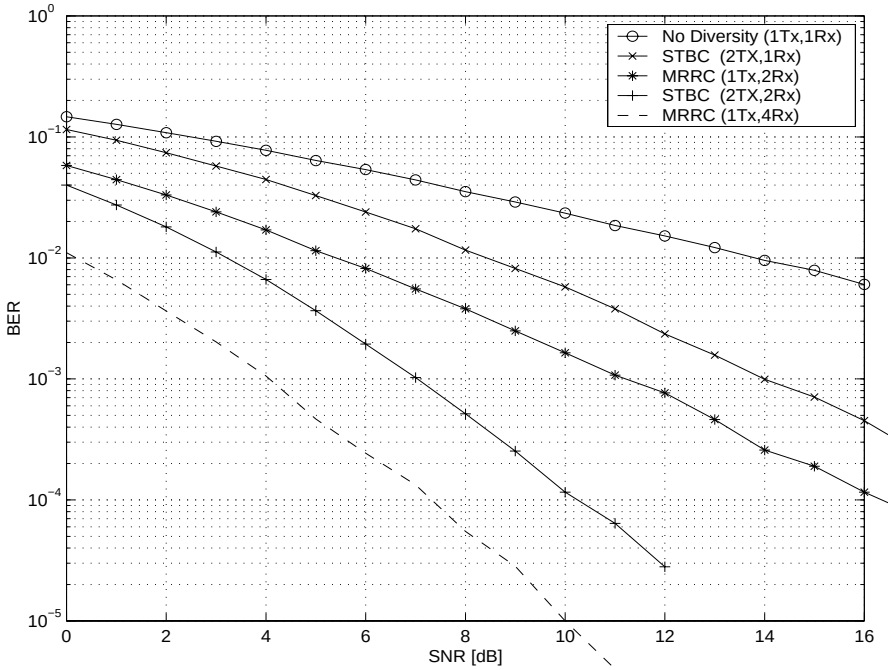

Figure 5.4: STBC Vs. MRC in Rayleigh fading channel

which is distributed equally across the 2 transmit antenna elements, is summed back at the receiver combining stage, resulting without any aperture gain. As a reference curve, performance of BPSK with no diversity is included to demonstrate the large performance gains (at the order of 15dB-25dB) attainable by a simple form of spatial diversity.

5.2.2 C-STBC with Multiple Receive Elements and QAM Modulation

Simulation results are presented in Figure 5.5 for 1 [bps/Hz] schemes with $1, 2$ and 3 antenna elements at the transmitter and 2 antenna elements at the receiver. Note that the diversity advantage offered by the multiple elements at both ends of the link has the order of $n_T n_R$. Also, note that with 2 elements at the receiver, the improvement offered by adding more elements at the transmitter is reduced as compared to single receive antenna element systems (Figure 5.1). The reason is that most of the diversity gain has been already achieved by the 2Tx-2Rx antenna array architecture.

Next, the performance of STBC with spectral efficiencies of 2 and 3 [bps/Hz] is presented. For spectral efficiency of 2 [bps/Hz], QPSK is paired with G_2 orthogonal design, and is compared to 16QAM with G_3 orthogonal design ($r = 1/2$). For spectral efficiency of 3 [bps/Hz], 8PSK is paired with G_2 orthogonal design, and is compared to 16QAM with H_3 and H_4 orthogonal designs ($r = 3/4$). Antenna configurations are $n_T = 2, 3, 4$ and $n_R = 1$.

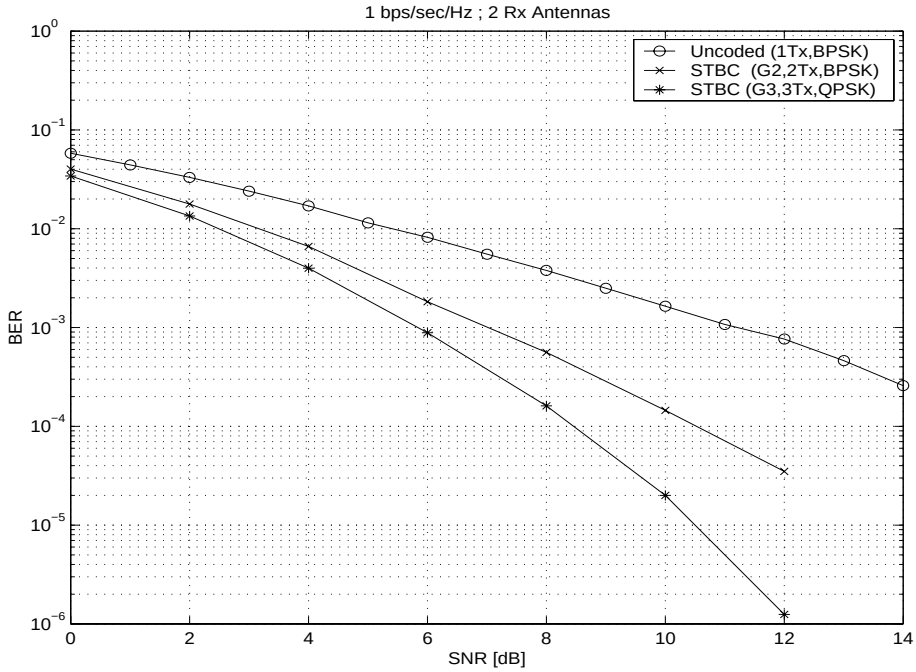

Figure 5.5: STBC in Rayleigh fading channel; $b = 1$ [bps/Hz], $n_T = 1, 2, 3$, $n_R = 2$

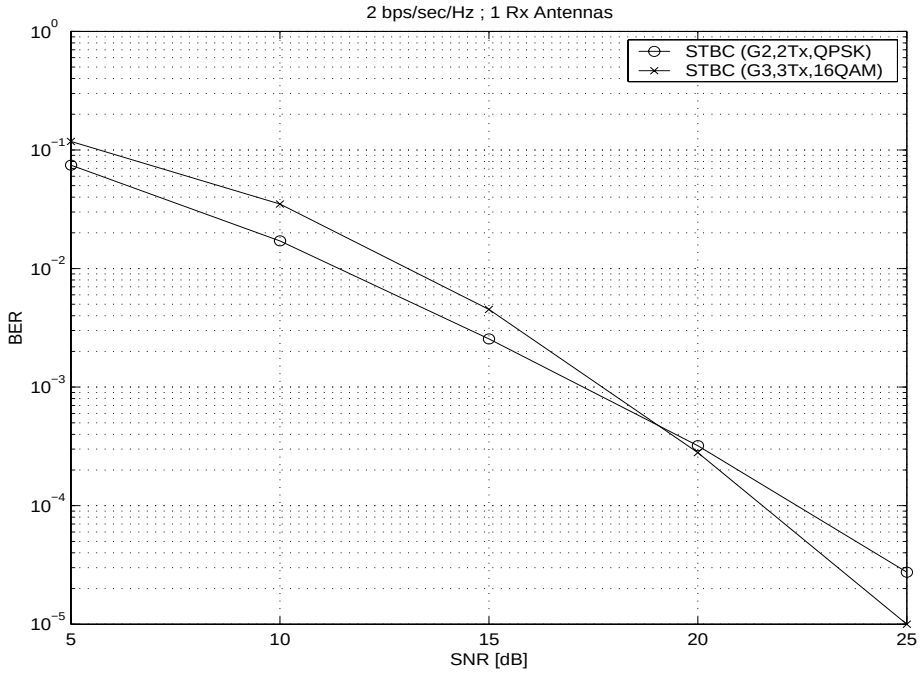

Figure 5.6: STBC in Rayleigh fading channel; $b = 2$ [bps/Hz], $n_T = 2, 3$, $n_R = 1$

A crossover effect of the two curves is observed. In low SNR region (SNR¡15 dB), the dominant factor in determining performance is the alphabet size (16 QAM is inferior to QPSK scheme due to reduced Euclidean distance). However, asymptotically (SNR¿20dB), diversity advantage dominates performance (The G_3 orthogonal design outperforms the dual diversity order offered by the G_2 scheme).

Next, Figure 5.7 presents results for schemes with high spectral efficiency of 3 [bps/Hz]. For these schemes, the rate 3/4 16QAM code gives about 7 dB gain over the 8 PSK full rate code at a fixed BER of 10^{-5}. Comparing with the results presented in Table 5.1, it is noticed that STBC with 16QAM modulation outperforms STBC paired with 16PSK for the same number of antenna elements and spectral efficiency.

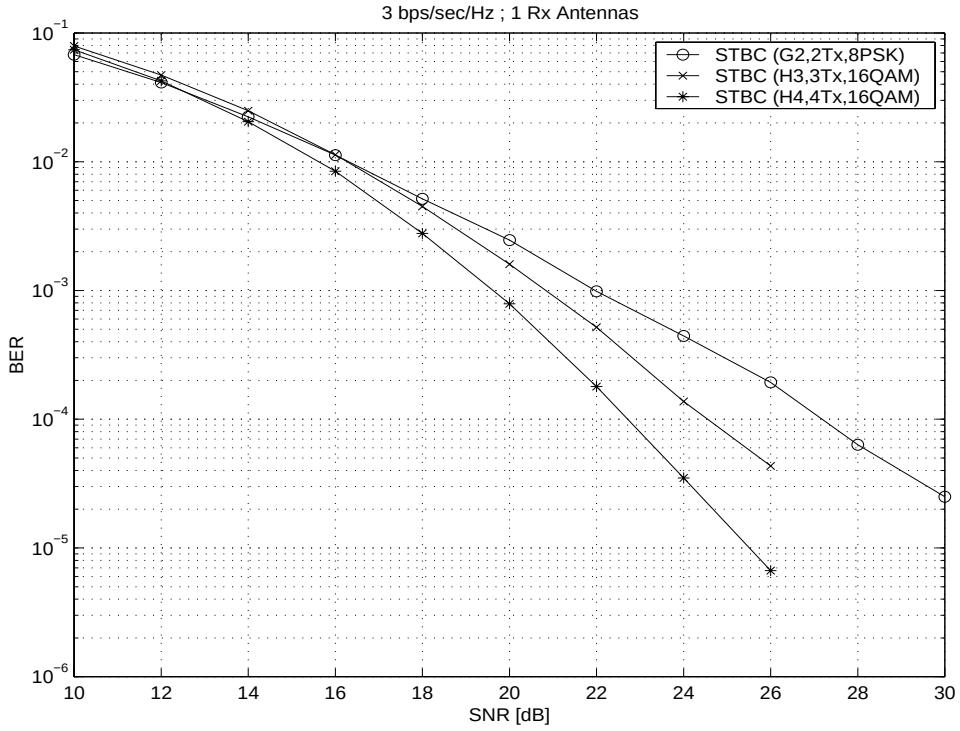

Figure 5.7: STBC in Rayleigh fading channel; $b = 3$ [bps/Hz], $n_T = 2, 3, 4$, $n_R = 1$

5.2.3 Concatenated C-STBC with TCM

Because of the low decoder complexity of STBC, it is possible to concatenate an outer error correction code such that coding gain in conjunction with spatial diversity advantage is achieved. The encoding and decoding mechanisms of STBC lend themselves naturally to a concatenated scheme. An example for such a concatenation scheme is shown in the block diagram of Figure 5.8. The outer error correction encoder is a trellis code whose output

symbols are fed into the STBC orthogonal design. At the receiver, decision statistics at the combiner output of the inner code are used as branch metrics of the outer error correction decoder.

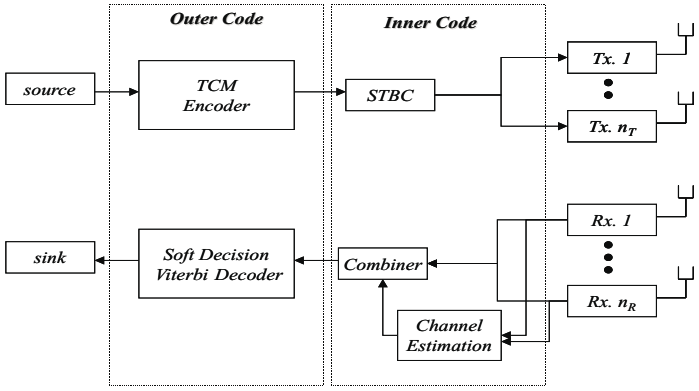

Figure 5.8: Concatenated STBC with TCM in Rayleigh fading channel

Since the effect of the diversity advantage is converting the Rayleigh fading channel into a Gaussian channel, the coding gain provided by the outer code is similar to the gain achieved by that code on a Gaussian channel [88, 85]. Simulation results for a concatenated TCM (rate $r = 2/3$, 8 PSK modulation, 4 state) and STBC (G_2 orthogonal design, $n_T = 2$, $n_R = 1, 2$) are given in Figure 5.9.

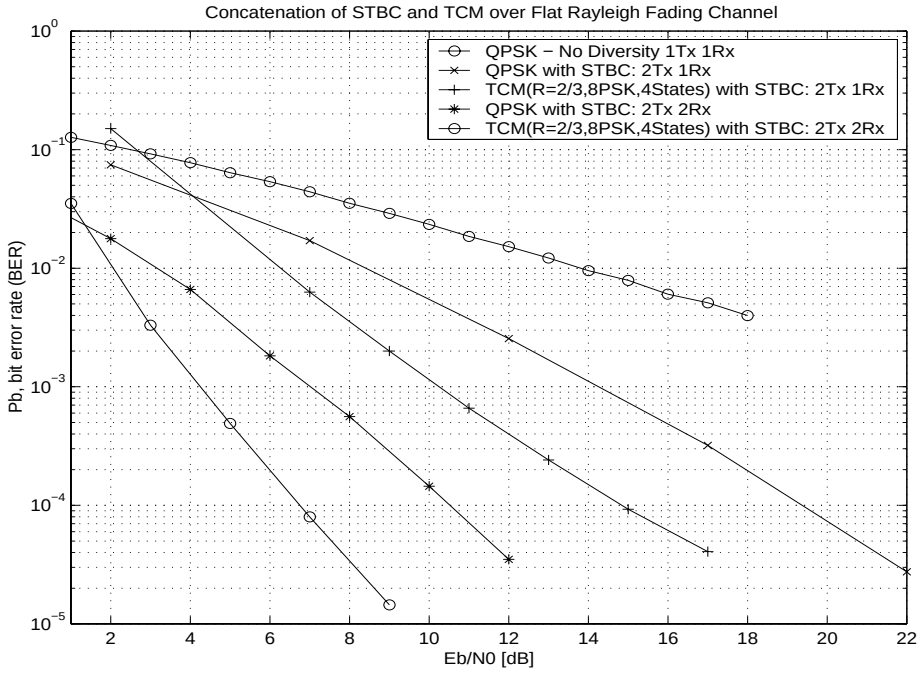

Figure 5.9: Performance of concatenated STBC with TCM in Rayleigh fading channel

It is observed that coding gain of 3 dB is achieved in addition to diversity levels of 2 and 4 (for 2Tx-1Rx and 2Tx-2Rx, respectively) without sacrificing spectral efficiency (2 [bps/Hz]). The concatenation of "turbo"-TCM codes with STBC is the subject of [31].

5.2.4 Sensitivity of C-STBC to Phase and Frequency Errors

This section studies the sensitivity of coherent STBC schemes to carrier recovery mismatch. This may rise from residual frequency offset between the receiver local oscillator and the center frequency of the incoming signal. Results are shown in Figure 5.10 for QPSK modulation, paired with G_2 orthogonal design and 2×2 antenna array configuration. Frequency mismatch ranges from 0 to 100Hz for a data rate of 100 [Kbaud].

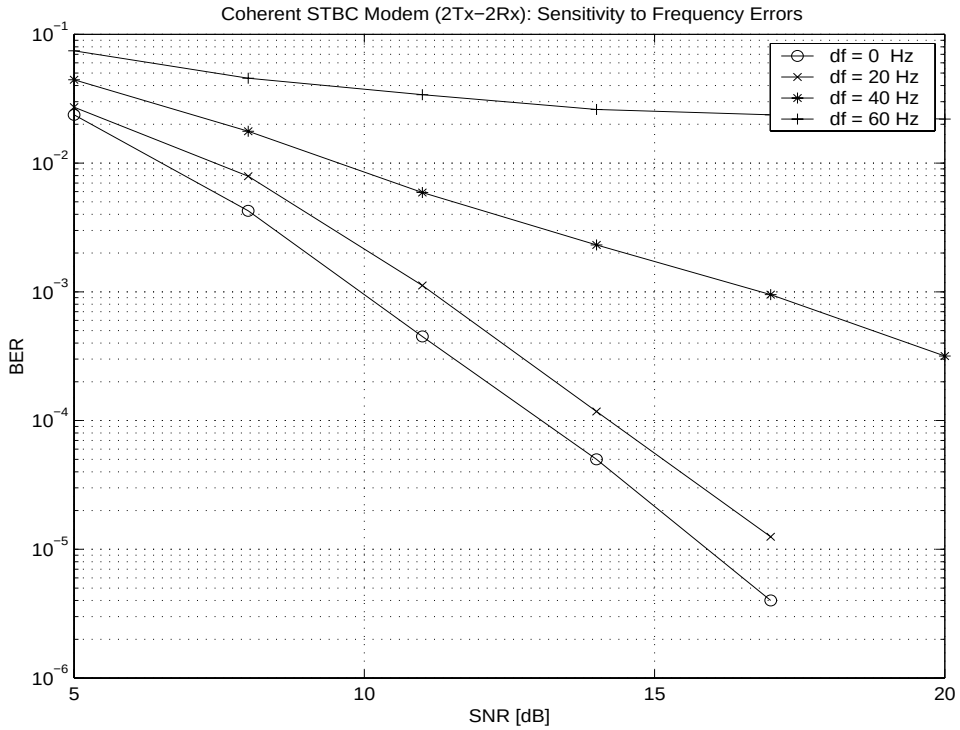

Figure 5.10: Sensitivity of C-STBC to phase and frequency errors

It is observed that frequency offset of more than 20Hz results in a significant performance degradation. This implies stringent requirement for the accuracy of the carrier recovery loop. Also, the authors in [89] have shown that the scheme is sensitive to channel estimation errors. These problems demonstrate the need for non-coherent detection techniques, which are more robust to frequency and phase offsets and do not rely on channel estimation. The performance of such scheme, known as differential STBC (D-STBC), is the subject of the next section.

5.3 Performance of Differential STBC (D-STBC)

The performance of D-STBC, which does not require explicit knowledge of CSI nor accurate carrier recovery at the receiver, is presented. The D-STBC scheme, originally proposed by Tarokh in [28], was described in details in section 3.2. Simulation results indicate that while C-STBC outperforms D-STBC by 3 dB in ideal channel tracking conditions, D-STBC offers much larger robustness to phase and frequency errors and does not rely on channel estimation. These benefits pose D-STBC as a promising candidate for deployment in transmit diversity schemes of practical wireless systems.

5.3.1 C-STBC vs. D-STBC

In traditional single transmit antenna element systems, it is well known that a coherent demodulator outperforms a differential demodulator by 3 dB. This is due to the fact that the differential scheme uses a noisy reference to extract information embedded in phase differences of consecutive symbols. Thus, noise enhancement is inherent to the differential demodulation process. Performance comparison of D-STBC and C-STBC under the assumption of ideal knowledge of CSI at the receiver and perfect carrier recovery is illustrated in Figure 5.11.

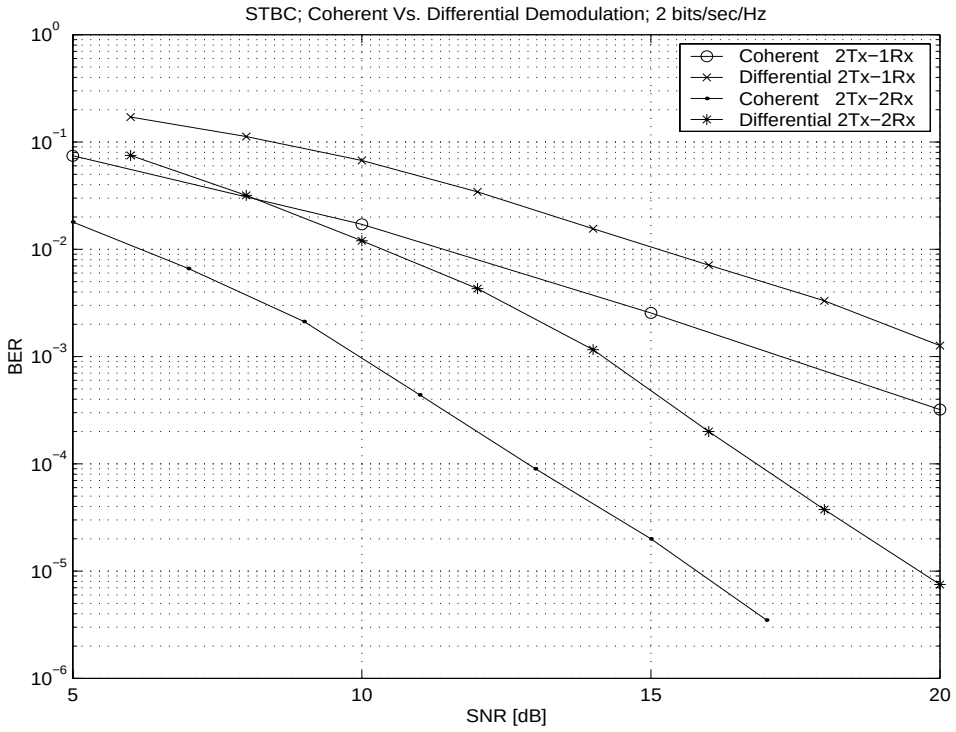

Figure 5.11: Coherent STBC Vs. differential STBC

It is observed that the performance of D-STBC is worse by 3 dB as compared to C-STBC scheme for both 2×1 and 2×2 antenna array configurations. However, the differential STBC scheme achieves the same diversity order as of the coherent scheme (2 and 4, for the two antenna configurations, respectively) without explicit knowledge of CSI. Next, the robustness of this scheme to carrier recovery mismatch is investigated.

5.3.2 Sensitivity of D-STBC to Phase and Frequency Errors

Carrier recovery mismatch in the range $0 - 2000$Hz is simulated for a baud rate of 100 [Kbaud]. Results are shown in Figure 5.12 for QPSK modulation, paired with G_2 orthogonal design, differential encoding-decoding and 2×2 antenna array configuration.

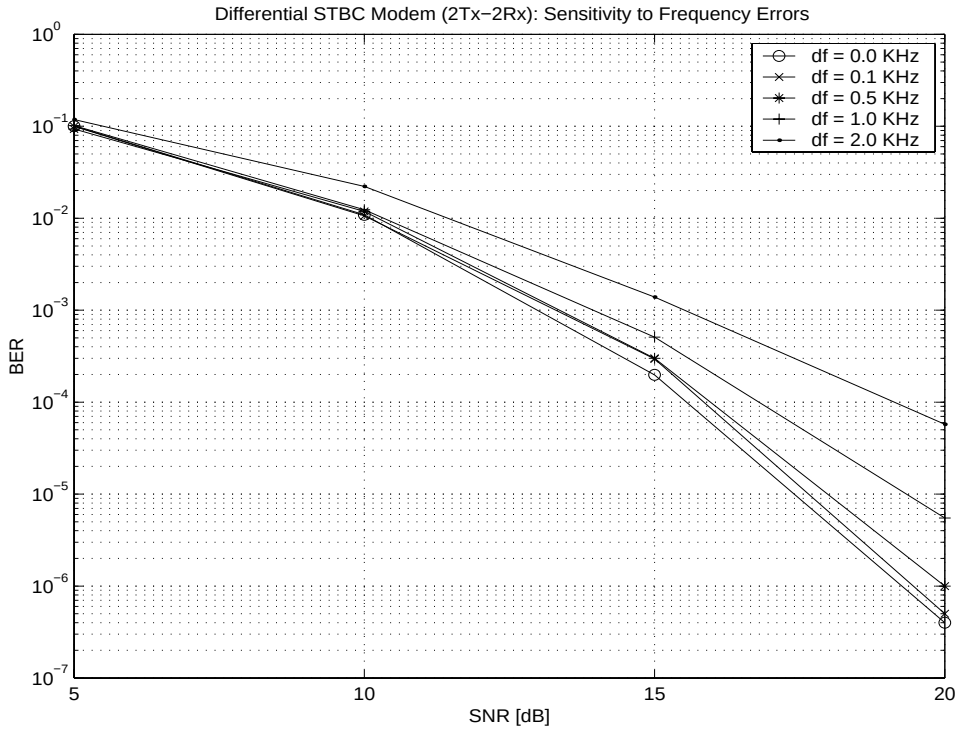

Figure 5.12: Sensitivity of D-STBC to phase and frequency errors

It is shown that the differential demodulation process is robust to residual frequency errors. Note that up to 1 KHz of frequency offset, negligible performance degradation is observed. Also, D-STBC schemes are not sensitive to phase errors as long as the phase error remains constant for a block of four consecutive symbols. The differential detection mechanism inherently eliminates the phase error created by a free-running local oscillator.

5.3.3 D-STBC in Correlated Rayleigh Fading Channels

Performance results for D-STBC scheme, operating over correlated Rayleigh fading channels, are presented. Figure 5.13 illustrates Monte Carlo simulation results for the scheme paired with QPSK and 2Tx-1Rx or 2Tx-2Rx antenna array configurations. The effect of correlation on the diversity performance of D-STBC schemes was examined by varying cross-correlation coefficients across transmit paths. Similar to C-STBC, results indicate that the effectiveness of D-STBC transmit diversity schemes is retained for cross-correlation coefficients as high as 0.5, with a limited penalty of 1 dB at BER of 10^{-3}.

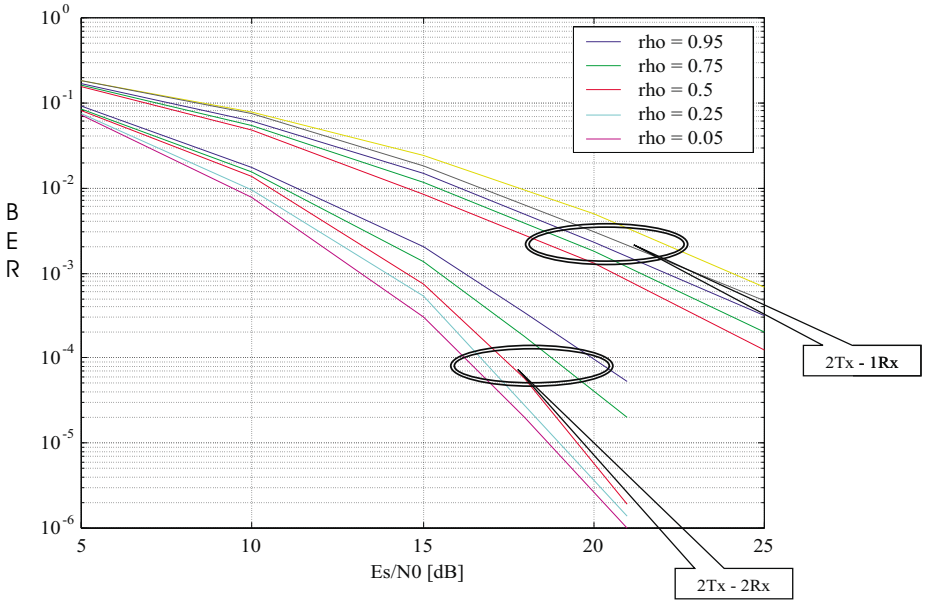

Figure 5.13: D-STBC over correlated fading channels; 2 [bps/Hz], 2Tx-1Rx, 2Tx-2Rx

5.4 Chapter Summary

This chapter presents BER analysis of space-time block codes in a variety of configurations. First, a simple analytic framework for coherent STBC, operating over independent and correlated fading channels, is presented. Tight upper bounds on the error probability of the scheme are derived and shown to be functions of the number of antenna elements at both ends of the link, the alphabet size, the orthogonal design rate, the signal-to-noise ratio and the array geometry. The analysis presented herein shows that the scheme is robust to spatial fading correlation and that the effective diversity order is determined by the geometric mean of the covariance matrix eigenvalues. This performance analysis will be presented at the 2002 International Symposium on Information Theory (ISIT) in Lausanne, Switzerland [83] and at the 2002 Spring Vehicular Technology Conference (VTC) in Birmingham, Alabama [84]. We have submitted the combined performance analysis over independent and correlated fading channels to *IEEE Communications Letters* [90].

Performance results for STBC schemes concatenated with outer error correction codes were also presented, showing that coding gain can be achieved in conjunction with spatial diversity order without sacrificing spectral efficiency. Finally, the chapter deals with the sensitivity of C-STBC to frequency and phase errors and explores the performance of differential STBC (D-STBC) architecture in independent and correlated environments. For its robustness, the D-STBC scheme has been selected as the first phase of implementation on the Virginia Tech Space-Time Advanced Radio (VT-STAR). The architecture of this laboratory testbed including the implementation details of the D-STBC on DSP platform is the subject of the next chapter.

Chapter 6

Virginia Tech Space-Time Advanced Radio (VT-STAR)

In previous chapters, the theoretical aspects of space-time coding techniques were investigated using analysis techniques and Monte Carlo simulation methods. In order to fully explore some of the implementation details of these schemes, a hardware platform is desired. While it is possible to study the performance of these algorithms in simulation, the assumptions inherent to simulation lead to results that may not match those of a practical real-world systems. In most of the work in this area, researchers have assumed ideal timing and phase tracking at the receiver as well as a perfect channel estimation process for their simulations. In practical systems, however, these assumptions are not realistic. In fact, the performance of the space-time architecture relies heavily on accuracy in tracking the channel [91].

In this chapter, the design and implementation of the Virginia Tech Space-Time Advanced Radio (VT-STAR) [92], a multiple antenna element space-time (ST) processing prototype testbed, is presented. The testbed is a research tool for comparing practical and theoretical performance metrics (e.g., throughput, link reliability) in different wireless channel conditions. The prototype builds around Software Defined Radio (SDR) concepts on a DSP platform and provides the flexibility to implement various forms of ST techniques. Different components of the system are described in detail, including the physical layer, DSP implementation, multi-channel data converters and Radio Frequency (RF) units. Two different example realizations are presented, a real-time demonstration and an off-line measurement tool. Finally, some representative measurement results obtained in indoor environments are presented. These results show VT-STAR to be a promising tool for performing MIMO experiments and generating channel measurements that can complement

simulation studies in this area.

There are several other MIMO testbed systems under development that have been reported in the recent literature. For example, a system with a single antenna element at the transmitter and 8 antenna elements at the receiver, denoted 1×8 architecture, operating at 2.4 GHz was developed at Ohio State University to measure the wireless channel in receive diversity settings [93]. Another approach to measure the characteristics of the MIMO channel is to use a wide variety of single input single output (SISO) measurements with static channel conditions [94]. By performing this series of measurements, the authors claim to measure the behavior of a MIMO channel. In [95], the authors estimate the channel using a 4×4 MIMO system that performs pseudo parallel transmissions, switching through antennas every 200 us, and performing parallel receptions of the signals. Wallace and Jensen in [96] implemented a 4×4 MIMO system with a wide variety of antenna geometries. This system is capable of performing measurements of the MIMO channel in the range of 0.8-6 GHz with a maximum bandwidth of 625 kHz. In comparison to these measurement platforms, the novel feature of the VT-STAR is that it allows channel measurements and real-time algorithm development on the same platform through the use of SDR concepts.

6.1 System Architecture

Some form of programmable processing is necessary to implement a variety of space-time algorithms. Two primary options are available that allow both programmability and high performance: FPGA (field programmable gate array) and DSP (digital signal processor). While FPGA offers a powerful platform that can provide higher performance than DSP, it suffers from one major drawback: a difficult programming interface. DSP, on the other hand, can be programmed in a high level language such as C, and can be programmed using floating point arithmetic, significantly reducing the complexity of the software. The major drawback in DSP is that it is not as fast or computationally efficient as an FPGA, limiting the complexity of the real-time algorithms that can be tested on the system. One of the fastest floating-point platforms available, the Texas Instruments TMS320C67 DSP [97] was selected as the computational platform, which is capable of 1350 MFLOPS. While a powerful processor was selected as the core of the VT-STAR, its real-time data exchange (RTDX) feature allows it to operate as an acquisition unit that stores the raw received data samples. Algorithms that are beyond the capabilities of the real-time processor or research that does not have real-time demands may be implemented using post-processing.

The architecture of the system, as illustrated in Figure 6.1, is based on a 2×2 antenna element array architecture, which allows the exploitation of transmit and receive diversity

mechanisms at the signal processing level. The processing on the transmitter side is carried out with a TI TMS320C6711 DSP Starter Kit (DSK) while that on the receiver side, with a TI TMS320C6701 Evaluation Module (EVM). Quarter wavelength vertically polarized monopoles on ground plane were used as the antenna elements because they offer a form factor that is close to the antennas on practical handheld wireless devices. Antenna spacing can be varied on the VT-STAR to study the impact of spatial correlation on performance. The Radio Frequency (RF) transmit and receive front ends accommodate a multi-channel two-stage up (and down) conversion between the RF section, which is centered at 2050 MHz, and the baseband section. The system bandwidth at the baseband level spans up to 750 kHz. Four identical and time-synchronized TI THS5661 EVMs, connected to the C67 DSK through custom interface boards, performed the Digital to Analog Conversion (DAC). A multi-channel TI THS1206 EVM, mated to the TMS320C67 EVM without an external interface board, performed the Analog to Digital Conversion (ADC) on the receiver side.

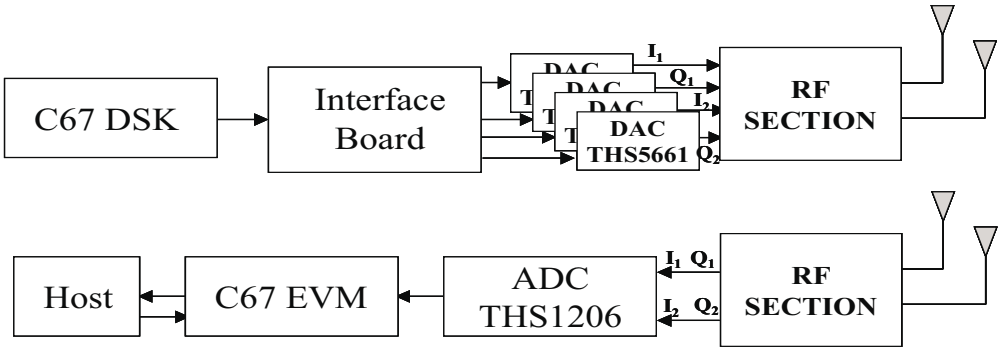

Figure 6.1: VT-STAR System architecture overview

The core algorithms, implemented on TMS320C67 floating-point DSP processors, include space-time encoding along with modulation and pulse shaping at the transmitter side and matched filtering, space-time processing, automatic gain control (AGC), channel estimation, timing recovery and maximum likelihood decoding at the receiver side. The RTDX feature of the C67 supports host target communications at the receiver side, and offers both real-time monitoring of physical layer parameters (e.g., bit-error rate, diversity gain, constellation diagrams) and data acquisition operation. A host PC, which runs a multi-threaded application to manage a MATLAB session is used to display the physical layer parameters, or perform post-processing of stored data.

6.2 Physical Layer Design

A general description of the physical layer structure is given in Figure 6.2.

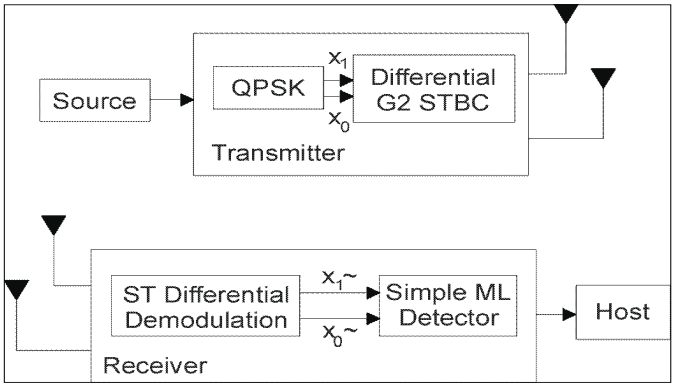

Figure 6.2: D-STBC transmitter/receiver structure

The encoding and decoding algorithms are described in this section followed by a description of the MIMO channel estimation process employed in VT-STAR. Also, the DSP implementation details of D-STBC are described including the software flow diagrams and the profiling of the code on C67 floating point processors.

6.2.1 Encoding/Decoding Algorithms

A. Encoding Algorithms

The D-STBC processing on the transmitter side commences with an information sequence denoted by I_k in Figure 6.3.

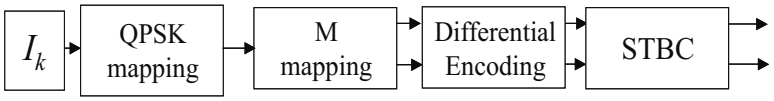

Figure 6.3: D-STBC transmission algorithm

The bits I_k are mapped to QPSK symbols coupled with Gray encoding. These QPSK symbols then undergo the core D-STBC processing, which is partitioned into three entities: M-mapping, differential encoding and STBC processing.

1. M Mapping: Perform change of basis from the natural basis to an orthonormal design described by the following M Matrix:

$$M = \begin{pmatrix} a_1 & a_2 \\ -a_2^* & a_1^* \end{pmatrix} \tag{6.1}$$

Mathematically,

$$\begin{aligned} A &= a_3 a_1^* + a_4 a_2^* \\ B &= -a_3 a_2 + a_4 a_1 \end{aligned} \tag{6.2}$$

where $(a_1, a_2) = (\frac{1}{\sqrt{2}}, \frac{1}{\sqrt{2}})$ is a reference vector, and (a_3, a_4) is a pair of QPSK information symbols.

2. Differential Encoding: The differential encoder uses previously transmitted symbols and current input symbols to compute a pair of symbols to be transmitted next.

$$\begin{aligned} s_3 &= A s_1 - B s_2^* \\ s_4 &= A s_2 + B s_1^* \end{aligned} \tag{6.3}$$

where (s_1, s_2) is a pair of previously transmitted symbols. The procedure is repeated in an inductive manner.

3. STBC: The outputs from the differential encoding process are mapped by G_2 mapping to form two parallel baseband complex symbol streams for two antenna branches.

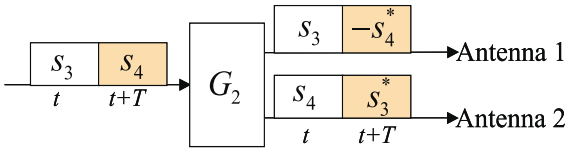

Figure 6.4: G_2 mapping

The G_2 mapping maps block of $k = 2$ symbols (s_3 and s_4) to two orthogonal sequences of length $p = 2$. G_2 mapping provides an orthogonal design, which facilitates the space-time processing stage at the receiver in order to decouple the symbols and obtain an estimate for the pair (A, B).

The resulting baseband complex symbols, I_1, Q_1 for antenna 1 and I_2, Q_2 for antenna 2 were individually pulse shaped by square root-raised-cosine (SRRC) filters with rolloff factor of 0.35. The pulse-shaping filters are of finite impulse response (FIR) filters with 19 taps. Four filters (I and Q each for two antennas) with over-sampling factor of 3 were implemented. Finally the filter outputs were properly formatted in the data-packing segment to match the output interface requirements.

B. Decoding Algorithms

A block diagram of the core detection modules is illustrated in Figure 6.5. The raw in-

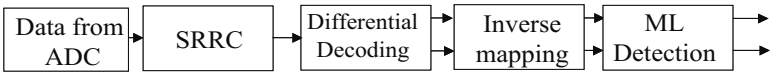

Figure 6.5: Signal flow diagram of DSP Rx

phase and quadrature samples, collected from the ADC FIFO, are first processed by a SRRC matched filter with rolloff factor 0.35. The matched filter is a mirror image of the pulse shape at the transmitter. Next, the following sub-algorithms are performed:

1. Space-Time Processing: Perform differential demodulation for both receive channels:

$$\begin{aligned} R_1^j &= (r_{2t+1})^j (r_{2t-1}^*)^j + (r_{2t+2}^*)^j (r_{2t})^j \\ R_2^j &= (r_{2t+1})^j (r_{2t}^*) j - (r_{2t+2}^*)^j (r_{2t-1})^j, j = 1, 2 \end{aligned} \tag{6.4}$$

where $r^j = (r_{2t-1}^j, r_{2t}^j, r_{2t+1}^j, r_{2t+2}^j)$ denotes the jth receive vector of 4 consecutive symbols.

2. Automatic Gain Control (AGC): the norm of the vector $(R_1, R_2)^j, j = 1, 2$ is evaluated for receiver chains 1 and 2. This norm is averaged by a first order Infinite Impulse Response (IIR) filter to obtain average gain of each channel.

$$AGC^j = \alpha d^j + (1 - \alpha) AGC^j, \tag{6.5}$$

where $d^j = ||(R_1, R_2)^j||, j = 1, 2$.

3. Rx Combining: decision statistics are summed across the two receive antenna elements using an Equal Gain Combining (EGC) approach.

$$\begin{aligned} R_1 &= R_1^1 + R_1^2 \\ R_2 &= R_2^1 + R_2^2 \end{aligned} \tag{6.6}$$

4. Maximum Likelihood (ML) Decoding: ML detector is performed to determine the vector $(\hat{A}, \hat{B})$ that is the closest (in terms of Euclidean distance) to the decision statistics vector (R_1, R_2). Choose $(\hat{A}, \hat{B}) = (A, B)_i$ such that

$$min(d^2((R_1, R_2), (A, B)_i)). \tag{6.7}$$

6.2.2 MIMO Channel Estimation in VT-STAR

Assuming flat fading environment, the received signals at receive antenna j at times t and $t + T$ are modeled by:

$$\begin{aligned} r_t^j &= h_{1j} s_3 + h_{2j} s_4 + \eta_t^j \\ r_{t+T}^j &= h_{1j} (-s_4^*) + h_{2j} s_3^* + \eta_{t+T}^j, \end{aligned} \tag{6.8}$$

where h_{ij} corresponds to the complex fade coefficient from transmit antenna i to receive antenna j, η_t^j is the additive white Gaussian noise term at receive antenna j at time instant t and $\{s_3, s_4\}$ are the two M-ary PSK symbols at the input of the space-time block encoder.

Based on channel estimation of the fade coefficients h_{ij}, a simple linear processing rule can decouple the symbols s_3 and s_4 from the above superposition to yield a separate decision statistics with diversity fold of $2n_R$ [19], where n_R correspond to the number of antenna elements at the receiver.

On the other hand, assuming knowledge of the symbols s_3 and s_4 (either via pilot symbols transmission in "data-aided" mode or symbol decisions in "decision-directed" mode), it was shown by Tarokh et al. in [21] that a linear processing rule can extract an estimate for the MIMO channel fade coefficients. This linear processing is described by:

$$\begin{aligned} \tilde{h}_{1j} &= \frac{r_t^j s_3^* - r_{t+T}^j s_4}{|s_3|^2 + |s_4|^2} = h_{1j} + \frac{s_3^* \eta_1^j + s_4 \eta_{t+T}^j}{|s_3|^2 + |s_4|^2} \\ \tilde{h}_{2j} &= \frac{r_t^j s_4^* + r_{t+T}^j s_3}{|s_3|^2 + |s_4|^2} = h_{2j} + \frac{s_4^* \eta_1^j + s_3 \eta_{t+T}^j}{|s_3|^2 + |s_4|^2}, \end{aligned} \tag{6.9}$$

where $\tilde{h}_{1j}$ and $\tilde{h}_{2j}$ represent noisy estimates of the channel fade coefficients h_{ij}. The symbols s_3 and s_4 can be either regenerated at the receiver in "decision-directed" mode or based on transmission of known pilot symbols. In the "decision-directed" mode, regenerating the symbols s_3 and s_4 includes: QPSK mapping, M mapping and differential encoding. Simulation results for this technique are illustrated in Figures 6.6, 6.7, 6.8 for noise free, $SNR = 17$dB and $SNR = 12$dB, respectively. The Doppler frequency to symbol duration product is assumed to be $f_d T = 0.00333$. Antenna configuration is 2×2 and each sub-figure corresponds to the fade coefficient $\tilde{h}_{ij}$ (original and estimated).

For high SNR, the proposed algorithm performs very well. However, for low regions of SNR, the variance of channel estimates increases as expected from Eq. (6.9). Once decision errors occur, the algorithm suffers from error propagation process. This is illustrated in Figure 6.8 where in some instants, channel estimates are wrong as compared to the original fading envelopes. In our actual MIMO channel measurement campaign, we select to use the data-aided mode where a pre-defined (known) set of symbols is transmitted and used at the receiver to guarantee a robust estimation process.

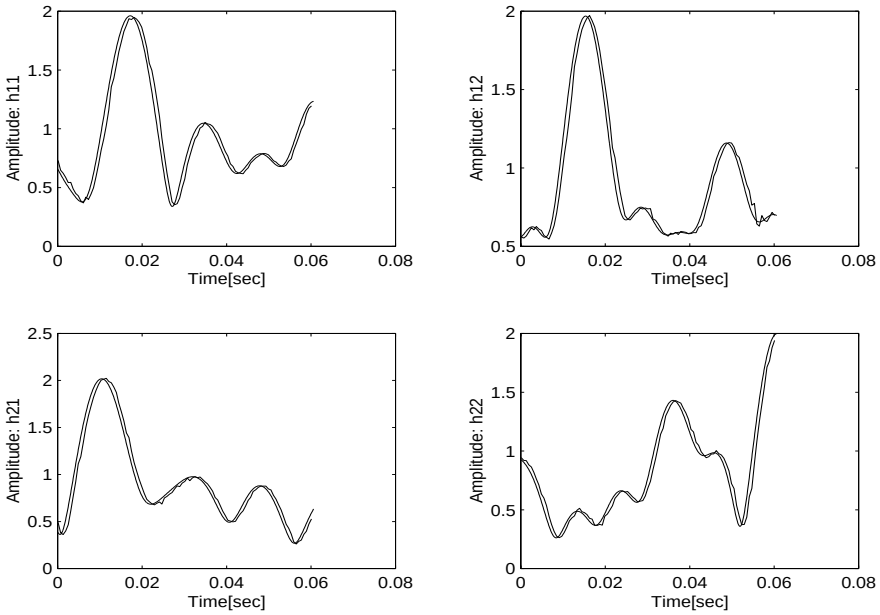

Figure 6.6: Simulated blind MIMO channel estimation for D-STBC - noise free channel

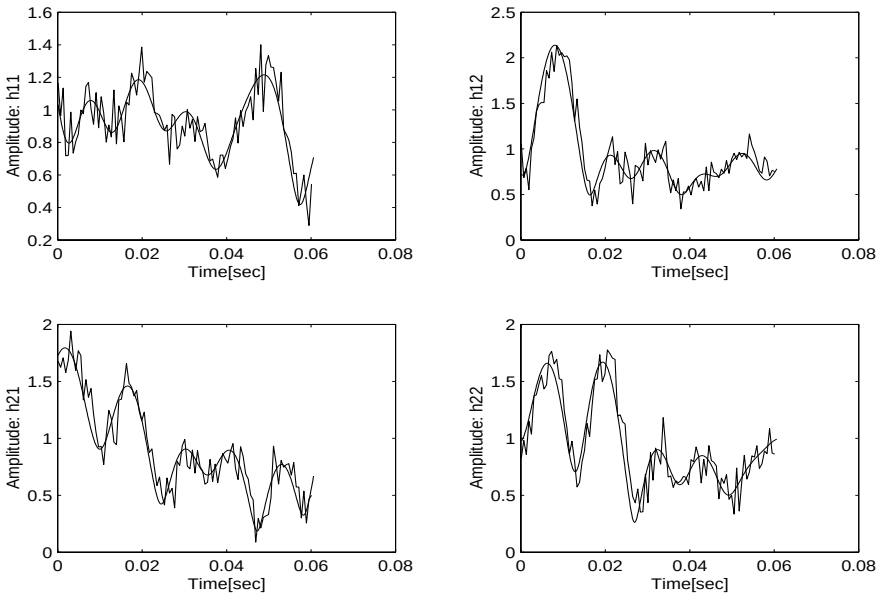

Figure 6.7: Simulated blind MIMO channel estimation for D-STBC ; $SNR = 17$ dB

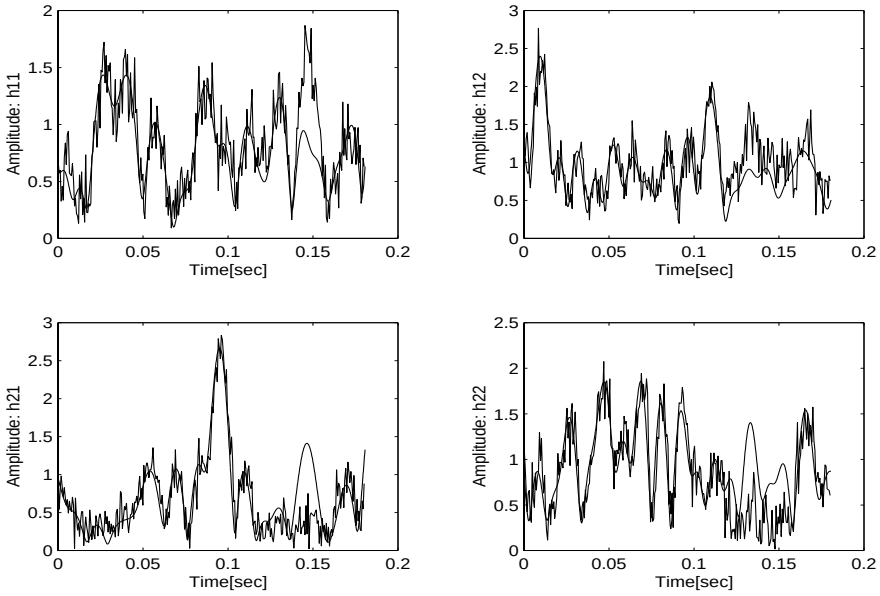

Figure 6.8: Simulated blind MIMO channel estimation for STBC ; $SNR = 12$ dB

6.2.3 DSP Implementation

Prior to implementing the algorithms on the DSP, a complete link level simulation was developed in MATLAB. The simulation tools played an important role in the design process of the radio, providing a verification of system level issues such as performance versus complexity tradeoffs. These tools also act as a source for generating test vectors for validating the different DSP functional blocks, simplifying the debugging process of the DSP code.

The flow diagrams of the software implemented on C67 are shown in Figures 6.9 and 6.10 for the transmitter and receiver, respectively.

Most of these modules were implemented in C, while some of the computationally dominant segments were programmed in assembly. The pulse shaping filtering was identified as the computationally dominant segment, and as such was targeted for optimization. The code optimization process for the filters included transition from C implementation to linear assembly and finally to hand-coded assembly with circular buffers [98]. This optimization process reduced the number of clock cycles required for the filtering operation by more than an order of magnitude. Since the filter was designed to be 19 taps long, circular addressing had to be rounded to the next power of 2 (32). Other optimization segments included removal of division, power and square root operations. Since multiple function calls affect performance, code readability had to be compromised for speed.

Profiling was performed on the overall code and the resulting number of clock cycles required for each functional block are shown in Figures 6.11 and 6.12 for the transmitter

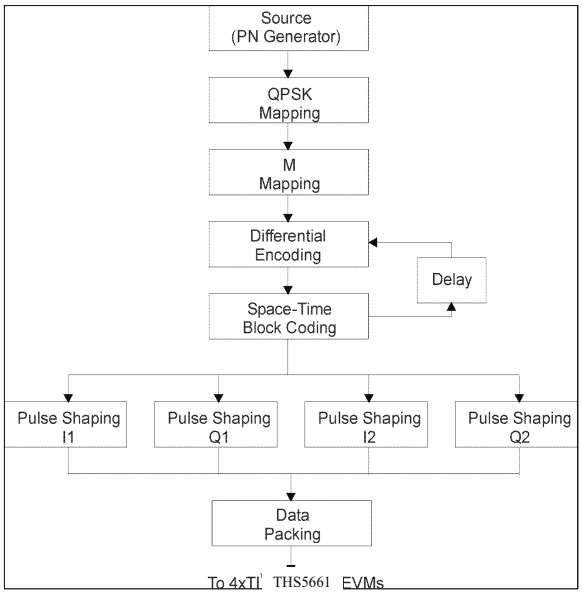

Figure 6.9: Transmitter software flow chart

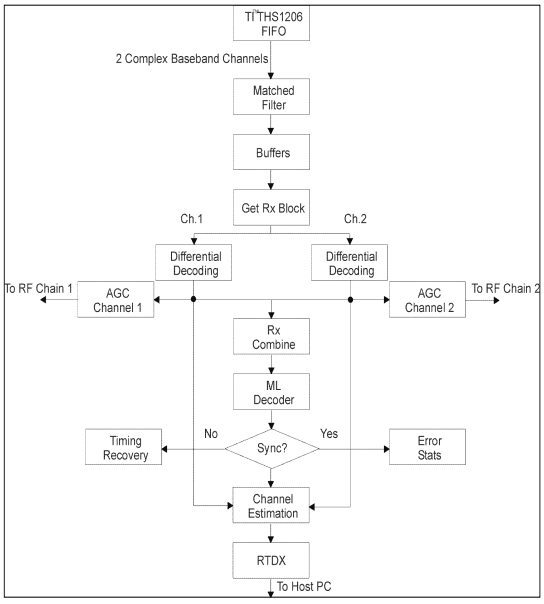

Figure 6.10: Receiver software flow chart

and receiver, respectively. Note that the instruction cycle of the DSK (transmitter) is 6.7 nanoseconds (ns), while an instruction cycle of the EVM (receiver) is 7.5 ns.

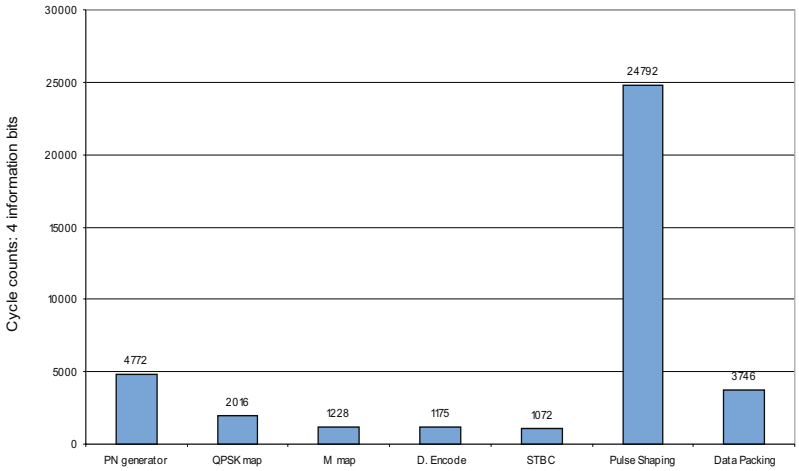

Figure 6.11: VT-STAR transmitter DSP profiling results

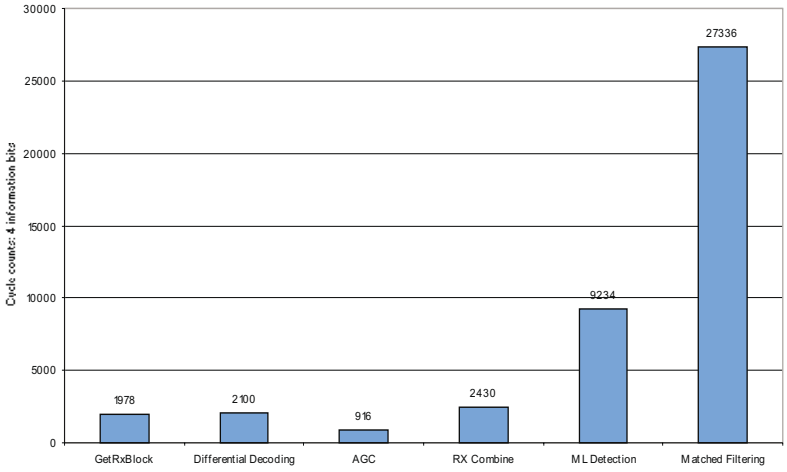

Figure 6.12: VT-STAR receiver DSP profiling results

The cycle counts represent the time required for processing 4 information bits. Pulse shaping block represents SRRC filtering in assembly on 24 samples and presents itself as the most computationally intensive process. Pseodu-Noise (PN) generator and data packing at the transmitter and Maximum Likelihood detection at the receiver dominate the remaining processes.

6.3 Multi-Channel Data Conversion

A complex baseband output and input was selected for the digital hardware at the transmitter and receiver, respectively. In order to represent two complex baseband channels, 4-channel ADC and DAC were used. A key requirement for the operation of the space-time coding modem is to have synchronous transmission and reception at the antenna arrays. The ADC was implemented using the TI THS1206 ADC EVM [99, 100], allowing a 4-channel ADC to be mated directly to the TI C67 EVM as a mezzanine board. Since a 4-channel DAC was not avaliable on a single board, four TI THS5661 DAC boards [101] were placed in parallel, driven from a common clock. A block diagram of the transmitter is shown in Figure 6.13.

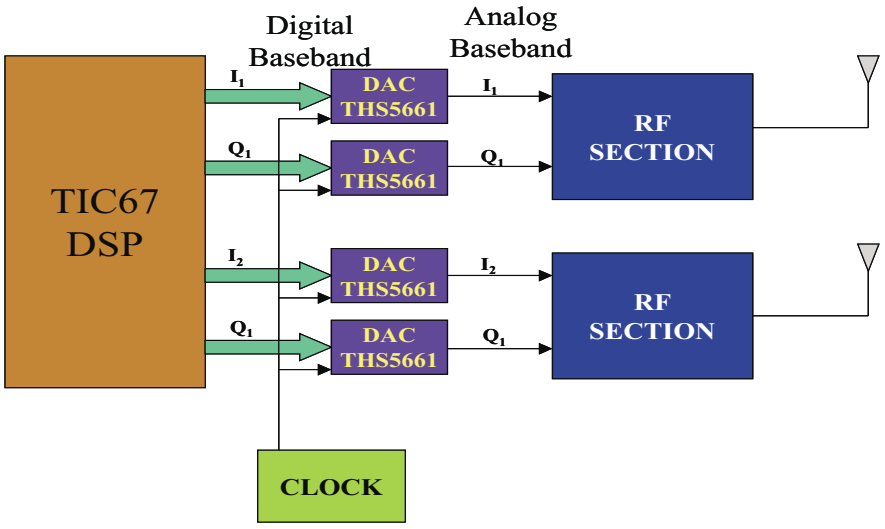

Figure 6.13: VT-STAR multi-channel DAC architecture

The signals to these 4 boards were driven from a single TI C67 DSK board via the expansion peripheral bus. To allow this interface, two custom-designed boards were developed. First, an adapter board, seen in Figure 6.14, which interfaces a 50-mil surface-mount connector (J6 or J7) to a regular 100-mil type connectors to allow ribbon cable connectivity. Second, an interface board, seen in Figure 6.15, which performs splitting of the DSP timer signal via a clock distribution chip (CDC) and splitting of 32-bit word into four 8-bit words, each of which drives a single TI THS5661 DAC board.

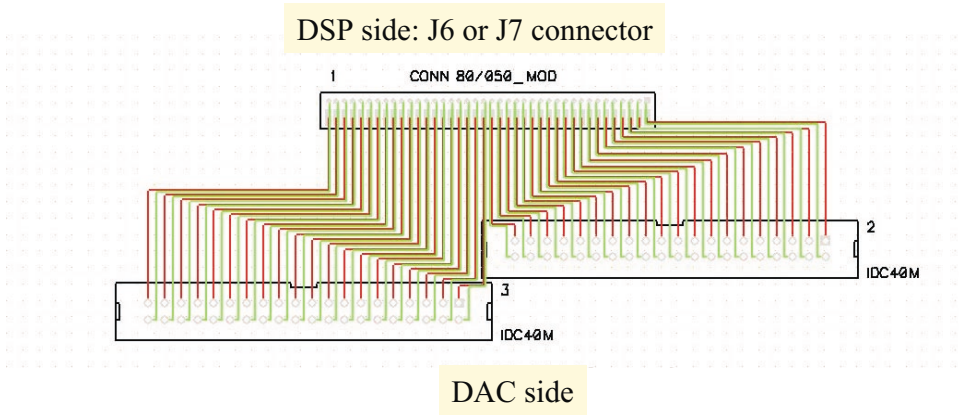

Figure 6.14: VT-STAR adapter board for 4xTI THS5661 / TI TMS320C67

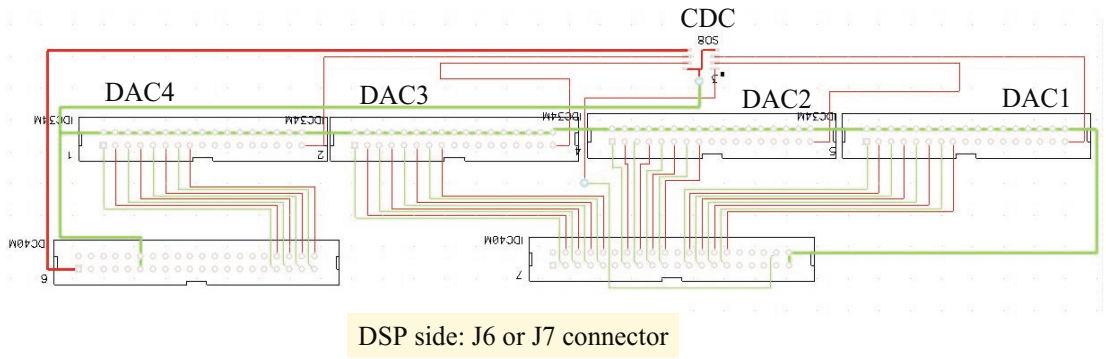

Figure 6.15: VT-STAR 4-way interface board for TI THS5661 DAC

6.4 RF Design

The RF section of the transmitter accepts complex baseband signals (I and Q) produced by the digital hardware and generates RF signals, which are transmitted using two separate transmit antennas. The signals are then down-converted to a band suitable for use by the sampling hardware. The VT-STAR operates at the 2050 MHz band because of the band's similarity in propagation characteristics to the U.S. PCS and worldwide 3G radio bands. Performance improvements demonstrated in the 2050 MHz band by VT-STAR would be realizable by worldwide wireless communication systems operating in nearby bands. Table 6.1 summarizes key parameters used in the design of the radio front-end.

Table 6.1: VT-STAR RF specification summary

RF Parameter	*Value*
Center Frequency	2050MHz
Maximum Signal Bandwidth	750kHz
Receiver Noise Floor	-110 dBm
Maximum Receiver Input Power	-50 dBm
Spurious-Free Dynamic Range (SFDR)	60 dB
Transmitter Input Baseband I/Q	35mV RMS
Receiver Output Baseband I/Q	140mV RMS
Transmit Power (Maximum/Nominal)	28 dBm / 0 dBm
Transmitter/Receiver Input/Output Impedance	50W

Two vertically polarized, co-planar, quarter-wavelength monopole antennas are used to transmit the signal through the radio channel. The architecture of the receiver and transmitter stages was designed based on the availability of RF components. The 68 MHz IF selection was based on the availability of I/Q demodulators, and two stages of frequency conversion allows amplification to be divided among the stages, preventing the possibility of receiver instability. A block diagram of the transmitter and receiver are given in Figures 6.16 and 6.17, respectively.

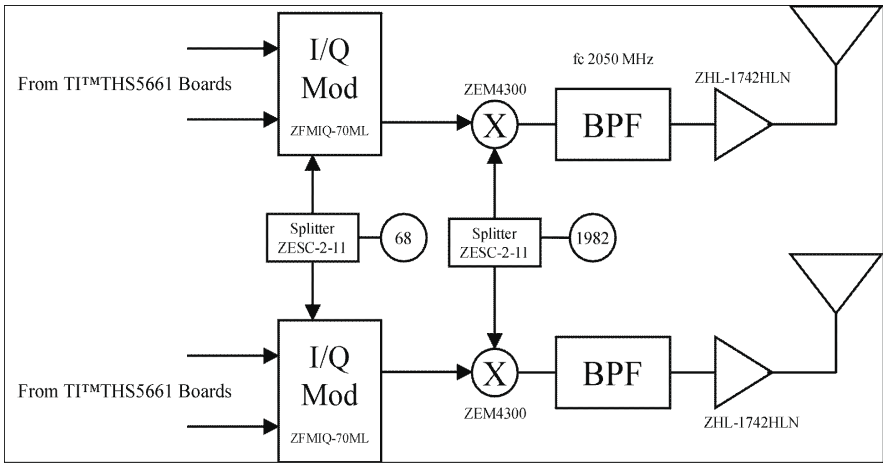

Figure 6.16: VT-STAR transmitter radio front-end

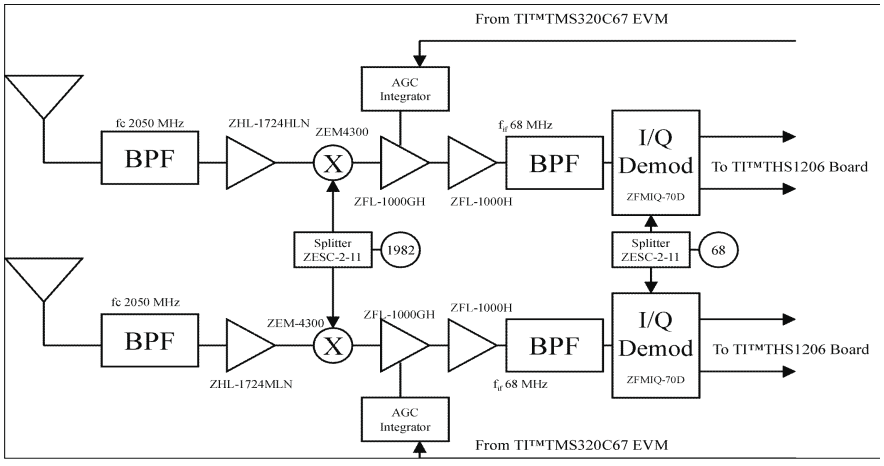

Figure 6.17: VT-STAR receiver radio front-end

6.5 Receiver Operating Modes

The VT-STAR receiver has two modes of operation: continuous mode and snapshot mode. In the continuous mode, the receiver DSP operates in real-time, performing full space-time demodulation and decoding and sending relevant physical layer parameters to the host PC via the RTDX. This mode is used to demonstrate the capabilities of space-time coding and to study the interactions between space-time decoding, timing recovery and channel estimation. In the snapshot mode, the receiver DSP is used as a data acquisition device. It collects raw data into buffers and dumps the buffer contents into the host PC's hard drive for post-processing in MATLAB. This mode is used to study the spatial and temporal characteristics of the MIMO channel. MIMO channel measurements are post-processed to address the achievable throughput and reliability in a variety of indoor realizations.

Communications between the host computer and the C67 EVM are performed through the EVM's RTDX capabilities. RTDX supports bi-directional real-time transfer of data between the host PC and the target DSP through the JTAG interface such that the target application is almost not affected [102]. Target-host communications protocol used by the RTDX is shown in Figure 6.18. The asynchronous nature of the protocol guarantees that buffer overflow does not occur.

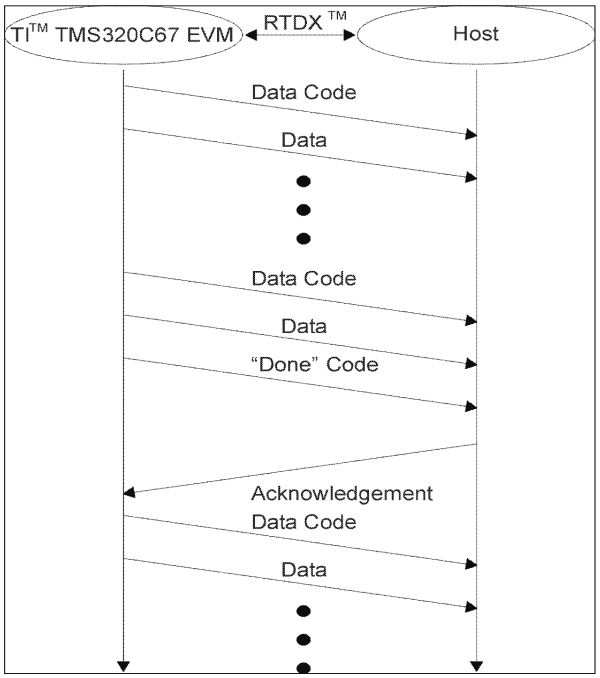

Figure 6.18: Communications protocol over RTDX

Each "data code" in Figure 6.18 corresponds to a specific type of data to be transported in the next data set, while "done code" indicates the completion of data transfer.

The data collected by the host PC is passed to the MATLAB environment for post processing and display. A sample of the telemetry data sent from the receiver processor is shown in Figure 6.19, including constellation diagrams at the matched filter output before and after the decimation process (over sampling factor = 3), AGC curves for estimated received signal power in dBm, fading profiles of the MIMO channel, diversity gain curves and bit error rate (BER) measurements. This sample was collected from the target DSP by using synthetic data at the input to the DSP. It validates the real-time processing at the DSP receiver and the communication protocol with the host PC via RTDX.

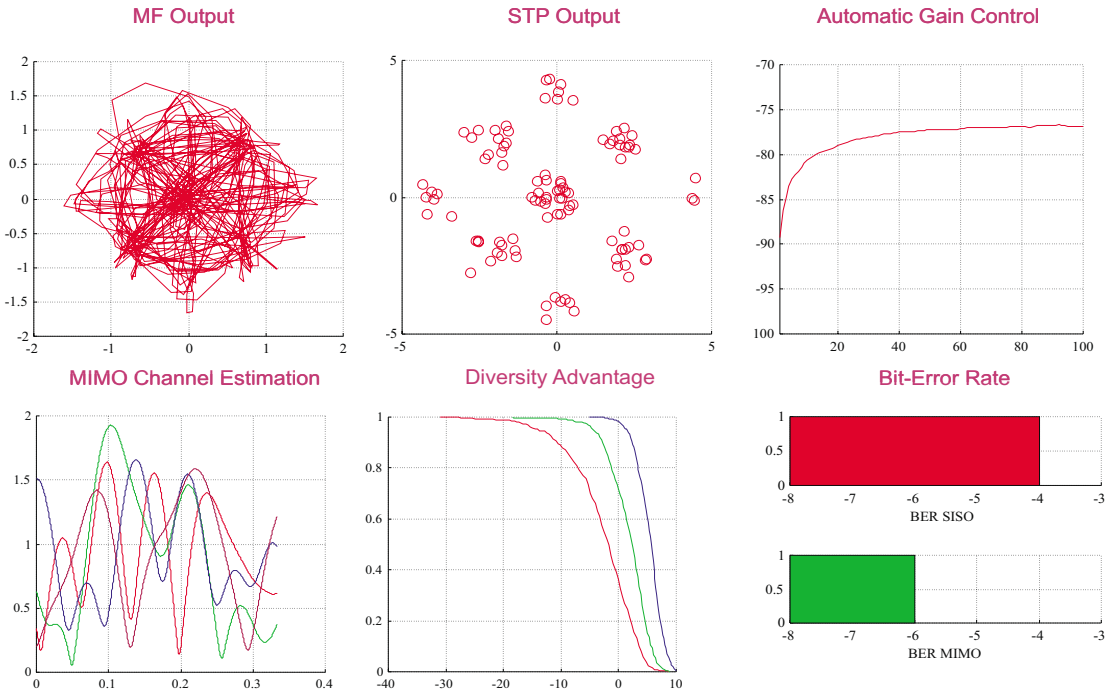

Figure 6.19: VT-STAR physical layer display

In the sanspshot mode, the receiver DSP collects and temporarily stores a preset number of received samples within the snapshot window, and transfers these samples to the host PC memory using the RTDX [102]. The stored data is retrieved by MATLAB and post-processed to characterize the MIMO channel.

6.6 Validation Process and Pattern Distortion

In this section, the measurement methodology and setup are presented. Prior to the collection and processing of Non Line-Of -Sight (NLOS) MIMO channel measurements, we perform validation process based on back-to-back settings and controlled over-the-air transmission.

6.6.1 Back-to-back Testing

The functionality of the complete system excluding the RF hardware is validated by connecting the baseband processing units on both sides of the link in a back-to-back manner and collecting data in this settings. The setup is shown in Figure 6.20. The principle behind this testing is to estimate and validate the channel gains, which represent two uncoupled SISO links between the transmitter and the receiver.

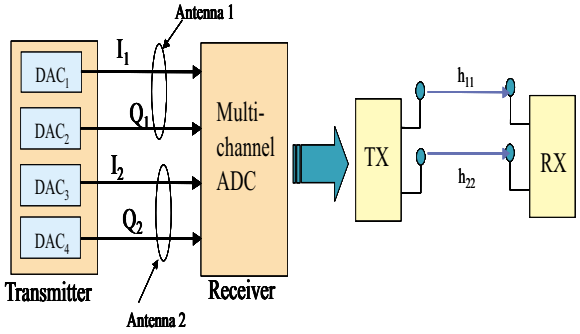

Figure 6.20: Back-to-Back Testing Configuration

Figure 6.21 presents the estimated squared channel gains. The path gains h_{11} and h_{22}, which represent the uncoupled LOS single-input single-output channels are constant and centered at 0dB while the cross-channels h_{12} and h_{21} are 25dB down. This confirms that our data collection mode is functioning correctly.

6.6.2 Over-the-air Testing

The transmitter and the receiver are calibrated in a LOS environment with the end-fires of both transmitter and receiver facing each other as shown in Figure 6.22. This forms an inline orientation between the arrays. MIMO Channel measurements are presented in Figure 6.23.

The estimated channel envelope profiles reveal that the environment is stationary and that the order of the MIMO channel estimates follows the following pattern: $|h_{22}| > |h_{21}| >$

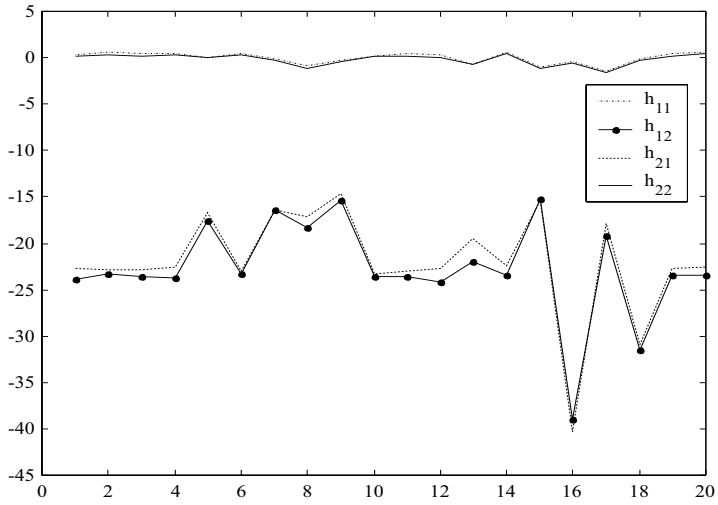

Figure 6.21: MIMO channel estimations ($|h_{ij}|^2$ in dB) using VT-STAR in back-to-back testing mode

Figure 6.22: Over-the-air testing Configuration

$|h_{12}| > |h_{11}|$. That is, the channel gains from transmit antenna 2 are stronger than the corresponding gains from transmit antenna 1. This is in agreement to what is expected due to the nature of pattern distortion for inline orientation [103, 104]. Radiation pattern plots for an individual element from electromagnetic modeling, using NEC software are presented in Figure 6.24.

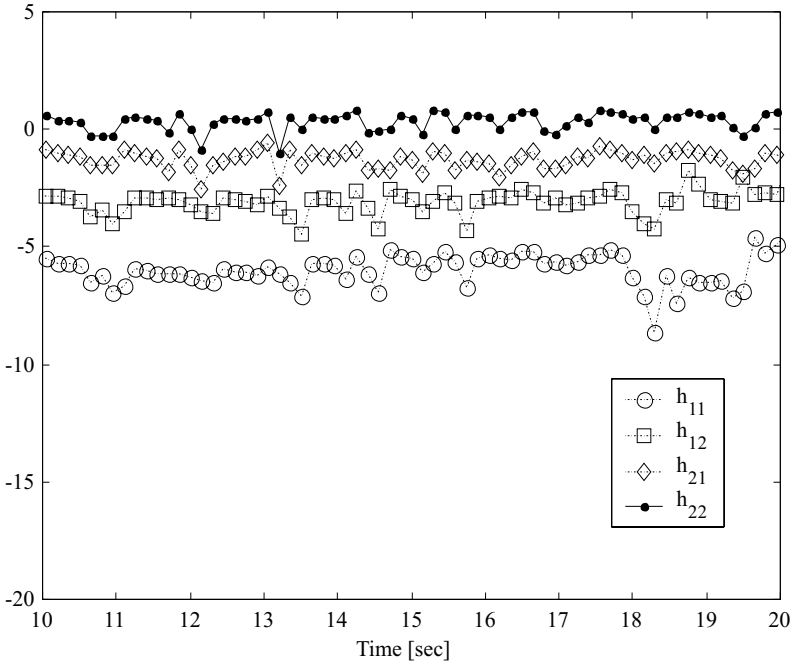

Figure 6.23: Over-the-air testing Results, $(|h_{ij}|^2$ in dB)

The radiation pattern plot corresponds to a dipole antenna element in a 2-element array with inter-element distance of 0.5λ (elements marked with X). It is assumed that the same general pattern would hold for a monopole on a ground plane. The radiation pattern for the other element will be a mirror image of the pattern shown here. The resulting pattern distortion would affect propagation characteristics and consequently diversity performance of the antenna array.

This experiment validates the functionality of the overall VT-STAR system, operating over a wireless MIMO link.

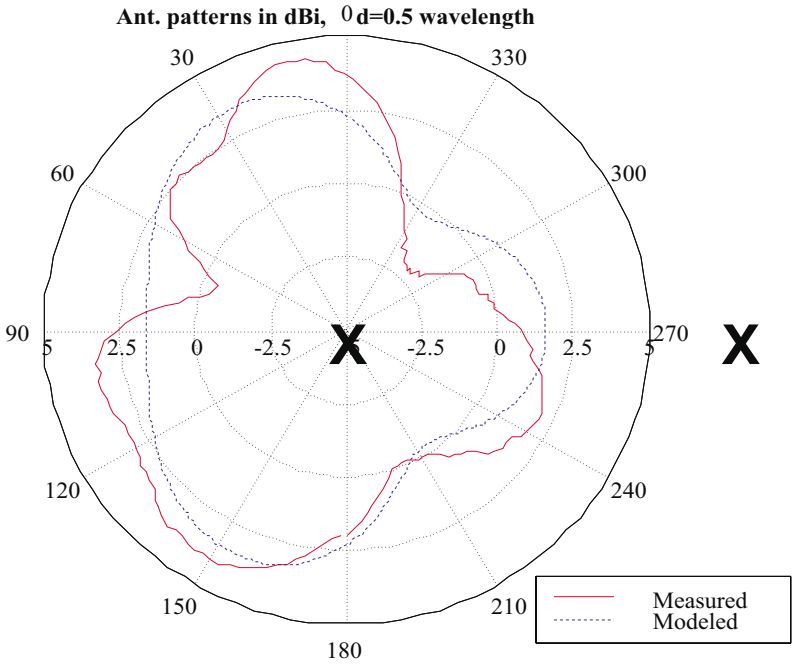

Figure 6.24: Measured Antenna Pattern Distortion

6.7 MIMO Capacity Measurements

In this section, we use the MIMO channel estimates, collected in various locations, to compute the capacity achieved by various antenna array configurations [105]. Capacity in this case refers to throughput, normalized with respect to the bandwidth and is measured in [bps/Hz]. The measurements have been collected by placing the receiver and transmitter in two fixed locations in MPRG's DSP lab, using obstructions to maintain a NLOS link. The DSP lab presents an indoor environment rich with local scatterers, and a concrete column in this lab served to provide a NLOS link.

To calculate the capacity of the MIMO channel, we use the result of Foschini et al. [2]:

$$C = log_2 det\left[I_{n_R} + (SNR/n_T)HH^{\dagger}\right]. \tag{6.10}$$

where $H = [h_{ij}]$ and $H^{\dagger}$ is the transpose conjugate of H. Each element h_{ij} refers to the channel gain from the ith transmit antenna to the jth receive antenna. SNR is the signal-to-noise ratio at the jth receive branch and I_{n_R} is an $n_R \times n_R$ identity matrix. Figure 6.25 compares measured capacity in NLOS environment of each one of the SISO links ($C_{h_{11}}$, $C_{h_{12}}$, $C_{h_{21}}$ and $C_{h_{22}}$) with the capacity achieved by employing MIMO configuration. The SNR is fixed to 20 dB. With the use of 2×2 antenna array configuration, 2-fold capacity

increase is observed as compared to any one of the SISO channels.

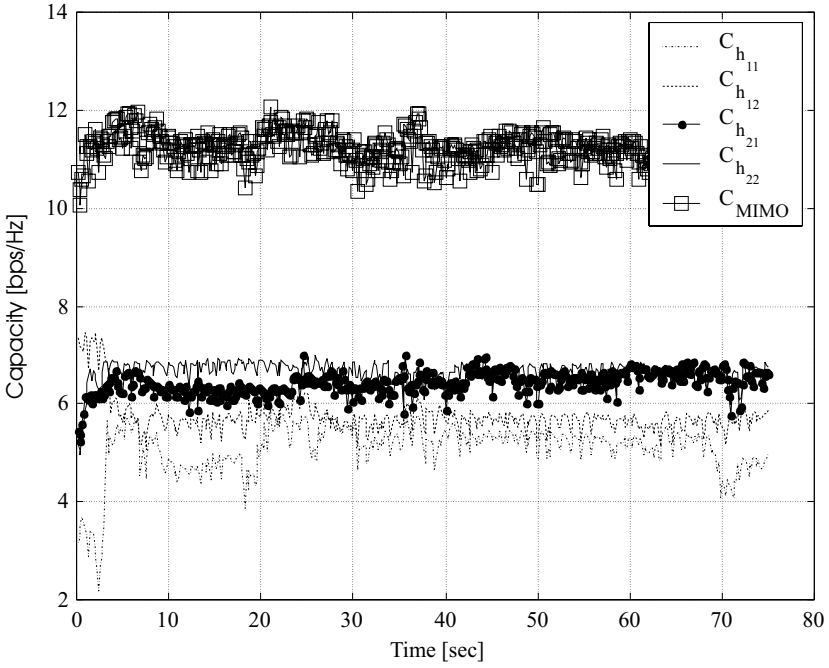

Figure 6.25: Channel capacity; SISO vs. MIMO channel

Next, we compare the capacity of the MIMO channel with the capacity achieved by a single-input multiple-output (SIMO) channel with either optimal combining (OC) or diversity selection (DS) criteria, multiple-input single-output (MISO) channel employing transmit diversity only and single-input single-output (SISO) channel. Figure 6.26 illustrates the measured histograms for these cases. Similar to the theoretical results of [2], MIMO channel capacity outperforms receive (SIMO) or transmit diversity (MISO). Within receive diversity schemes, optimal combining is better than selection diversity as expected. Note that receive diversity outperforms transmit diversity due to the constraint of same total radiated power in both schemes. In the transmit diversity case, power is distributed equally across transmit antenna elements, resulting in lower effective SNR at the combiner output.

To compare the empirical findings with theoretical ones, theoretical capacity results in the form of complementary cumulative distribution functions (CCDF) are presented in Figure 6.27. We observe that only 30% of channel realizations will achieve capacities comparable to those measured in our lab. An on-going goal of this test-bed is to perform an extensive measurement campaign to capture more channel realizations in indoor NLOS settings.

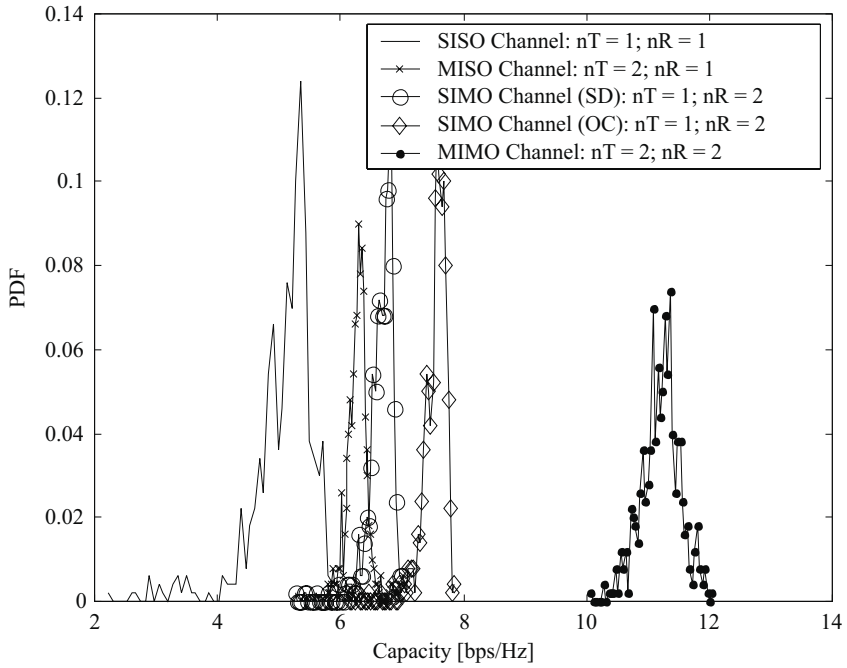

Figure 6.26: Capacity histograms: SISO, transmit diversity, receive diversity and MIMO channels

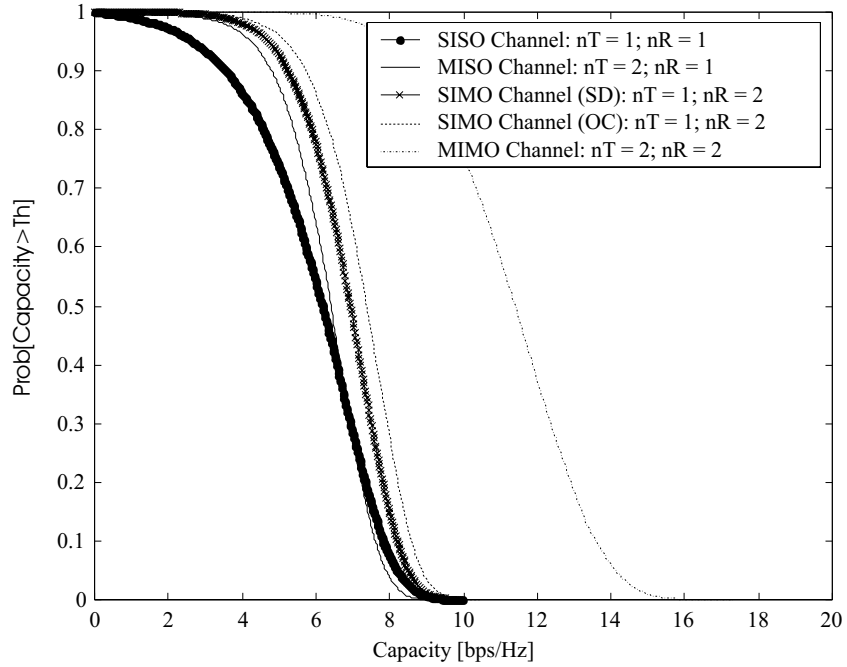

Figure 6.27: Theoretical capacity; SNR = 20dB

6.8 Limitations of the Design and Key Issues

This section summarizes some of the limitations of the hardware test bed along with possible expansions.

- Limitations on Bandwidth and Throughput -
  The bandwidth of the signal is limited to 750 KHz due to limitations imposed by the sampling hardware at the receiver (the THS1206 ADC's maximum sampling rate is 1.5 Msps/channel, assuming that all four channels are active). However, the bottleneck in terms of signal bandwidth and throughput is the processing unit which is based on a single processor. As an example, maximum data rate of 50 Kbps was achieved for the computational complexity of space-time block codes with 2×2 antenna array architecture. To allow for higher data rates and/or higher number of antenna elements, it is recommended to consider board with multiple processors than has parallel processing capabilities or a reconfigurable hardware architecture that combines Field Programmable Gate Array (FPGA) with DSP.

- Interface Issues -
  Interfacing the multi-channel DAC architecture to a single DSP requires custom designed hardware to be developed. This hardware was described in section 6.3, which was one of the most time consuming efforts throughout the design of the prototype. At the receiver side, this was inherently solved as the THS1206 EVM board mates directly to the $C67$ DSP board as a mezzanine board.

- DC Offset -
  THS56x1 DAC has DC offset in its single ended output for low update rates (< 100 Ksamp/sec). This is undesirable since DC offset translates into a carrier after upconverting. The differential output can be used to avoid DC offsets but it does not function at low data rates. The solution for the VT-STAR test bed was based on placing a DC blocking capacitor at the single ended output of each DAC.

- Reconstruction Filter at DAC output -
  The THS56x1 DACs do not have reconstruction filter at their outputs and thus harmonic distortion is present.

- DAC Resolution -
  Since the space-time coding algorithm requires simultaneous transmission of 4 pulse shaped samples, parallel data transfer between the DSP and data converters has to be performed. The Expansion Memory Interface (EMIF) of the DSP board was used

to transfer in parallel 32 bit words, containing four simultaneous samples (I and Q for two transmit antennas). Thus, the 32-bit word supports 4 pulse shaped samples each of which is 8-bit wide. Therefore, the floating point sample is quantized into an 8-bit sample rather than utilizing the 12-bit resolution of the THS5661 DAC.

- FIFO Memory in Multi-Channel DAC -
  For the real-time data transfer between the DSP and multi-channel DAC at the transmitter, DSP memory is used since FIFO on the DAC is not available. A DAC with a FIFO settings might be beneficial for efficient memory utilization in real time transmission.

- Multi-Channel ADC -
  The THS 1206 multi-channel ADC has problems in its FIFO functionality. Whenever all four channels are used, the FIFO has overflow occurring. Only reseting of the FIFO with a command from the DSP will assure continuous operation. This phenomenon is undesirable as the FIFO reset introduces time jitter.

- Timing Issues -
  Since the DAC and ADC at the transmitter and receiver, respectively, are driven from different clock sources, time drift occurs. This implies a requirement for a symbol tracking algorithm in addition to the acquisition algorithm. At each side of the link, the multi-channel data converters have to be driven from a single source to guarantee synchronous transmission and reception. This is achieved by distribution of the clock signal form the DSP using a Clock Distribution Chip (CDC).

- Hooks for expansion -
  Expansions can be performed in the following directions:

  1. Range of operation - to allow for outdoor MIMO experiments, an additional amplification unit at the transmitter RF front end should be added. The maximum range of the current hardware is 70 meters and is intended for indoor studies.
  2. Numbers of antenna elements - The array architecture can be expanded from 2×2 to 4×4 by applying IF sampling rather than baseband sampling. This operation requires Direct Digital Synthesis (DDS) and Digital Down Conversion (DDC) operations at the transmitter and receiver, respectively.
  3. Closed Loop Transmit Diversity - Adding a feedback link between the receiver and transmitter (via a wire or Ethernet link) will allow closed loop transmit diversity experiments.

6.9 Chapter Summary

The Virginia Tech Space-Time Advanced Radio (VT-STAR) architecture is presented. This test bed presents a visual demonstration of the capabilities of space-time coding schemes utilizing multiple element array technology at both ends of the wireless link. The transmitter and receiver sections of VT-STAR were examined in detail, outlining some of the challenges and design issues that needed to be resolved in the development of this prototype. The novel feature of the VT-STAR is its open SDR architecture, facilitating both MIMO channel measurements and real-time algorithm development on the same platform. Results indicate that there are improvements in a wireless link's capacity and reliability through the use of MIMO technology.

The architecture of the radio was presented at the 2001 Radio and Wireless Conference (RAWCON) in Boston, MA [92]. MIMO channel measurements and capcity results obtained by the VT-STAR architecture will be presented at the 2002 Fall Vehicular Technology Conference (VTC) in Vancouver, Canada [105]. A journal paper on the design, architecture and results of VT-STAR was submitted to *EURASIP Journal on Applied Signal Processing, Special Issue on Rapid Prototyping of DSP Systems* [106].

Chapter 7

Iterative Processing of STC in Frequency Selective Channels

Space-time coding schemes have been shown to perform remarkably well in flat fading environments, achieving full spatial diversity order along with coding gain. For large delay spread environments, however, both STTC and STBC suffer from severe performance degradation due to channel-induced Intersymbol Interference (ISI). To overcome this effect, two main approaches were proposed in the literature including concatenation of space-time codes with OFDM [22] or concatenation of equalization and decoding [66].

We focus in this chapter on the latter approach by considering iterative processing between the equalization stage and the decoding stage. The space-time encoder and the time dispersive channel can be formulated as two Markov processes. These Markov processes are combined using interleaving and serial concatenation. At the receiver, the problem of estimating the entire process is broken into smaller problems, one that deals with equalization of the ISI channel and the other that performs space-time decoding. While it is possible to form a joint solution using a single processor, large savings in complexity are possible by decomposing the estimation problem into separable processes. Both the equalizer and decoder produce not only hard decisions of their estimates, but also reliability information of their decisions. This information is shared between the processes in an iterative manner. As more iterations are executed, the performance of this iterative processor converges to the performance of the joint solution.

In the work of Bauch and Naguib in [66], the performance of iterative equalization decoding of STC was reported for 2 iterations only and for a specific 8 state code. In [107], the authors have shown that the achievable diversity of a space-time code, operating over time dispersive channels, is a function of the spatial diversity order times the number

of independent ISI taps, indicating that multipath diversity can be exploited to enhance performance. To that end, the authors derive special design criteria for space-time codes operating over frequency selective channels. In this chapter, we show that with the use of interleaving, the originally designed codes for flat fading channels [18], achieve full spatial and frequency (multipath) diversity order with an additional iterative processing gain. It is also shown that there is an effective number of iterations that provides significant performance enhancement, while more iterations result in diminishing returns.

The space-time encoder and the channel are separated by n_T identical interleavers, such that a serially concatenated code is formed. At the receiver, a concatenation of two Aposteriori Probability (APP) algorithms [108] that produce APPs of the encoded symbols is considered. The MAP equalizer uses channel estimates in its forward-backward recursions to compute the APPs, which are de-interleaved and passed as inputs to the decoding stage. The space-time (ST) decoder produces both APPs of the encoded symbols which are fed back to the equalization stage and Log-Likelihood Ratios (LLR) of the decoded bits. The improvement introduced by this scheme relies on sharing information between the two stages in an iterative manner.

Unlike linear equalization techniques, APP or Maximum Likelihood Sequence Estimation (MLSE) techniques [109] do not suffer from error propagation or noise enhancement [71]. On the other hand, the complexity of these type of equalizers increases exponentially with the cardinality of the signal. That is, for time dispersive channel of L_{ISI} taps, the equalizer has $|M|^{L_{ISI}-1}$ states, where $|M|$ is the cardinality of the signal and $(L_{ISI}-1)$ is the channel memory. In space-time coding, this cardinality is equal to the alphabet size to the power of n_T. Thus, complexity increases exponentially with channel memory and with the number of transmit antenna elements. Reduced complexity approaches such as decision-feedback sequence estimation are discussed in [110, 111, 112].

Assuming perfect knowledge of CSI at the receiver, we explore in section 7.3.1 the gains associated with the iterative process as well as the importance of random interleaving between the equalization and decoding stages. Performance results in terms of bit-error rate curves as well as histograms of the aposteriori probabilities and log likelihood ratios are provided for $4, 8$ and 16 state STTC with QPSK signaling format operating over 2 and 3-tap time dispersive channels.

We note that a frequency selective MIMO channel requires estimation of $n_T \times n_R \times L_{ISI}$ fade coefficients within the time coherence of the channel. In practical systems such as GSM for example, the coherence time of the channel at 60 MPH mobile velocity is approximately 12.5 [msec]. It is necessary therefore to complete the estimation process

within a relatively short period (≤ 1 [msec]). Both data-aided channel estimation techniques (using pilot symbols) or blind techniques may suffer from channel estimation errors. To address that, section 7.3.2 quantifies the degradation associated with imperfect channel estimation process. It is shown that the diversity advantage of the scheme relies heavily on accurate channel estimation. For example, a phase error of up to 10 degrees and an amplitude error below 15% are found to be tolerable, such that the diversity advantage of the scheme is maintained. Within these limits, the iterative process provides significant performance gains in the first and second iterations, while diminishing returns are observed for more than two iterations. Finally, simulation results for these cases are compared with outage probability analysis bounds, calculated in Chapter 2 for MIMO frequency selective channels.

7.1 System Model

The system model is described in Figures 7.1 and 7.2 for the transmitter and receiver, respectively.

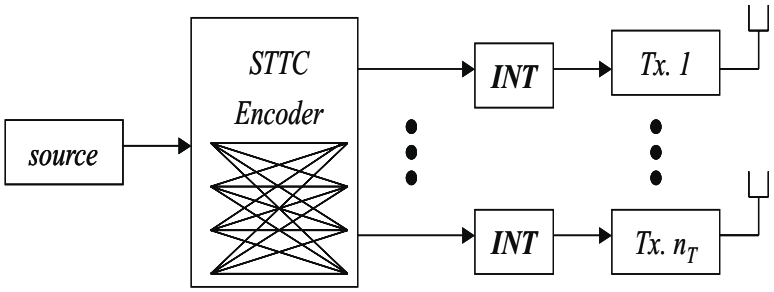

Figure 7.1: STTC in frequency selective fading

The channel between transmit antenna i and receive antenna j is modeled by an FIR filter with L_{ISI} taps. All channels are assumed to have the same channel memory. The lth tap of the $(i,j)th$ channel is denoted $\alpha_{i,j}(l)$ and is modeled as a zero mean complex Gaussian random variable with variance 0.5 per dimension. The taps of each FIR channel are normalized ($\sum_{l=0}^{L_{ISI}-1} |\alpha_{i,j}(l)|^2 = 1$) such that the channel has unit energy gain. Also, the codeword duration is assumed to be shorter than the time coherence of the channel. That is, the channel taps remain constant for the duration of a codeword and are changed between codewords.

The trellises of the $4, 8$ and 16 state STTC with QPSK mapping and 2 transmit antenna elements [18] are depicted in Figure 7.3.

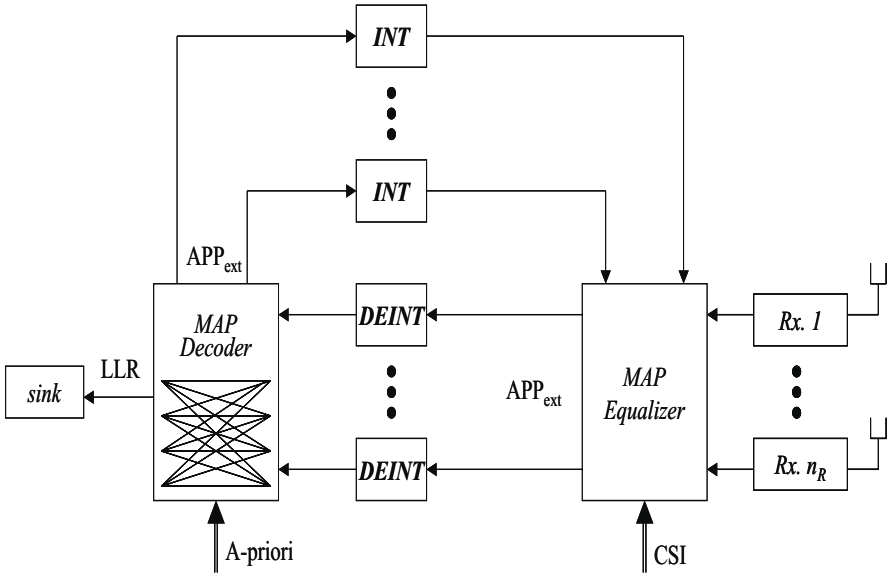

Figure 7.2: Iterative "turbo"-equalization of STTC

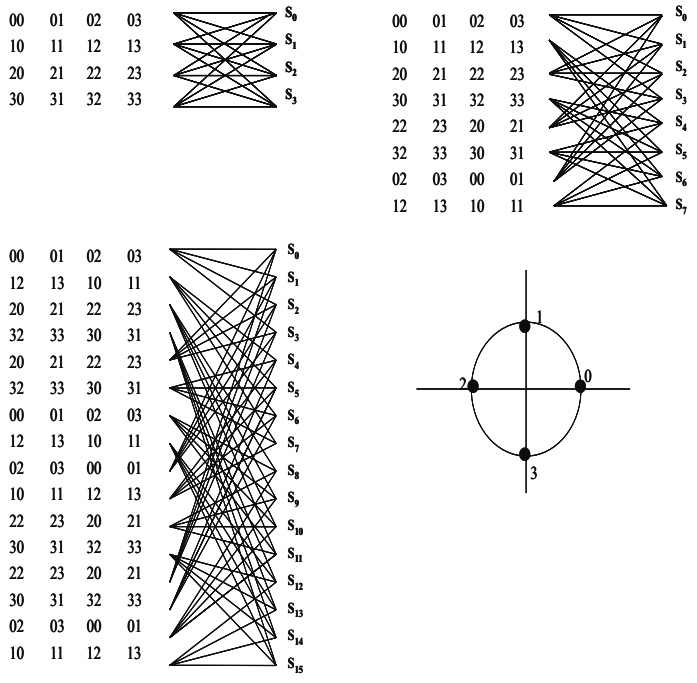

Figure 7.3: 4, 8 and 16 state STTC, QPSK mapping, 2 transmit antennas

The model of the channel estimation mismatch, to be used in section 7.3.2, is given by

$$\hat{\alpha}_{i,j}(l) = K_e \left|\alpha_{i,j}(l)\right| exp\left\{j(\Phi_{\alpha_{i,j}(l)} + \Phi_e)\right\}, \tag{7.1}$$

where K_e and Φ_e represent the magnitude gain factor and phase error deviation from the perfect channel fade coefficients, $\alpha_{i,j}(l)$ where $i \in [1, 2, \ldots, n_T]$, $j \in [1, 2, \ldots, n_R]$ and $l \in [0, 1, \ldots, L_{ISI} - 1]$.
The received signal at antenna j at time k is modeled by

$$r^j(k) = \sum_{i=1}^{n_T} \sum_{l=0}^{L_{ISI}-1} \alpha_{i,j}(l) c^i(k-l) + \eta^j(k), \tag{7.2}$$

where $c^i(k-l)$ are the encoded interleaved symbols from transmit antenna i at times $[k, k-1, \cdots, k-L_{ISI}+1]$ and $\eta^j(k)$ denotes the AWGN term and is modeled as i.i.d zero mean complex Gaussian random variable with variance σ_n^2. L denotes the length of the transmitted codeword.

The processing at the receiver includes channel estimation followed by MAP equalization, which produces a matrix of aposteriori probabilities with dimensions $M \times n_T$ per symbol transition, where M is the size of the alphabet. The extrinsic information is deinterleaved to break up bursts of errors at the equalizer output and then ST decoded using a second MAP algorithm. The MAP ST decoder produces log-likelihood ratios for the decoded bits along with aposteriori probabilities of the encoded symbols, which are fed back to the equalizer and used to update the a-priori probabilities. The two stages are separated by interleaving-deinterleaving rule that provides the equalizer/decoder with almost independent a-priori information. Based on turbo processing principles, the feed back contains only the extrinsic part of the aposteriori information in order to minimize correlation with previous inputs and outputs of the previous stage. A detailed description of the algorithms used in this iterative equalization decoding scheme is provided in the next section.

7.2 MAP Equalization/Decoding of STTC

The symbol-by-symbol MAP algorithm was originally proposed by Bahl, Cocke, Jeinek and Raviv as an alternative to the Viterbi algorithm for decoding convolutional codes [108][1]. Based on noisy observations (received signal), the algorithm calculates aposteriori probabilities (APP) of each encoded symbol, message bit, and/or state transition produced by a Markov process. The properties of the Markov process are used to partition calculations of the joint transition probability of each valid transition to quantities that can be computed

[1]In some texts, the algorithm is referred as the BCJR algorithm according to the initials of the authors.

using forward and backward recursion formulas. Once APPs are computed, a hard decision can be made by taking the quantity with the highest probability. This section describes the application of MAP principles to the problem of turbo equalization of STC in MIMO time dispersive channels.

The space-time encoder transmits a vector of n_T symbols from the array, denoted $c^i(k), i = [1, \cdots, n_T]$ at time $t = k$. The encoded interleaved symbols are independent and equiprobable and since the channel impulse response is convolved with the signal, a Hidden Markove Model (HMM) can be formed. The Markov state is the previous $(L_{ISI} - 1)$ transmitted symbols per transmit antenna. The channel trellis has $(M^{L_{ISI}-1})^{n_T}$ states where M branches emanating from and diverging to each state. The channel output is denoted by R, which is a space-time matrix of received samples with dimensions $L \times n_R$, whose $(k, j)th$ entry is described in Eq. (7.2).

The MAP equalizer uses the channel output matrix R, channel estimation information $\hat{\alpha}_{i,j}(l)$, apriori probabilities and channel trellis, to compute n_T marginal APP vectors (of length M each) per symbol transition. The marginal APPs computed by the equalizer are given by

$$P\left[x^i(k) = x_0|R\right] = \sum_{(m' \to m : x^i(k) = x_0)} P(m' \to m, R), \tag{7.3}$$

where $m' \to m$ corresponds to the transition from state m' to state m in the channel trellis and x_0 represents a given alphabet candidate. Note that the summation is over all transitions in which the condition $x^i(k) = x_0$ is satisfied. Thus, this is a marginalization process that results in the marginal aposteriori probability $P\left[x^i(k) = x_0|R\right]$. Since this process is repeated for all candidate symbols in the alphabet and also for all transmit antennas, n_T APP vectors of length M each are computed per symbol transition. The joint transition probability is the product of the following three terms:

$$P(m' \to m, R) = \alpha_{k-1}(m')\gamma_{k-1}(m', m)\beta_k(m), \tag{7.4}$$

where $\alpha_{k-1}(m')$ and $\beta_k(m)$ are the forward and backward probabilities, respectively, which can be computed recursively by:

$$\alpha_k(m) = \sum_{m'} \alpha_{k-1}(m')\gamma_k(m', m), \tag{7.5}$$

$$\beta_{k-1}(m') = \sum_{m} \beta_k(m)\gamma_k(m', m), \tag{7.6}$$

and $\gamma_k(m', m)$ is the branch transition probability which can be expressed as the product of the a priori probability and the channel transition probability:

$$\gamma_k(m', m) = P(R_k|m', m)P(m|m'). \tag{7.7}$$

A-priori probabilities are initialized to $1/M$ before feedback from the decoder is available but after the first iteration, they are replaced by the product of the extrinsic probabilities $P_e\left[x^i(k) = x_0|R\right]$ obtained from the decoder.

$$P(m|m') = \prod_{i=1}^{n_T} P_e\left[x^i(k) = x_0|R\right]. \tag{7.8}$$

The channel transition probability is exponentially related to the Squared Euclidean Distance (SED), which forms the following branch metric:

$$SED(k) = \sum_{j=1}^{n_R} \left| r^j(k) - \sum_{i=1}^{n_T} \sum_{l=0}^{L_{ISI}-1} \hat{\alpha}_{i,j}(l) x^i(k-l) \right|^2, \tag{7.9}$$

where $x^i(k-l), l = [1, \cdots, L_{ISI}-1]$ represents the encoded symbols that form the current state of the channel trellis transition $m' \rightarrow m$, and $\hat{\alpha}_{i,j}(l)$ are the $(i,j)th$ channel estimates vector of length L_{ISI} taps. The channel transition probability is given by

$$P(R_k|m',m) = \frac{1}{2\pi\sigma_n^2} exp\left(-\frac{SED(k)}{2\sigma_n^2}\right). \tag{7.10}$$

Note that in the forward and backward recursions, the states at the beginning and at the end of a data block are known with probability 1 and thus $\alpha_{k=1}(0)$ and $\beta_{k=L}(0)$ are initialized to 1 [113].

In order to make sure that the decoder is provided with only extrinsic information, the contribution of the a-priori information is removed from the aposteriori probabilities to prevent correlation with previous inputs. This extrinsic APPs undergo deinterleaving and passed to the ST decoder.

Within the ST decoder, a forward-backward recursions over the trellis diagram of the space-time code with 2^ν states are performed with the channel transition probability given by

$$BM(k) = \prod_{i=1}^{n_T} P_e\left[x^i(k) = c^i(k)|R\right]. \tag{7.11}$$

According to the set of n_T symbols $c^i(k)$, associated with a given code trellis transition, we multiply the marginal extrinsic probabilities obtained from the equalizer. Note that it is assumed that the channels from multiple transmit antennas are independent and therefore the joint probability is equal to the product of the marginal probabilities.

The MAP ST decoder produces log-likelihood ratios for the decoded bits, which are described by

$$LLR = log\frac{P(u=1|R)}{P(u=0|R)} = log\frac{\sum_{\tilde{m}'\rightarrow\tilde{m}:u=1} P(\tilde{m}',\tilde{m},R)}{\sum_{\tilde{m}'\rightarrow\tilde{m}:u=0} P(\tilde{m}',\tilde{m},R)}. \quad (7.12)$$

That is, $P(u=1|R)$ and $P(u=0|R)$ are obtained by marginalization process of the joint transition probabilities over all transitions that correspond to information bit 1 and 0, respectively. In our notations, $(\tilde{m}',\tilde{m})$ and (m',m) denote states of the space-time code and channel trellises, respectively. Note that $P(\tilde{m}',\tilde{m},R)$ is equal to the product of $\tilde{\alpha}_{k-1}(\tilde{m}')$,$\tilde{\beta}_k(\tilde{m})$ and $\tilde{\gamma}_{k-1}(\tilde{m}',\tilde{m})$. Finally, the decoder produces aposteriori probabilities of the encoded symbols by marginalizing $P(\tilde{m}',\tilde{m},R)$ over each symbol in the alphabet.

7.3 Simulation Results

7.3.1 Known Channel Estimation

In the simulation results that follow, codeword length is set to 200 symbols. Identical random interleaving rule is used across the multiple transmit antennas and perfect knowledge of CSI at the receiver is assumed to be available. Figures 7.4, 7.5, 7.6 illustrate the performance of the $4, 8$ and 16 state STTC, respectively, with 2Tx-1Rx antenna array configuration operating over 2-tap time dispersive channel. For all of these codes, we perform 4 iterations in which extrinsic probabilities are passed between the MAP equalizer and the MAP ST decoder. We include in these Figures (as reference curves) the performance of MLSE space-time decoder (with the corresponding number of states) in flat fading environment. It is shown that the MAP equalizer does not only compensate for the channel induced ISI, rather, it provides an additional form of diversity by gathering energy from all the channel taps. This is observed by the asymptotic slope of the error rate curves, which is steeper than spatial diversity order of two, which is provided by the space-time code in a flat fading environment. Also, the iterative process enhances performance in the second iteration by 3 dB at BER of 10^{-3} with additional gain of 1 dB obtained by the third iteration. However, it is observed that this process reaches a saturation point at the fourth iteration, resulting in diminishing performance returns after that point. We note that with no iterative processing, the 16 state code outperforms the 4 state code by more than 2 dB, which is attributed to the additional coding gain of the 16 state code. However, with the iterative processing, since most of the temporal gain has been already achieved, increasing the number of states does not result in enhanced performance. This trend is illustrated in Figure 7.7 even for large interleaver depth (codeword length) of 2000 symbols.

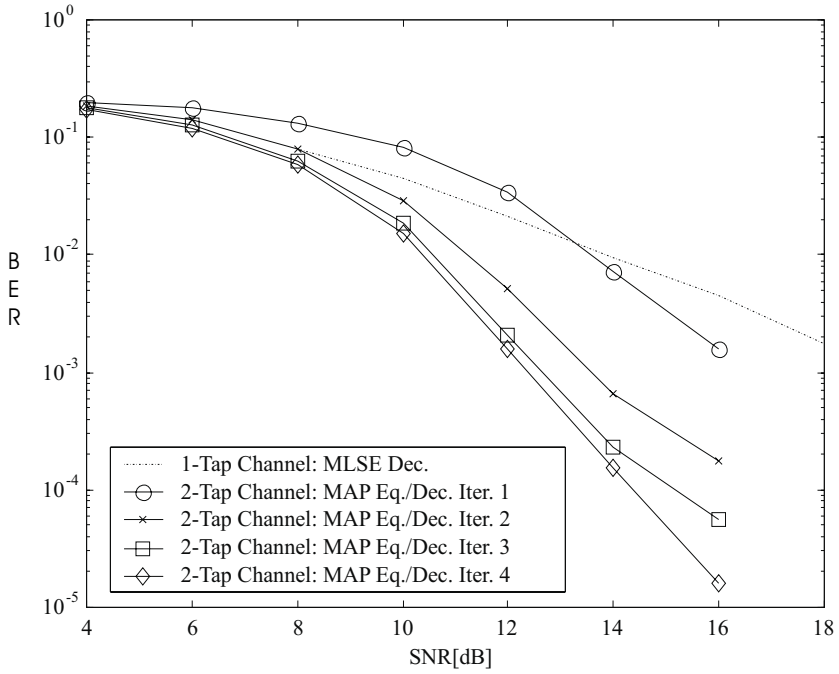

Figure 7.4: 4 state STTC, 2 taps channel, QPSK, perfect CSI, random interleaving

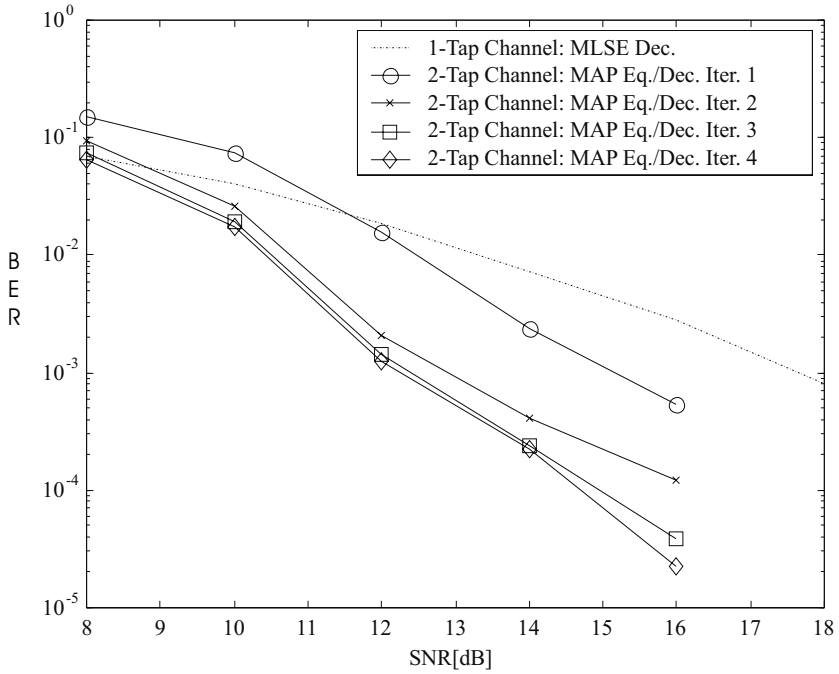

Figure 7.5: 8 state STTC, 2 taps channel, QPSK, perfect CSI, random interleaving

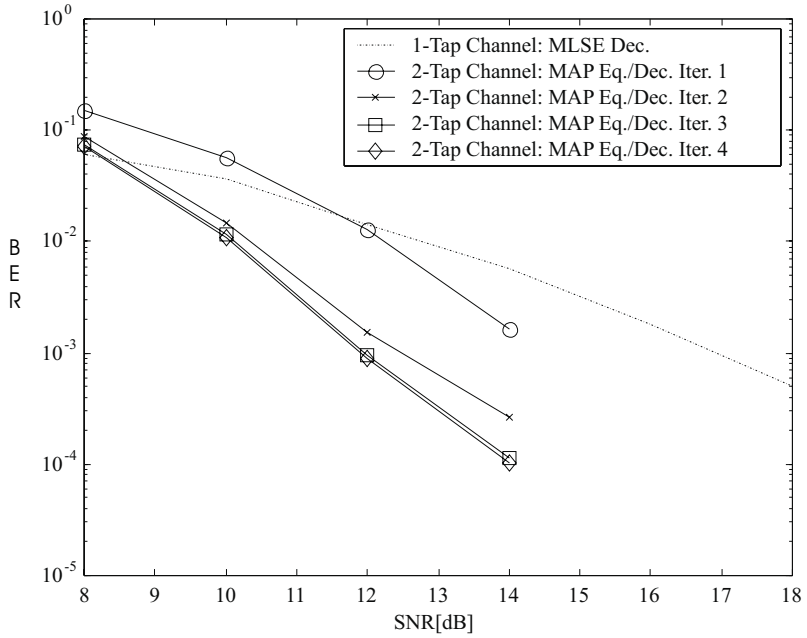

Figure 7.6: 16 state STTC, 2 taps channel, QPSK, perfect CSI, random interleaving

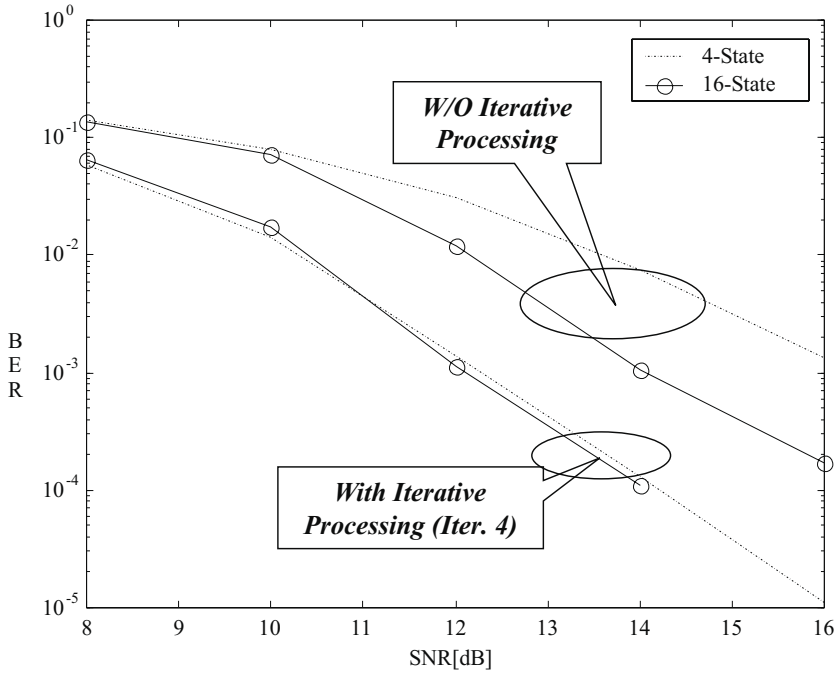

Figure 7.7: 4 state Vs. 16 state STTC, 2-taps channel, random interleaving, $L = 2000$

Next, we explore the effectiveness of the iterative process by constructing histograms of the encoded symbols APPs at the MAP equalizer output and LLRs of the decoded bits at the MAP ST decoder output. The decoder calculates the APPs of the message bits, $P(u = 1|R)$ and $P(u = 0|R)$, which are then put into LLR form according to Eq. (7.12). The MAP algorithm used in the decoder does not make hard-decisions on the message bits until after the last iteration. In addition to the LLRs, it produces extrinsic probabilities of the encoded symbols and pass those to the equalization stage.

Figure 7.8 describes the histogram of the equalizer APPs of a 16 state STTC as a function of the number of iterations, for a fixed SNR of 10 dB. Since on a per symbol transition, the MAP equalizer produces a matrix of APPs that cover all possible vectors of symbols in the alphabet, we construct the histogram of the APPs of the transmitted (correct) symbols only. This histogram shows that the second iteration is dominant in enhancing the APPs while the improvement obtained by the fourth iteration is negligible. Note that there are some APPs of transmitted symbols with probabilities near zero. These are attributed to the errors at the equalizer output at SNR of 10 dB.

Figure 7.9 illustrates the histogram of the decoded bits LLRs at the ST MAP decoder output for a fixed SNR of 10 dB. The LLRs are bounded to ± 100 to prevent stability problems in taking the logarithm of Eq. (7.12). Since bit decisions are based on the sign of the LLRs, it is shown that the iterative process increases the distance between the decision statistics associated with bit 0 or bit 1. Also, the major improvement is obtained by the second and third iterations with minimal improvement in the fourth iteration.

Figures 7.10 and 7.11 show the histograms of LLRs as a function of SNR for the first and fourth iterations, respectively. It is shown that without iterative processing (Figure 7.10), improving SNR results in gradual separation of the decision statistics, while upon completion of the fourth iteration (Figure 7.11), iterative processing provides large separation of the decision statistics even in low SNR regions. The outcome of this effect is minimization of the bit and frame error rates.

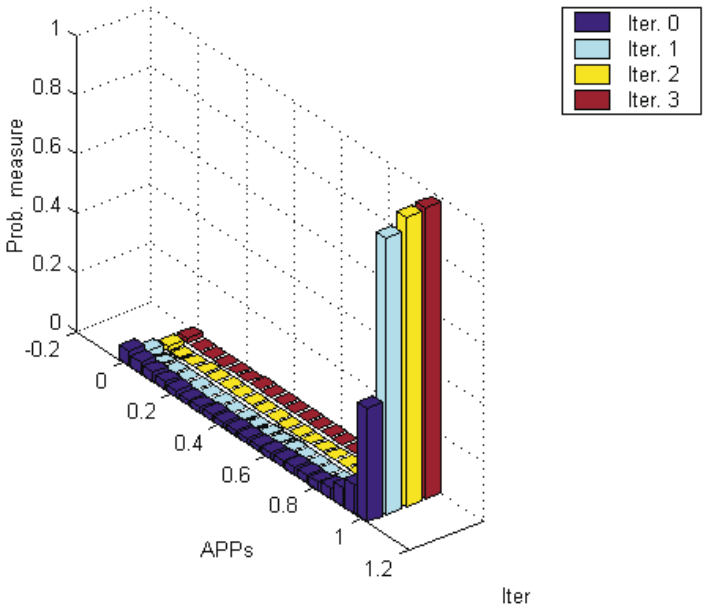

Figure 7.8: APPs histogram at MAP equal. output for 16 state STTC, 2 taps channel, QPSK, perfect CSI, random interleaving, $SNR = 10$ dB

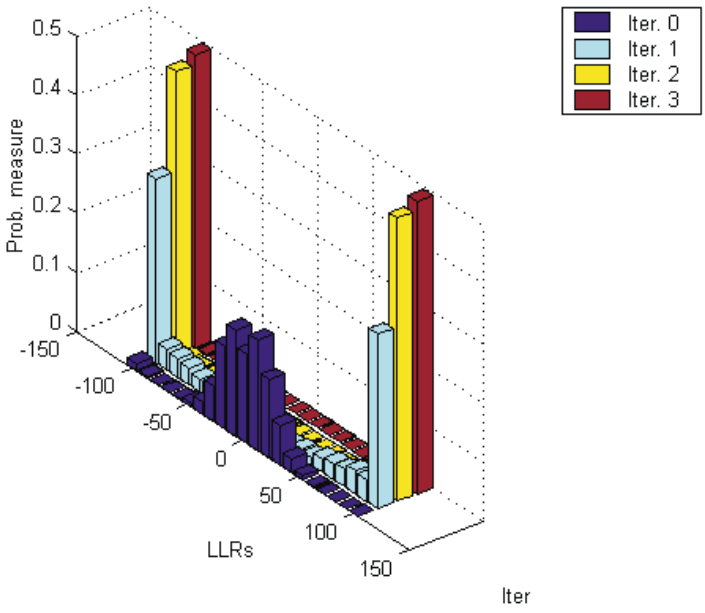

Figure 7.9: LLRs histogram at ST decoder output for 16 state STTC, 2 taps channel, QPSK, perfect CSI, random interleaving, $SNR = 10$ dB

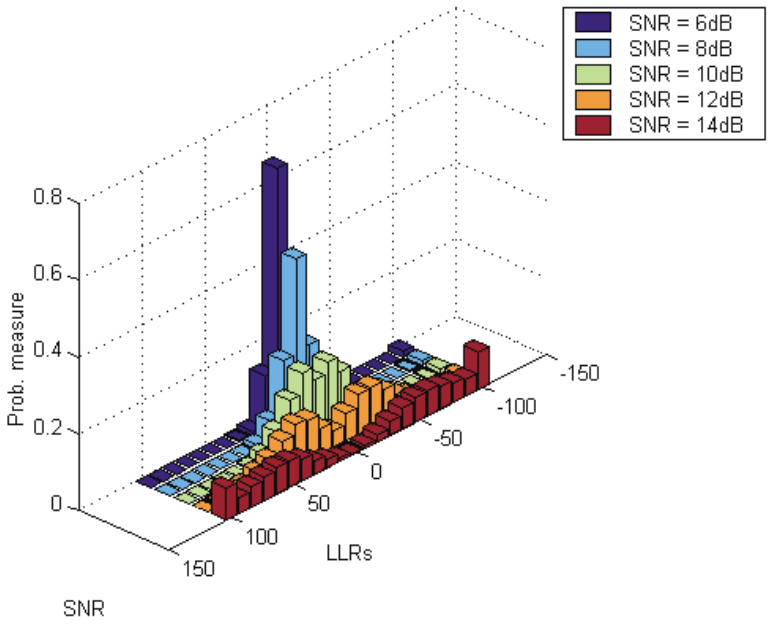

Figure 7.10: LLRs histogram at ST decoder output as a function of SNR, 16 state STTC, 2 taps channel, QPSK, perfect CSI, random interleaving, iteration 1

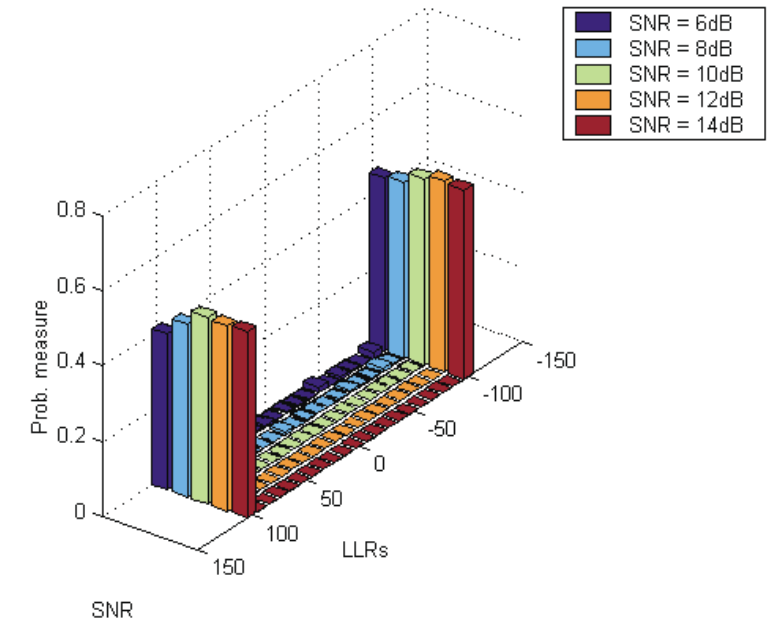

Figure 7.11: LLRs histogram at ST decoder output as a function of SNR, 16 state STTC, 2 taps channel, QPSK, perfect CSI, random interleaving, iteration 4

Figure 7.12 illustrates the performance of the 4 state STTC over a 3-tap time dispersive channel. As a reference curve, the bit-error rate of MLSE decoding of the same code operating over flat fading channel is included. It is observed that the MAP equalization-decoding scheme exploits multipath diversity in addition to the spatial diversity offered by the STTC. Comparing with the results over 2-tap time dispersive channel (Figure 7.4), the asymptotic slope of the error rate curve in the case of a 3-tap channel is steeper than in the case of a 2-tap channel. Also, an additional performance gain of 4 dB at BER of 10^{-3} is achieved by the iterative process.

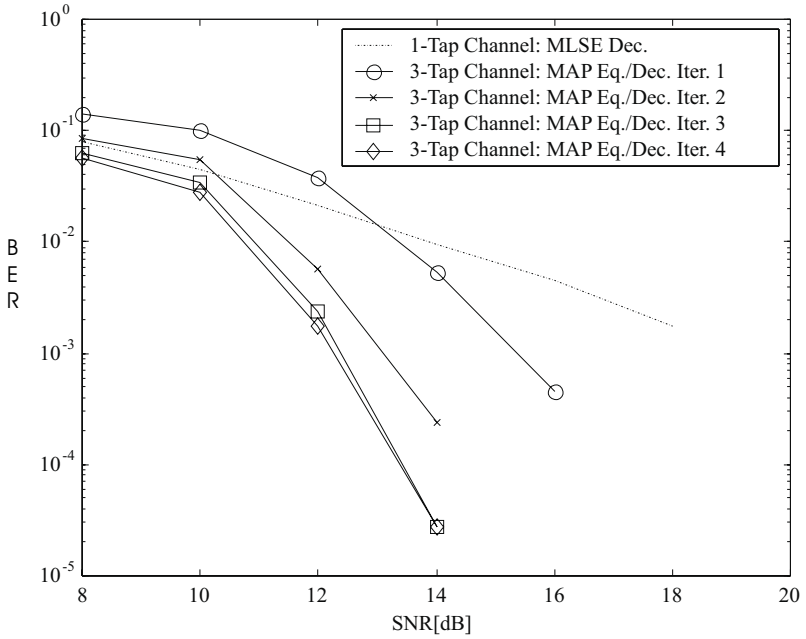

Figure 7.12: 4 state STTC, 3 taps channel, QPSK, perfect CSI, random interleaving

Random interleaving between the equalization and decoding stages breaks up bursts of errors and provides the stages with almost independent extrinsic probabilities. In order to quantify the importance of interleaving for the iterative scheme, performance results for the 4 and 8 state STTC with no interleaving are provided in Figures 7.13 and 7.14, respectively.

Comparing results with the case of random interleaving (Figures 7.4 and 7.5), it is observed that without iterative processing (iteration 1), the use of random interleaving enhances performance by not more than 1 dB, while for the second and third iterations, schemes with random interleaving outperform the schemes with no interleaving by more than 2.5 dB. That is, the large performance gains associated with the iterative process are dependent upon using interleaving between the stages.

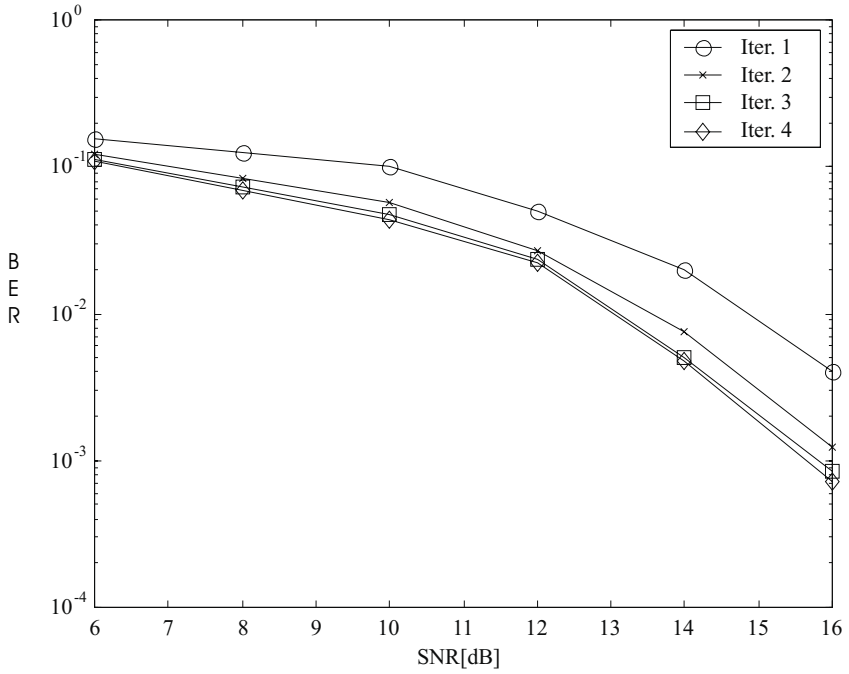

Figure 7.13: 4 state STTC, 2 taps channel, QPSK, perfect CSI, no interleaving

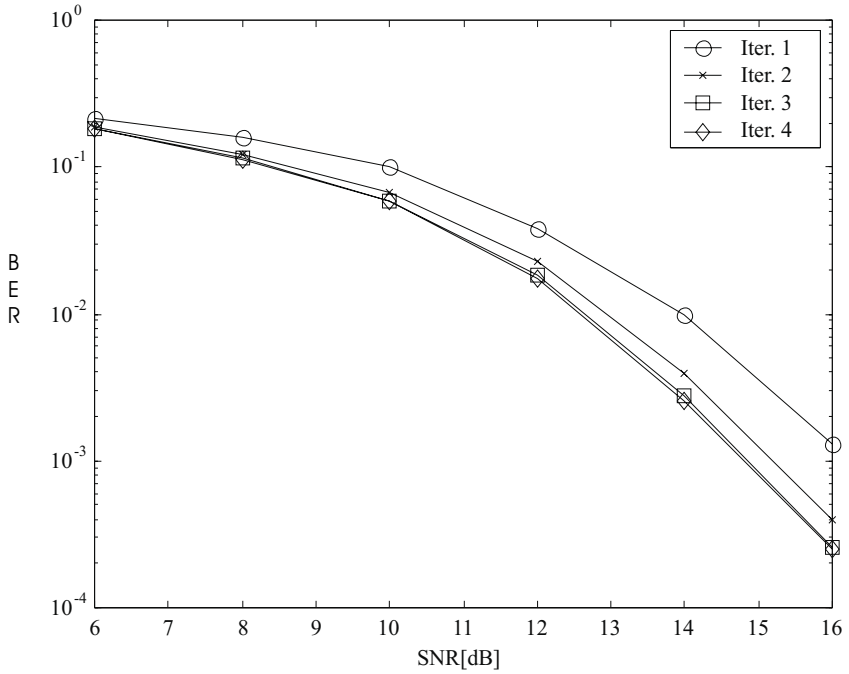

Figure 7.14: 8 state STTC, 2 taps channel, QPSK, perfect CSI, no interleaving

7.3.2 Imperfect Channel Estimation

Armed with the performance of the scheme under ideal channel estimation assumption, we apply the channel estimation mismatch model of Eq. (7.1) to examine the effect of channel estimation errors. Performance results are presented in the form of a three dimensional surface plot, associating BER to SNR for various phase or magnitude errors.

Figure 7.15 demonstrates the sensitivity of the scheme to phase errors upon completion of the third iteration. It is shown that as long as the phase error is below 10 degrees, the diversity advantage of the scheme is retained (as seen by the asymptotic slope of the BER in the SNR dimension). However, phase error of 15 degrees results in an irreducible error floor.

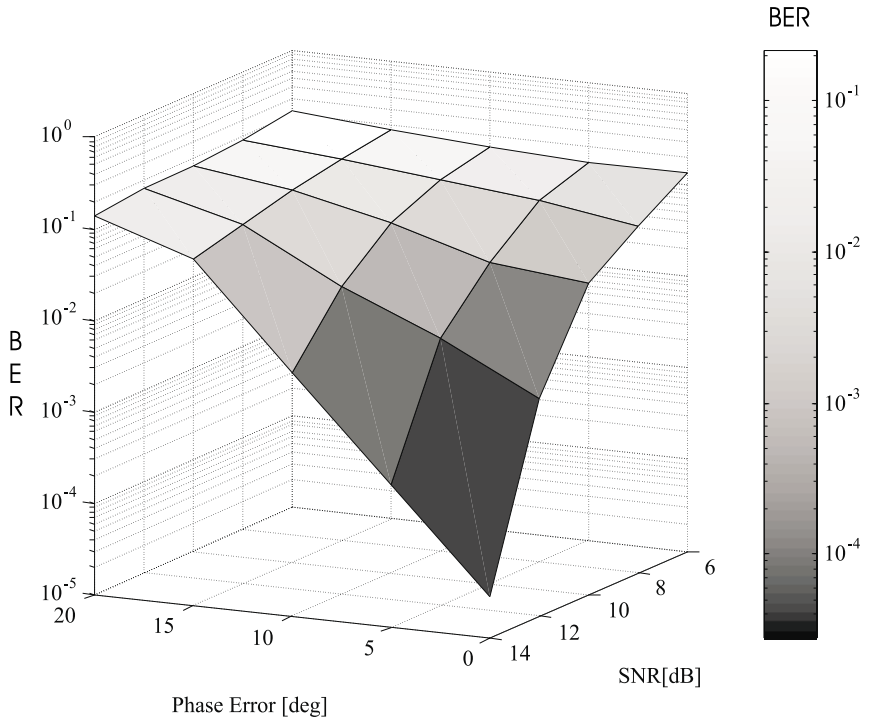

Figure 7.15: Phase estimation errors; 4-state STTC, QPSK, 2Tx-1Rx, 3-tap channel, third iteration

Figure 7.16 presents three error rate surfaces for the three iterations. It is observed that for phase error of less than 10 degrees, the iterative process provides significant performance gains in the first and second iterations (3.5dB @ BER of 10^{-3}), while diminishing returns are observed for more than two iterations. Moreover, the performance gains associated with the iterative process are eliminated for larger phase estimation errors.

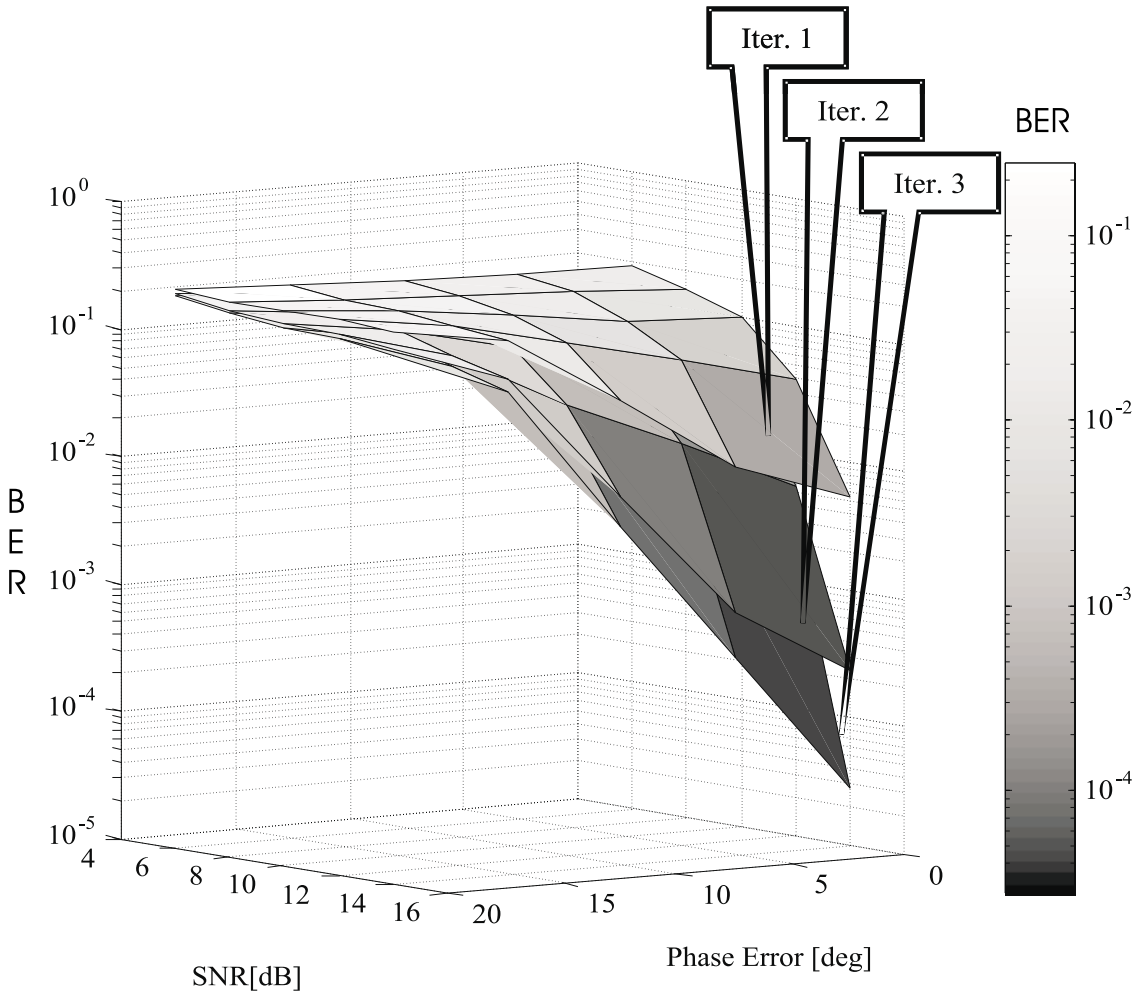

Figure 7.16: The role of iterative processing in the presence of phase estimation errors; 3-tap time dispersive channel, 4-state STTC, QPSK, 2Tx-1Rx

Next, we examine the sensitivity of the scheme to amplitude estimation errors. Figure 7.17 demonstrates the performance of the scheme in the presence of amplitude errors for 2-tap time dispersive channel. As one would expect, a symmetry about $K = 1$ (ideal CSI) is obtained. It is also shown that up to 15% error in the channel gain estimates ($K_e = 1.15, 0.85$), the diversity advantage of the scheme is retained. However, magnitude error that exceeds this limit results in a significant degradation loss.

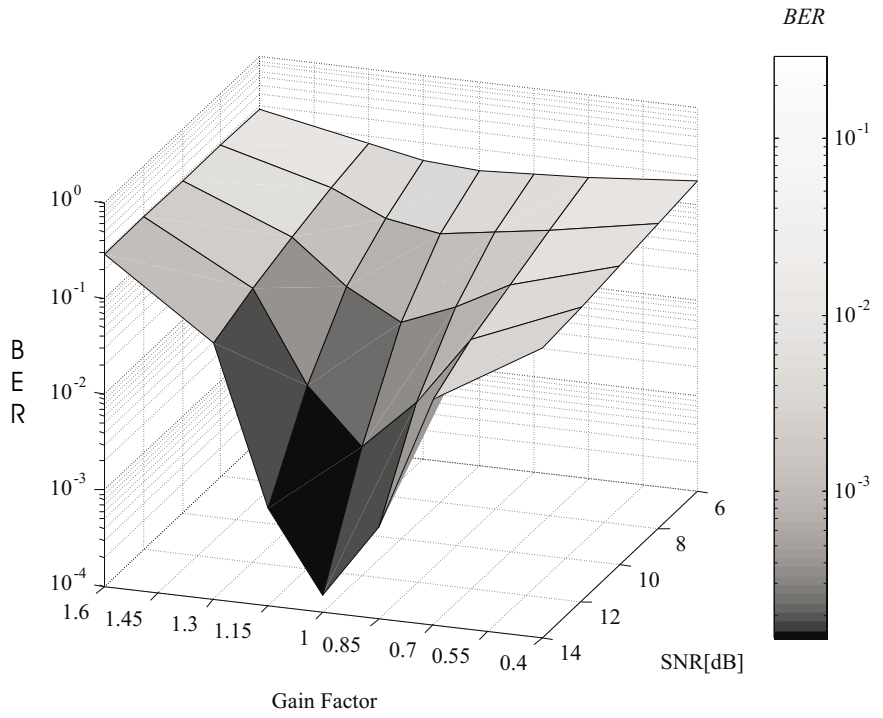

Figure 7.17: Amplitude estimation errors; 4-state STTC, QPSK, 2Tx-1Rx, 2-tap channel, third iteration

Figure 7.18 presents three error rate surfaces for the three iterations. It is shown that as long as the amplitude error is below 15%, the iterative process provides significant performance gains in the first and second iterations, while diminishing returns are observed for more than two iterations. Furthermore, it is observed that the gains associated with the iterative processing are eliminated for larger amplitude estimation errors.

In order to ensure that the scheme tolerates 10 degrees phase error and 15% amplitude deviation, we compare the frame error rate (FER) with the outage probability lower bound obtained in section 2.2 for schemes operating over MIMO frequency selective channels with a fixed spectral efficiency of 2 [bps/Hz]. Figure 7.19 compares the simulated FER performance of the scheme with the outage probability lower bound. We examine phase errors of $10, 6$ and 0 degrees (ideal CSI) and observe that indeed up to 10 degrees phase error, the asymptotic

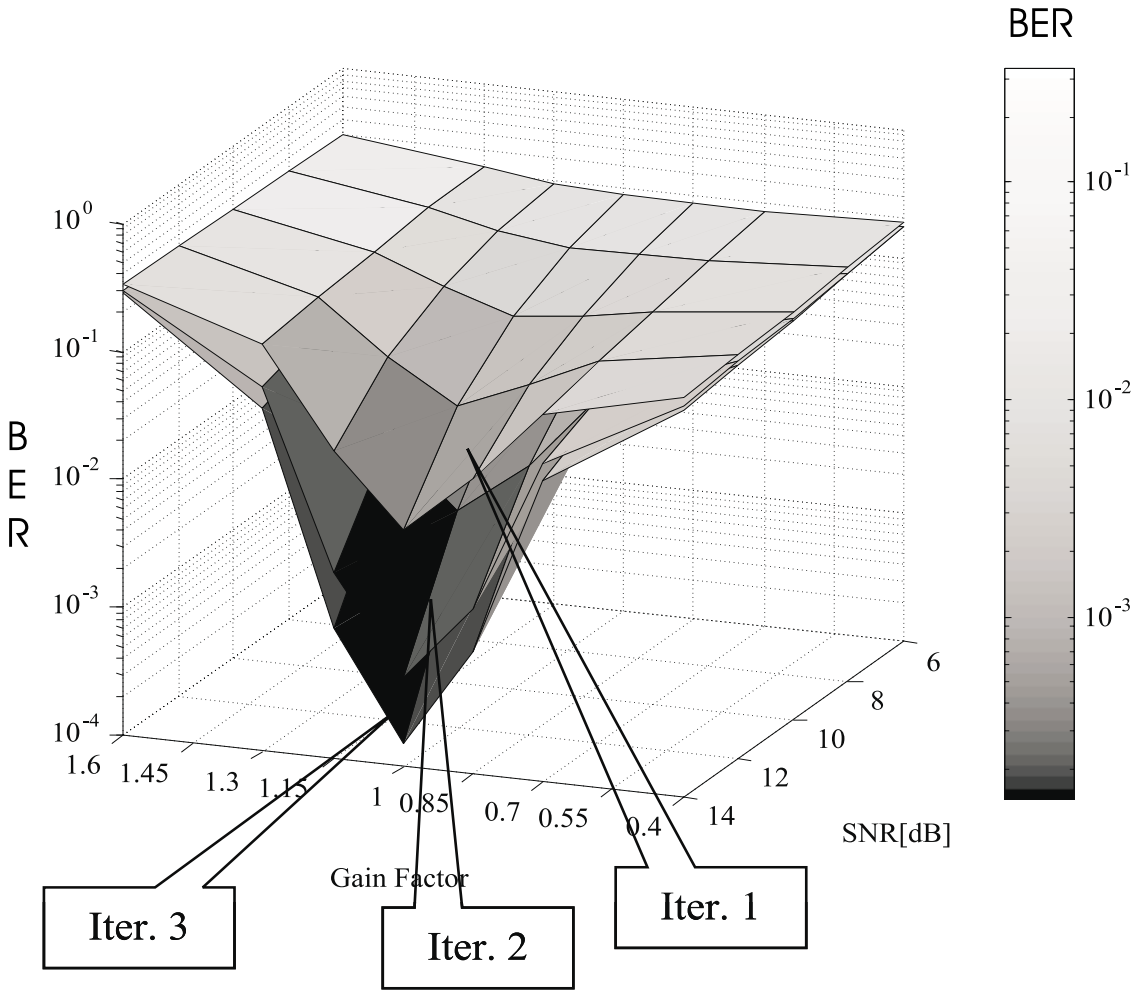

Figure 7.18: The role of iterative processing in the presence of amplitude estimation errors; 2-tap time dispersive channel, 4-state STTC, QPSK, 2Tx-1Rx

slope of the FER follows that of the lower bound. This indicates that full spatial and frequency diversity level are achieved. It is noticed however, that at a target 1% FER the scheme with perfect CSI performs within $2-3$ dB from outage capacity while phase estimation mismatch of 10 degrees causes an additional performance degradation of 5 dB.

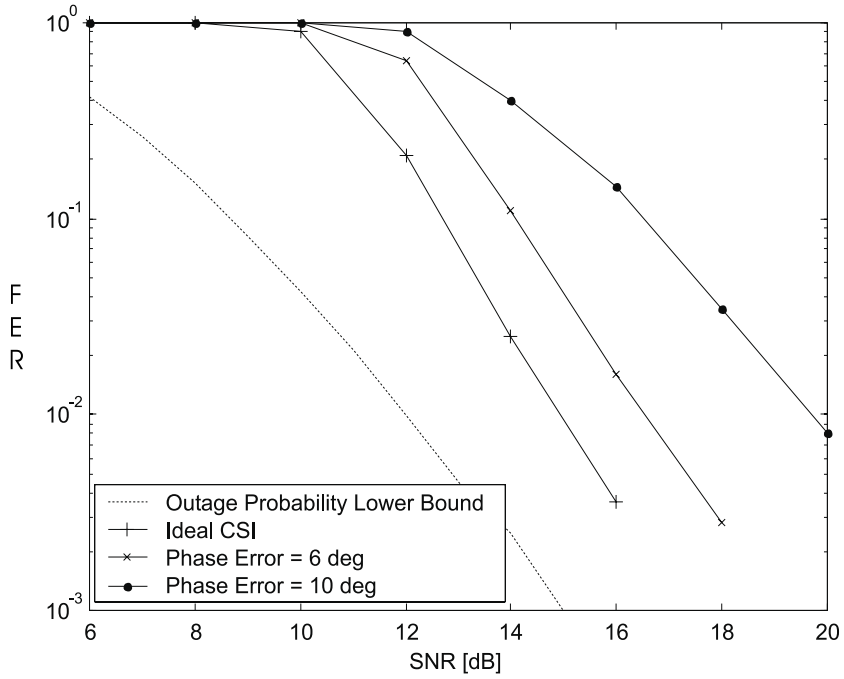

Figure 7.19: Outage probability vs. frame error rate; phase estimation errors; 4-state STTC, QPSK, 2Tx-1Rx, 2-tap time dispersive channel, third iteration

Figure 7.20 repeats the above comparison for amplitude errors of $20\%, 10\%$ and 0% (ideal CSI) with the outage probability as a lower bound. For 20% amplitude error, a loss in diversity order is observed. In addition, the scheme with amplitude estimation mismatch of 10% performs within 4 dB from the outage capacity.

7.4 Chapter Summary

In this chapter, performance results of iterative equalization decoding of space-time trellis codes, operating over MIMO frequency selective fading channels with perfect or imperfect channel estimation, are presented. Two APP algorithms for equalization and decoding are concatenated and share soft information in the form of extrinsic probabilities to achieve multipath diversity along with spatial diversity and coding gain. This scheme extends the suitability of STC to outdoor wireless communications where the channel exhibits frequency

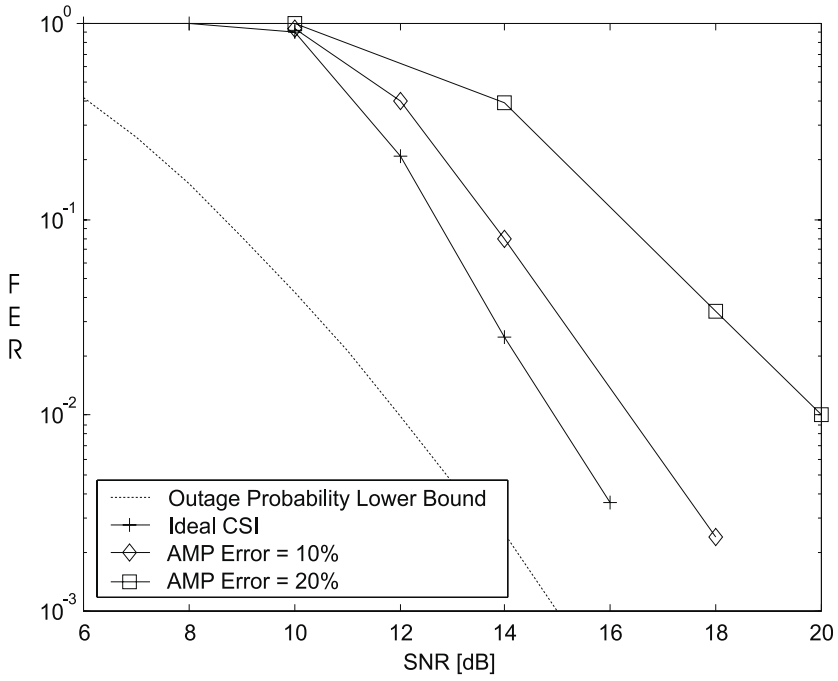

Figure 7.20: Outage probability vs. frame error rate; amplitude estimation errors; 4-state STTC, QPSK, 2Tx-1Rx, 2-tap time dispersive channel, third iteration

selectivity. Finally, we showed that the effectiveness of the iterative process relies heavily on accurate channel estimation and quantified the degradation associated with imperfect channel estimation. This work will be presented at the 2002 Spring Vehicular Technology Conference (VTC) in Birmingham, Alabama [91] and at the Wireless Personal Multimedia Communications (WPMC) Conference in Honolulu, Hawaii.

Note that the complexity of this scheme increases exponentially with channel memory and number of antenna elements. Thus, even for moderate channel memory, complexity becomes prohibitive for implementation and reduced complexity approaches are desirable. Iterative equalization and decoding with channel shortening filters that reduce the number of equalizer states are the topic of [114, 115].

In the next chapter, another example of applying iterative processing principles to space-time architectures is presented, demonstrating that BLAST type detectors can improve their energy efficiency significantly by employing an appropriate iterative interference cancellation decoding mechanism.

Chapter 8

Iterative Interference Cancellation Decoding for BLAST

The Bell-Labs Layered Space-Time Architecture (BLAST) [47, 48] utilizes multiple antenna elements at both ends of the wireless link to offer unprecedented spectral efficiencies as compared with traditional single transmit antenna systems. The underlying signal processing at the receiver is based on multi-user detection, where the various layers (signals coming from multiple transmit antennas) are treated as interferences and cancelled using beam forming (nulling) and interference cancellation (IC) techniques. Two linear nulling criteria were considered in the literature including the Minimum-Mean Squared Error (MMSE) [20] and Zero-Forcing (ZF) decorrelator [116]. The original BLAST approach [47] was based on a successive interference cancellation (SIC) mechanism such that the layers are detected and cancelled in a successive manner. Later, parallel interference cancellation (PIC) schemes were also proposed [117].

Both SIC and PIC detectors suffer from an error propagation problem, associated with feed backing unreliable decisions to the cancellation unit. This results in a poor energy efficiency due to loss of diversity order, which could be achieved if the previously detected layers were cancelled perfectly. For example, to achieve BER of 10^{-5}, V-BLAST with 4 layers and QPSK signaling format requires SNR at the order of 30 dB. This high SNR requirements imply large transmitted power that results in an increased interference levels to neighboring systems/users. In attempt to improve BLAST performance, the authors in [20] have proposed to combine space-time block codes and iterative decoding with SIC based BLAST detectors. Their results indicate that the error propagation still exists and limits the diversity advantage of the scheme. For PIC detectors, a novel "Turbo"-BLAST architecture that mitigates the error propagation problem effectively was proposed in [118].

In this chapter, we characterize the error propagation problem of both SIC and PIC BLAST detectors and propose two simple candidate schemes to mitigate the phenomenon. Both schemes rely on introducing channel coding with appropriate interleaving over the layers. In the SIC case, since the reliability of previously detected layers is crucial to the diversity advantage of successive layers, we place a more powerful code over the layer to be detected first. As will be shown in the sequel, this unequal error protection facilitates an increased level of diversity. The order of detection and cancellation of layers at the receiver is fixed according to the code rate assignment at the transmitter. From an implementation point of view, we adopt the pragmatic code design proposed by Viterbi et al. in [119], where a single rate convolutional code, paired with puncturing at the transmitter and erasing at the receiver, is used to obtain any rate $(n-1)/n$ code. These settings provide a convenient way to trade energy and spectral efficiency. For PIC BLAST detectors, a constant rate channel code is placed over each layer and iterative parallel interference cancellation decoding is incorporated at the receiver. Upon completion of the fourth iteration, almost error-free decisions are fed into the IC unit, thus offering maximum diversity level to all detected layers.

This chapter is organized as follows. Section 8.1 describes the principles of both SIC and PIC based BLAST detectors. Section 8.2 formulates the error propagation problem for both schemes. Section 8.3 presents the architecture of the proposed schemes. In section 8.4, simulation results are provided for the schemes over independent and correlated fading channel conditions.

8.1 SIC and PIC BLAST Detectors

Let us first describe the principles of uncoded V-BLAST receivers, based on successive or parallel interference cancellation paired with ZF or MMSE nulling criteria.

The architecture of V-BLAST was described briefly in section 3.3. The transmitter is based on n_T independent M-ary PSK or QAM modulators operating in a co-channel manner with synchronized symbol timing and using the entire bandwidth of the system. A generic block diagram for V-BLAST is illustrated in Figure 8.1. The received vector is modeled by

$$r = Ha + \nu, \tag{8.1}$$

where H represents the channel matrix with dimensions $n_R \times n_T$, whose entry $\alpha_{i,j}$ represents the complex fade coefficient for the path from transmit antenna i to receive antenna j. This fade coefficient is modeled as an independent zero mean complex Gaussian random variable with variance 0.5 per dimension. a is the transmitted vector with size $n_T \times 1$, which is

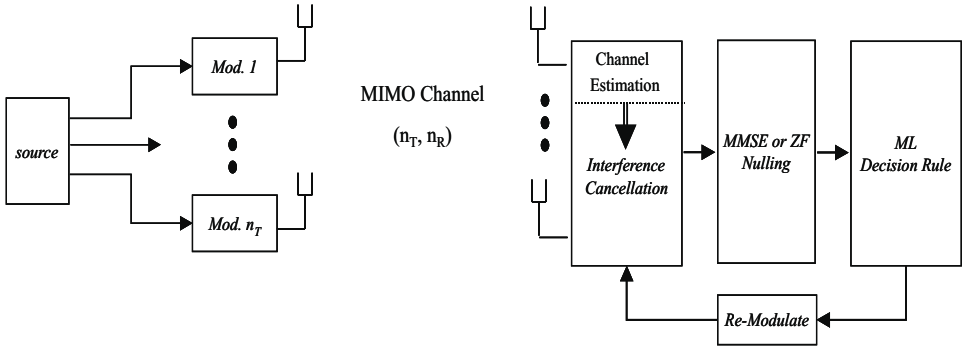

Figure 8.1: V-BLAST Architecture

composed of a set of symbols, each of which is a member of M-PSK or QAM alphabet. ν represents a complex vector of independent samples of AWGN over the n_R receive antenna chains with zero mean and variance σ_n^2 per dimension.

The nulling matrix, which is based on the pseudo-inverse of the channel matrix H, is described in Eq. (8.2) and (8.3) for the ZF and MMSE criteria, respectively.

$$G = \left(H^\dagger H\right)^{-1} H^\dagger. \tag{8.2}$$

$$G = \left(H^\dagger H + \frac{\sigma_n^2}{A^2} I\right)^{-1} H^\dagger. \tag{8.3}$$

Here, $\frac{A^2}{\sigma_n^2}$ denotes the signal-to-noise ratio at each receive antenna branch. The ith row of the nulling matrix is multiplied with the received vector to suppress all but the ith layer component, thus yielding the decision statistics of the ith layer:

$$\tilde{a}_i = G_i r. \tag{8.4}$$

A symbol-by-symbol maximum likelihood (ML) detector derives decisions based on minimum Euclidean distance to all possible candidates in the alphabet $\mathcal{A}$:

$$\hat{a}_i = argmin_{a \in \mathcal{A}} \parallel a - \tilde{a}_i \parallel^2 . \tag{8.5}$$

The computation of the nulling matrix, nulling operation and ML detection are common to both successive and parallel interference cancellation type detectors. Both techniques cancel previously detected layers from the received signal vector by reconstructing the interference components based on decisions of the ML detector. Following the cancellation, the nulling operation is repeated by computing again the nulling matrix of Eq. (8.2) or (8.3). Prior to this computation, it is crucial to strike out the columns of the channel matrix H, associated with previously detected layers. This operation is indeed what leverages the potential for

diversity advantage since there are potentially less number of interfering signals to suppress and same number of receive antenna elements. The next subsections describe the differences between SIC and PIC type detectors.

8.1.1 Successive Interference Cancellation (SIC)

The SIC detector operates successively by cancelling one layer per each iteration. It has been shown in [47] that the performance of the SIC detector is affected by the order in which layers are detected. Since the nulling matrix is calculated each iteration with different channel matrix H (after striking out the column of the previously detected layer), the ordering of the layers determines which subset of columns the nulling vector should be constrained by. The optimal ordering of the layers is determined according to the maximum post-detection SNR or the minimum norm row of the nulling matrix G, which is computed each iteration. The cancellation process at iteration $i+1$ (assuming for simplicity of presentation that the decoding of the ith layer has been completed) is described by

$$r_{i+1} = r_i - \hat{a}_i H_i, \tag{8.6}$$

where H_i denotes the ith column of the channel matrix, $\hat{a}_i$ is the reconstructed symbol of the ith layer based on the decision device output, and r_{i+1} is the received signal vector after cancellation of the ith layer component. Following, the nulling matrix is computed again based on only $n_T - i$ remaining layers. This is achieved by striking out the ith column of the H matrix before recomputing the pseudo-inverse of the new channel matrix. This process is performed successively until all components of the a vector are recovered. The performance of SIC type detectors for V-BLAST with ZF or MMSE nulling criteria with and without ordering of layers, is presented in Figure 8.2.

It is observed that the ordering of layers, which is performed each iteration, enhances performance considerably. Also, MMSE nulling outperforms ZF decorrelator by 3 dB in the case of no ordering and 8 dB when ordering is applied. Nevertheless, even the best scheme (MMSE nulling, ordering of layers) suffers from poor energy efficiency (SNR of 30 dB is required to guarantee BER of 10^{-5}), which is attributed to the lack of error correction code and the error propagation mechanism.

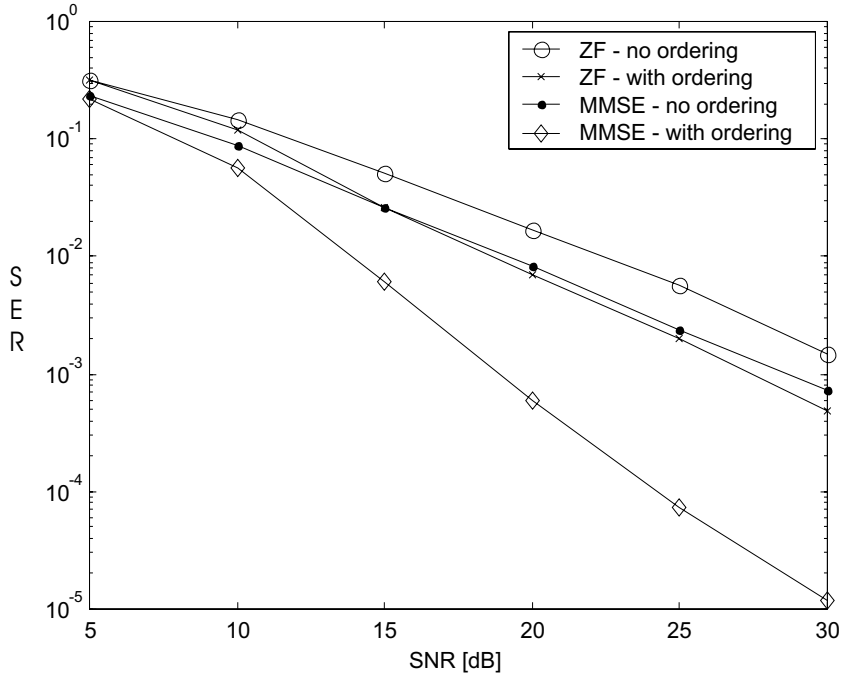

Figure 8.2: SIC V-BLAST Performance; ZF versus MMSE; with and without ordering; 4Tx-4Rx, QPSK

8.1.2 Parallel Interference Cancellation (PIC)

Unlike the SIC detector, the PIC detector does not rely on ordering of layers. In the first stage, decision statistics for all layers are derived simultaneously. That is given by

$$\tilde{a} = Gr, \tag{8.7}$$

where G is the nulling matrix with dimensions $n_T \times n_R$, r is the received vector and $\tilde{a}$ is a vector of decision statistics for the n_T symbols transmitted simultaneously from the array. Following, n_T ML decoders are operated in parallel to obtain the decisions associated with the transmitted vector a. The cancellation process subtracts for each layer the contribution of the other $(n_T - 1)$ interfering layers. This is described by

$$r_k = r - \sum_{j \neq k} \hat{a}_j H_j \quad \forall k \in [1, \cdots, n_T], \tag{8.8}$$

where r_k is the received signal after cancellation of all but the kth layer. Next, the nulling matrix is calculated again by striking out all but the kth column. The nulling matrix in the second stage of the PIC detector is a row vector with n_R elements and can be expressed as $G_k = CH_k^{\dagger}$, where C is an arbitrary complex constant that does not affect post-detection

SNR. Following the multiplications of r_k with G_k ($\forall k \in [1, \cdots, n_T]$), n_T ML detectors operate in parallel to recover the components of the vector a. The performance of PIC detector paired with ZF or MMSE nulling is illustrated in Figure 8.3.

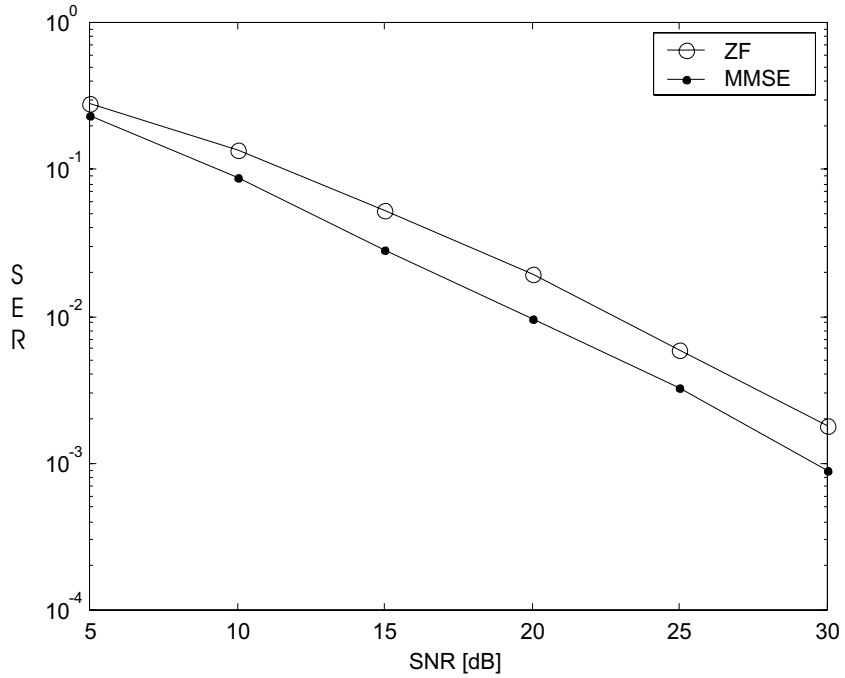

Figure 8.3: PIC V-BLAST Performance; ZF versus MMSE; 4Tx-4Rx, QPSK

The MMSE nulling outperforms ZF decorrelator by 3 dB. Comparing with SIC results (Figure 8.2), the PIC detector achieves similar results to SIC with no ordering of layers. The next section characterizes the error propagation problem of both SIC and PIC type detectors, which is found to be the primary reason for their poor energy efficiency.

8.2 Error Propagation Problem

The error propagation problem in BLAST corresponds to decision errors that are fed back from the decision device to the cancellation unit and thus propagate to successive iterations or stages. The effect of this problem on the energy efficiency of the scheme is significant, since the potential for an increased diversity advantage is not utilized.

In the SIC case, the received signal after cancellation of $k-1$ layers is formulated by

$$r_{i+k} = \underbrace{H_k a_k(i)}_{Desired\ Layer} + \underbrace{\sum_{j=1}^{k-1} H_j \left(a_j(i) - \hat{a}_j(i)\right)}_{(k-1)\ Cancelled\ Layers} + \underbrace{\sum_{j=k+1}^{n_T} H_j a_j(i)}_{(n_T-k)\ Uncancelled\ Layers} + \underbrace{\nu(i)}_{AWGN}. \quad (8.9)$$

Assuming ideal cancellation (no errors are fed to the IC unit), $\hat{a}_j(i) = a_j(i)$, and thus the second term of Eq. (8.9) goes to zero. This allows for spatial diversity order to increase as detection proceeds from layer to layer. Note that at the kth iteration, there are $(n_T - k)$ uncancelled layers (interfering signals) to suppress with $n_R > (n_T - k)$ antenna elements at the receiver. Winters and Salz in [120] have proven rigorously that in such a scenario, in addition to the suppression of $(n_T - k)$ interferers the array processor can achieve diversity order of $n_R - (n_T - k)$.

In hard cancellation however, the second term does not converge to zero and rather, it contributes to the interference level. To illustrate this phenomenon further, Figure 8.4 presents the performance of SIC BLAST detector paired with MMSE nulling with and without error propagation. In these curves, "genie" cancellation corresponds to error-free cancellation process where rather than feedback actual ML detector decisions, correct decisions are forced (second term in Eq. (8.9) is zero). The error rate on a per detected layer basis is plotted for both the "genie" case and the hard cancellation. It is observed that with perfect cancellation, the diversity advantage (as seen by the asymptotic slope of the error rate curve) increases as we proceed from layer to layer. Clearly, hard cancellation suffers from error propagation such that the potential increase in diversity level is not achieved.

In the PIC case, the received signal after first stage cancellation is formulated by

$$r_k(i+1) = \underbrace{H_k a_k(i)}_{Desired\ Layer} + \underbrace{\sum_{j \neq k} H_j \left(a_j(i) - \hat{a}_j(i)\right)}_{(n_T-1)\ Cancelled\ Layers} + \underbrace{\nu(i)}_{AWGN}, k \in [1, \cdots, n_T]. \quad (8.10)$$

That is, since all $(n_T - 1)$ layers are cancelled simultaneously, the received signal is composed of three terms only: the desired signal, the cancelled $(n_T - 1)$ layers and the noise term. In the case of ideal cancellation (denoted "genie"), the second term is forced to zero, and the received signal of the kth layer takes the form $r_k(i+1) = H_k a_k(i) + \nu(i)$. Thus, applying the nulling vector using either MMSE or ZF criteria ($G_k = C H_k^{\dagger}$) results in effective maximal ratio combining of n_R-fold diversity. In hard cancellation however, since there are errors in the decision process, the interference level is enhanced. This is illustrated in Figure 8.4. Note that due to the symmetry in the processing of all layers, we plot the average error rate over the four layers rather than error rate curve per each layer.

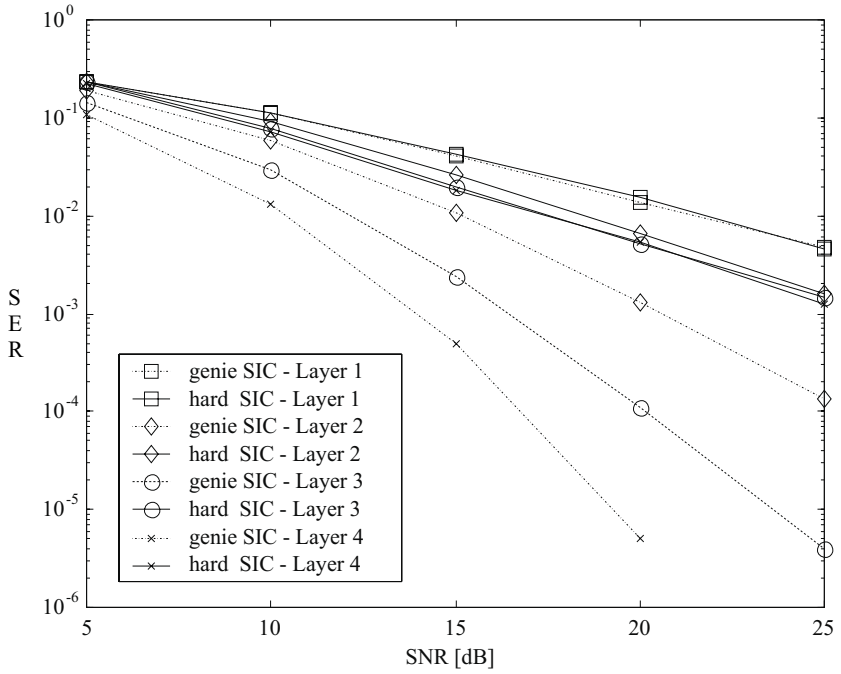

Figure 8.4: Error propagation of SIC BLAST detector, 4Tx-4Rx, QPSK, MMSE nulling

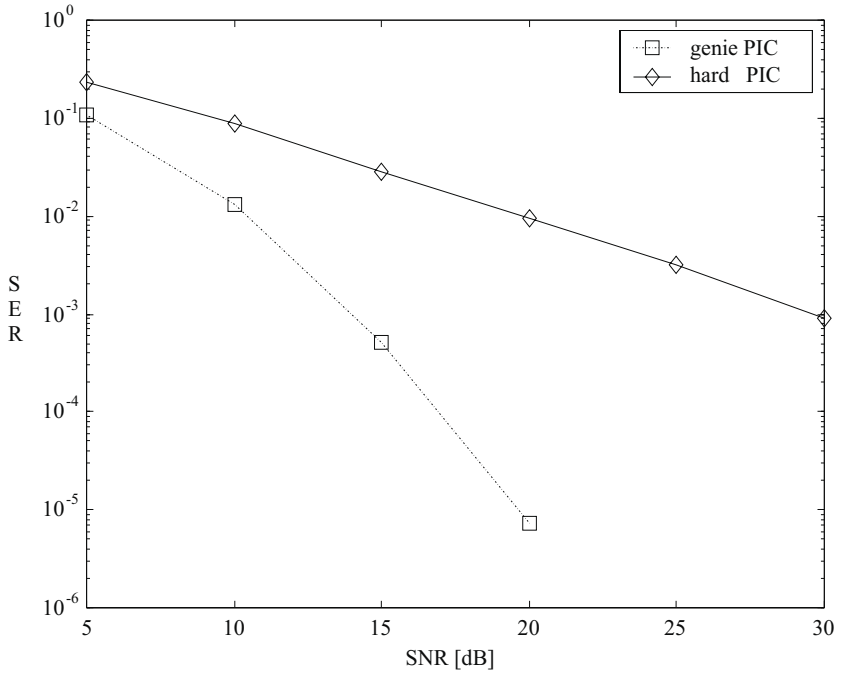

Figure 8.5: Error propagation of PIC BLAST detector, 4Tx-4Rx, QPSK, MMSE nulling

While perfect cancellation results in a 4-fold diversity level to all layers, the hard cancellation process suffers from significant degradation due to the error propagation problem.

These observations lead us to the conclusion that enhancing the reliability of previously detected layers has a significant impact on the overall performance of the scheme. We thus consider in the following section two candidate schemes that employ coding and interleaving in order to not just achieve coding gain but rather to offer the interference cancellation unit a more reliable decision feedback link, resulting in a higher overall diversity level.

8.3 Proposed Schemes

This section proposes two candidate schemes to mitigate the error propagation problem of SIC and PIC BLAST detectors. For the SIC type detectors, a pragmatic channel code paired with puncturing and erasing is introduced to improve the reliability of first detected layers with minimum penalty in spectral efficiency. In the PIC case, iterative interference cancellation decoding is performed such that after a few iterations the decisions fed into the interference cancellation unit are almost error free, and thus the MMSE nulling criteria converts its role to maximal ratio combining and offers maximum diversity level to all detected layers.

8.3.1 Variable Rate SIC Coded BLAST

A block diagram of the proposed variable rate coded BLAST is illustrated in Figure 8.6. Information bits are split into n_T parallel streams. The lth layer is encoded using a con-

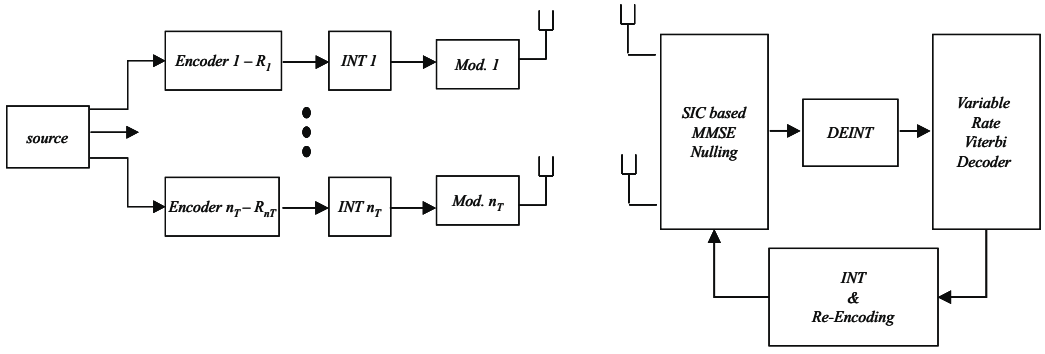

Figure 8.6: Unequal error protection for SIC based BLAST architecture

volutional code of rate R_l, block interleaver and M-ary PSK or QAM modulator. The coding rates of the layers are chosen such that $R_1 \leq R_2 \leq R_3 \cdots \leq R_{n_T}$. In these settings, symbols transmitted from the first layer will have better immunity to channel errors than

symbols transmitted from lower layers. The SIC based BLAST receiver orders its detection/cancellation process according to the assigned code rates. In the first iteration, the MMSE nulling process yields decision statistics that are fed in the form of soft decisions to the Viterbi decoder after deinterleaving. Decisions from the first layer are re-encoded, interleaved and modulated such that an estimate for the transmitted symbols of layer 1 is fed into the cancellation unit. These estimates are more reliable than their uncoded counterparts since they benefit from the error protection of a low rate code. Given that the error propagation is reduced, successive layers would "enjoy" an increased level of diversity and thus would not require the protection of a powerful error correction code, which degrades spectral efficiency. To keep the complexity of the scheme reasonable, we adopt the pragmatic code approach of Viterbi et al. in [119], where a single rate 1/2 convolutional code, paired with puncturing and erasing, is used to obtain any rate $(n-1)/n$ code. This facilitates the use of the same decoder for all layers, with a minor change in the metric generation process, which inserts erasures for the punctured symbols.

Note that the interleaving operation is crucial for the effectiveness of the channel code. By allowing the interleaver depth to be larger than the duration of a block (codeword), we distribute the bursty errors from the channel across the frame to allow for coding gain at the expanse of reasonable delay. In order to minimize latency, it is also possible to use diagonally layered space-time (DLST) encoding as proposed in [48, 49], where symbols are mapped along diagonals in space-time, utilizing the spatial dimension of the transmitter array to introduce time selectivity at the receiver. In such schemes, the nulling operation is performed over diagonals in space-time rather than over the spatial domain only.

8.3.2 Iterative PIC/Decoding for Coded BLAST

A block diagram of the iterative PIC decoding BLAST architecture is given in Figure 8.7.

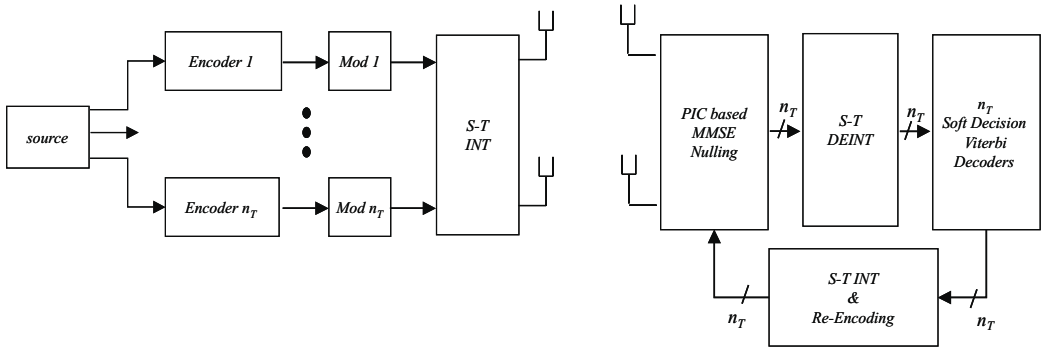

Figure 8.7: Iterative PIC/decoding BLAST architecture

At the transmitter, an equal rate error correction code is employed over each layer. The space-time interleaver is a random inter-substream permuter of size $n_T \times L$, where L corresponds to the length of the block. This operation uses the spatial dimension at the transmitter to form time-selectivity at the receiver (after deinterleaving), such that effective coding gain is achieved with minimum latency.

At the receiver, the nulling operation derives decision statistics for all layers simultaneously, which are space-time deinterleaved and fed into n_T parallel Viterbi decoders. The decisions are used to reconstruct the symbols transmitted from all layers. The PIC unit subtracts the contribution of these estimates from the received vector as described in Eq. (8.8) and the nulling and decoding operations are performed again. This process is repeated for multiple iterations until the reconstructed estimates are almost error-free, thus yielding n_R-fold diversity and substantial coding gain. The performance of the proposed schemes over independent and correlated fading channels are described in the next section.

8.4 Simulation Results

8.4.1 Independent Fading Channels

Figure 8.8 illustrates the symbol error rate (SER) of the variable rate SIC coded BLAST architecture with 4Tx-4Rx antenna array architecture and convolutional code rates of $1/2, 2/3, 3/4$ and $4/5$ for the four layers, respectively. Interleaver depth is selected to be 12 blocks long, with overall frame length of 600 QPSK symbols. The dash line curves correspond to the case of perfect cancellation, similar to those illustrated earlier in Figure 8.4. Since these "genie" curves correspond to the best-case scenario (decisions for feedback are error free), we refer to them as lower bounds.

It is observed that with the variable rate coding scheme (solid-line curves), similar diversity advantages for the various layers are achievable as the asymptotic slopes of the error-rates follow the corresponding slopes of the lower bounds. This indicates that the error propagation problem is significantly reduced by introducing variable rate channel coding and interleaving over the layers.

Note however that with the coding employed, the ordering in which layers are detected and cancelled is fixed according to the code rates. This inability to employ ordering based on post-detection SNR may have a negative impact on the performance of the SIC detector. To address that, we compare our coded bit-error rate (BER) results with the case of uncoded BER with and without ordering. All curves correspond to SIC with MMSE nulling. Results are depicted in Figure 8.9.

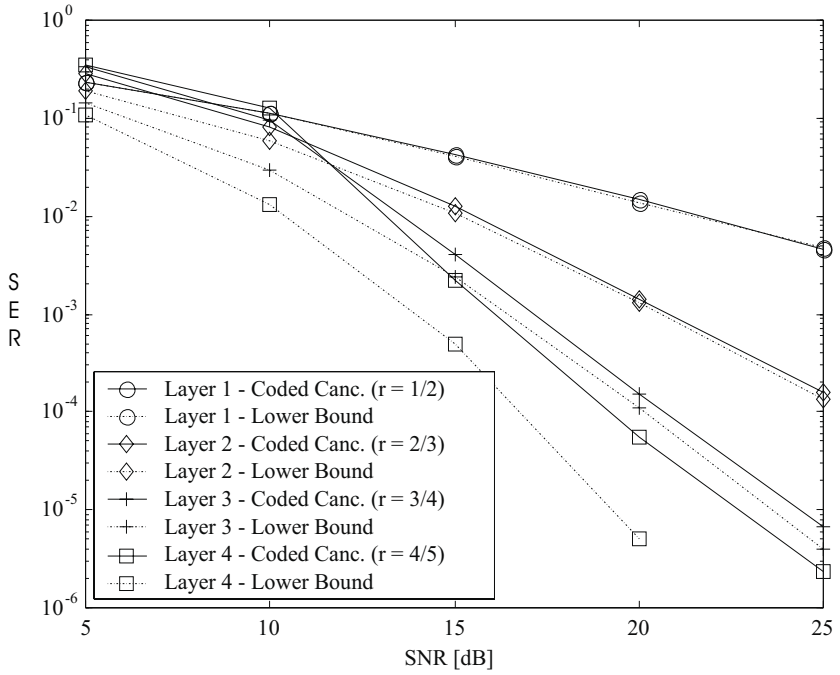

Figure 8.8: Uncoded performance; unequal error protection, SIC detector, MMSE nulling, 4Tx-4Rx, QPSK

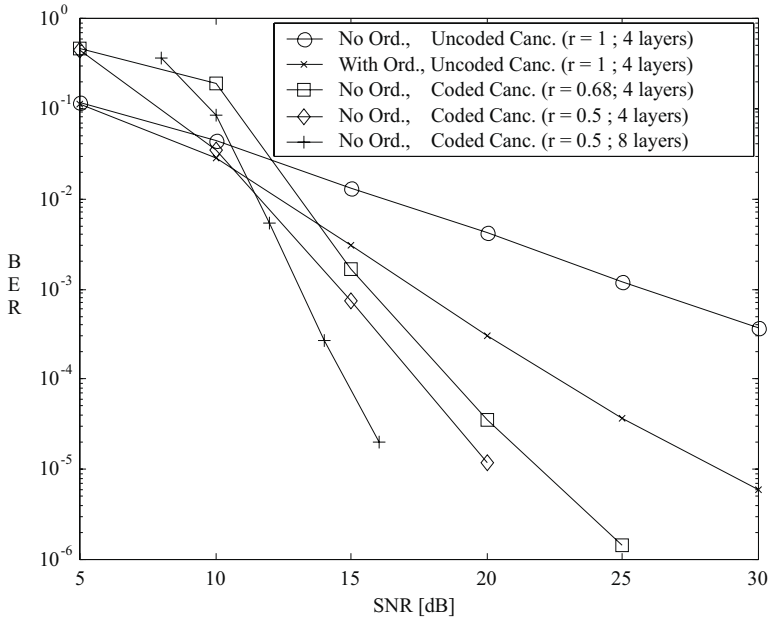

Figure 8.9: Coded performance; unequal error protection, SIC detector, MMSE nulling, 4Tx-4Rx, QPSK

It is first observed that the ordering is crucial to the performance of the V-BLAST SIC detector. However, by employing the variable rate coding scheme, gains of 6 and 8 dB are achieved at $BER = 10^{-5}$ for average code rate of 0.68 (composed of four convolutional codes with rates $1/2, 2/3, 3/4, 4/5$) and 0.5 (composed of four rate $1/2$ codes), respectively. These gains should not be interpreted as coding gains only. Rather, they result from an increase in diversity level (asymptotic slope of the error-rate curve is steeper) combined with coding gain. This improvement in performance comes at the expense of spectral efficiency. If one would like to keep the spectral efficiency the same and can tolerate higher complexity in both ends of the link, 8Tx-8Rx architecture with average rate $1/2$ codes can achieve overall gain of more than 10 dB at a target BER of 10^{-5} for the same spectral efficiency (8 [bps/Hz]). It is interesting to note that although the interleaving operation is performed in the time domain only, similar results can be obtained by diagonal layering as performed by Foschini in [48] and Da-Shan in [49].

Next, we explore the performance of the proposed iterative PIC decoding architecture. Figure 8.10 presents the uncoded SER of the 8Tx-8Rx PIC BLAST architecture as a function of SNR for a few consecutive stages/iterations.

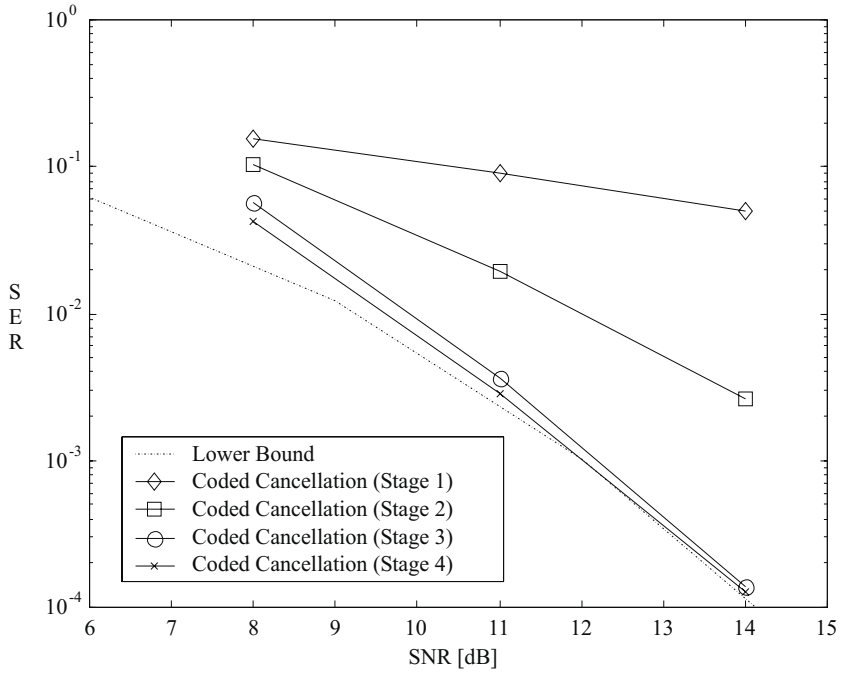

Figure 8.10: Uncoded Performance; iterative PIC/decoding; 4 iterations; 8Tx-8Rx; QPSK

It is observed that upon completion of the fourth iteration (stage 4), SER converges to the lower bound, indicating that the decisions fed into the cancellation unit are nearly error-free and thus eightfold diversity order is achieved.

Figure 8.11 demonstrates the uncoded performance of three PIC coded BLAST architectures with $4, 8$ and 16 layers. Clearly, the lower bound is achieved upon completion of the fourth iteration. We note that while large array sizes imply high computational complexity (n_T Viterbi decoders operate in parallel) and high implementation costs (in terms of hardware), both the spectral and energy efficiency of the scheme are enhanced.

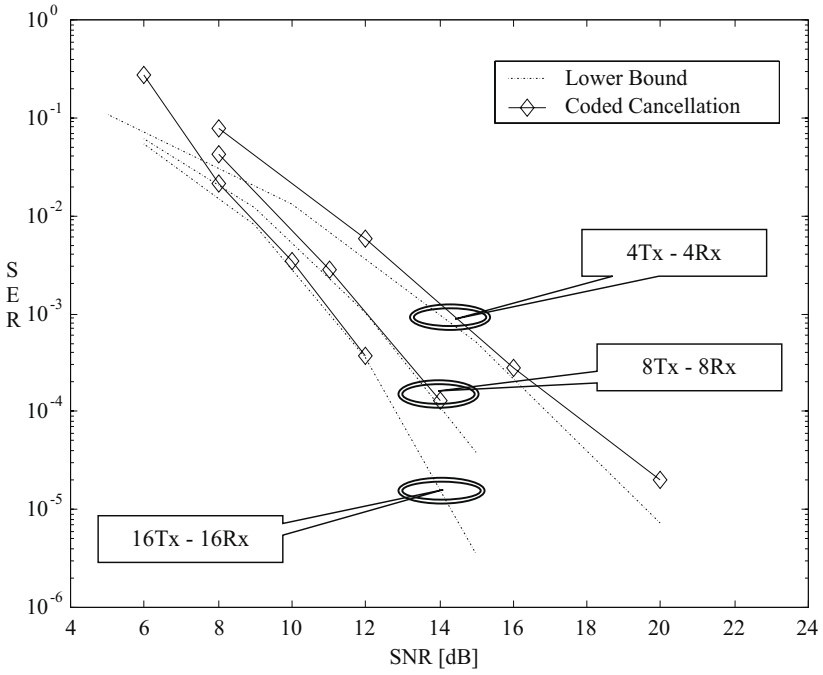

Figure 8.11: Iterative PIC/decoding; 4 iterations; MMSE nulling, $r = 1/2$, $K = 7$, QPSK

Finally, the performance of uncoded PIC scheme is compared with the performance of the iterative coded PIC scheme of 16×16 antenna array configuration. We observe dramatic improvements in the energy efficiency of the scheme. In fact, throughput of 16 [bps/Hz] is achieved with BER of 10^{-5} at SNR of 9.5 dB over quasi-static Rayleigh Fading channel. This is remarkable energy efficiency, which is comparable to the well-known energy efficiency of uncoded QPSK modulation in AWGN channel.

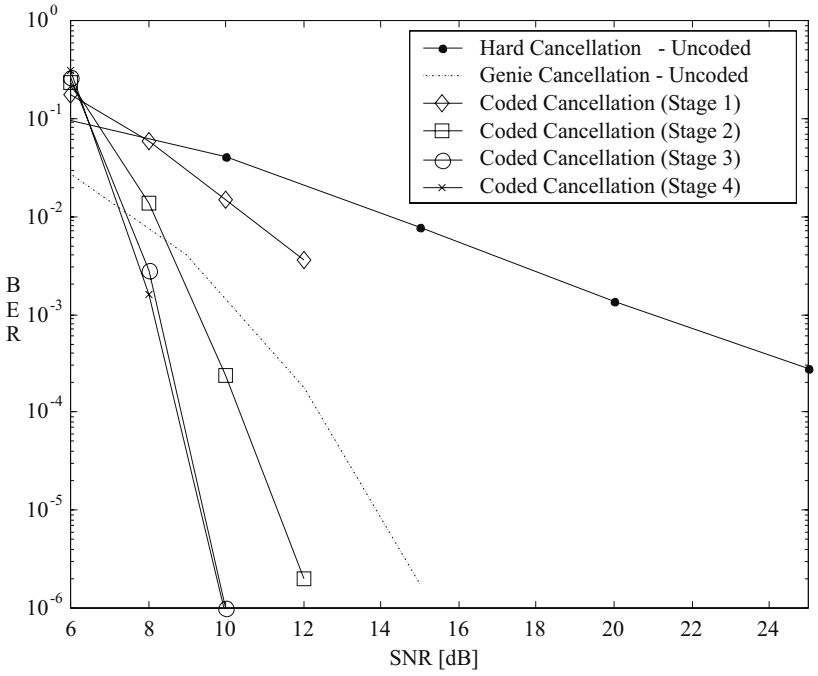

Figure 8.12: Coded performance; PIC detector, MMSE nulling, 16Tx-16Rx, $r = 1/2$, $K = 7$, QPSK

8.4.2 Correlated Fading Conditions

In practical terminals (e.g., laptops, personal digital assistants, etc.), antenna separation may be limited such that fading paths exhibit significant correlation. In this section, we address the performance of the iterative PIC decoding BLAST scheme under correlation conditions at the transmitter or receiver. We consider both uniformly spaced linear or circular antenna array configurations and quantify the degradation associated with spatial correlation. Furthermore, in practical terminals where the spatial dimensions are limited, we demonstrate that adding more antenna elements does not necessarily result in an improved performance.

In the case of linear array, the elements of the covariance matrix are assumed to be functions of antenna separation only, i.e., $R_{mn} = f(m-n)$ and thus the resulting matrix has a Toeplitz form, which is described by:

$$R_{mn} = \begin{cases} 1, & m = n \\ \rho^{|m-n|}, & m \neq n \end{cases}, \tag{8.11}$$

where ρ represents the cross-correlation coefficient between the fade coefficients associated with two adjacent antenna elements.

In the circular array case, the covariance matrix has a circulant form, given by

$$R_{mn} = \begin{cases} 1, & m = n \\ \rho^{min\{|m-n|, n_T - |m-n|\}}, & m \neq n \end{cases}, \tag{8.12}$$

Examples of both Toeplitz and circulant matrices are given in Figure 8.13 for 8 and 16 antenna elements with $\rho = 0.25$ and 0.5, respectively. We use these matrices and adopt the procedure proposed in [68, 69] (see also Appendix E), for generating equal power correlated Rayleigh fading envelopes.

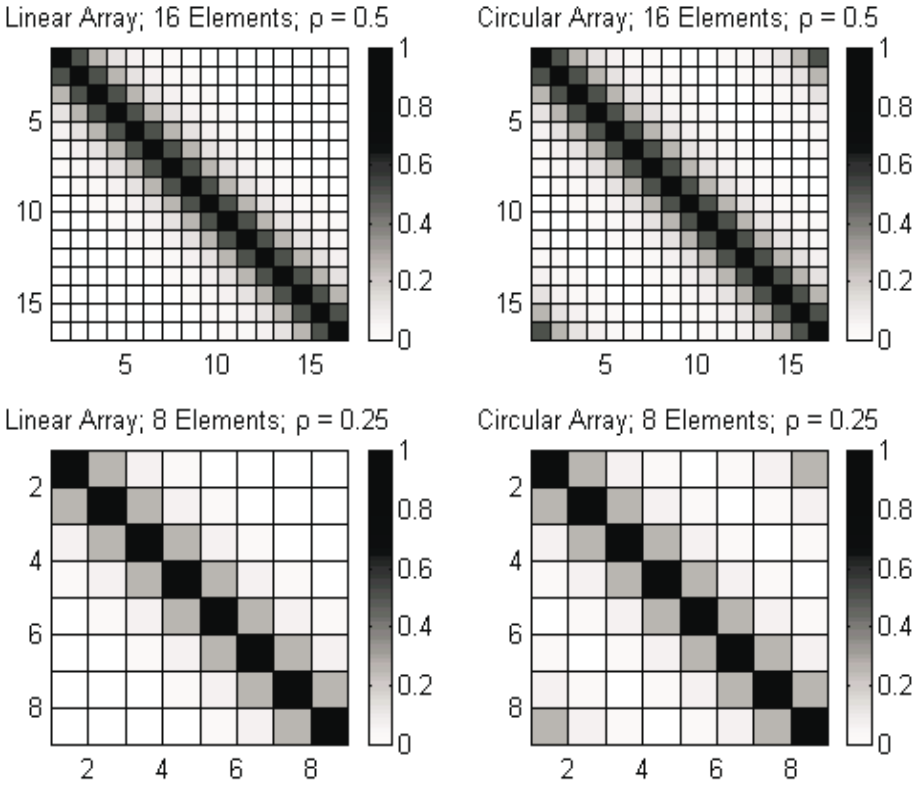

Figure 8.13: Toeplitz and circulant covariance matrices

Figure 8.16 presents bit error rate results of the PIC coded BLAST as a function of the cross-correlation coefficient between two adjacent antennas at the receiver. In these simulations, the signal-to-noise ratio is held to a constant, at 12 dB. While the geometry of the receiver array is assumed to be linear, the transmit array is assumed to have sufficient spatial separation between elements to guarantee independent transmissions. The scheme employs QPSK Mapping, 8Tx-8Rx antenna array size, MMSE nulling, rate 1/2 constraint length 7 convolutional code and space-time interleaver with $L = 600$ symbols.

It can be seen that for $\rho > 0.25$, performance is degraded significantly in all stages. However, as long as $\rho \leq 0.5$, iterative processing is still effective. It is noted that $\rho > 0.6$ results in error floor, such that additional iterations degrade performance.

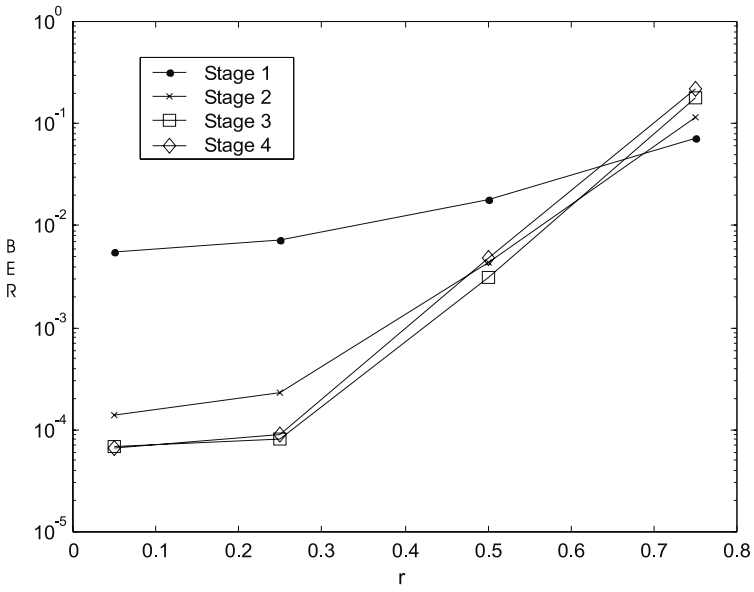

Figure 8.14: Correlation at the receiver; PIC detector, MMSE nulling, 16Tx-16Rx, $r = 1/2$, $K = 7$, QPSK, SNR= 12 dB

A comparison of the impact of correlation at the transmitter and receiver is illustrated in Figure 8.15. Bit error rate results of the PIC coded BLAST are described as a function of the cross-correlation coefficient between two adjacent antennas upon completion of the fourth iteration for a fixed SNR of 12 dB. It is observed that the iterative PIC coded BLAST scheme is more sensitive to correlation at the receiver than at the transmitter.

Next, we compare the performance of 16Tx-16Rx with 8Tx-8Rx with the spatial dimensions held constant. That is, we assume that the limited spatial dimensions of a portable device imply half-wavelength antenna spacing for 8 elements, and quarter-wavelength for 16 elements. The corresponding cross-correlation coefficients, derived based on Jakes model [70] (assuming uniform angular distribution) are 0.25 and 0.5, respectively. Figure 8.16 presents results for various antenna array configurations with linear or circular array geometries. In the uncorrelated case, the scheme with 16 elements outperforms the scheme with 8 elements due to the increased diversity advantage. However, in correlated conditions, no significant difference can be observed. This leads us to the conclusion that performance gains associated with increased number of antenna elements may not be realized in correlated fading environments.

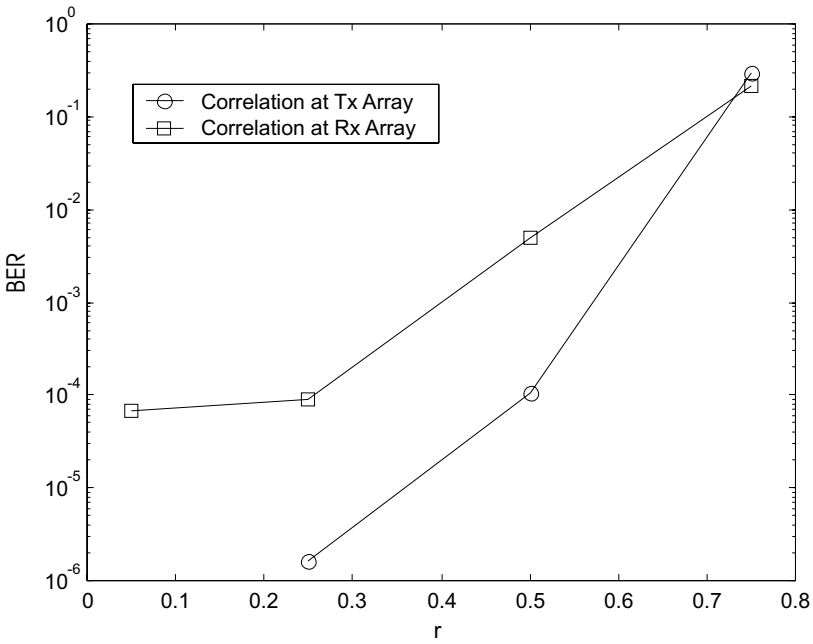

Figure 8.15: Impact of correlation at the transmitter and receiver; PIC detector, MMSE nulling, 16Tx-16Rx, $r = 1/2$, $K = 7$, QPSK, SNR= 12 dB

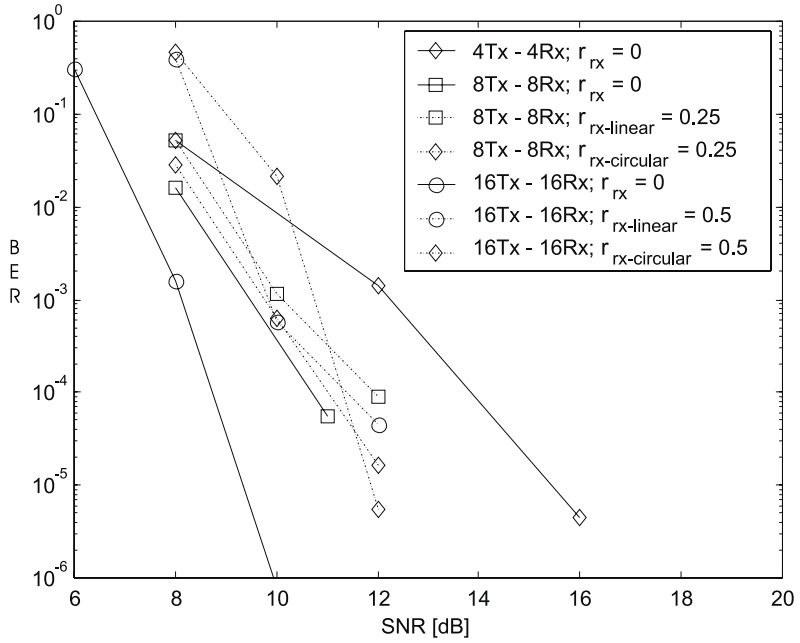

Figure 8.16: Limited physical dimensions for linear or circular array; PIC detector, MMSE nulling, 16Tx-16Rx, $r = 1/2$, $K = 7$, QPSK

8.5 Chapter Summary

In this chapter, the error propagation problem of both successive interference cancellation (SIC) and parallel interference cancellation (PIC) BLAST detectors is characterized. Two candidate schemes that mitigate the phenomenon are proposed. For the SIC based detectors, a pragmatic channel code paired with puncturing and erasing is introduced to improve the reliability of first detected layers with minimum penalty in spectral efficiency. In the PIC case, iterative interference cancellation decoding is performed such that after couple of iterations the decisions fed into the interference cancellation unit are almost error-free and thus the MMSE nulling criteria converts its role to maximal ratio combining and offers maximum diversity level to all detected layers.

Although both schemes reduce significantly the error propagation problem, the iterative PIC decoding scheme achieves higher overall diversity advantage than the corresponding SIC scheme. In the latter case, the diversity advantage increases as detection proceeds from layer to layer, but the former guarantees n_R-fold diversity to all detected layers. Also, the latency associated with the PIC scheme increases linearly with the number of stages/iterations while the latency of the SIC coded scheme increases linearly with the number of layers to be detected. Usually, the number of layers is higher than the number of stages/iterations required. On the other hand, the complexity of the PIC scheme is higher than the complexity of the SIC scheme since n_T Viterbi decoders have to operate in parallel. Also, the SIC based scheme possesses an inherent feature of trading energy and spectral efficiency by employing different sets of code rates.

Finally, we study the impact of spatial correlation on the performance of the iterative PIC decoding scheme. It is shown that the scheme is more sensitive to correlation at the receiver than at the transmitter. In practical portable devices, where the spatial dimensions are limited, it is shown that adding more antenna elements does not necessarily result in improved performance.

The work presented in this chapter has been submitted to the 2002 Fall Vehicular Technology Conference in Vancouver, Canada [121].

Chapter 9

A Unified Comparison of Space-Time Architectures

Space-time architectures have been developed to improve the reliability and throughput of wireless systems using multiple antenna element technology. In previous Chapters, we have shown that both block and trellis-type space-time codes improve the energy efficiency over fading channels by exploiting their spatial and temporal diversity. It was also shown that the original BLAST architecture (V-BLAST) significantly improves the spectral efficiency of the scheme with limited energy efficiency[1]. An effort to improve the energy efficiency of BLAST detectors was made in Chapter 8, by introducing iterative cancellation decoding mechanism. A vast body of research has been published on the performance and structure of these techniques separately. In this chapter, we aim to compare these architectures in a unified manner such that both the spectral and energy efficiencies are addressed. To that end, we define a new performance metric of averaged "good throughput", termed "goodput". This metric can be defined as the inherent spectral efficiency of the scheme times the correct frame rate. Using this metric, we assess on the impact of scheduling algorithms, which may be performed in the access-control (MAC) layer of a wireless network, on the performance of space-time architectures, employed at the physical (PHY) layer of the system.

One important application to space-time architectures may be high-data-rate downstream wireless Internet access to nomadic users [122]. The nature of such data traffic is asymmetric, requiring a much higher downlink rate from the base station (BS) than that generated in the uplink channel by the user terminal. In addition to traffic asymmetry, data services differ from voice services also in their tolerance to delay. In this chapter, we consider a scenario where a single BS provides data services to K users, each of which

[1]For definitions of spectral and energy efficiency, please see section 1.5

is equipped with multiple antenna elements. Since the data rate that can be supported to each user is proportional to its received SNR, it may be beneficial to use CSI and the unequal latency property of the service to serve multiple users with disparate SNRs. This may improve the overall throughput of the system as compared with the case of equally served users regardless of their channel conditions. The BS applies one of the space-time architectures (e.g., STBC, STTC or BLAST) paired with a scheduling protocol that routes the transmission of packets to users based on their reported CSI in the uplink channel.

Two extreme scheduling algorithms are considered. The first one, denoted "greedy", routes each transmission to the user with the best instantaneous channel conditions. The second, denoted "round robin" (RR), routes the transmission of packets equally across users. Results indicate that the "greedy" scheduler gives rise to multiuser diversity mechanism, where the link with the best instantaneous SNR is selected (out of K independent links) on a per frame basis. The round robin scheduler is equivalent to the single user case since all users are equally served in an orthogonal TDM-like manner. The multiuser diversity, introduced by the "greedy" scheduler, enhances the averaged SNR and thus improves the performance of the space-time architecture. We study the interactions of multiuser diversity and spatial diversity by calculating the statistics of the effective SNR at the space-time combiner output with and without K-fold multiuser diversity. It is shown that in some cases, schemes with multiuser diversity only can (surprisingly) outperform schemes with spatial and multiuser diversity. An explanation for this phenomenon is provided in section 9.2.

9.1 Scheduling Algorithms over STC

Let us consider a scenario in which K active data users, each of which is equipped with multiple antenna elements, are served by a single multi-antenna element base station (BS). The users report their CSI to the BS on a per frame basis. Using a scoring function at the BS, time resources are allocated to the user with the best instantaneous channel conditions. This scheme is denoted "greedy" and its performance in Rayleigh fading environment is compared with the case of equally served users in a round robin fashion.

We compare various combinations of scheduling algorithms and space-time architectures using a single metric of averaged "good throughput", which encapsulates both the spectral and energy efficiency of the scheme. The metric is defined by

$$\overline{\rho} = \eta \frac{K}{L} \sum_{k=1}^{K} N_k (1 - FER(k, SNR)), \tag{9.1}$$

where η is the theoretical spectral efficiency of the scheme in [bps/Hz], K denotes the number of users, L is the total number of data frames to all users, N_k is the number of

actual transmitted frames to the kth user (need not be constant in "greedy" mode) and $FER(k, SNR)$ is the FER of the kth user for a given signal-to-noise ratio.

The following four specific space-time architectures are considered for the PHY layer, assuming that both the base station and the terminal are equipped with 4 antenna elements:

1. Space-time block code (STBC) with M-ary PSK and H_4 orthogonal design.
2. STBC (same as in 1) as inner code concatenated with an outer convolutional code (rate 1/2, constraint length 7).
3. Uncoded V-BLAST with MMSE nulling, successive interference cancellation (SIC) and ordering of layers.
4. Coded PIC BLAST with iterative cancellation decoding.

For simplification purposes, we assume perfect channel tracking at the terminal and perfect feedback of these estimates to the BS. We also assume that the K users experience the same average SNR and that each MIMO link exhibits quasi-static flat fading conditions. We note that the transmitted power is held constant for all cases.

Figure 9.1 presents simulated results for various combinations of space-time architectures and scheduling algorithms. The effectiveness of the metric $\overline{\rho}$ is demonstrated by addressing both the energy and spectral efficiency of the scheme. We observe that each scheme has a different operating point, where the "goodput" $\overline{\rho}$ converges to the theoretical throughput η. For example, V-BLAST with QPSK modulation requires SNR of 20 dB to guarantee 8 [bps/Hz], coded BLAST requires SNR of 11 dB to provide 4 [bps/Hz], uncoded STBC with QPSK modulation requires SNR of 6 dB to provide 1.5 [bps/Hz] and coded STBC can operate reliably at SNR of 0 dB with spectral efficiency of 0.75 [bps/Hz]. This provides an insight for the benefits (and drawbacks) of the various space-time architectures. It is further observed that the "greedy" scheduling algorithm enhances throughput significantly due to multiuser diversity. A detailed treatment of the impact of multiuser diversity on space-time architectures is provided in the next section and in [123]. As reference curves, we also include the 1% outage capacity of the MIMO channel (see Chapter 2) computed with and without multiuser diversity. These curves serve as an upper bound on the throughput of practical space-time architectures. It is observed that the coded PIC BLAST scheme, proposed in Chapter 8 operates within 5 dB from channel capacity.

Zooming into the good energy efficiency-low spectral efficiency regions of this two dimensional space, Figure 9.2 demonstrates the "goodput" of STBC with and without outer error correction code paired with "greedy" ($K = 20$) or round robin scheduling algorithm.

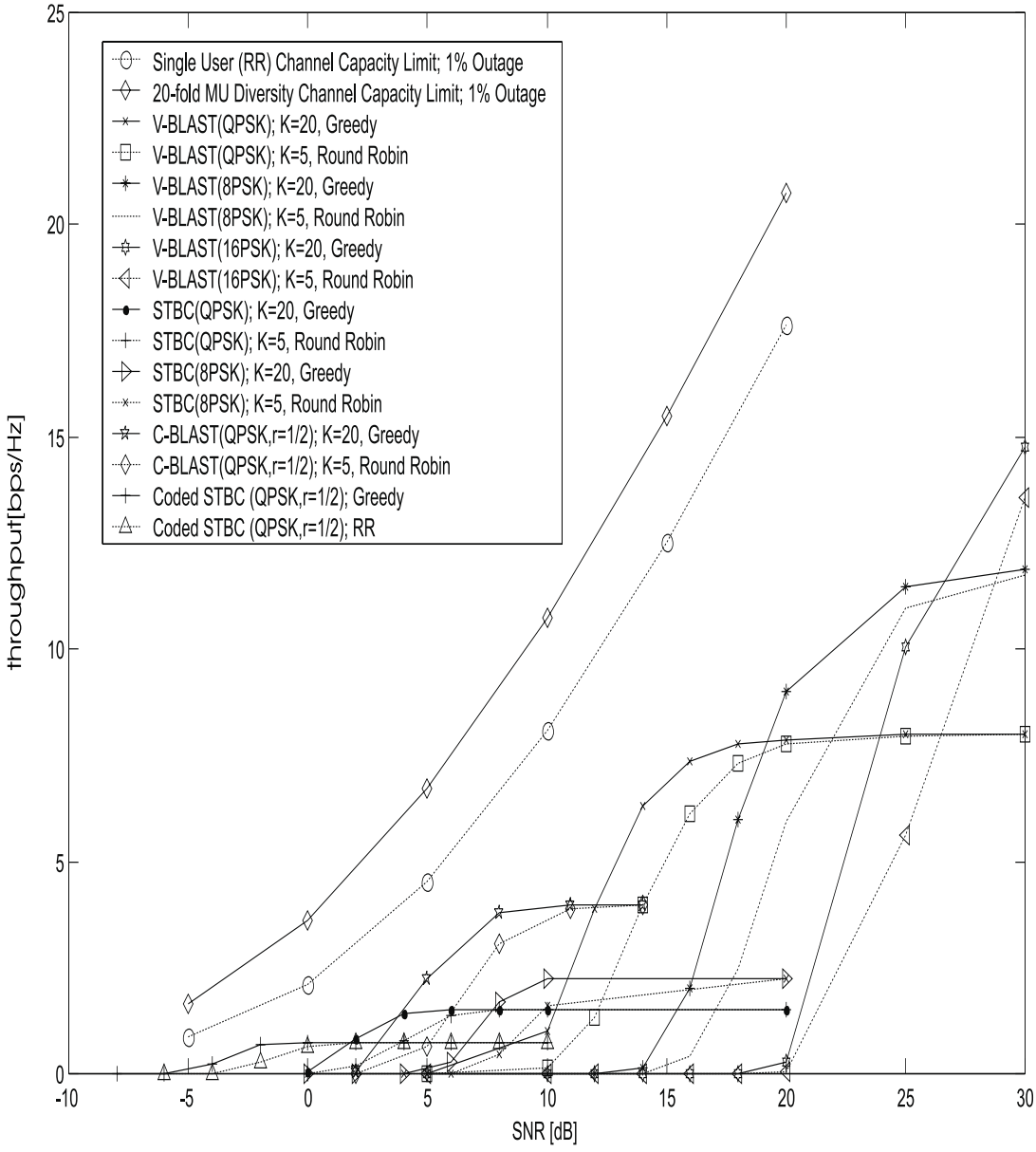

Figure 9.1: "Goodput" of scheduling over space-time architectures (4Tx-4Rx)

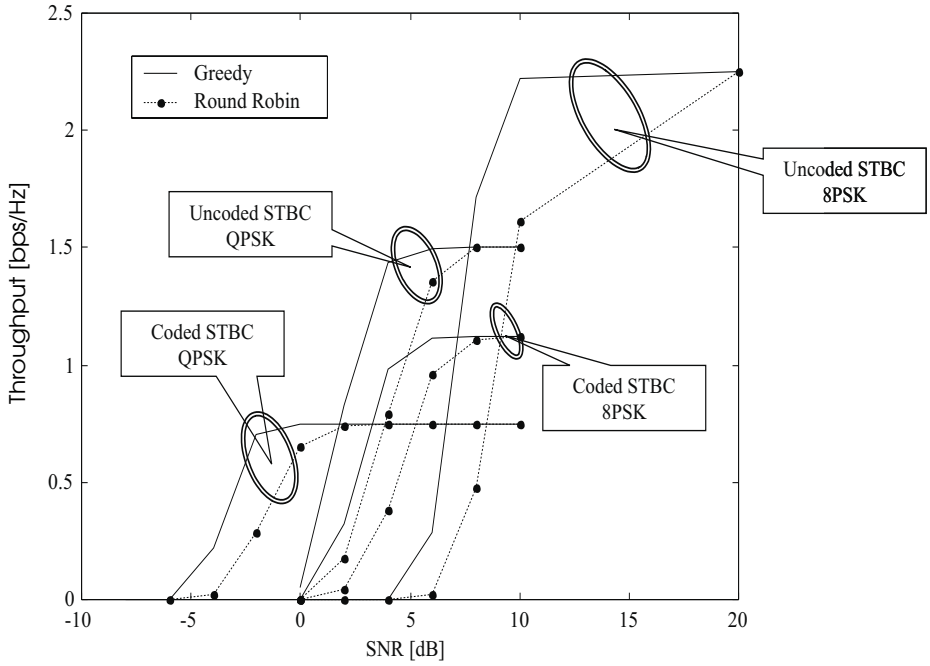

Figure 9.2: "Goodput" of scheduling over space-time block codes (4Tx-4Rx)

Again, the "greedy" scheduler increases throughput quite significantly due to enhancement of SNR. Note that coded STBC with 8PSK is inferior to uncoded STBC with QPSK. This is due to the rate loss associated with the use of convolutional code. As was shown in section 5.2, trellis codes may be a better choice for an outer error correction code of STBC as they facilitate coding gain without sacrificing spectral efficiency.

One disadvantage of the "goodput" metric is that not all points on the curve are valid operating points (i.e., acceptable FER values). To address that, Figure 9.3 presents a "sample" of the throughput curves at a fixed FER of 1% for the four disparate space-time architectures operating with round robin scheduling algorithm. Also here, we include the 1% outage capacity of the MIMO channel as a reference curve.

Results show that V-BLAST architecture paired with QPSK, 8PSK and 16PSK achieves $8, 12$ and 16 [bps/Hz] at SNRs of $20, 30$ and 35 dB, respectively. Space-time block code (H_4 orthogonal design) paired with QPSK and 8PSK requires SNRs of 6 and 11 dB, to achieve 1.5 and 2.25 [bps/Hz], respectively. Upon completion of the fourth iteration, the iterative coded BLAST with QPSK achieves 4 [bps/Hz] at SNR of 11 dB. If one would like to achieve extremely good energy efficiency, STBC concatenated to a rate $1/2$ convolutional code yields spectral efficiency of 0.75 [bps/Hz] at a low SNR of 2 dB.

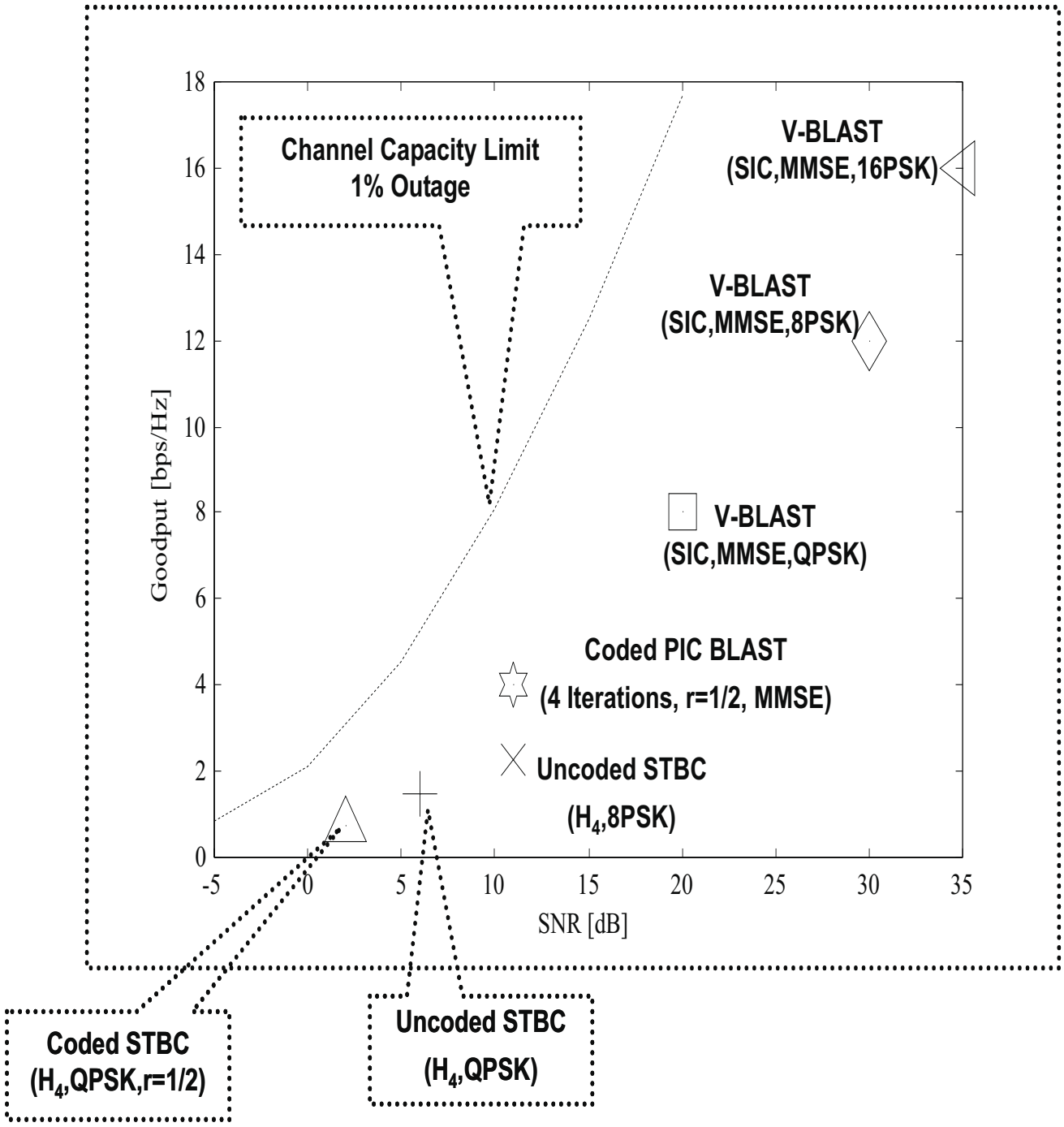

Figure 9.3: "Goodput" of round robin scheduling over space-time architectures for a fixed FER of 1% (4Tx-4Rx)

Next, FER results as a function of SNR for the four schemes with "greedy" or round robin scheduling algorithms are presented. Note that the information presented in this plot has been already embedded into Figure 9.1 (see Eq. (9.1)). Here, we focus on the energy efficiency of the scheme and observe that with the "greedy" scheduling, 1% FER is achieved at $SNR = -1, 4, 11$ and 21 dB for coded STBC, uncoded STBC, coded PIC BLAST and uncoded V-BLAST, respectively. Using the round robin scheduling algorithm, 1% FER is achieved at $SNR = 2, 8, 13$ and 23 dB for the four schemes, respectively. Thus, the "greedy" scheduling algorithm enhances the performance of the scheme by about 2.5 dB.

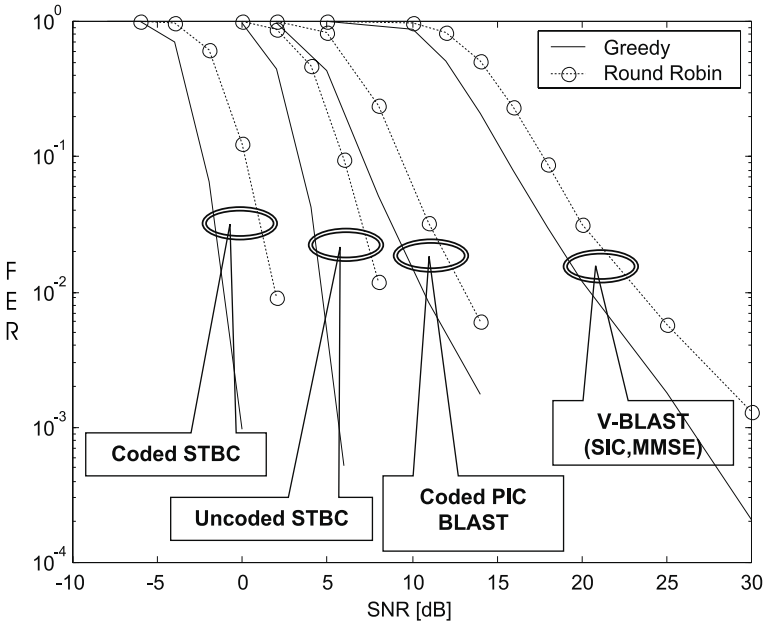

Figure 9.4: FER results for scheduling over space-time architectures (4Tx-4Rx;$K = 20$)

A surprising result is that the "greedy" scheduler, which introduces multiuser diversity, enhances the performance of STBC with 4Tx-4Rx antenna array configuration. Since the spatial diversity order of this scheme is 16, the MIMO Rayleigh fading channel has been approximately transformed to an equivalent single-input single-output AWGN channel. It is well known [85, 124] that by increasing the spatial diversity order of STBC further, performance in terms of reliability and capacity is bounded by AWGN results. Natural questions are therefore: 1) How does multiuser diversity enhance performance further ? 2) Is multiuser diversity mechanism equivalent to spatial diversity ? The answer to these questions is provided in the following section.

9.2 The Impact of Multiuser Diversity on STBC

The "greedy" scheduling algorithm, which gives rise to multiuser diversity, was shown to result in an enhanced performance. Using order statistics [125], we quantify the benefits of multiuser diversity on the effective SNR at the space-time combiner output. We study the interactions of multiuser diversity and spatial diversity order, associated with transmit diversity only or transmit-receive diversity schemes.

The channel of the kth user is modeled by an $n_T \times n_R$ matrix $\Omega_k = [\alpha_{i,j}^{(k)}]$, whose entry $\alpha_{i,j}^{(k)}$ represents the complex fade coefficient for the path from transmit antenna i to receive antenna j of the kth user. These fade coefficients are assumed to be zero mean complex Gaussian random variables with variance 0.5 per dimension. Assuming a rate r STBC used for each link, the effective SNR at the space-time combiner output of the kth user is given by

$$\gamma = \frac{SNR}{rn_T} \sum_{j=1}^{n_R} \sum_{i=1}^{n_T} \left| \alpha_{i,j}^{(k)} \right|^2 . \tag{9.2}$$

This is a chi-square random variable with $n_T n_R$ degrees of freedom. The probability density function of this random variable is given by [71]

$$f_\gamma(\gamma) = \frac{1}{(n_T n_R - 1)! \left(\frac{SNR}{rn_T}\right)^{n_T n_R}} \gamma^{n_T n_R - 1} e^{-\frac{\gamma}{SNR/rn_T}} . \tag{9.3}$$

Let us define new variables μ, n and C as: $\mu = \frac{rn_T}{SNR}$, $n = n_T n_R - 1$ and $C = \frac{\mu^{n+1}}{n!}$. This allows us to write a simplified form of (9.3):

$$f_\gamma(\gamma) = C\gamma^n e^{-\mu\gamma}. \tag{9.4}$$

In our "greedy" scheduling algorithm, the base station selects (on a per frame basis) the user k with the best instantaneous channel realization. That is:

$$arg\ max_{k \in \{1,2,\cdots,K\}} \sum_{j=1}^{n_R} \sum_{i=1}^{n_T} \left| \alpha_{i,j}^{(k)} \right|^2 . \tag{9.5}$$

This multiuser diversity mechanism creates a new random variable, denoted $\tilde{\gamma}$, which represents the effective SNR at the space-time combiner output with K-fold multiuser diversity. The probability density function (pdf) of this random variable is computed using order statistics results [125]:

$$g_{\tilde{\gamma}}(y) = K f_\gamma(y) F(y)^{K-1}, \tag{9.6}$$

where K is the number of users and $F(y)$ denotes the cumulative distribution function (CDF) of the original random variable γ. The CDF of γ is given by

$$F(y) = \int_{\gamma=0}^{y} f_\gamma(\gamma) d\gamma = 1 - \mu^{n+1} e^{-\mu y} \sum_{m=0}^{n} \frac{y^m}{m! \mu^{n-m+1}}. \tag{9.7}$$

Plugging Eqs. (9.7) and (9.4) into (9.6), we obtain a closed form expression for the pdf of the effective SNR at the space-time combiner output with K-fold multiuser diversity. Results in the form of cumulative distribution functions (CDFs) are plotted in Figure 9.5 using Monte Carlo simulations and the analysis presented for STBC with 4Tx-4Rx, paired with $50, 20, 5$ and 1-fold multiuser diversity.

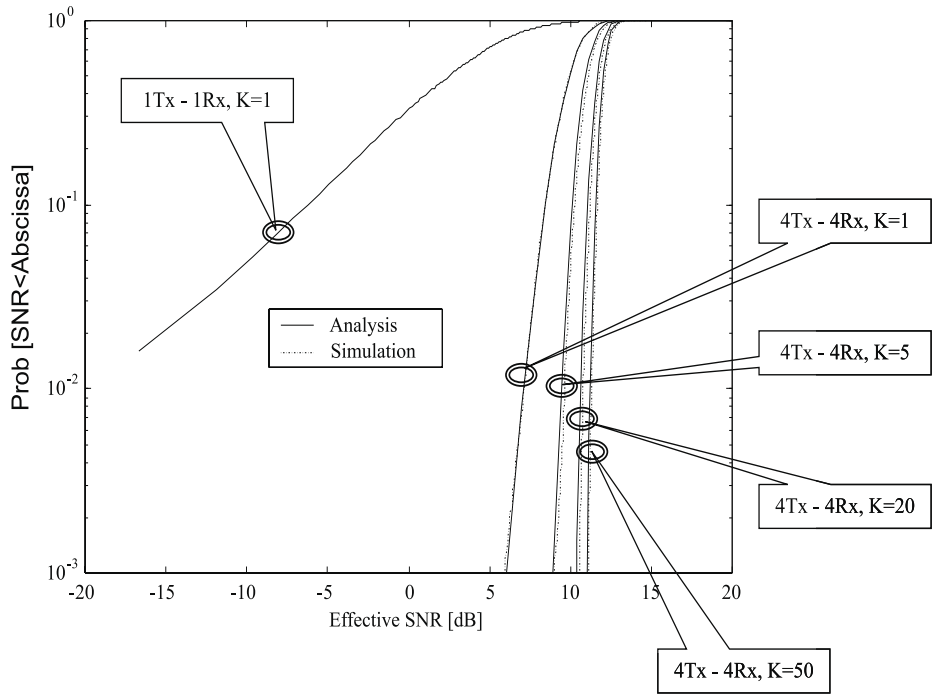

Figure 9.5: The effect of multiuser diversity on the average effective SNR ; $SNR = 4dB$

As a reference, we include the CDF of a single-input single-output (SISO) link with no multiuser diversity. For a given CDF level of 1%, the effective SNR is enhanced by $2.3, 3.3$ and 4 dB for $K = 5, 20$ and 50 users, respectively. An excellent match is demonstrated between the closed form expression and the Monte Carlo simulation results.

This SNR enhancement yields an improved performance in terms of frame error rate. Figures 9.6 and 9.7 present FER and "goodput" results, respectively, for a rate 3/4 STBC with QPSK modulation and 4Tx-4Rx antenna array configuration with and without multiuser diversity. The outer error correction code used herein is a constraint length 7, rate 1/2 convolutional code.

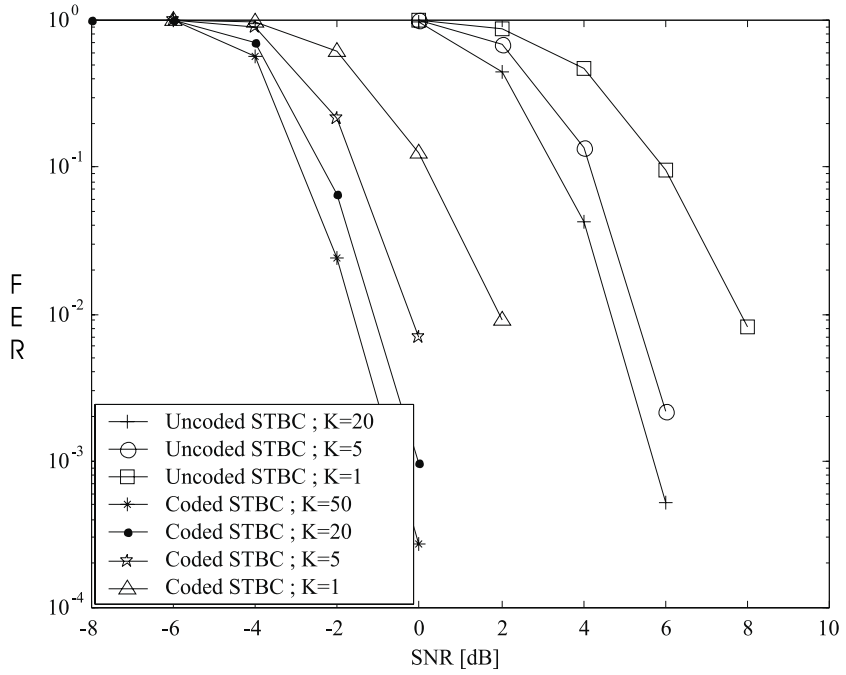

Figure 9.6: FER of STBC with K-fold multiuser diversity (4Tx-4Rx, QPSK, H_4, $r = 1/2$)

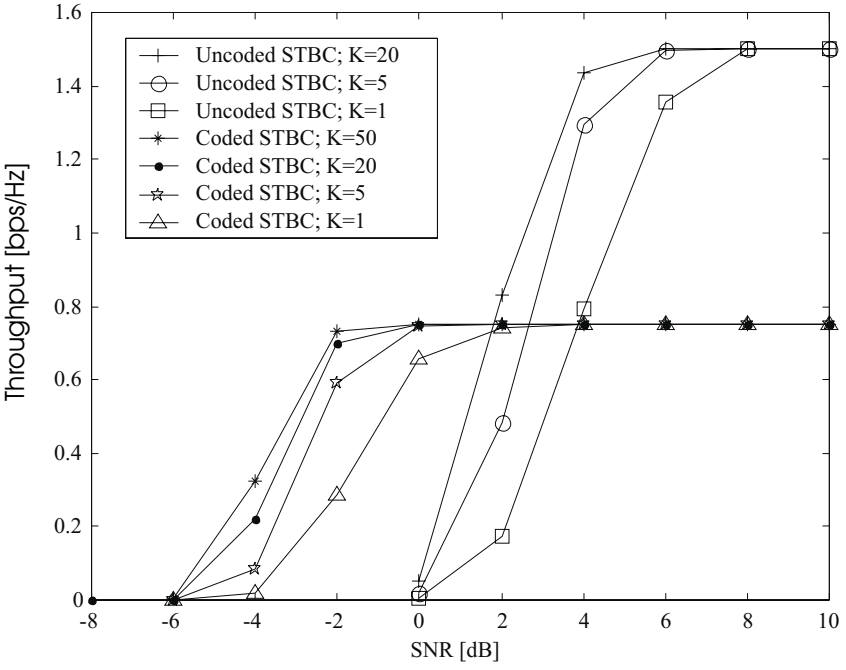

Figure 9.7: "Goodput" of STBC with K-fold multiuser diversity (4Tx-4Rx, QPSK, H_4, $r = 1/2$)

The mth moment of the effective SNR at the output of the space time combiner with K-fold multiuser diversity is computed by

$$E[y^m] = \int_{y=0}^{\infty} y^m g_{\tilde{\gamma}}(y)dy = K \int_{y=0}^{\infty} y^m f_{\gamma}(y)F(y)^{K-1}dy, \tag{9.8}$$

Using the first moment of Eq. (9.8), Figure 9.8 illustrates the effective SNR gain due to multiuser diversity for various array configurations. It is noticed that the SNR gain reaches a saturation point for all array sizes, where increasing the number of users further (amount of links to choose from) results in diminishing returns in SNR enhancement. More important, it is observed that as the array size increases (higher spatial diversity order), the gain associated with the multiuser diversity decreases.

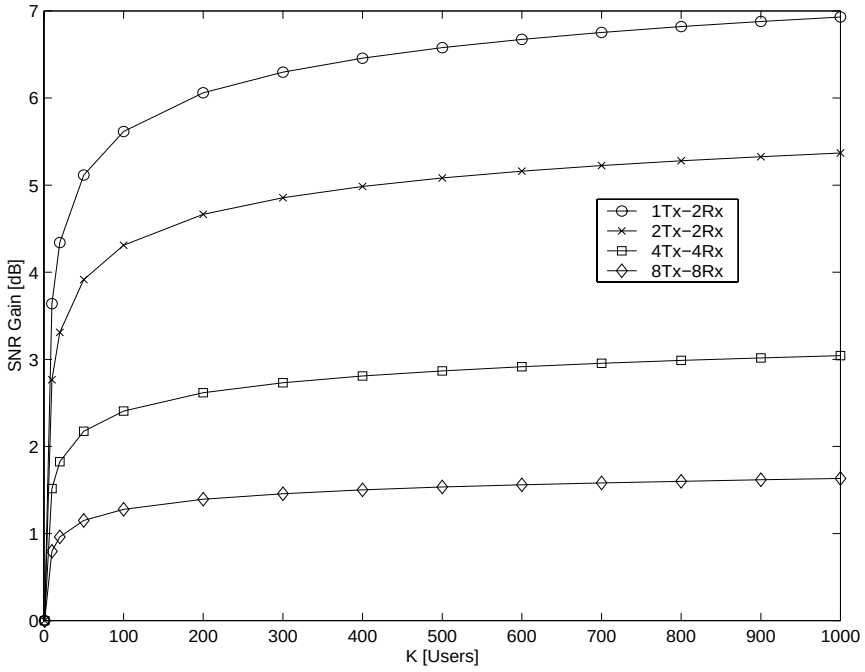

Figure 9.8: Multiuser diversity over STBC; averaged effective SNR gain

Similarly, we compute the standard deviation of the effective SNR using the first and second moments of Eq. (9.8). Results are illustrated in Figure 9.9. We notice that the variance of the effective SNR decreases with the number of users and as the spatial diversity order increases.

In order to assess on the interactions of multiuser diversity and spatial diversity further, we plot in Figure 9.10 the CDF of the effective SNR with the "greedy" ($K = 50$) and round robin scheduling algorithms for various spatial diversity orders that arise from transmit diversity only.

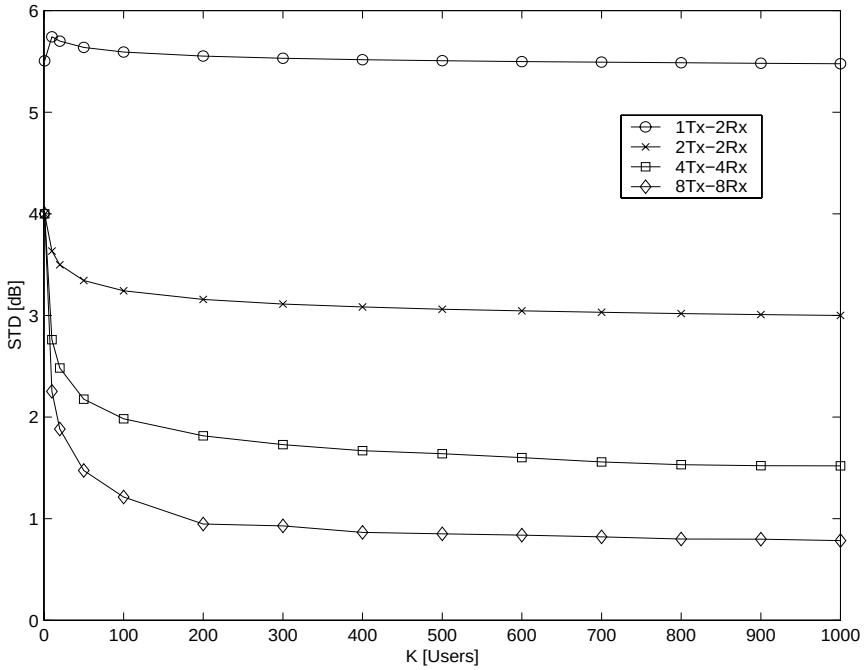

Figure 9.9: Multiuser diversity over STBC; standard deviation of the effective SNR

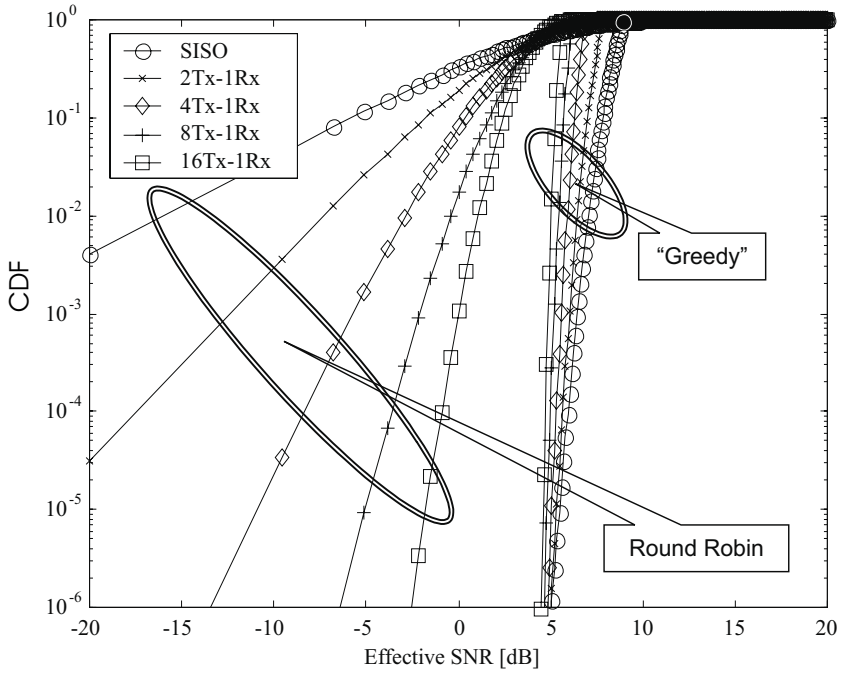

Figure 9.10: CDF of effective SNR with and without 50-fold multiuser diversity; $n_R = 1$

It is observed that in the round robin case, as the size of the transmitter array increases, the steepness of the CDF slope increases, indicating the increased spatial diversity order. However, with multiuser diversity, an opposite trend occurs. That is, multiuser diversity with no spatial diversity outperforms schemes that employ both multiuser diversity and spatial diversity. Although this result may seem surprising at first, it can be explained as follows. The "greedy" scheduler takes advantage on the constructing characteristics of the Rayleigh fading channel. The spatial diversity order of the STBC does not only reduce the probability of having deep fades but also the probability of having constructive fades, thus limiting the benefits that could be achieved by multiuser diversity. In other words, while the performance of STBC schemes with multiple transmit antenna elements and a single receive antenna element is bounded by AWGN results, schemes with multiuser diversity can outperform those of a single input single output AWGN channel. In Figure 9.11 we include schemes that employ multiple antenna elements at the receiver. It is observed that the receive diversity provides antenna aperture gain that shifts the curves by 3 and 6 dB, for the 2 and 4 receive antenna elements, respectively.

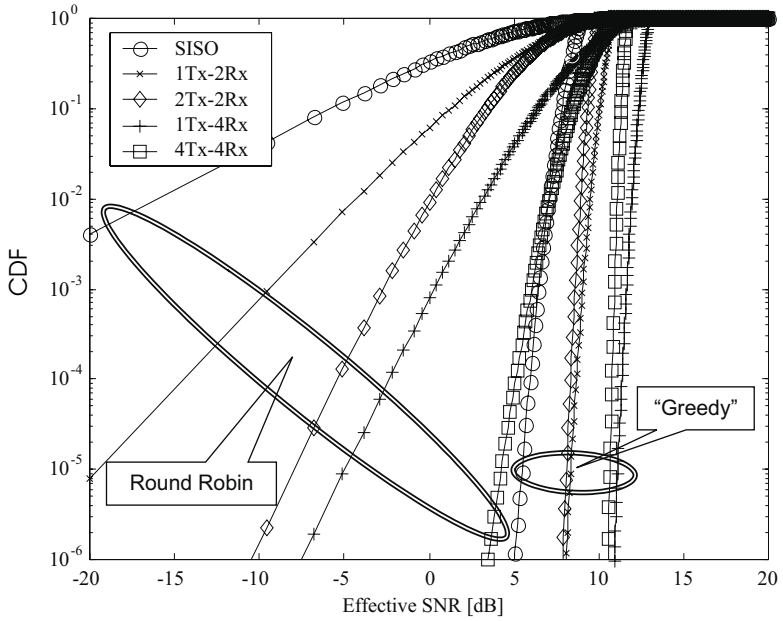

Figure 9.11: CDF of effective SNR with and without 50-fold multiuser diversity; various array sizes

In the "greedy" mode, it is observed that although the slop of the 4Tx-4Rx configuration may be steeper than the slope of the 1Tx-4Rx configuration, schemes with multiuser diversity would perform better in the case of smaller spatial diversity order.

9.3 Chapter Summary

In this chapter, we have investigated the performance of space-time architectures paired with scheduling algorithms. A unified approach to compare the performance of various space-time architectures is presented, based on a metric that encapsulates both the spectral and energy efficiency of the scheme. Two scheduling algorithms, known as the "greedy" and round robin approaches, applied different routing protocols for the transmission of packets to users in the service area. This work has been submitted to the 2002 Fall Vehicular Technology Conference in Vancouver, Canada [126].

The "greedy" scheduling algorithm was shown to yield multiuser diversity, resulting in an enhanced averaged effective SNR. Using order statistics, histograms and cumulative distribution functions of the effective SNR at the space-time combiner output were calculated with and without K-fold multiuser diversity. It is shown that the multiuser diversity does not only reduce the variance of the effective SNR but also enhances its mean value. Moreover, multiuser diversity can exploit constructive instances of the fading channel thus outperforming the performance of spatial transmit diversity. The impact of multiuser diversity on the performance of STBC is the topic of a paper submitted to the 2002 Fall Vehicular Technology Conference in Vancouver, Canada [123].

Chapter 10

Conclusions

In this dissertation, the theoretical and practical aspects of space-time codes have been investigated. STC represent a novel transmission scheme that was originally introduced by a group of researchers from AT&T research labs in an effort to achieve portion of the capacity growth offered by employing antenna arrays at both ends of the wireless link. The main features of these codes are their holistic design principles, combining entities that were traditionally designed independently (e.g., error correction code, modulation and array processing). This joint design allows STC to achieve the benefits of coded-modulation techniques with full spatial diversity order, and thus offering significant improvements in throughput and link reliability. The schemes are particularly suited for improving the downlink performance, which is the bottleneck in asymmetric applications such as Internet browsing and downloading.

10.1 Summary of Contributions and Publications

Three original contributions to the field of STC have been presented. First, the development of analytic tools that determine the fundamental limits on the performance of trellis and block type space-time codes (Chapters 4 and 5, respectively). These analytic results facilitate rapid calculation of error rate curves, and provide insights into parameter optimization in code design and system behavior in variety of channel conditions, including Rayleigh or Rician distributed fading and independent or correlated fading processes. Second, the architecture of the Virginia Tech Space-Time Advanced Radio (VT-STAR), a MIMO laboratory test bed, is shown to facilitate characterization of the MIMO channel and validation of various space-time approaches. Using this test bed, we were offered the rare opportunity to investigate real-world challenges in STC implementation (Chapter 6). In the third part

of the dissertation, two novel schemes that apply iterative processing principles to STC were presented. These include iterative equalization decoding of STC in frequency selective fading channels (Chapter 7) and iterative interference cancellation decoding for BLAST detectors (Chapter 8). Results indicate that remarkable energy and spectral efficiencies are achievable by combining concepts drawn from space-time coding, multiuser detection, array processing and iterative decoding. Finally, Chapter 9 presents a unified comparison of various multi-antenna systems, addressing the interactions of scheduling algorithms and space-time architectures. To summarize, the original contributions of this research include:

1. A comprehensive overview of STC and capacity of MIMO channels
2. Upper bounds on the performance of STTC using generating function techniques
3. Performance analysis of STTC in correlated fading channels
4. Performance analysis of orthogonal design transmit diversity (STBC) over independent and correlated fading channels
5. Design and implementation of the Virginia Tech Space-Time Advanced Radio
6. Iterative equalization decoding of STC in frequency selective fading channels
7. Novel schemes for successive and parallel interference cancellation coded BLAST
8. Performance analysis of scheduling algorithms over space-time architectures

The work summarized in this dissertation has resulted in several published papers, and transactions manuscripts currently under review. A list follows:

- R. Gozali and B.D. Woerner "Performance analysis of space-time trellis codes in Rayleigh, Rician and correlated fading channels," IEEE Transactions on Communications, in review.
- R. Gozali and B.D. Woerner "Theoretic bounds of orthogonal design transmit diversity over independent and correlated fading channels," IEEE Communications Letters, in review.
- R. Mostafa, R. Gozali, P.M. Robert, R.C. Palat, B.D. Woerner and J.H. Reed, "Virginia Tech Space-Time Advanced Radio: A DSP-based multiple input multiple output (MIMO) system prototype", EURASIP Journal on Applied Signal Processing, Special Issue on: Rapid Prototyping of DSP Systems, in review.

- R. Gozali, R. Mostafa, R.C. Palat, R. Nori, B.D. Woerner and J.H. Reed, "On the performance of orthogonal STBC in indoor and outdoor MIMO channels using analysis, measurements and simulation results", Journal on Selected Areas of Communications (JSAC), Special Issue on MIMO Systems and Applications, in preparation.

- R. Gozali and B.D. Woerner, "Applying the Calderbank-Mazo algorithm to space-time trellis codes," Proceedings, IEEE SouthEastCon, pp. 303-309, Nashville Tennessee.

- R. Gozali,"Space-time coding and MIMO channels - A tutorial," In Propagator, Fall 2000.

- R. Gozali and B.D. Woerner, "Upper bounds on the bit-error probability of space-time trellis codes using generating function techniques," Proceedings, Vehicular Technology Conference - Spring VTC '01, pp. 1318 -1323, Rhodes Greece.

- R. Gozali, S. Bayram, J.A. Tsai, J.H. Reed and B.D. Woerner, "Interpolation based data-aided timing recovery scheme for multiuser DS-CDMA receivers," in Proceedings, Wireless 2001 Conference, Calgary Canada.

- R. Gozali and B.D. Woerner, "Performance analysis of space-time trellis codes in correlated Rayleigh fading channels," 3G Wireless '02, San Francisco, CA.

- R. Gozali, R. Mostafa, R.C.Palat, S. Marikar, P.M. Robert, W.G. Newhall, C. Beaudette, S.A. Tsiakkoris, C. Anderson, J. Neel, B.D. Woerner and J.H. Reed,"Virginia-Tech Space-Time Advanced Radio (VT-STAR)," in Proceedings, Radio and Wireless Conference (RAWCON '01), pp. 223-227, Boston MA.

- R. Gozali and Brian D. Woerner, "Space-time coding and MIMO channels for high data rate wireless communications," A tutorial, IEEE SoutheastCon 2002, Columbia, South Carolina.

- R. Gozali and B.D. Woerner, "On the robustness of space-time block codes to spatial correlation", Vehicular Technology Conference - VTC Spring '02, Birmingham Alabama.

- R. Gozali and B.D. Woerner, "The impact of channel estimation errors on space-time trellis codes paired with iterative equalization decoding," Vehicular Technology Conference - VTC Spring '02, Birmingham Alabama.

- R. Gozali and B.D. Woerner, "Theoretic bounds on orthogonal design transmit diversity," International Symposium on Information Theory - ISIT '02, Lausanne, Switzerland.

- R. Gozali, R.M. Buehrer and B.D. Woerner, "On the performance of scheduling over space-time architectures," submitted to Vehicular Technology Conference - VTC Fall '02, Vancouver, Canada.

- R. Gozali, R.M. Buehrer and B.D. Woerner, "The impact of multiuser diversity on space-time block coding," submitted to Vehicular Technology Conference - VTC Fall '02, Vancouver, Canada.

- R. Gozali, B.D. Woerner, "Mitigating the error propagation problem of SIC and PIC BLAST detectors," submitted to Vehicular Technology Conference - VTC Fall '02, Vancouver, Canada.

- R. Gozali, R. Mostafa, R.C. Palat, P.M. Robert, W.G. Newhall, B.D. Woerner and J.H. Reed, "MIMO channel capacity measurements using the VT-STAR architecture," submitted to Vehicular Technology Conference - VTC Fall '02, Vancouver, Canada.

- R. Gozali and B.D. Woerner "Iterative processing of space-time trellis codes in frequency selective channels," submitted to Wireless Personal Multimedia Communications - WPMC' 02.

- R.C. Palat, R. Gozali, R. Mostafa, P.M. Robert, "Virginia Tech Space-Time Advanced Radio," Propagator Spring 2002.

10.2 Future Research Issues

This dissertation attempts to explore the performance of STC operating over MIMO fading channels. Like trellis coded modulation and turbo codes, space-time codes pose another example for the benefits associated in combining modules that were traditionally designed in a segragated manner. This approach to system design has demonstrated the saying of Ida P. Rolf: "The whole is greater than the sum of its parts". Indeed, not only that STC achieve spatial diversity order (due to the use of multiple antenna elements) and coding gain (due to the use of redundant information), they also enhance throughput (due to the use of the spatial dimension in the transmission process). The notion of joint design in the physical layer can be further extended across layers of the communications network. An example was discussed in Chapter 9 where functions that are executed in different layers (e.g., scheduling at the MAC layer and STC at the PHY layer), were shown to impact each other's performance and thus overall system performance. It is our belief that a more holistic approach to system design may be a major avenue for communication researchers in the next decade. Specific suggestions for extensions of this dissertation work may include:

1. In Chapter 4, the derivation of the pairwise error probability (PWEP) was based on an upper (Chernoff) bound. Recently, it has been shown that exact calculation of the PWEP is possible (see [58, 67, 57]). It may be useful to embed the exact PWEP into the GFT directly and evaluate how tight are the resultant analytic results. In addition, the performance analysis performed for STTC in correlated fading channels has assumed independent fade coefficients at the receiver. This assumption can be relaxed to support arbitrary correlations at the transmitter and receiver by restructuring the channel matrix as performed in Eq. (5.8).

2. The results in Chapter 5 can be applied to arbitrary channel models, including geometrical based channel models (e.g., circular and elliptical) or channel measurements obtained from a hardware test bed. The measured or computed eigenvalues of the channel covariance matrix can be used by Eq. (5.14) to assess on the performance of STBC over these channel conditions. Also, the analysis in Chapter 5 can be easily extended to support QAM signaling format with complex orthogonal designs.

3. An extension of the measurement campaign using the VT-STAR architecture may include space-time correlation studies for indoor narrowband MIMO channels. This can be performed by placing the ground plane of the antennas on a sliding track and collecting MIMO measurements as the track slides from one end to the other. As mentioned in Chapter 6, the array size can be expanded from 2×2 to 4×4

by applying IF sampling rather than baseband sampling. This operation requires direct digital synthesis (DDS) and digital down conversion (DDC) operations at the transmitter and receiver, respectively. Another extension may be to add a feedback link between the receiver and transmitter (via a wire or wireless link) to facilitate closed loop transmit diversity experiments.

4. The MAP equalizer of Chapter 7 suffers from high complexity that increases exponentially with channel memory and number of antenna elements. Thus, even for moderate channel memory, complexity becomes prohibitive for implementation and reduced complexity approaches are desirable. Other researchers have begun to look at this topic - see for example [114, 115].

5. The iterative interference cancellation decoding proposed in Chapter 8 for BLAST detectors is based on the soft-in hard-out Viterbi algorithm, such that hard decisions are fed back into the interference cancellation unit. Soft-input soft-output algorithms such as MAP or SOVA may reduce the number of iterations required to achieve an effective interference cancellation mechanism. Such an effort is discussed in [118].

6. An interesting extension for the problem of scheduling over STC, discussed in Chapter 9, may be to incorporate a cellular coverage model, including log-normal shadowing, path loss and distribution of users in the service area. Another extension may be to consider more sophisticated scheduling algorithms than the "greedy" and round robin, based on various scoring functions at the base station (BS). The availability of CSI at the BS facilitates also adaptive space-time modulation schemes that strive to improve the overall throughput of the system by adapting the physical layer according to instantaneous channel conditions.

7. While the focus in this dissertation was on the fundamental theory and practice of STC in single user settings, it is important to evaluate the performance of these schemes in the presence of multiple access interference (MAI). The space-time architectures investigated herein can be applied to a certain common air interface (e.g., CDMA) in order to assess on the performance of K users operating simultaneously with multiple antenna elements each.

8. Space-time coding techniques have shown to introduce diversity advantage and coding gains over independent or slightly correlated channels using omni-directional antenna patterns. In outdoor wireless environment, where the angular spread is small, the multiple paths may be highly correlated. Unlike spatial receive diversity, transmit

diversity schemes do not provide antenna gain aperture in AWGN. Beam forming techniques on the other hand direct the energy towards the desired user, thus providing the downlink channel with antenna gain. By directing energy to the desired user, the interference levels to other users in the cell are reduced, such that the overall system capacity is enhanced. In [80, 127, 128, 129, 130, 131], beam forming schemes were proposed for the downlink channel, based on minimization of the SIR to other users or maximization of the desired user SNR. An interesting research effort may be directed towards the development of a hybrid scheme that combines the benefits of both techniques in an adaptive manner. The functionality of this scheme relies on the existence of a feedback link between the terminal and the base station and thus the impact of imperfect feedback link should be also addressed.

9. In application such as satellite communications and ad-hoc networks, coordinated communications from distributed antennas can exploit the benefits of STC even when each transmitter is equipped with one antenna element only. For example, consider the transmission from two different and spatially separated geosynchronous satellites. Additional link margin at the mobile receiver can be achieved by using coordinated STC transmission. In these settings, each channel operates on its own frequency and undergoes slow flat fading due to scintillation, which is uncorrelated from one channel to another. Note that the antennas are not co-located, and thus timing estimates that accounts for the disparate propagation delays have to be embedded into the demodulation process. This problem can be applied also in ad-hoc military networks, where inactive terminals may support a coordinated transmission scheme that delivers information reliably between network nodes.

Appendix A

List of Acronyms

ADC Analog-to-Digital Conversion

AGC Automatic Gain Control

AMPS Advanced Mobile Phone System

APP Aposteriori Probability

AWGN Additive White Gaussian Noise (channel)

BER Bit Error Rate

BLAST Bell Labs Space-Time Architecture

bps bits per second

BPSK Binary Phase Shift Keying (modulation)

BS Base Station

CAI Common Air Interface

CCDF Complementary Cumulative Distribution Functions

CCGRV Correlated Complex Gaussian Random Vector

CDMA Code Division Multiple Access

CM Calderbank-Mazo Algorithm

CRC Cyclic Redundancy Check (code)

CSI Channel State Information

DAC Digital-to-Analog Conversion

DQPSK Differential Quadrature Phase Shift Keying

DSK DSP Starter Kit

DSP Digital Signal Processor

DSTBC Differential Space-Time Block Codes

ETSI European Telecommunications Standards Institute

EVM Evaluation Module

FCC Federal Communications Commission

FDD Frequency Division Duplexing

FDMA Frequency Division Multiple Access

FPGA Field Programmable Gate Array

FEC Forward Error Correction

FER Frame Error Rate

FIR Finite Impulse Response (filter)

FPLMTS Future Public Land Mobile Telecommunications System

GFT Generating Function Techniques

GMSK Gaussian Minimum Shift Keying (modulation)

GSM Global System for Mobile communications

IC Interference Cancellation

IEEE Institute of Electrical and Electronics Engineers

i.i.d. independent and identically distributed

IIR Infinite Impulse Response (filter)

IMT-2000 International Mobile Telecommunications by 2000

IS Interim Standard

ISDN Integrated Services Digital Network

ISI InterSymbol Interference

ITU International Telecommunications Union

ISM Industrial Scientific and Medical

LLR Log-Likelihood Ratio

LOS Line Of Site

MAI Multiple Access Interference

MAC Access Control Layer

MAP Maximum Aposteriori

MF Matched Filter

MFLOPS Million Floating Pint Operations per Second

MIMO Multiple-Input Multiple-Output (antenna elements)

MISO Multiple-Input Single-Output (transmit diversity)

MLSE Maximum Likelihood Sequence Estimator

MMSE Minimum Mean-Square Error

MPSK M-ary Phase Shift Keying (modulation)

MRC Maximal Ratio Combining

NAMPS Narrowband Advanced Mobile Phone System

NLOS Non Line Of Site

OFDM Orthogonal Frequency Division Multiplexing

pdf probability density function

PHI Physical Layer

PIC Parallel Interference Cancellation

PWEP Paireise Error Probability

QAM Quatrature Amplitude Modulation

RF Radio Frequency

RM Reed Muller (code)

RS Reed Solomon (code)

RSC Recursive Systematic Convolutional (code)

RTDX Real-Time Data Exchange

SDR Software Defined Radio

SER Symbol Error Rate

SIC Successive Interference Cancellation

SIMO Single-Input, Multiple-Output (receive diversity)

SIMO-OC Single-Input, Multiple-Output Optimal Combining

SIMO-SD Single-Input, Multiple-Output Selection Diversity

SISO Single-Input, Single-Output (antenna elements)

SNR Signal to Noise power Ratio

SOVA Soft-Output Viterbi Algorithm

SRRC Square-Root Raised Cosine

STBC Space-Time Block Codes

STC Space-Time Codes

STTC Space-Time Trellis Codes

TCM Trellis Coded Modulation

TDD Time Division Duplexing

TDMA Time Division Multiple Access

TIA Telecommunications Industry Association

VA Viterbi Algorithm

VTSTAR Virginia Tech Space-Time Advanced Radio

USDC United States Digital Cellular System

WCDMA Wideband Code Division Multiple Access

WLAN Wireless Local Area Network

ZF Zero Forcing

Appendix B

Review of Important Concepts in Matrix Analysis

Important results from linear and matrix algebra are reviewed in this appendix.

- For square matrices A and B the following relationships are useful.

$$\begin{aligned}
(AB)^T &= B^T A^T \\
\overline{AB} &= \overline{A}\,\overline{B} \\
(A^T)^{-1} &= (A^{-1})^T \\
(AB)^{-1} &= B^{-1}A^{-1} \\
det(A^T) &= det(A) \\
det(cA) &= c^n det(A)\ (c\ is\ scalar) \\
det(AB) &= det(A)det(B) \\
det(A^{-1}) &= \frac{1}{det(A)}
\end{aligned}$$

- Dot product of two complex vectors in the n-dimensional complex space C^n is defined by

$$(x, y) = \sum_{i=1}^{n} x_i \overline{y}_i,$$

  where $\overline{y}_i$ denotes the complex conjugate of y_i.

- An $n \times n$ matrix A is invertible (nonsingular) if and only if its columns (or rows) are linearly independent or, equivalently, if its determinant is nonzero. In such a case, A is full rank. Otherwise, it is singular.

- An $n \times n$ matrix A is Hermitian if and only if $A = A^\dagger$ where $A^\dagger = \overline{A^T}$ or A is equal to its transpose conjugate. Note that over the real space R^n, Hermitian matrix is equivalent to symmetric matrix.

- An $n \times n$ matrix V is unitary if $VV^\dagger = I$ where I is the identity matrix. In other words, the inverse of a unitary matrix always exists and is equal to its own transpose. Note that over the real space R^n, unitary matrix is equivalent to orthogonal matrix.

- An eigenvector of a square $n \times n$ matrix A is an $n \times 1$ vector v satisfying $Av = \lambda v$, where λ is the eigenvalue of A associated with the eigenvector v. It is assumed that the eigenvector is normalized to have unit length, or $||v|| = 1$.

- An Hermitian matrix A is diagonalizable. Also, there exist a unitary matrix V, which is composed of the eigenvectors of A and diagonalizes A such that

$$VAV^\dagger = D = diag(\lambda_1, \lambda_2, \cdots, \lambda_n),$$

  where D is a real diagonal matrix with the eigenvalues of A in its diagonal.

- Let an Hermitian matrix A be full rank, then its determinant is equal to the product of its eigenvalues. That is $det(A) = \prod_{i=1}^{n} \lambda_i$. Sketch of proof follows.

$$\begin{aligned}
\prod_{i=1}^{n} \lambda_i &= det(D) \\
&= det(VAV^\dagger) \\
&= det(V)det(A)det(V^\dagger) \\
&= det(V)det(V^\dagger)det(A) \\
&= det(VV^\dagger)det(A) \\
&= det(I)det(A) \\
&= det(A)
\end{aligned}$$

  If an Hermitian matrix A has rank r, where $r < n$, then there are $n - r$ zeros in the diagonal matrix D.

- The determinant of a square $n \times n$ matrix is computed as

$$det(A) = \sum_{j=1}^{n} a_{ij} C_{ij},$$

  where $C_{ij} = (-1)^{i+j} M_{ij}$. M_{ij} is the determinant of the sub matrix of A obtained by deleting the ith row and the jth column and is termed the minor of a_{ij}. C_{ij} is the cofactor of a_{ij}.

- A quadratic form Q of an Hermitian matrix A is defined as

$$Q = \sum_{i=1}^{n}\sum_{j=1}^{n} a_{ij}x_i\overline{x}_j = xAx^\dagger$$

- A quadratic form Q of an Hermitian matrix A is always real. Sketch of proof follows.

$$\begin{aligned}
\overline{Q} &= \overline{xAx^\dagger} \\
&= \overline{x}\ \overline{A}\ \overline{x^\dagger} \\
&= \overline{x}\ \overline{A}\ x^T \\
&= (\overline{x}\ \overline{A}\ x^T)^T \quad (scalar) \\
&= xA^\dagger x^\dagger \\
&= xAx^\dagger \quad (A\ is\ Hermitian) \\
&= Q
\end{aligned}$$

- Principal Axes Theorem: Let A be Hermitian matrix with eigenvalues $\lambda_1, \lambda_2, \cdots, \lambda_n$. V is orthonormal (unitary) matrix that diagonalizes A. Given a quadratic form $Q = xAx^\dagger$ of the Hermitian matrix A, is possible to transform the quadratic form into a standard form by the following change of basis: $x = yV$ such that

$$Q = \sum_{i=1}^{n} \lambda_i |y_i|^2,$$

  Sketch of proof follows.

$$\begin{aligned}
Q &= xAx^\dagger \\
&= (yV)A(yV)^\dagger \\
&= y(VAV^\dagger)y^\dagger \\
&= yDy^\dagger \\
&= \sum_{i=1}^{n} \lambda_i |y_i|^2
\end{aligned}$$

- An $n \times l$ matrix B is a square root of an $n \times n$ matrix A if $BB^\dagger = A$.
- The matrix A is nonnegative definite if $xAx^\dagger \geq 0$ for any $1 \times n$ complex vector x.
- Any matrix A with a square root B is nonnegative definite.
- The eigenvalues of a nonnegative-definite Hermitian matrix are nonnegative.

Appendix C

Generating Function Techniques for AWGN and BSC

The generating function is a closed form expression, whose expansion provides all distance information of the code directly. This section shows how the generating function yields an upper bound on the bit-error probability for both Binary Symmetric Channels (BSC) and Additive White Gaussian Noise (AWGN) channel. We start with the trellis diagram and assume the codes to be either linear or Geometrically uniform. This allows us to assume that the all-zero codeword was transmitted, without any loss of generality.

Figure C.1 illustrates a typical trellis diagram with $2^{\nu} = 4$ states and l transitions. The branch label contains the information bit sequence and the coded symbols sequence. The all-zero codeword is referred as the correct path while all other codewords are referred as error events.

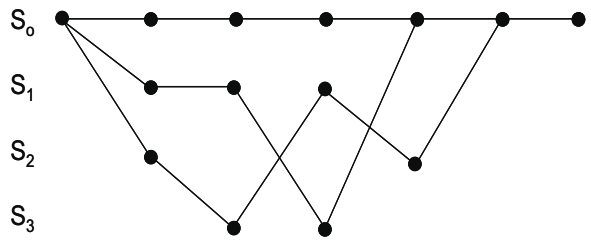

Figure C.1: Typical trellis diagram

The probability of error is the probability of diverging from the all-zero codeword

$$P_e = P(\sum_{d=d_f}^{\infty} E_d),$$

where E_d represents an error event to a codeword that has distance d with respect to the

all-zero codeword and d_f is the free distance of the code, meaning the minimum distance between two codewords of the codebook.
Applying the union bound,

$$P_e \leq \sum_{d=d_f}^{\infty} P(E_d).$$

The probability of an error event E_d is described by

$$P(E_d) = a_d P_d = a_d P(C \to C'),$$

where a_d denotes the number of codewords (error events) in distance d (from the all-zero codeword) and $P(C \to C')$ denotes the pair-wise error probability (PWEP) in between C, the all-zero codeword and C', the codeword that was erroneously decoded.
The PWEP for BSC and AWGN is given, respectively, as:

$$P(C \to C') \leq \begin{cases} \left[\sqrt{2p(1-p)}\right]^d, & BSC \\ \left[exp^{-\frac{E_s}{N_0}}\right]^d, & AWGN \end{cases}$$

where p is the crossover probability of the BSC channel and $\frac{E_s}{N_0}$ is the SNR of the AWGN channel. Note that in both cases, the PWEP is bounded by the form D^d where D is given by:

$$D = \begin{cases} \sqrt{2p(1-p)}, & BSC \\ exp^{-\frac{E_s}{N_0}}, & AWGN \end{cases}$$

Plugging this form into the error event probability, we get:

$$P_e \leq \sum_{d=d_f}^{\infty} a_d P_d \leq \sum_{d=d_f}^{\infty} a_d D^d,$$

which is the infinite power series of the generating function $T(D)$.
The general form of the generating function is given by:

$$T(D, I) = \sum_{d=d_f}^{\infty} a_d D^d I^{n_d},$$

where n_d is the number of information bits that are in error associated with the error event. Differentiating the transfer function with respect to I and plugging $I = 1$, we get

$$\left.\frac{\partial T(D, I)}{\partial I}\right|_{I=1} = \sum_{d=d_f}^{\infty} n_d \underbrace{a_d D^d}_{P_d} = E[n_d].$$

This is a weighted sum of the pair-wise error probabilities, weighted with the number of information bits in error. Thus, this is equal to the expected (average) number of information bits in error.

Therefore, the bit-error probability can be bounded using the generating function by

$$P_b = \frac{1}{k} E[n_d] \leq \frac{1}{k} \frac{\partial T(D, I)}{\partial I}\bigg|_{I=1},$$

where k denotes the number of information bits per trellis transition.

Appendix D

Quadratic Form of a Correlated Complex Gaussian Random Vector

In the performance analysis of digital communication systems, the squared Euclidean distance often takes the form of a quadratic form of the channel fade coefficients. The characteristic function of this squared Euclidean distance is of great interest as it yields an upper bound on the pair-wise error probability.

This section provides reformulation of Turin's Theorem (described in details in [7, 73]), which provides a closed form solution to the characteristic function of a quadratic form of a complex correlated Gaussian random vector (CCGRV).

Turin's Theorem: (For proof: See [73])

Let Q_j be a quadratic form of a zero mean $N \times 1$ complex Gaussian random vector Ω_j:

$$Q_j \quad = \quad \Omega_j^{\dagger} A \Omega_j,$$

where A is an $N \times N$ Hermitian matrix.

The Characteristic function of Q_j is then given by :

$$\Phi_{Q_j}(t) \quad = \quad E[exp(jtQ_j)] = \frac{1}{det(I_N - jtC_{\Omega_j}A)},$$

where C_{Ω_j} is the covariance matrix of Ω_j and I_N is an $N \times N$ identity matrix.

Defining $W = C_{\Omega_j}A$, the above result can be simplified to:

$$\Phi_{Q_j}(t) \quad = \quad \prod_{i=1}^{N} \frac{1}{1 - jt\lambda_i},$$

where $\lambda_i, i = [1, \cdots, N]$ are the eigenvalues of W.

Appendix E

Generation of Correlated Rayleigh Fading Envelopes

This appendix is based on the following references [68, 69, 74]. It is well known that Rayleigh random variables can be generated by taking the absolute value of a complex Gaussian random variable. Assume we want to generate N Rayleigh envelopes $(r_1, r_2, \cdots, r_N)$ with a normalized covariance matrix:

$$C = \begin{bmatrix} 1 & \rho_{12} & \cdots & \rho_{1N} \\ \rho_{21} & 1 & \cdots & \rho_{2N} \\ \cdots & \cdots & \cdots & \cdots \\ \rho_{N1} & \rho_{N2} & \cdots & 1 \end{bmatrix} \tag{E.1}$$

We first convert this covariance matrix into a corresponding covariance matrix of the complex Gaussian random variables $(g_1, g_2, \cdots, g_N)$, such that $r_i = |g_i|, \forall i = [1, \cdots, N]$. The new covariance matrix is denoted by $\tilde{C}$ and given by:

$$\tilde{C} = \begin{bmatrix} 1 & \tilde{\rho}_{12} & \cdots & \tilde{\rho}_{1N} \\ \tilde{\rho}_{21} & 1 & \cdots & \tilde{\rho}_{2N} \\ \cdots & \cdots & \cdots & \cdots \\ \tilde{\rho}_{N1} & \tilde{\rho}_{N2} & \cdots & 1 \end{bmatrix} \tag{E.2}$$

The analytical relationship between ρ_{ij}, the (i, j)th cross-correlation coefficient across Rayleigh envelopes and $\tilde{\rho}_{ij}$, the (i, j)th cross-correlation coefficient across complex Gaussian variates, is based on the following formula [70]:

$$\rho_{ij} = \frac{(1 + |\tilde{\rho}_{ij}|) E_i \left(\frac{2\sqrt{|\tilde{\rho}_{ij}|}}{1+|\tilde{\rho}_{ij}|} \right) - \frac{\pi}{2}}{2 - \frac{\pi}{2}} \tag{E.3}$$

where $E_i(\eta)$ denotes the complete elliptic integral of the second kind with modulus η. Since there is no closed form solution to this equation, numerical methods can be used [68, 74] to form a look-up table that relates ρ_{ij} to $\tilde{\rho}_{ij}$. This is given in table E.1.

Table E.1: Correlation of Rayleigh envelopes for values of complex Gaussian correlation

ρ_{ij}	0.00	0.05	0.10	0.15	0.20	0.25	0.30	0.35	0.40	0.45
$\tilde{\rho}_{ij}$	0.0000	0.0047	0.0056	0.0243	0.0337	0.0559	0.0737	0.0965	0.1494	0.1836
ρ_{ij}	0.50	0.55	0.60	0.65	0.70	0.75	0.8	0.85	0.9	0.95
$\tilde{\rho}_{ij}$	0.2227	0.2752	0.3327	0.4133	0.4562	0.5410	0.6073	0.6974	0.7913	0.9005

Once the covariance matrix of the complex Gaussian random variables is computed, A Cholesky decomposition of this matrix is performed to yield a lower triangular coloring marix L, such that:

$$LL^{\dagger} = \tilde{C} \tag{E.4}$$

This coloring matrix is used in transforming uncorrelated complex Gaussian random vectors to correlated ones. Assume W is an $N \times l$ matrix with zero mean complex Gaussian random vectors of length l as rows. Then, the product $X = LW$ yields a matrix of N vectors with covariance $\tilde{C}$. That is,

$$E\left\{XX^{\dagger}\right\} = E\left\{LWW^{\dagger}L^{\dagger}\right\} = LL^{\dagger} = \tilde{C} \tag{E.5}$$

Finally, the envelopes of X are the desired Rayleigh faded samples with the covariance matrix C.

N vectors with covariance $\tilde{C}$. That is,

$$E\left\{XX^{\dagger}\right\} = E\left\{LWW^{\dagger}L^{\dagger}\right\} = LL^{\dagger} = \tilde{C} \tag{E.6}$$

Finally, the envelopes of X are the desired Rayleigh faded samples with the covariance matrix C.

Bibliography

[1] D.H. Johnson and D.E. Dudgeon, *Array Signal Processing: Concepts and Techniques*. Englewood, New Jersey: Prentice Hall, 1993.

[2] G.J. Foschini and M.J. Gans, "On limits of wireless communications in a fading environment when using multiple antennas," *Wireless Personal Communications*, vol. 6, pp. 311–335, March 1998.

[3] T.S. Rappaport, *Wireless Communications - Principles and Practice*. Prentice Hall PTR, 1996.

[4] W.C.Y. Lee, "Smaller cells for greater performance," *IEEE Commun. Magazine*, pp. 19–23, 1991.

[5] B. Sklar, "Rayleigh fading channels in mobile digital communication systems. i. characterization," *IEEE Communications Magazine*, pp. 90–100, 1997.

[6] E. Berruto, M. Gudmundson, R. Menolascino, W. Mohr, and M. Pizarroso, "Research activities on UMTS radio interface, network architectures, and planning," *IEEE Commun. Magazine*, pp. 82–95, 1998.

[7] M. Schwartz, W.R. Bennett, and S. Stein, *Communication Systems and Techniques*. McGraw-Hill, 1st ed., 1966.

[8] J.L. Massey, "Coding and modulation in digital communications," *International Zurich Seminar on Digital Communications*, pp. E2(1)–E2(4), March 1974.

[9] G. Ungerboeck, "Channel coding with multilevel phase signals," *IEEE Transactions on Information Theory*, vol. IT-28, pp. 56–66, Jan. 1982.

[10] G. Ungerboeck, "Trellis coded modulation with redundant signal sets, parts I and II," *IEEE Communications Magazine*, vol. 25, no. 2, pp. 5–21, 1987.

[11] C.E. Shannon, "A mathematical theory of communication," *Bell Labs Technical Journal*, 1948.

[12] D.J. Costello, J. Hagenauer, H. Imai, and S.B. Wicker, "Applications of error-control coding," *IEEE Transactions on Information Theory*, vol. 44, pp. 2531–2560, Oct. 1998.

[13] O.M. Collins, "The subleties and interacies of building a constraint length 15 convolutional codes," *IEEE Transactions on Communications*, vol. 40, pp. 1810–1819, Dec. 1992.

[14] C. Berrou, A. Glavieux, and P. Thitimasjshima, "Near shannon limit error-correction coding and decoding," *IEEE International Conference on Communications - ICC 93*, pp. 1740–1745, 1993.

[15] E. Telatar, "Capacity of multi-antenna gaussian channels," *ATT-Bell Labs Internal Tech. Memo.*, 1995.

[16] T.L. Marzetta and B.M. Hochwald, "Capacity of a mobile multiple-antenna communication link in Rayleigh flat fading," *IEEE Transactions on Information Theory*, vol. 45, pp. 139–157, Jan. 1999.

[17] A. Narula, M.D. Trott, and G.W. Wornell, "Performance limits of coded diversity methods for transmitter antenna arrays," *IEEE Transactions on Information Theory*, vol. 45, pp. 2418–2433, Nov. 1999.

[18] V. Tarokh, N. Seshadri, and A.R. Calderbank, "Space-time codes for high data rates wireless communications: Performance criterion and code construction," *IEEE Transactions on Information Theory*, vol. 44, pp. 744–765, March 1998.

[19] S. Alamouti, "A simple transmit diversity technique for wireless communications," *IEEE Journal On Selected Ares in Communications*, vol. 16, pp. 1451–1458, Oct. 1998.

[20] S. Baro, G. Bauch, A. Pavlic, and A. Semmler, "Improving BLAST performance using space-time block codes and turbo decoding," in *Global Telecommunications Conference - GLOBECOM 2000*, vol. 2, pp. 1067–1071, 2000.

[21] V. Tarokh, S.M. Alamouti, and P. Poon, "New detection schemes for transmit diversity with no channel estimation," in *International Conference on Universal Personal Communications - ICUPC*, vol. 2, pp. 917–920, 1998.

[22] D. Agrawal, V. Tarokh, A. Naguib, and N. Seshadri, "Space-time coded OFDM for high data-rate wireless communication over wideband channels," in *Vehicular Technology Conference*, May 1998.

[23] A.F. Naguib, V. Tarokh, N. Seshadri, and A.R. Calderbank, "A space-time coding modem for high data rate wireless communications," *IEEE Journal On Selected Areas in Communications*, pp. 1459–1478, Oct. 1998.

[24] V. Tarokh, A.F. Naguib, N. Seshadri, and A.R. Calderbank, "Space-time codes for high data rate wireless communication: performance criteria in the presence of channel estimation errors, mobility, and multiple paths," *IEEE Transactions on Communications*, vol. 47, pp. 199–207, Feb. 1999.

[25] V. Tarokh, H. Jafarkhani, and A.R. Calderbank, "Space-time block coding for wireless communications: performance results," *IEEE Journal On Selected Areas in Communications*, vol. 17, pp. 451–460, March 1999.

[26] V. Tarokh, A.F. Naguib, N. Seshadri, and A.R. Calderbank, "Combined array processing and space-time coding," *IEEE Transactions on Information Theory*, vol. 45, pp. 1121–1128, May 1999.

[27] V. Tarokh, H. Jafarkhani, and A.R. Calderbank, "Space-time block codes from orthogonal designs," *IEEE Transactions on Information Theory*, vol. 45, pp. 1456 –1467, July 1999.

[28] V. Tarokh and H. Jafarkhani, "A differential detection scheme for transmit diversity," *IEEE Journal On Selected Areas in Communications*, vol. 18, pp. 1169–1174, July 2000.

[29] J. Wolfowitz, *Coding Theorems of Information Theory*. Springer-Verlag, 3rd ed., 1978.

[30] J.-C. Guey, M.P. Fitz, M.R. Bell, and W.-Y. Kuo., "Signal design for transmitter diversity wireless communication systems over Rayleigh fading channels," in *Vehicular Technology Conference*, pp. 136 –140, 1996.

[31] G. Bauch, "Concatenation of space-time block codes and turbo-TCM," in *IEEE International Conference on Communications - ICC 99*, vol. 2, pp. 1202–1206, 1999.

[32] A.F. Naguib, N. Seshadri, and A.R. Calderbank, "Applications of space-time block codes and interference suppression for high capacity and high data rate wireless systems," in *Conference Record of the Thirty-Second Asilomar Conference on Signals, Systems and Computers*, vol. 2, pp. 1803–1810, 1998.

[33] H. El Gamal, A.R. Hammons Jr., Y. Liu, M.P. Fitz, and O.Y. Takeshita, "On the design of space-time and space-frequency codes for MIMO frequency selective fading channels," *Submitted to IEEE Transactions on Information Theory*, April 2001.

[34] N. Seshadri and J.H. Winters, "Two signaling schemes for improving the error performance of frequency-division-duplex (FDD) transmission systems using transmitter antenna diversity," *Int. J. Wireless Inform. Networks*, vol. 1, no. 1, 1994.

[35] M. Cimini and A. Wittneben, "OFDM with diversity and coding for high bit-rate mobile data applications," *Int. Workshop on Mobile Multimedia Communications*, 1996.

[36] V. Weerackody, "Diversity for direct-sequence spread spectrum system using multiple transmit antennas," *International Conference on Communications*, pp. 1775–1779, 1993.

[37] J.M. Wozencraft and I.M. Jacobs, *Principles of Communication Engineering.* New York: Wiley, 1965.

[38] P.V. O'neil, *Advanced Engineering Mathematics.* Brooks/Cole Publishing, 4th ed., 1995.

[39] R.A. Horn and C.R. Johnson, *Matrix Analysis.* New York: Cambridge Univ. Press, 1988.

[40] D. Divsalar and M.K. Simon, "The design of trellis coded MPSK for fading channels: Performance criteria," *IEEE Transactions on Communications*, pp. 1004–1012, 1988.

[41] D. Divsalar and M.K. Simon, "The design of trellis coded MPSK for fading channels: Set partitioning for optimum code design," *IEEE Transactions on Communications*, pp. 1013–1021, 1988.

[42] E. Biglieri, D. Divsalar, P.J. Mclane, and M.K. Simon, *Introduction to Trellis-Coded Modulation with Applications.* Macmillan Publishing Company, 1st ed., 1991.

[43] A.V. Geramita and J. Seberry, *Orthogonal Designs, Quadratic Forms and Hadamard Matrices, Lecture Notes in Pure and Applied Mathematics*. New York and Basel: Marcel Dekker, 1979.

[44] B.L. Hughes, "Differential space-time modulation," *IEEE Transactions on Information Theory*, vol. 46, pp. 2567 –2578, Nov. 2000.

[45] G. Ganesan and P. Stoica, "Differential modulation using space-time block codes," *Conference Record of the Thirty-Fourth Asilomar Conference on Signals, Systems and Computers*, pp. 236–240, 2001.

[46] Meixia Tao and R.S. Cheng, "Differential space-time block codes," in *Global Telecommunications Conference - GLOBECOM 2001*, vol. 2, pp. 1098–1102, 2001.

[47] P.W. Wolniansky, G.J. Foschini, G.D. Golden, and R.A. Valenzuela, "V-BLAST - an architecture for realizing very high data rates over the rich-scattering wireless channel," *URSI International Symposium on Signals, Systems, and Electronics*, pp. 295–300, 1998.

[48] G.J. Foschini, "Layered space-time architecture for wireless communications in a fading environmenet when using multi-element antennas," *Bell Labs Technical Journal*, 1996.

[49] Da-Shan Shiu and J.M. Kahn, "Scalable layered space-time codes for wireless communications: performance analysis and design criteria," *Wireless Communications and Networking Conference - WCNC 99*, vol. 1, pp. 159–163, 1999.

[50] A.R. Calderbank and J.E. Mazo, "A new description of trellis codes," *IEEE Transactions on Information Theory*, vol. 30, pp. 784–791, Nov. 1984.

[51] R. Gozali and B.D. Woerner, "Applying the Calderbank-Mazo algorithm to space-time trellis codes," in *IEEE Proceedings of Southeastcon*, pp. 309–314, 2000.

[52] S. Baro, G. Bauch, and A. Hansmann, "Improved codes for space-time trellis coded modulation," *IEEE Communications Letters*, vol. 4, pp. 20–22, Jan. 2000.

[53] R. Gozali and B.D. Woerner, "Upper bounds on the bit-error probability of space-time trellis codes using generating function techniques," in *Vehicular Technology Conference*, vol. 02, pp. 1318 –1323, May 2001.

[54] D. Aktas and M.P. Fitz, "The distance spectra of space-time trellis coded modulations in quasi-static Rayleigh fading channels," *Submitted to IEEE Transactions on Information Theory*, Jan. 2001.

[55] D. Kucukyavuz and M.P. Fitz, "New views of transfer function based performance analysis of coded modulations," *Conference Record of the Thirty-Fourth Asilomar Conference on Signals, Systems and Computers*, vol. 01, pp. 42–46, 1999.

[56] R. Gozali and B.D. Woerner, "Performance analysis of space-time trellis codes in correlated Rayleigh fading channels," in *Accepted for publication at the Third Generation Wireless Conference, San Francisco, CA*, 2002.

[57] G. Taricco and E. Biglieri, "Exact pairwise error probability of space-time codes," *IEEE Transactions on Information Theory*, pp. 510–513, Feb. 2002.

[58] M. Uysal and C.N. Georghiades, "Error performance analysis of space-time codes over Rayleigh fading channels," in *Vehicular Technology Conference*, pp. 2285–2290, 2000.

[59] M.K. Simon and M.S. Alouini, *Digital Communications over Fading Channels*. New York: Wiley, 1st ed., 2000.

[60] A.J. Viterbi and J.K. Omura, *Principles of Digital Communication and Coding*. McGraw-Hill, 3rd ed., 1979.

[61] D. Divsalar and M.K. Simon, "Trellis-coded modulation for 4800-9600 bps transmission over a fading satellite channel," *IEEE Journal On Selected Areas in Communications*, vol. 5, pp. 162–175, Feb. 1987.

[62] E. Zehavi and J.K. Wolf, "On the performance evaluation of trellis codes," *IEEE Transactions on Information Theory*, vol. 33, pp. 196–202, Feb. 1987.

[63] R.G. McKay, P.J. McLane, and E. Biglieri, "Error bounds for trellis-coded MPSK on a fading mobile satellite channel," *IEEE Transactions on Communications*, vol. 39, pp. 1750–1761, Dec. 1991.

[64] J.K. Cavers and P. Ho, "Analysis of the error performance of trellis-coded modulations in Rayleigh-fading channels," *IEEE Transactions on Communications*, vol. 40, pp. 74–83, Jan. 1992.

[65] G. Forney, "Geometrically uniform codes," *IEEE Transactions on Information Theory*, vol. 37, pp. 1241–1260, Sep. 1991.

[66] G. Bauch and A. Naguib, "MAP equalization of space-time coded signals over frequency selective channels," in *Wireless Communications and Networking Conference - WCNC'*, pp. 261–265, 1999.

[67] M. Uysal and C.N. Georghiades, "Effect of spatial fading correlation on performance of space-time codes," *IEEE Electronic Letters*, pp. 181–183, Feb. 2001.

[68] R.B. Ertel and J.H. Reed, "Generation of two equal power correlated Rayleigh fading envelopes," *IEEE Communications Letters*, vol. 2, pp. 276–278, Oct. 1998.

[69] N.C. Beaulieu, "Generation of correlated Rayleigh fading envelopes," *IEEE Communications Letters*, vol. 3, pp. 172–174, June 1999.

[70] W.C. Jakes, *Microwave Mobile Communications*. Wiley, 1st ed., 1974.

[71] J.G. Proakis, *Digital Communications*. McGraw-Hill, 1995.

[72] M.P. Fitz, J. Grimm, and S. Siwamogsatham, "A new view of performance analysis techniques in correlated Rayleigh fading," in *Wireless Communications and Networking Conference*, vol. 1, pp. 139 –144, March 1999.

[73] G.L. Turin, "The characteristic function of Hermitian quadratic forms in complex normal variables," *Biometrica*, pp. 199–201, 1960.

[74] B. Natarajan, C.R. Nassar, and V. Chandrasekhar, "Generation of correlated Rayleigh fading envelopes for spread spectrum applications," *IEEE Communications Letters*, vol. 4, pp. 9–11, Jan. 2000.

[75] R. Gozali and B.D. Woerner, "Performance analysis of space-time trellis codes in rayleigh, rician and correlated fading channels," *Submitted to IEEE Transactions on Communications*, 2001.

[76] D. Aktas and M.P. Fitz, "Computing the distance spectrum of space-time trellis codes," in *Proceedings, IEEE Wireless Communications and Networking Confernce*, vol. 01, pp. 51–55, 2000.

[77] D. Aktas and M.P. Fitz, "Distance spectra of space-time trellis coded modulations," in *Proceedings, International Symposium on Information Theory*, p. 328, 2001.

[78] TIA, *TR45.5, Physical Layer Standard for CDMA2000 Spread Spectrum Systems*. TIA/EIA/IS-2000.2, 1999.

[79] A. Annamalai and C. Tellambura, "Error rates for nakagami-m fading multichannel reception of binary and m-ary signals," *IEEE Transactions on Communications*, pp. 58–68, 2001.

[80] C. V. Rensburg and B. Friedlander, "Transmit diversity for arrays with correlated Rayleigh fading," *Conference Record of the Thirty-Fourth Asilomar Conference on Signals, Systems and Computers*, pp. 301–305, 2000.

[81] Tai-Ann Chen, M.P. Fitz, Wen-Yi Kuo, M.D. Zoltowski, and J.H. Grimm, "A space-time model for frequency non-selective Rayleigh fading channels with applications to space-time modems," *IEEE Journal on Selected Areas in Communications*, pp. 1175–1190, 2000.

[82] S. Sandhu and A. Paulraj, "Union bound on error probability of linear space-time block codes," in *IEEE International Conference on Acoustics, Speech, and Signal Processing*, vol. 4, pp. 2473–2476, 2001.

[83] R. Gozali and B.D. Woerner, "Theoretic bounds on orthogonal design transmit diversity," in *Accepted for publication at the IEEE International Symposium on Information Theory - ISIT'*, 2002.

[84] R. Gozali and B.D. Woerner, "On the robustness of space-time block codes to spatial correlation," in *Vehicular Technology Conference*, 2002.

[85] G. Bauch and J. Hagenauer, "Analytical evaluation of space-time transmit diversity with FEC-coding," in *Global Telecommunications Conference - GLOBECOM 2001*, vol. 2, pp. 435–439, 2001.

[86] S. Verdu, *Multiuser Detection*. New York: Cambridge Univ. Press, 1998.

[87] S. Sandhu, R. Heath, and A. Paulraj, "Space-time block codes versus space-time trellis codes," *IEEE International Conference on Communications - ICC 01*, vol. 4, pp. 1132–1136, 2001.

[88] S.M. Alamouti, V. Tarokh, and P. Poon, "Trellis-coded modulation and transmit diversity: design criteria and performance evaluation," in *International Conference on Universal Personal Communications - ICUPC*, vol. 1, pp. 703–707, 1998.

[89] D. Baker and M.C. Valenti, "The impact of channel estimation errors on space time block codes," in *11th Annual MPRG/Virginia Tech Wireless Communications Symposium*, 2001.

[90] R. Gozali and B.D. Woerner, "Theoretic bounds of orthogonal design transmit diversity over independent and correlated fading channels," *Submitted to IEEE Communications Letters*, 2002.

[91] R. Gozali and B.D. Woerner, "The impact of channel estimation errors on space-time trellis codes paired with iterative equalization/decoding," in *Vehicular Technology Conference*, 2002.

[92] R. Gozali, R. Mostafa, R.C. Palat, S. Marikar, P.M. Robert, W.G. Newhall, C. Beaudette, S.A. Tsiakkouris, C. Anderson, J. Neel, B.D. Woerner, and J.H. Reed, "Virginia Tech space-time advanced radio (VT-STAR)," in *IEEE Proceedings of Radio and Wireless Conference (RAWCON), Boston, MA.*, pp. 227–231, 2001.

[93] S. Ellington and J. Hetrick, "An 8-element dual-frequency array receiver for propagation measurements near 2.4 ghz," in *Electromagnetic Range Consortium Meeting - The Ohio State University ElectroScience Laboratory*, 2001.

[94] M. Stoytchev, J.B. Raveche, and H.F. Safar, "Joint spatial and temporal characterization of the wideband wireless communication channel for MIMO applications," in *IEEE Proceedings of RAWCON, Boston*, pp. 233–236, 2001.

[95] J.P. Kermoal, P.E. Mogensen, and K.I. Pedersen, "Experimental investigation of correlation properties of MIMO radio channels for indoor picocell scenario," in *Vehicular Technology Conference*, pp. 14–21, 2002.

[96] J.W. Wallace and M.A. Jensen, "Measured characteristics of the MIMO wireless channel," in *Vehicular Technology Conference*, vol. 4, pp. 2038–2042, 2001.

[97] TI, *TMS320C62x/C67x Programmers Guide, SPRU198B.* Texas Instruments, 1998.

[98] TI, *TMS320C6x Assembly Language Tools Users Guide, SPRU186C.* Texas Instruments, 1998.

[99] TI, *THS1206, THS12082, THS10064, THS10082 Evaluation Module Users Guide, SLAU042A.* Texas Instruments, 1999.

[100] TI, *Designing With the THS1206 High-Speed Data Converter Application Report, SLAA094.* Texas Instruments, 1999.

[101] TI, *THS56x1EVM for the THS5641/51/61/71 8-Bit,10-Bit,12-Bit,14-Bit D/A Conversion, SLAU032A.* Texas Instruments, 1999.

[102] TI, *TMS320C6000 Real-Time Data Exchange (RTDX) Tutorial.* Texas Instruments, 1998.

[103] R. Mostafa, A. Hannan, and J.H. Reed, "Narrowband transmit diversity measurements at the handset for an indoor environment," *3rd International Conference on Information, Communications, and Signal Processing*, 2001.

[104] C.B. Dietrich, Jr., K. Dietze, J.R. Nealy, and W.L. Stutzman, "Spatial, polarization, and pattern diversity for wireless handheld terminals," *IEEE Transactions on Antennas and Propagation*, vol. 49, pp. 1271–1281, Sept. 2001.

[105] R. Gozali, R. Mostafa, R.C. Palat, P.M. Robert, W.G. Newhall, B.D. Woerner, and J.H. Reed, "MIMO channel capacity measurements using the VT-STAR architecture," in *Submitted to VTC Fall*, 2002.

[106] R. Mostafa, R. Gozali, P.M. Robert, R.C. Palat, B.D. Woerner, and J.H. Reed, "Virginia Tech space-time advanced radio: A DSP-based multiple input multiple output system prototype," *Submitted to EURASIP Journal on Applied Signal Processing, Special Issue on: Rapid Prototyping of DSP Systems*, 2002.

[107] Y. Liu, M.P. Fitz, and O.Y. Takeshita, "Space-time codes performance criteria and design for frequency selective fading channels," in *International Conference on Communications*, pp. 2800–2804, 2001.

[108] L.R. Bahl, J. Cocke, F. Jelinek, and J. Raviv, "Optimal decoding of linear codes for minimizing symbol error rate," *IEEE Transactions on Information Theory*, pp. 284–287, 1974.

[109] G.D. Forney, "Maximum likelihood sequence estimation of digital sequences in the presence of intersymbol interference," *IEEE Transactions on Information Theory*, pp. 363–378, 1972.

[110] M.V. Eyuboglu and S.U. Qureshi, "Reduced-state sequence estimation with set-partitioning and decision feedback," *IEEE Transactions on Communications*, pp. 12–20, 1988.

[111] A. Duel-Hallen, "Delayed decision-feedback sequence estimation," *IEEE Transactions on Communications*, no. 5, pp. 428–436, 1989.

[112] A. Hafeez and W.E. Stark, "Decison feedback sequence estimation for unwhitened ISI channels with aplications to multiuser detection," *IEEE Journal on Selected Areas in Communications*, no. 9, pp. 1785–1795, 1998.

[113] M.C. Valenti, *Iterative Detection and Decoding for Wireless Communications, Ph.D. Dissertation.* Virginia Poly. Inst. and State University, 1999.

[114] S. Baro, G. Bauch, A. Pavlic, and A. Semmler, "Iterative equalization and decoding with channel shortening filters for space-time coded modulation," in *Global Telecommunications Conference - GLOBECOM 2000*, vol. 2, pp. 1067–1071, 2000.

[115] G. Bauch and N. Al-Dhahir, "Iterative equalization and decoding with channel shortening filters for space-time coded modulation," in *Vehicular Technology Conference*, vol. 4, pp. 1575–1582, 2000.

[116] G.D. Golden, G.J. Foschini, R.A. Valenzuela, and P.W. Wolniansky, "Detection algorithm and initial laboratory results using v-blast space-time communication architecture," *IEE Electronic Letters*, pp. 14–16, 1999.

[117] M. Sellathurai and S. Haykin, "A simplified diagonal blast architecture with iterative parallel-interference cancelation receivers," *IEEE International Conference on Communications - ICC 01*, vol. 10, pp. 3067–3071, 2001.

[118] M. Sellathurai and S. Haykin, "Turbo-blast for high-speed wireless communications," *Wireless Communications and Networking Conference - WCNC 00*, vol. 1, pp. 315–320, 2000.

[119] A.J. Viterbi, J.K. Wolf, E. Zehavi, and R. Padovani, "A pragmatic approach to trellis-coded modulation," *IEEE Communications Magazine*, pp. 11–19, 1989.

[120] J.H. Winters, J. Salz, and R.D. Gitlin, "The impact of antenna diversity on the capacity of wireless communication systems," *IEEE Transactions on Communications*, pp. 1740–1751, 1994.

[121] R. Gozali and B.D. Woerner, "Mitigating the error propagation problem of SIC and PIC BLAST detectors," in *Submitted to VTC Fall*, 2002.

[122] P. Bender, P. Black, M. Grob, R. Padovani, N. Sindhushayana, and A. Viterbi, "Cdma/hdr: A bandwidth-efficient high-speed wireless data service for nomadic users," *IEEE Communications Magazine*, pp. 70–77, 2000.

[123] R. Gozali, R.Michael Buehrer, and B.D. Woerner, "The impact of multiuser diversity on space-time block coding," in *Submitted to VTC Fall*, 2002.

[124] S. Sandhu and A. Paulraj, "Space-time block codes: a capacity perspective," *IEEE Communications Letters*, vol. 4, pp. 384–386, Dec. 2000.

[125] D. Neal, "Order statistics," *http://www.wku.edu/ neal/probability/order.html*, 2002.

[126] R. Gozali, R.Michael Buehrer, and B.D. Woerner, "On the performance of scheduling over space-time architectures," in *Submitted to VTC Fall*, 2002.

[127] M.A. Ingram, K.H. Li, A. Van Nguyen, and T. Pratt, "Beamforming, doppler compensation, and differential space-time coding," *Conference Record of the Thirty-Fourth Asilomar Conference on Signals, Systems and Computers*, pp. 158–162, 2000.

[128] A.M. Tehrani, R. Negi, and J. Cioffi, "Space-time coding and transmission optimization for wireless channels," *Conference Record of the Thirty-Fourth Asilomar Conference on Signals, Systems and Computers*, vol. 02, pp. 1798–1802, 1998.

[129] R.W. Heath and A. Paulraj, "Multiple antenna arrays for transmitter diversity and space-time coding," *Proceedings, International Conference on Communications*, vol. 01, pp. 36–40, 1999.

[130] R. Negi, A.M. Tehrani, and J. Cioffi, "Adaptive antennas for space-time coding over block-time invariant multipath fading channels," *Vehicular Technology Conference*, vol. 01, pp. 70–74, 1999.

[131] M. Katz and J. Ylitalo, "Extension of space-time coding to beamforming wcdma base stations," *Vehicular Technology Conference*, vol. 02, pp. 1230–1234, 2000.

[132] J.E. Padjett, C.G. Gunther, and T. Hattori, "Overview of wireless personal communications," *IEEE Commun. Magazine*, pp. 28–41, 1995.

[133] D.J. Goodman, *Wireless Personal Communication Systems.* Addison Wesley, 1997.

[134] J.K. Cavers, J.H. Kim, and P. Ho, "Exact calculation of the union bound on performance of trellis-coded modulation in fading channels," *IEEE Transactions on Communications*, no. 5, pp. 576–579, 1998.

[135] R. Knopp and H. Leib, "M-ary phase coding for correlated Rayleigh fading channels," in *The 5th IEEE International Symposium on Personal, Indoor and Mobile Radio Communications - PIMRC '94.*, pp. 563–567, 1994.

[136] D. Divsalar and M.K. Simon, "Multiple trellis coded modulation (MTCM)," *IEEE Transactions on Communications*, pp. 410–419, 1988.

[137] S.H. Jamali and Tho Le-Ngoc, *Coded-Modulation Techniques For Fading Channels*. Kluwer Academic Publisher, 1995.

[138] S.B. Wicker, *Error Control Systems for Digital Communication and Storage*. Prentice Hall, 1995.

[139] V. Tarokh, A.F. Naguib, N. Seshadri, and A.R. Calderbank, "Low-rate multi-dimensional space-time codes for both slow and rapid fading channels," in *The 8th IEEE International Symposium on Personal, Indoor and Mobile Radio Communications - PIMRC '97.*, vol. 3, pp. 1206–1210, 1997.

[140] Da-Shan Shiu, G.J. Foschini, M.J. Gans, and J.M. Kahn, "Fading correlation and its effect on the capacity of multi-element antenna systems," *IEEE Transactions on Communications*, vol. 48, pp. 502–513, March 2000.

[141] R. Gozali, "Space-time coding and MIMO channels - a tutorial," *MPRG Propagator*, Sept. 2000.

[142] A.F. Naguib, "Equalization of transmit diversity space-time coded signals," in *Global Telecommunications Conference - GLOBECOM 2000*, vol. 2, pp. 1077–1082, 2000.

[143] A.F. Naguib and N. Seshadri, "MLSE and equalization of space-time coded signals," in *Vehicular Technology Conference*, vol. 3, pp. 1688–1693, 2000.

[144] P. Balaban and J. Salz, "Optimum diversity combining and equalization in digital data transmission with application to cellular mobile radio," *IEEE Transactions on Vehicular Technology*, pp. 342–354, 1991.

[145] P. Balaban and J. Salz, "Optimum diversity combining and equalization in digital data transmission with application to cellular mobile radio - part I: Theoretical considerations," *IEEE Transactions on Communications*, pp. 885–894, 1992.

[146] C. Douillard, M. Jezequel, C. Berrou, G.A. Picart, and P. Didier, "Iterative correction of intersymbol interference: Turbo-equalization," *European Transactions on Telecommunications*, pp. 507–511, 1995.

[147] P.R. Chevillat and E. Eleftheriou, "Decoding of trellis-encoded signals in the presence of intersymbol interference," *IEEE Transactions on Communications*, no. 7, pp. 669–676, 1989.

[148] P. Hoeher, "TCM on frequency-selective fading channels: a comparison of soft-output probabilistic equalizers," in *Global Telecommunications Conference - GLOBECOM 1990*, vol. 1, pp. 376–381, 1990.

[149] S.M. Kay, *Fundamentals of Statistical Signal Processing- Volume I: Estimation Theory*. Prentice Hall, 1993.

[150] A. Papoulis, *Probability, Random Variables, and Stochastic Processes*. McGraw-Hill, 1965.

[151] B. Sklar, "A primer on turbo code concepts," *IEEE Communications Magazine*, pp. 94–102, 1997.

[152] A. Reial, *Concatenated Space-Time Coding, A Dissertation Proposal*. University of Virginia, 1999.

[153] J. Salz and J.H. Winters, "Effect of fading correlation on adaptive arrays in digital mobile radio," *IEEE Transactions on Vehicular Technology*, pp. 1049–1057, 1994.

[154] C. Chuah, J.M. Kahn, and D. Tse, "Capacity of multi-antenna array systems in indoor wireless environment," in *Global Telecommunications Conference - GLOBECOM 1998*, 1998.

[155] G.G. Raleigh and J.M. Cioffi, "Spatio-temporal coding for wireless communications," *IEEE Transactions on Communications*, pp. 357–366, 1998.

[156] T.M. Cover and J.A. Thomas, *Elements of Information Theory*. New York: Wiley, 1991.

[157] R.B. Ertel, P. Cardieri, K.W. Sowerby, T.S. Rappaport, and J.H. Reed, "Overview of spatial channel models for antenna array communication systems," *IEEE Personal Communications*, pp. 10–22, 1998.

[158] O. Tirkkonen and A. Hottinen, "Square-matrix embeddable space-time block codes for complex signal constellations," *IEEE Transactions on Information Theory*, vol. 48, pp. 384–395, Feb. 2002.

[159] H. Jafarkhani, "A quasi-orthogonal space-time block code," *IEEE Transactions on Communications*, vol. 49, pp. 1–4, Jan. 2001.

[160] M.O. Damen, K. Abed-Meraim, and J.-C. Belfiore, "Diagonal algebraic space-time block codes," *IEEE Transactions on Information Theory*, vol. 48, pp. 628–636, March 2002.

[161] M. Uysal and C.N. Georghiades, "New space-time block codes for high throughput efficiency," in *Global Telecommunications Conference - GLOBECOM 2001*, vol. 2, pp. 1103–1107, 2001.

[162] G. Ganesan and P. Stoica, "Space-time block codes: a maximum snr approach," *IEEE Transactions on Information Theory*, vol. 47, pp. 1650–1656, May 2001.

[163] G. Ganesan and P. Stoica, "Achieving optimum coded diversity with scalar codes," *IEEE Transactions on Information Theory*, vol. 47, pp. 2078–2080, July 2002.

[164] Xiangming Li, Tao Luo, Guangxin Yue, and Changchuan Yin, "A squaring method to simplify the decoding of orthogonal space-time block codes," *IEEE Transactions on Communications*, vol. 49, pp. 1700 –1703, Oct. 2001.

Vita

Ran Gozali was born on April 4, 1970, in Haifa, Israel. He received his B.Sc. degree magna cum laude in electrical & computer engineering from Ben Gurion University, Israel in 1994, and his M.Sc. degree in electrical engineering from the Technion, Israel Institute of Technology in 1999. From 1994-1999, he was a technical staff member of the Communication Systems Directorate at Rafael Inc., Israel, conducting research that supports algorithm development and system engineering of advanced wireless modems. Currently, Ran is a Ph.D. candidate at the Mobile and Portable Radio Research Group, Virginia Tech, working in the area of space-time coding, array processing and iterative decoding with Prof. Brian Woerner. His research interests include reliable data transmission techniques over wireless links, development of analytic tools for communication systems design, diversity techniques, coding and modulation. During the summers of 2000 and 2001, Ran served the department of Electrical and Computer Engineering at Virginia Tech as an instructor, teaching Analog and Digital Communications. Ran serves as a reviewer for the IEEE Communications Letters and has been nominated for the Virginia Tech Sigma XI research award.